Miniaturized Engineering of Human Cells using Droplet Microfluidics

Samuel R. Little

A Thesis
In the Department
of
Electrical and Computer Engineering

Presented in Partial Fulfillment of the Requirements
For the Degree of
Doctor of Philosophy (Electrical and Computer Engineering) at

Concordia University
Montreal, Quebec, Canada

July 2024

Concordia University
School of Graduate Studies

This is to certify that the thesis prepared

By: ***Samuel Raymond Little***

Entitled: ***Miniaturized Engineering of Human Cells using Droplet Microfluidics***

And submitted in partial fulfillment of the requirements for the degree of:

DOCTOR OF PHILOSOPHY *(Electrical and Computer Engineering)*

Complies with the regulations of the University and meets the accepted standards with respect to originality and quality.

Signed by the final examining committee:

_____ Chair
Dr. Brandon Helfield

_____ External Examiner
Dr. Tania Konry

_____ Examiner
Dr. Elena Kuzmin

_____ Examiner
Dr. Nawwaf Kharma

_____ Examiner
Dr. Mojtaba Kahrizi

_____ Thesis Supervisor
Dr. Steve Shih

Approved by _____
Dr. Jun Cai, Graduate Program Director

July 30, 2024 _____
Dr. Mourad Debbabi, Dean
Faculty of Engineering and Computer Science

Abstract

Miniaturized Engineering of Human Cells using Droplet Microfluidics

Samuel Raymond Little, Ph.D.
Concordia University, 2024

Inserting foreign biomolecules into human cells is at the heart of cell engineering protocols. By taking nucleic acids or fully formed proteins and shuttling them across the cell membrane in a process known as transfection, cells can either temporarily or permanently gain or lose functionalities. This capability has been used extensively for applications including fundamental research into genetics, industrial production of high value biomolecules, and of interest to this thesis, the production of novel cell therapies – where human cells are repurposed to fight disease.

Numerous techniques have been developed to perform transfection on human cells with a specific focus on technologies that can engineer enough cells for clinical use (often > 10^9 cells are needed to treat a single patient). However, a currently unmet need in this field, is a miniaturized platform for the research and development of new cell therapies. For this application, large libraries of cellular modifications need to be tested in hopes of discovering one with clinical potential. To do this economically, testing each modification in the library must be done rapidly while consuming as few resources as possible.

Bulk microfluidics has emerged as an ideal technology for high throughput clinical cell therapy production; however, it is unsuited to processing numerous unique small-scale reactions in parallel. To address the unmet need, in this thesis we demonstrate that droplet microfluidics – the science of controllably manipulating sub-microliter volumes of liquid – can serve as the ideal platform for cell therapy R&D.

Acknowledgements

I would like to express a sincere appreciation for my supervisor and mentor Dr. Steve CC Shih who has both challenged and encouraged me to be a better scientist and engineer. I would not have achieved success without your guidance.

I would also like to thank my committee, Dr. Tania Konry, Dr. Mojtaba Kahrizi, Dr. Nawwaf Kharma, and Dr. Elena Kuzmin. I look forward to your comments and questions and I appreciate any feedback you have that will help me improve the quality of this work.

I have been fortunate throughout my PhD journey to have numerous capable and enthusiastic collaborators. I would like to thank Dr. Peter J Darlington and his students Fatemeh Gholizadeh and Mehri Hajiaghayi, the extensive work with primary human immune cells in this thesis would not have been possible without their expertise and generosity. I would like to thank Dr. David JHF Knapp and his student Fanny-Mei Cloarec-Ung for sharing their gene editing expertise. I would like to thank Hugo Sinha and Dr. Alison Hirukawa as well as the entire team at Drop Genie for challenging me to solve hard problems and for being superb industrial collaborator.

I additionally would like to acknowledge collaborators in the Shih Microfluidics Laboratory. My time has been both intellectually stimulating and professionally fruitful, I will forever be grateful for the willingness to collaboratively problem solve and relentlessly pursue good science. I would like to specifically acknowledge the following: Ziuwin Leung, with whom I experienced a truly tremendous amount of failure, but also a good deal of success; Angela Quach, who patiently taught a clumsy engineer every aspect of cell culture etiquette; Niloufar Rahbari, who has been an attentive and hardworking mentee. I would also like to acknowledge Dr. James Perry, Dr. Fatemeh Ahmadi, Zhiyang Deng, and Chiara Leal Alves for entertainment, brainstorming, and – more than anything – friendship.

I want to extend a sincere thank you to my family, friends, and loved ones. Becky Fixman, and Brian Ward for welcoming me into their home. My little sister Maggie, who I have looked to for guidance and looked up to for quite some time. My dad, who has been a remarkable bedrock of support especially during the hardest days of this PhD. And finally, to my partner Zoë. As much as I have learned in grad school, it pales in comparison to what you have taught me. Thank you for filling my life with love and affection, for being at my side, for being my home.

Dedications

This thesis is dedicated to my mom, Leslee McCarthy, who passed on June 17, 2020. Despite this, she still managed to be by my side every step of the way. Thank you for teaching me how to persevere, to believe, to fight .

Contributions

Chapter 2

The research was designed by Angela B.V. Quach (ABVQ) and Steve C.C. Shih (SCCS). All experiments and analysis were conducted by ABVQ and SCCS. Biological and microfluidic methods were developed by ABVQ and Samuel R Little (SRL). All authors wrote, revised, and reviewed the manuscript.

Chapter 3:

The novel electroporation system was designed by SRL, Alison Hirukawa (AH), and SCCS. The experiments were designed by SRL, Ziuwin Leung (ZL), and SCCS. All experiments and analyses were conducted by SRL and ZL. Biological and microfluidic methods and DMF control software were developed by SRL and ZL. Mathematical modeling and simulations were designed and performed by ZL. Electroporation control circuits and software were designed and built by SRL. Methodology for cell isolation and freezing from fresh blood was developed by Fatemeh Gholizadeh (FG), Mehri Hajiaghayi (MH), and Peter J Darlington (PJD) and FG and MH performed the isolation and freezing protocols. All authors wrote, revised, and reviewed the manuscript.

Chapter 4:

Experiments were designed by SRL, and SCCS. SRL and Niloufar Rahbari (NR) performed transcriptomic analysis. NR and Joel Phillips (JP) designed qPCR primers, qPCR was optimized and performed by NR. DMF control software along with electroporation hardware and software were developed by SRL. FG, MH, and PJD developed the methodology for cell isolation and freezing from fresh blood and FG and MH performed the isolation and freezing protocols as well as all ELISAs. Fanny-Mei Cloarec-Ung (FMCU) and David JHF Knapp (DJHFK) developed CRISPR knock in methodology. SCCS secured required funding for the project. SRL and SCCS wrote the manuscript which was revised and reviewed by all authors.

Table of Contents

Table of Figures

Table of Tables

List of Symbols and Units

θ – Contact angle [degrees]

ϵ_0 – Permittivity of vacuum [F/m]

ϵ_r – Relative permittivity or dielectric constant [unitless]

γ_{LV} – surface tension at liquid vapor interface [N/m]

C – Capacitance [F]

f – Frequency [Hz]

V_{RMS} – Root mean squared voltage [V]

$V_{P\text{-}P}$ – Peak-to-peak voltage [V]

E – Energy [J]

F – Force [N]

ρ – resistivity [Ω/m]

Δp – change in pressure [N/m^2]

I - Current [A]

R – Resistance [Ω]

r – radius [m]

EF – Electric field [kV/cm]

List of Abbreviations

AC – Alternating current

CRISPR – Clustered regularly interspaced short palindromic repeats

DC – Direct current

DEP – Dielectrophoresis

DMEM - Dulbecco's Modifed Eagle Medium

DMF – Digital microfluidics

DNA – Deoxyribonucleic acid

EP – Electroporation

E. coli – *Esterichia coli*

ELISA – Enzyme-linked immunosorbent assay

EWOD – Electrowetting-on-dielectric

FACS – Fluorescence-activated cell sorting

FBS – Fetal bovine serum

FDA – Food and drug administration

FITC – Fluorescein isothiocyanate

GE – Ground electrode

GFP – Green fluorescent protein

HDR – Homology directed repair

ITO – Indium tin oxide

KO – Knock out

MFI – Mean fluorescence intensity

mRNA – Messenger ribonucleic acid

NHEJ – Non-homologous end joining

PBS – Phosphate buffer saline

PE – Phycoerythrin

PCB – Printed circuit board

PCR – Polymerase chain reaction

PDMS – Polydimethylsiloxane

PI – Propidium iodide

PE – Pulsing electrode

QC – Quality control

R&D – Research and development

RNA – Ribonucleic acid

RNP – Ribonucleic protein

RT-qPCR – Reverse transcription quantitative (real-time) polymerase chain reaction

SCL – Serial clock line

SDA – Serial data line

ssODN – Single stranded oligodeoxynucleotide

TE – Transfection efficiency

VR – Viability ratio

Chapter 1. Introduction

This chapter serves as an introduction to the key topics relevant to this thesis. We first introduce cellular therapies and the need for new technologies to advance this field, subsequently we discuss droplet microfluidics and digital microfluidics with an emphasis on how these fluid handling paradigms can be applied to work with small populations of mammalian cells. We conclude the chapter with a look at how microfluidics can be applied to engineering mammalian cells.

1.1 Motivation

Prior to 2013, the care of patients with Acute Lymphoblastic Leukemia (ALL) relied on traditional cancer treatment paradigms. Patients diagnosed with ALL could expect to receive chemotherapy, radiation therapy, or in certain cases stem cell transplants and monoclonal antibody treatments.[1] Overall survival rates for patients with ALL was 40 - 50 % and declined sharply in patients diagnosed over the age of 50.[2] However, in 2013, Brentjens et al.[3] demonstrated that T cells recovered from a cancerous patient could be genetically reprogrammed to express synthetically designed Chimeric Antigen Receptors (CAR). The CAR molecules could be designed to attack cell markers present on malignant cells and absent on most healthy cells, effectively engineering the human immune system to target certain cancers. Once genetically reprogrammed, modified T cells could be reinjected back into the patient and allow that patient to mount an immune response against the cancer cells. In this initial study, complete tumor eradication was achieved in five chemotherapy resistant adults, and in a long term follow-up from the same group 83% (44 out of 53) of treated patients had complete remission.[4] This success demonstrated that genetically engineered T cells with enhanced immune functions are a powerful new class of therapeutic.[5] Since this time, T cell engineering, and cell engineering in general have expanded to treat not just hematological cancers (as shown by Brentjens), but also solid cancers,[6] infections,[7] autoimmune diseases,[8] and neurodegenerative diseases.[9] As of 2021, there were 28 globally approved cellular therapies and over 1700 on going clinical trials.[10] The research and development of new cellular therapies represents one of the most important medical developments of the 21st century.

To continue the advancement of cellular therapies, extensive research and development (R&D) is required to solve persistent problems (such as toxic side effects,[11] or premature cell exhaustion),[12] and to find new targets that direct immune cells towards malignancy while sparing healthy cells. With these R&D pursuits have come a demand for new technologies to accelerate and improve cell therapy pipelines. Current workflows are resource intensive and laborious, driving up the cost of R&D and limiting the ability to test novel genetic manipulations. Techniques to miniaturize and automate cell therapy R&D hold the promise of accelerating timelines to clinic while limiting prohibitive development costs.[13] Microtools, purpose built to aid in the cell engineering process, could help supercharge the next stage in the cell therapy revolution.

This thesis describes the authors contribution to the field of automated and miniaturized cell engineering platforms. The thesis is divided into four core chapters. Chapter 2 documents a technique for viral transduction on a digital microfluidic (DMF) chip. We show how the unique droplet geometries achieved on our microfluidic platform facilitate improved interactions between viral particles and target cells improving transduction in challenging cell lines compared to well-plate approaches. Despite early success using viral particles for cell engineering, concerns over immunogenicity are causing this technique to fall out of favour. To this end, chapter 3 presents a DMF-based droplet electroporation (EP) method that relies on the application of electric pulses to facilitate the non-viral delivery of biomolecules to primary human cells. We document how our approach solves three significant problems that have led to failure in previous droplet-based EP systems and show how this technique can be applied to both immortalized and primary immune cells for the delivery of complex biomolecules. Chapter 4 continues out investigation into our novel DMF-EP technique. In this chapter we directly compare our miniaturized method against two commercially available state-of-the-art EP platforms. Using our system, we are able to achieve equivalent gene editing efficiencies while using up to 20-fold fewer cells and reagents. Additionally, we demonstrate that cells engineered on our platform have better viability, improved proliferation capabilities, less transcriptomic dysregulation, and improved functionality in immunotherapeutic assays.

1.2 Microfluidic Theory

In his now famous essay "*Plenty of room at the bottom*", physicist Richard Feynman called for an enhanced interest in miniaturization describing it as a field "in which an enormous amount can be

done", and that "would have an enormous number of technical applications".[14] At the microscale, Reynold's numbers plummet and viscous forces dominate inertial forces, turbulence disappears, diffusion becomes the dominant mode of mixing and surface tension can overwhelm other forces[15,16]. It is by taking advantage of this counter-intuitive world that microfluidics aims to achieve the novel technical application of laboratory functionality on a palm-sized chip (lab-on-a-chip). Microfluidic technologies allow scientist to miniaturize lab procedures allowing for a several order of magnitude reduction in the consumption of often expensive reagents,[17] additionally, the control of microfluidic chips lends itself to automation opening the possibility of limiting the laborious nature of many common lab tasks. However, an often under appreciated benefit of microfluidics is the novel physics paradigms that exist at the microscale where heat transfer is nearly instantaneous, and mass transfer is limited by diffusion.[18] By leveraging microfluidics, experimental procedures and apparatuses can be designed to perform tasks that would never be possible at the macroscale.

Microfluidics is a multifaceted field. It can be roughly grouped into three main sub-categories: 1. bulk flow, 2. droplet in channel and, 3. droplet movement on wettable surfaces.[19] In this work, we will focus on the second two categories.

1.3 Droplet Microfluidics

1.3.1 Droplet in Channel

Droplet-in-channel microfluidics describes the science of generating 100s to > 10^6 discreet fluid compartments segmented by an immiscible phase.[20] Droplet volumes can range from femto – microliters (fL - μL) and high throughput analysis of droplet in channel systems have led to significant advancements in diverse fields including single-cell analysis,[21] antibody discovery,[22] and directed evolution.[23]

Generally, droplets are created using passive techniques such as T-junctions, flow-focusing geometries, and co-flow structures.[18] Active techniques, such as the controllable application of electrowetting forces[24] are also used for on-demand droplet generation. Since its invention, numerous technological advancements have been made to increase the controllability of droplet microfluidic systems. A collection of droplet manipulation tools are highlighted in **Figure 1-1**. These include the ability to mix, split, and merge droplets (**Figure 1-1a-c**), dilution, incubation,

and single particle encapsulation (**Figure 1-1d-f**), as well as controllable picoinjection, droplet sorting, capture, and detection (**Figure 1-1g-j**).[18]

Fabricating these systems usually relies on soft lithography techniques.[25] Briefly, a negative photoresist (such as SU-8) is deposited on to a physical substrate (such as a silicon wafer) to an known thickness by spin coating. Then, UV light is applied to the photoresist through a custom designed photomask, baked, and undeveloped photoresist is developed away leaving only

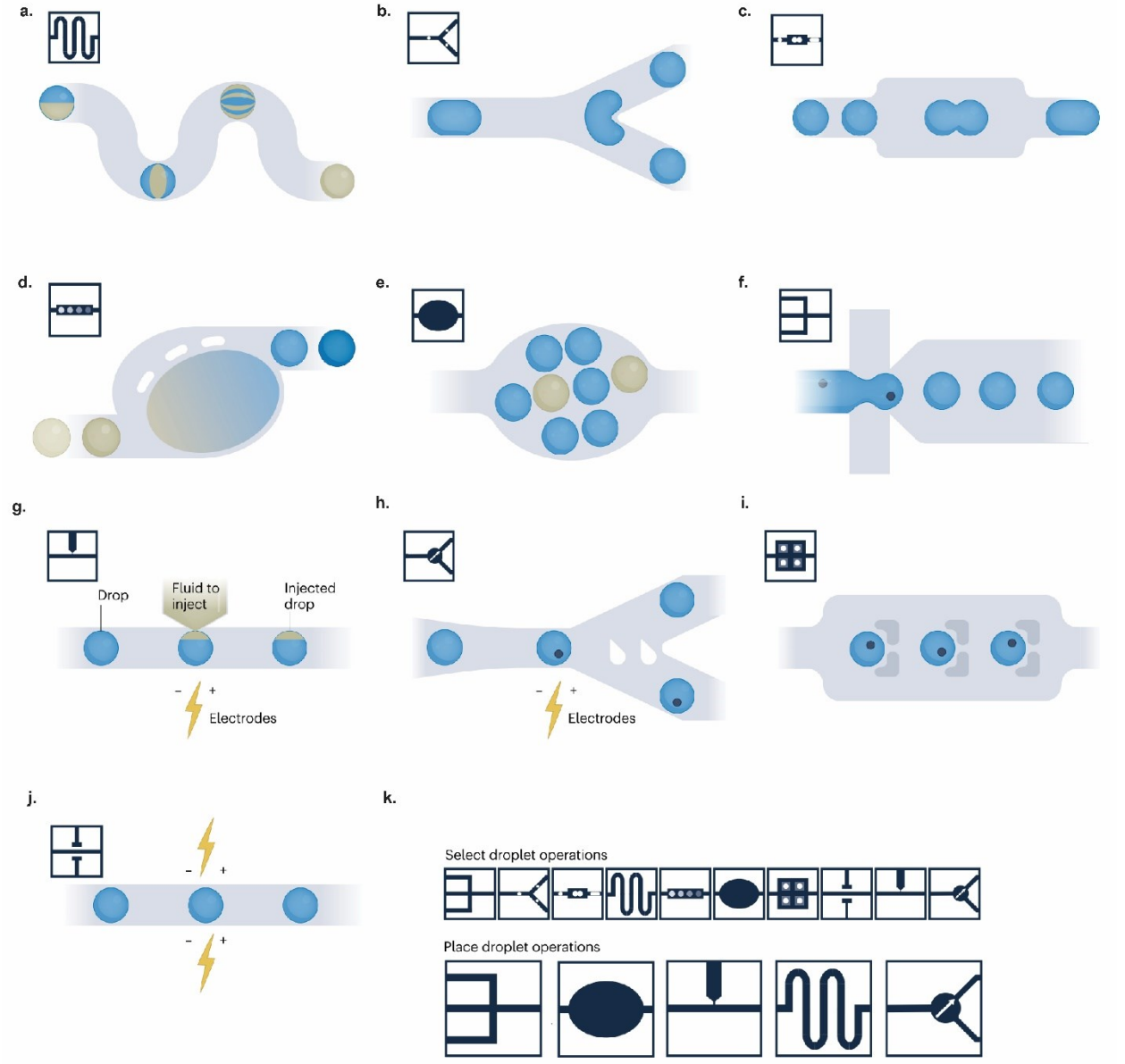

Figure 1-1: ***An overview of droplet in channel microfluidic techniques.*** *a) Droplet mixing, b) droplet splitting, c) droplet merging, d) droplet dilution, e) droplet incubation, f) single-particle encapsulation, g) picoinjection, h) droplet sorting, i) droplet trapping, j) droplet detection, k) overview of the modular nature of droplet in channel capabilities. Reproduced with permission from Moragues et al. 3:1 1-22 (2023) Copyright Nature Reviews Methods Primers.*

the negative of the desired channel network. Then a soft polymer such as polydimethylsiloxane (PDMS) is poured on to the channel mold. After solidifying the PDMS, the layer can be removed from the mold leaving the imprint of the channel network in the PDMS. Inlet and outlet ports can be punched into the PDMS allowing for fluidic connections with external pumps.

Of special interest to this study is the ability to use droplet-in-channel microfluidics for the manipulation of either primary or immortalized human cells. While single cell techniques have been mentioned above, techniques where droplets contain 10 - 10^4 cells are also of interest for performing more complex assays while maintaining the benefit of high throughput operation.[26] For instance, Eduati et al.[27] demonstrated a platform for performing combinatorial drug screening on cancer biopsies. In this work the authors generated 500 nL droplets containing ~100 cells. By using a custom droplet generator, the authors were able to generate 56 unique droplet compositions each with at least 20 replicates per condition allowing them to analyze a broad range of drug combinations while using cells from only a single patient biopsy. In another high impact application from Ronteix et al.[28] the authors generated 50 nL Matrigel droplets containing ~ 75 mouse B16 melanoma cells. After overnight incubation the cells grew into a 3-dimensional spheroid, subsequently, secondary droplets were generated containing a varying amount of cytotoxic T lymphocytes, these secondary droplets were then merged with the spheroid containing droplets and the authors were able to perform time-lapse microscopy to observe the interactions between the immune cells and the cancerous target in over 234 unique spheroid-containing droplets. The above applications along with a growing body of work show that while some of the most high-profile successes in the field of droplet microfluidics have come from single-cell applications, the ability to observe small populations of mammalian cells in droplets can give useful insights into cell-to-cell interactions[29,30], culture and coculture dynamics,[31] and the analysis of spheroids or organoids.[32]

1.3.2 Digital Microfluidics

A distinct paradigm of droplet microfluidics is the field of Digital Microfluidics (DMF) which is of particular interest to the work in this thesis. In the field of DMF, pico – micro liter (pL - µL) droplets are moved across an array of individually addressable electrodes coated in an insulating dielectric and hydrophobic layer. DMF systems usually manipulate 10 – 100 droplets at a time but as many as 10^3 droplets have been shown on a single platform.[33] By applying a voltage across a

driving and grounding electrode, a small force can be generated on a droplet between the two electrodes.[34] In a one-plate DMF configuration (**figure 1-2a**) the driving and grounding electrode are on the same plane and the droplet sits on top of the two electrodes, whereas in a two-plate configuration (**figure 1-2b**) the droplet is sandwiched between the driving and grounding plane (in both configurations an insulating dielectric layer is between the droplet and the electrodes). Two-plate DMF systems are slightly more complex however they are capable of a wide range of droplet manipulation procedures including merging droplets together and mixing their contents, precisely dispensing droplets from a reservoir, or splitting a large droplet into two smaller droplets.[34]

Two theoretical models have been developed to understand the droplet movement phenomena observed on DMF. The first is a thermodynamic model referred to as the Lippman Young model[35] detailed in **Equation 1.1**.

Equation 1-1

$$cos\theta_v = cos\theta_0 + \frac{1}{2\gamma_{LF}} CV^2$$

Where θ_v and θ_0 are the static contact angle of the droplet with and without the application of a voltage respectively. γ_{LF} is the surface tension between the liquid droplet and the filler media (ie. the fluid surrounding the droplet – usually air), C is the capacitance of the dielectric layer and V is the applied voltage. In this approach, droplet movement is attributed to capillary pressure (or Laplace pressure) resulting from asymmetric contact angles when part of a droplet is in contact

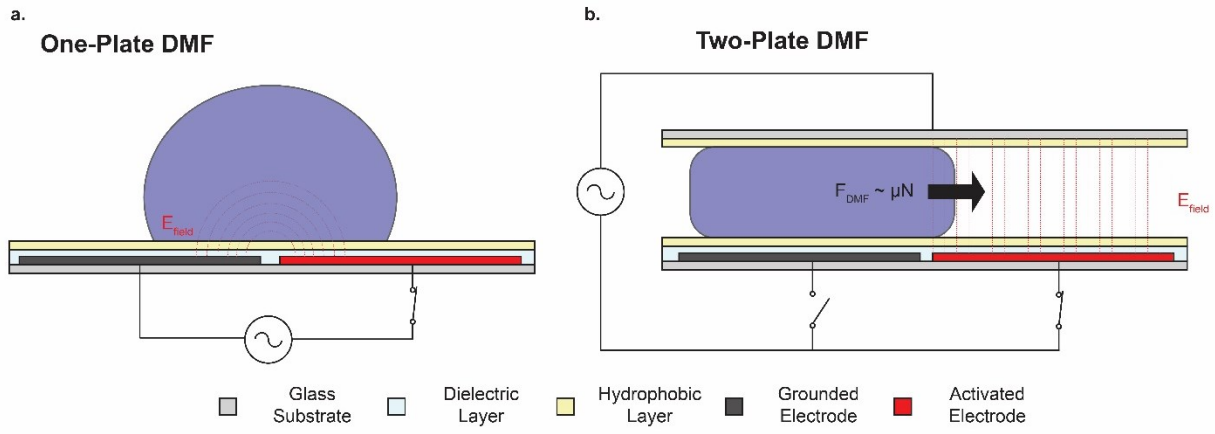

*Figure 1-2: **Digital microfluidic systems**. A schematic of an a) one-plate DMF configuration and b) a two-plate DMF configuration. Red lines indicate generated electric field.*

with a driving potential (θ_v) and part of the droplet is not (θ_0). The resulting pressure (Δp) for a droplet of height 'd' can be calculated using **Equation 1-2.**[36]

Equation 1-2

$$\Delta p = \frac{\gamma_{LF}}{d}(cos\theta_v - cos\theta_0)$$

This model has led to DMF often being referred to electrowetting on dielectric (EWOD). However, a number of non-aqueous solvents and solutions that have minimal or no voltage induced contact angle change have been observed to move on DMF platforms implying that the voltage induced contact angle change is an observable consequence of the application of an electric field but not a requirement for droplet movement.[36] As a result of this conclusion, an electromechanical theory of droplet movement has been developed that accounts for electrowetting forces as well as dielectrophoretic (DEP) forces that result when a non uniform electric field is generated and a polarized droplet is drawn to a region of high electric field intensity.[37] The electromechanical model attributes droplet movement to a gradient in stored energy where the DMF platform is modeled as a parallel-plate capacitor using **Equation 1-3**.

Equation 1-3

$$C = \frac{\epsilon_0 \epsilon_r A}{d}$$

Where ϵ_0 and ϵ_r are the permittivity of free space and relative permittivity of the dielectric layer respectively and A and d are the cross-sectional area of the capacitor and the thickness of the capacitor respectively. Since a DMF platform has numerous discreet layers (i.e. dielectric layer, hydrophobic layer, liquid layer), the total energy in a DMF system can be described with **Equation 1-4.**

Equation 1-4

$$E(x) = \sum_i \frac{C_i V_i^2}{2}$$

Where x is the horizontal position along a DMF system and i represents each discreet energy storing layer at position x. By taking the partial derivative of **Equation 1-4** with respect to x and substituting in **Equation 1-3,** an equation for applied force can be developed in **Equation 1-5**.

Equation 1-5

$$F = \frac{\partial E(x)}{\partial x} = \frac{L}{2}\left(\sum_i \frac{\epsilon_0 \epsilon_{ri,liquid} V_{i,liquid}^2}{d_i} - \sum_i \frac{\epsilon_0 \epsilon_{ri,filler} V_{i,filler}^2}{d_i}\right)$$

Where L is the length of droplet exposed to an applied voltage, i,liquid represents all the energy stored in regions covered by a droplet, and i,filler represents all the energy stored in regions covered by filler media. Key take aways from observing **Equation 1-5** are that actuation forces will be changed by modifying the composition of the droplet, the filler media, or the dielectric layer or by increasing or decreasing the applied voltage or the thickness of any of the layers.

For prototyping purposes, most DMF devices are fabricated in a cleanroom using photolithography techniques. More information on these techniques can be found in the experimental sections of chapters 2, 3, and 4 as well as in additional literature.[38] Briefly, a positive photoresist is spin coated on to substrate coated with a thin metal layer. By exposing the photoresist to UV light through a custom photomask and etching away the exposed metal an electrode pattern can be formed along with all required electrode wiring and contact pads to external circuitry. The electrodes are subsequently coated in a dielectric layer (parylene C or SU8-5 are both commonly used), followed by a hydrophobic layer such as Teflon. Glass chips coated in transparent Indium Tin Oxide (ITO) as well as a hydrophobic layer are separated from the electrodes by a spacer (commonly double-sided tape) and used as a grounding plate. Cleanroom fabrication gives the ability to rapidly produce DMF chips with near limitless customization allowing for quick prototyping and easy application in a laboratory setting. However it is worth noting that DMF platforms can also be fabricated using printed circuit board (PCB) technology[39] which can be expensive for prototyping purposes, but can be massively scaled for commercialized products. A schematic of a complete DMF system can be found in appendix C (**Figure 8-1)** and is thoroughly outlined in additional literature.[40] Briefly, the most common laboratory DMF system consists of an arbitrary function generator and high voltage amplifier used to generate a high voltage AC signal. The AC signal is then selectively delivered to electrodes using solid-state relays controlled by a micro controller generating controllable electrostatic forces for precise manipulation of droplets. This setup has also been miniaturized for portability and shown to be functional in remote settings.[41]

Due to the compact nature of DMF platforms, the ability to easily interface with existing lab hardware such as pipettes, and the unparalleled controllability of individual droplets, DMF has gained significant popularity for a wide range of lab-on-a-chip functions[42] including point-of-care diagnostics,[43] synthetic biology workflows,[44] and automating laborious lab tasks such as next generation sequencing (NGS) library prep.[33] To this end, numerous companies have emerged leveraging DMF capabilities for high-impact applications. Miroculus (now part of Integra),[45] Oxford Nanopore,[46] and Volta Labs[47] are all building products for automated NGS prep. Nuclera[48] has developed a platform for on-demand protein synthesis and Nicoya[49] sells a platform for biomolecular interaction analysis. A more exhaustive analysis of commercialized DMF platforms can be found in literature.[50] However, an additional company worth mentioning is Drop Genie,[51] which has a commercially available platform for the miniaturized and automated engineering of human cells that was developed as a direct result of the work documented in chapter 3 and 4 of this thesis.

While applications of DMF vary widely, of specific interest to this work is the ability to use DMF for assays with mammalian cells. Barbulvic-Nad et al.[52] demonstrated that 11 µL droplets containing ~ 6.6 x 10^5 cells could be actuated along a DMF electrode array and that after actuation these cells had no differences in viability, proliferation capacity, or cell biochemistry in comparison to cells that never experienced DMF actuations. This important work proved that DMF could serve as a platform for the manipulation of mammalian cells and since that time it has been used for both primary and immortalized mammalian cell culture,[53,54] single-cell omics,[55] and drug screening on organoids.[56] The ability to use a miniaturized platform such as DMF for primary cell based assays allows for complex experiments to be performed while reducing the consumption of precious cells (obtained through patient biopsies). Since the starting material of cells is often a limiting factor in experimental design,[57] needing substantially fewer cells for a single reaction on a DMF platform can make new discoveries possible with single donor resolution.[58] A significant contribution of this work (documented in chapters 2,3, and 4) include expanding the capability of DMF to work with mammalian cells.

1.4 Mammalian Cell Engineering

Since its first demonstration by Cong et al., and Mali et al., CRISPR/Cas systems have been widely used to engineer cellular genomes[59,60]. The Cas9 protein is a dsDNA binding protein that is guided

to its target site by reprogrammable short guide RNAs (sgRNAs), once the system has located its associated target sequence it can cut the dsDNA and knock-out the target gene through non-homologous end joining (NHEJ)[60]. Furthermore, by relying on homology directed repair (HDR), user-supplied donor DNA can be inserted into the targeted cut-site, thus allowing for both directed gene knock-outs as well as the addition of new genes into a cellular genome[61]. As previously discussed, the ability to generate synthetic receptors and insert them into T cells greatly expands the repertoire of the human immune system. It has also been shown that taking these synthetic receptors and directly inserting them at advantageous spots in the genome using CRISPR can enhance immune response to cancerous targets.[62] Further, it has been speculated that in order to design immune cell therapies that minimize side effect, persist long-term in a patient, and are truly "off-the-shelf", significant genetic engineering will be needed.[63–65] A substantial challenge in the CRISPR-Cas cell engineering pipeline is the delivery of the required biological payloads into the mammalian cells.[66] To do this successfully, payloads (such as sgRNA, Cas9 proteins, and HDR templates) must be transported across the cell membrane and into the cell without compromising cell viability and functionality.

The act of transporting these biomolecules across the cell membrane is referred to as transfection. Transfection can either be performed for clinical scale manufacturing where cells are being engineered to treat a patient, or for R&D scale manufacturing when novel modifications are being testing for efficacy in-vitro. During clinical-scale manufacturing, often 10^8 – 10^9 cells need to be engineered with a single, well-defined modification,[67] however it is worth noting that complete remission has been achieved where ~ 94 % of CAR T cells originated from a single clone.[68] Conversely, in R&D scale manufacturing, numerous unique modifications need to be screened in parallel. Since the pre-market phase makes up a significant portion of time and cost of developing cell therapies,[69] there is motivation to limit the required number of cells and reagents to save cost and time during the R&D phase.

1.4.1 Transfection Techniques

1.4.1.1 Viral Transduction

Figure 1-3a overview viral vector-based transduction which is a widely used technique for genetic engineering.[70] It involves using engineered viruses to deliver genetic materials into human cells, leveraging the viruses natural ability to infect cells and modify them to express new genetic constructs while removing the viruses pathogenic capabilities. A wide range of engineered viruses exist, the most commonly used for cell therapy applications are retroviruses,[71] lentiviruses (which are a subtype of retrovirus),[72,73] herpes simplex virus,[74] adenovirus,[75] and adeno-associated virus (AAV).[76] These viral systems can be broadly grouped as integrating vectors (retroviruses and lentiviruses) and non-integrating (herpes simplex virus, adenoviruses, and AAVs). Integrating vectors randomly insert their genetic payload into the host genome where it is subsequently expressed stably by the host,[73] and non-integrating systems insert their DNA into the nucleus but rarely integrate into the genome leading to transient expression.[75,76]

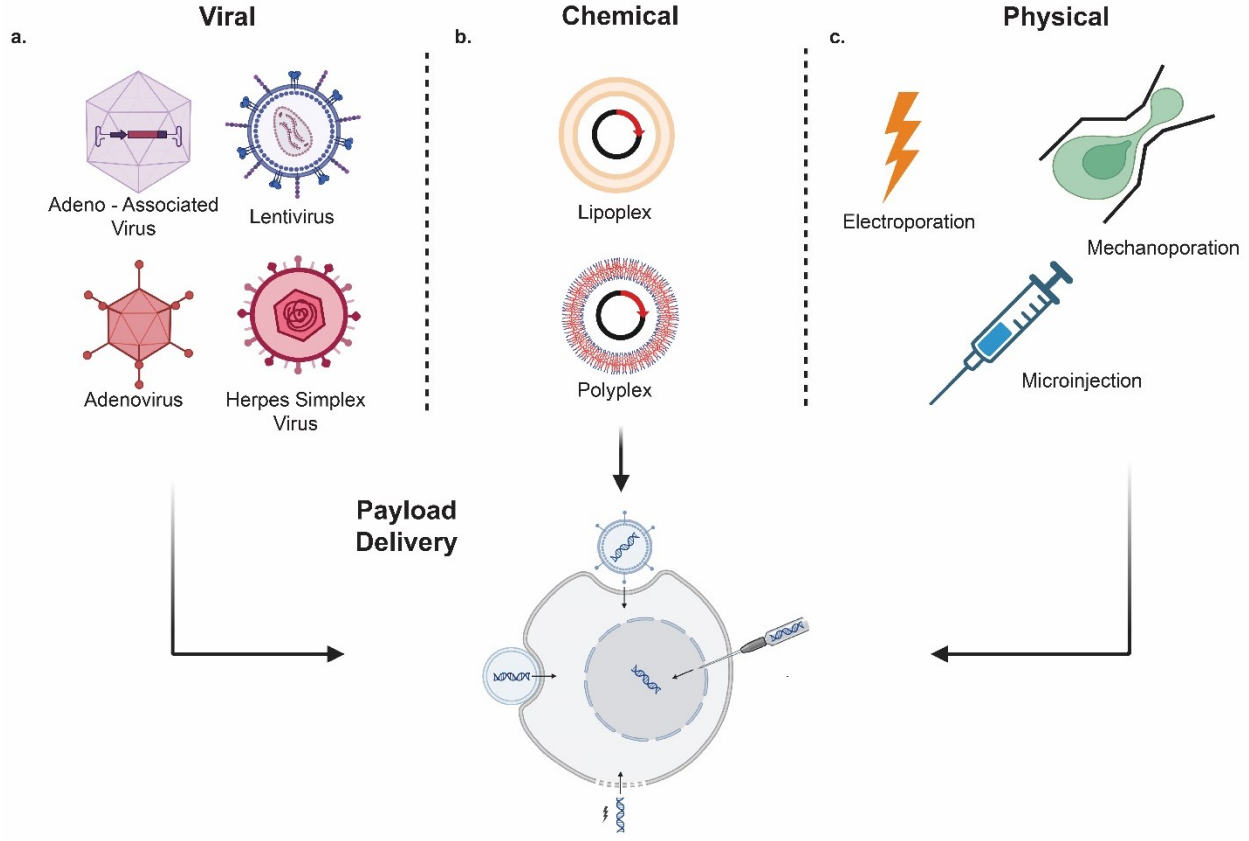

*Figure 1-3: **Overview of techniques for transfecting mammalian cells.** a) Viral transduction methods including adeno associated virus, adenovirus, lentivirus, and herpes simplex virus. b) chemical transfection methods including lipoplexes and polyplexes. c) physical transfection methods including electroporation, mechanoporation and microinjection. Created with Biorender.com.*

In part due to decades of study and development, viral transduction has become the leading technique for clinical cell therapy manufacturing and will continue to play a significant role for years to come.[77] However, adenoviruses have been shown to elicit an adverse cytokine response in transduced cells[78] and improper dosing of AAVs can lead to transduction related cytotoxicity.[79] Additionally, retroviruses and lentiviruses have raised concerns over random insertion disrupting host oncogenes.[80] These concerns, combined with the expensive and complex nature of developing viral vectors for transduction have led to calls for a change in the way cell therapies are developed for clinical applications.[81]

1.4.1.2 Chemical Delivery

A wide range of chemical transfection methods have been shown in literature and while differences exist between methods, they all have a similar underlying principle: briefly, positively charged chemicals form a complex with negatively charged nucleic acids to form a positively charged complex. This complex is then attracted to the negatively charged cell membranes, and through not-fully-understood mechanisms, the complex is shuttled across the cell membrane.[82] Cationic lipids have been widely shown for gene therapy applications[83] and lipid nanoparticles have been shown for the delivery of CRSPR reagents.[84]

Several chemical techniques have gained success in the clinic[85] and lipid nanoparticles in particular became universally recognized as a useful tool for the in-vivo delivery of COVID-19 mRNA vaccines.[86] However, as a tool for ex vivo gene therapy, preparation procedures can be complex meaning generating a wide range of unique delivery vectors is expensive and time consuming.[87]

1.4.1.3 Physical Transfection

Physical transfection methods encompass a wide range of payload delivery techniques that predominantly rely on suspending cells in a media with a high concentration of payload and using a physical stimulus to generate nanopores in the membrane of the cells. Once pores are generated the concentration gradient between the inside of the cell and the surrounding media will drive payload across the cell membrane where they remain once the pores are healed.[88] Usually, physical transfection must be performed ex-vivo, meaning cells must be first removed from the body prior to engineering, however it comes with the significant advantage that no additional vector is required to deliver the payload, payloads can be delivered into a wide range of dividing and non-

dividing cells, and most physical transfection methods are agnostic as to what the payload consist of.[89] This means a wide variety of unique materials can be delivered into almost any cell without additional preparation or modifications. While an exhaustive review of techniques used for physical transfection ca be found in literature,[89] a technique worth exploring in detail here is electroporation (EP) which is used extensively in chapters 3, 4 and 5 of this thesis.

1.4.1.4 Electroporation

EP works by neutralizing the membrane potential of a cell with an applied electric field in accordance with the Schwan equation seen in **Equation 1-6**.[90]

Equation 1-6

$$V_{cell} = fEFr\cos\theta\left(1 - e^{\frac{-t}{\tau}}\right)$$

Where V_{cell} is the voltage drop across an individual cell caused by an external electric field (EF), f is a dimensionless factor that is a function of the cell's electrical and geometric properties,[91] τ is the time constant of membrane charging, r is the radius of the cell, and t is the elapsed time since the onset of the electric field. When V_{cell} sufficiently neutralizes the cell's endogenous membrane potential, water molecules penetrate the lipid bilayer making up the cell membrane, this leads to a reorientation of the lipids adjacent to the water molecule resulting in the formation of nanopores on the surface of the cell.[90] EP has gained attention for its ability to be used as an affordable platform for rapid ex-vivo cell engineering[92] while also having been demonstrated as a safe and effective technique for clinical scale manufacturing.[93] Despite this success, recent criticisms have emerged claiming that EP results in functionally deficient cells.[94,95] To understand this criticism we must analyze how EP can cause harm to cells during the transfection process.

The two predominant causes of cell harm during EP are excessive current generation during pulsing leading to joule heating,[96,97] and the effects of electrochemical reactions occurring at the metallic anode and cathode.[96–98] However, it is important to note that since EP is a voltage based phenomena (**Equation 1-6**) both current generation and electrolysis are side effects of the EP process and not necessary to the success of EP.

Since the current through an electrical system is defined by Ohm's Law, in order to calculate the electrical current generated during a process such as electroporation, you must take the required applied voltage ($V_{applied}$) and divide it by the system resistance (R_{system}), where the

applied voltage can be calculated with **Equation 1-7** and the system resistance can be calculated with **Equation 1-8.**[99]

Equation 1-7

$$V_{applied} = EF_{cell}\ x\ d$$

Equation 1-8

$$R_{system} = \frac{\rho\ x\ d}{w\ x\ L}$$

Where EF_{cell} is the electric field required to permeabilize the cell. W and L are the dimensions of the cross-sectional area between the anode and cathode, d is distance between the anode and cathode, and ρ is the resistivity of the media. Since EF_{cell} is largely a biological parameter determined by cell size and membrane structure,[90] limiting the current generation during pulsing is predominantly a function of system design. Observing **Equation 1-8,** it can be seen that R_{system} can be maximized by increasing the media resistivity, increasing the distance between the electrodes, or minimizing the cross-sectional area between the electrodes. Combining **Equation 1-7**, with **Equation 1-8** through Ohm's law we can obtain **Equation 1-9** which can be used for calculating the current generated during an EP pulse (I_{pulse}).

Equation 1-9

$$I_{pulse} = \frac{V_{applied}}{R_{system}} = \frac{EF_{cell}\ x\ d}{\frac{\rho\ x\ d}{w\ x\ L}} = \frac{EF_{cell}\ x\ w\ x\ L}{\rho}$$

Equation 1-9 makes it clear that the most important factors for minimizing I_{pulse} is maximizing media resistivity and minimizing the dimensions that define the cross-sectional area of the EP systems. However, care should be taken when maximizing media resistivity as some EP buffers are known to by toxic to cells.[100]

Electrolysis at the anode and cathode leads to oxidation and reduction of water molecules inside of the EP chamber resulting in a substantial change in pH along with the production of hydrogen, oxygen, and chlorine gas bubbles.[101] It has been document that these pH changes are most severe near the metallic electrodes and that the closer a cell is to an electrode during EP the more likely it is to die.[98] Therefore, another concern for engineers building an EP system is to protect cells from the effects of electrolysis.

Despite concerns regarding cell functionality, electroporation is still becoming an increasingly popular approach both for clinical scale cell manufacturing and R&D scale T cell engineering and numerous commercial products have emerged to serve these needs including the MaxCyte,[102] Nucleofector,[103] and the Neon.[104] However for EP to truly become the optimal technique for developing new cell therapies, functionality concerns must be addressed.

1.4.2 Microfluidic Transfection

To address the demand for payload delivery techniques, bulk flow microfluidics has emerged as a promising technology and thorough reviews can be found in literature.[105] To date, the primary pursuit of the field of microfluidic payload delivery has been to develop a platform capable of clinical scale manufacturing, more specifically, a platform capable of high throughput (>10^6 cells per minute), and efficient delivery of functional materials into primary human cells.[105] A collection of successful techniques have been developed including techniques relying on mechanical squeezing or compression,[94,106–108] fluidic shearing,[109–111] and electroporation.[112] While these techniques excel at large scale processing, they are poorly suited to application where numerous conditions need to be tested in parallel due to their reliance on syringe pumps. In this paradigm, for each unique condition (i.e. unique type of payload or combination of payloads), a new aliquot of cells and payload would need to be prepared and loaded into the syringe which is then connected to the device through tubing. To account for dead volume, a relatively large volume would need to be loaded into the syringe. To prevent cross contamination between samples the device would need to be thoroughly flushed or a new device would need to be used. Alternatively, samples could be run simultaneously on a chip with several parallel channels, however this would require numerous syringe pumps which is expensive.

1.4.2.1 Droplet Microfluidic Transfection

Droplet microfluidics has the potential to become an ideal platform for massively parallelized, miniaturized, and automated transfection where each droplet could serve as a microreactor for a unique transfection condition. Exemplary of this vision are two works from Shih et al.[113] and Gach et al..[114] In the work from Shih et al., two combinatorial libraries each consisting of 16 unique plasmids were assembled on a DMF device using either Gibson, yeast, or golden gate assembly. Then a droplet containing the assembled plasmids and microbial cells were actuated to a microfluidic channel where droplet EP occurred. This platform allowed the author to generate and

screen a large library of payloads (32 unique plasmids) in an automated fashion while limiting the required input materials. Gach et al. used a similar workflow also using microbial cells however droplet transfection was performed on-chip using heat shock. While these works are promising,

Table 1-1: Overview of droplet-based methods for transfecting mammalian cells

Format	Transfection Method	Cell Type	Payload	Efficiency (%)	Viability (%)	# of cells / droplet	Citation
DMF	Chemical	H1299	Plasmid	65	Not Reported	~ 1 x 10^3	Sinha et al.[115]
Droplet in Channel	Physical (Mechanical)	Primary Human T - cells	Dextran, mRNA	90	80	1	Joo et al.[116]
				98	Not Reported	1	Lee et al. [117]
	Chemical + Physical (Mechanical)	Jurkat, THP-1, K562	Plasmid	~ 50	70 - 80	1	Li et al.[118]
	Chemical	hiPSC	Plasmid	~75	94	1	Perez-Sosa et al.[119]
	Physical (Electroporation)	CHO	Plasmid	11	68	1	Zhan et al.[120]
Droplet Pipetting	Physical (Electroporation)	Jurkat	Plasmid	66	70	~ 2 x 10^5	Jin–Im et al.[121]
Levitating Droplet	Chemical	HeLa, PC12	Plasmid	~ 10	Not Reported	1.5 x 10^4	Vasileiou et al.[122]
		Huh-7	Plasmid	Not Reported	80	8 x 10^4	Arai et al.[123]

translating the success of droplet transfection from microbial cells to mammalian cells has proven to be challenging. **Table 1-1** documents 9 publications attempting to achieve transfection of mammalian cells in microfluidic droplets. It can be seen that only two platforms have been validated with primary human cells. Additionally, the majority (5 out of 9) of these techniques rely on chemically mediated transfection and the majority (5 out of 9) are only for single-cell transfection. Both approaches will be limited in their ability to serve as a platform for cell therapy R&D. Chemical techniques such as Lipid Nanoparticle delivery are capable of efficient delivery to primary human T cells,[124] however the complex fabrication of Lipid Nanoparticles would make it challenging to generate and test different conditions at scale. Single-cell approaches will be limited for cell therapy R&D because typical in vitro killing assays require at least 10^2 cells and usually 10^3 – 10^4 cells to appropriately assess target cell killing at a range cell ratios.[125] The only

technique seen in **Table 1-1** that is shown to be capable of transfecting small populations of cells and can seamlessly transition between payloads is EP, however both droplet-EP methods in **Table 1-1** were limited to immortalized cells and had poor efficiency and viability. To better understand these shortcomings, it is worth looking closer and how droplet-EP has been performed on both DMF and droplet in channel platforms.

1.4.2.2 Droplet Electroporation

Approaches for performing electroporation in microfluidic droplets for either mammalian or microbial cells fall broadly into two categories where electrodes can either be arranged co-planar,[113,120,126–128] or parallel.[121,129–131] Each of theses arrangements have an opposing set of pros and cons. In a co-planar arrangement both the anode and cathode are located on the same plane either on top, or beneath the droplet (**Figure 1-4a**). Once the droplet is situated on the electrodes

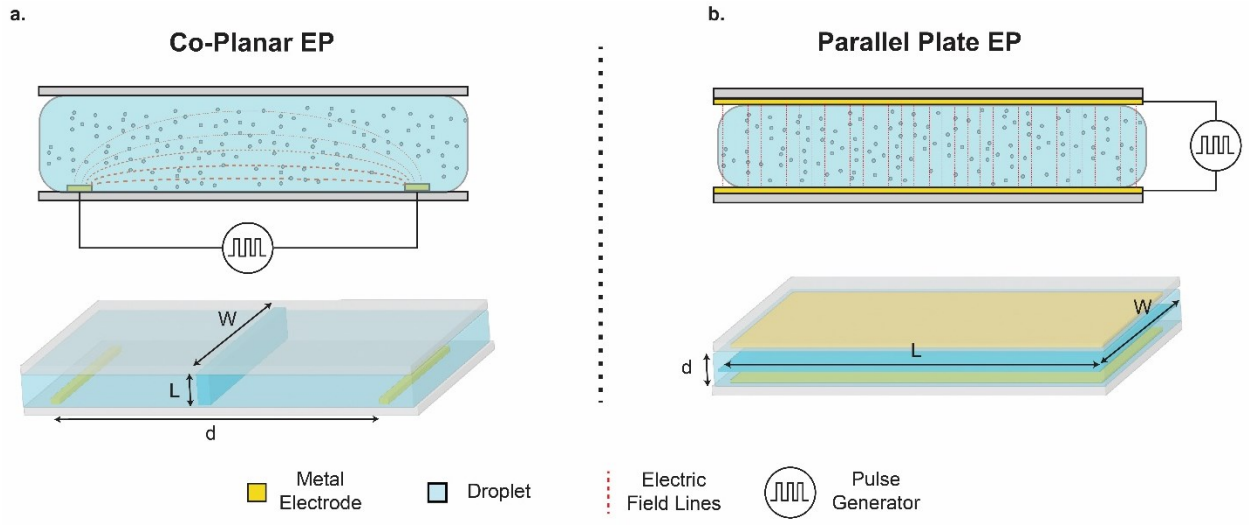

*Figure 1-4: **Existing configurations for droplet-based electroporation.** a) coplanar and b) parallel electrode configurations. Red dashed lines indicate electric field with line thickness standing in for intensity.*

a pulse is applied and an electric field is generated throughout the droplet. An advantage of this droplet EP format is that the electric field crosses horizontally across the droplet in a fashion that minimizes the cross-sectional area between the electrodes. Referencing **Equation 1-9**, this is an optimal way to minimize the generation of electrical current during pulsing which will reduce joule heating and minimize the severity of electrolysis. However, the disadvantage is that the electric field generated in this format is highly heterogenous. Since the distance between the electrodes varies depending on position within the droplet, the generated electric field will be strongest in the regions closest to the plane where the electrodes sit and weakest further away. This means that

cells at the bottom of the droplet would receive a lethal electric field and die, cells at the top would receive an insufficient electric field and not have pores generated, and only cells in a 'goldilocks' zone would both live, and have pores generated in their membranes. A parallel configuration consists of one electrode at the top and another at the bottom sandwiching the droplet (**Figure 1-4b**). This arrangement has an opposite set of advantages and disadvantages to a coplanar system. The entire droplet will experience a mostly homogenous electric field, however, since droplets are often much wider than they are tall (forming something more similar to a disk than a sphere), parallel electrodes maximize the cross-sectional area and minimize the distance between electrodes. This will minimize system resistance and increase pulse current during EP leading to more joule heating and exacerbating electrolysis. Additionally, the parallel configuration forces cells into close proximity with electrodes where pH change as a result of electrolysis is most severe.[98]

1.5 Outlook

In this thesis we aim to address key issues in the field of droplet-based transfection of mammalian cells. Given the historical emphasis on viral transduction as a vector for cell engineering, we first develop a platform capable of both the generation of viral particles as well as transduction on a DMF platform. This system, referred to as LENGEN, automates and miniaturizes the laborious process of viral transduction. In the future, we believe this platform will allow for large scale testing of viral particles allowing clinicians to experiment with a range of viral particles while optimizing dosage. Subsequently, we look to the future of cell engineering techniques by developing a non-viral payload delivery mechanism. To do this, we show for the first time a DMF-based droplet EP system that combines the benefits of a co-planar electrode configuration with the benefits of a parallel configuration while avoiding the pitfalls of each. Our novel method is able to generate a homogenous electric field, while producing minimal electric currents and protecting cells from heating and electrolysis. We characterize this system with both immortalized and primary human cells. Further, we compare our novel system against state-of-the-art commercially available EP methods demonstrating our novel platform requires significantly less cells and payload for successful transfection presenting an opportunity for cost saving during cell engineering. More importantly, we also show that cells engineered with our platform have

improved functionality after EP which leads to better viability and proliferation, and better performance in immunotherapeutic assays.

Chapter 2. Viral Generation, Packaging, and Transduction on a Digital Microfluidic Platform

This chapter is taken from a co-author research article reporting a novel microfluidic device that automates the viral transduction of mammalian cells. This chapter is adapted from the following publication: Viral Generation, Packaging, and Transduction on a Digital Microfluidic Platform. Angela B.V. Quach, Samuel R. Little, and Steve C.C. Shih. (2022) Analytical Chemistry 94(9): 4039–47

Abstract

Viral-based systems are a popular delivery method for introducing exogenous genetic material into mammalian cells. Unfortunately, the preparation of lentiviruses containing the machinery to edit the cells is labour-intensive, with steps requiring optimization and sensitive handling. To mitigate these challenges, we introduce the first microfluidic method that integrates lentiviral generation, packaging, and transduction. The new method allows production of viral titers between 10^6-10^7 (similar to macroscale production) and high transduction efficiency for hard-to-transfect cell lines. We extend the technique for gene-editing applications and show how this technique can be used to knockout and knockdown estrogen receptor gene – a gene prominently responsible for 70% of breast cancer cases. This new technique is automated with multiplexing capabilities, which have the potential to standardize the methods for viral-based genome engineering.

2.1 Introduction

Virus-mediated gene-editing is a widely used technique in which short-hairpin RNAs (shRNA)[132] or single-guide RNAs (sgRNA)[133] are packaged within viral particles and are delivered into the target cells. To prepare virus particles, co-transfection of three plasmids into a packaging cell line (e.g., HEK293T) are required to allow for efficient production of viral particles that are released into the cell's supernatant. The viral particles (whether adeno- or lenti-viral) can be harvested, purified, and titrated in preparation for infection. Using a viral mediated approach leads to applications including editing cells for the treatment of genetic diseases[134,135] and in achieving

highly specific immunotherapies[136–138], since viral delivery can integrate our gene of interest efficiently into the cells to create new designer antibodies or to gene-correct genetic deficiencies.

The most common method for preparing and producing viral vectors is to first seed a "packaging" cell line[139] in the presence of a nutrient-filled medium to form a monolayer culture. This is followed by preparing a co-transfection mixture (containing the packaging, envelope, and transfer plasmids) which is then added to the cells. This process requires that the reagent be added in a gentle drop-wise manner such that there is no immediate change to the pH of the medium, allowing for the cells to maintain good health and to efficiently uptake the plasmids for production. The supernatant is harvested and pooled with several rounds of centrifugation and purification to improve vector potency and purity making the overall process of preparing viral vectors tedious.[140] Once harvested, titration of viral vectors must be performed to determine the concentration of the viral titers where different methods can be selected for measurement.[141] Aside from production, optimizing vector transduction to boost efficiency is another bottleneck – which depends on lengthy trial-and-error procedures to find the optimal viral parameters (i.e. viral concentrations, multiplicity of infection (MOI), transduction times) to achieve high efficiency. Working with standard transduction systems[142,143] requires for large vector quantities which calls for large working volumes (> 100 μL) with much of the viral titer being wasted.

The challenges described above has driven much interest in miniaturizing lentiviral processes, especially transduction using a microfluidic device.[144–147] These approaches have shown to reduce volumes for transduction, to enable faster transduction rates, and to overcome limitations that hinder efficient gene transfer. Owing to the increased surface area to volume ratio at the miniaturized scale, these studies has shown fast lentiviral gene transfer kinetics and high transduction efficiency at lower volumes (~1-15 μL).[148] Thus, using microfluidics can be an enabling platform for lentiviral transduction. While these represent important steps forward, the methods do not integrate other important steps that are related to lentiviral transduction - generation and packaging – because they are limited in the complexities of cell cultivation of a packaging cell line, co-transfection of the plasmids, media and reagent exchange, and harvesting and purification the viral particles for direct on-device functional titration. To address the challenges described above, we introduce a technique for expediting LENtiviral GENeration, packaging, production and transduction (called LENGEN) on a digital-based microfluidic

platform (DMF). There are many advantages in using DMF for automating such a process[34], such as the ability to program all droplet operations and the ability to address each droplet individually. DMF is compatible for cell culturing, in which cells can be cultured in droplets[52], on protein spots[53] or on fabricated hydrophilic spots[54,55,149–151], enabling automating processes like gene-editing which requires culturing cells over weeks. Finally, because the two-plate DMF system has a removable top substrate, cells cultured on this platform can be easily removed by trypsinization and transferred to another platform (e.g., well-plate) for validation (RT-PCR, sequencing) and expansion.

Here, we describe a "proof-of-principle" method for viral generation, packaging and transduction by DMF to perform automated site-specific gene editing and silencing. We demonstrate that our LENGEN device is effective for packaging lentiviral vectors up to 15 kb in size and producing lentiviral titers comparable to the gold-standard techniques. Furthermore, to extend the technique to be useful for gene editing/silencing, we integrated the transduction process on the same device to directly target the estrogen receptor in breast cancer cells using the produced lentiviral particles and performed validation/expansion of the edited cells. Using our platform, we reduce the time to package, produce, and transduce target cells, to analyze their edits with virus and cell savings while achieving the same results as in the macroscale, and reduce manual intervention (i.e., pipetting steps, purification and filtering, transferring of precious cells). To our knowledge, this report is the first to describe a microfluidic technique that allow for lentiviral packaging, production, and transduction and we propose that the new techniques will be of value for automating procedures related to genome engineering applications.

2.2 Methodology

2.2.1 Cell Culture

Before seeding cells onto DMF devices, all cell types (H1299, HEK293T, MCF-7, MDA-MB-231, and T47D-KBLuc) used in this study were grown in 100 mm petri dishes and were washed with PBS buffer, trypsinized with 0.25% trypsin-EDTA and re-suspended in complete medium (with 10% heat-inactivated FBS). After centrifugation, the cell pellet was re-suspended in complete medium, and cells were counted such that dilutions made would reach the required cell density.

Aliquots of the cell suspension at densities (from ~1.0 x 10^6 to 2.5 x 10^6 cells/mL) were supplemented with 0.05% w/v Pluronics F-127.

For cell seeding of the target cells, we followed a similar protocol as described previously.[149] Briefly, 1.5 µL of the above cell suspension was pipetted onto the bottom plate at the edge of the top plate and loaded by applying driving potentials (400 V_{p-p}, 15 kHz) into the appropriate reservoirs. 1.5 µL droplets were formed by elongating the liquid from the reservoir and activating the potential on an active dispensing electrode. The dispensed droplets from the reservoirs were actuated across a hydrophilic site (on the top plate) generating 1.5 µL and 1 µL volumes for eventual viral production and transduction respectively. Excess liquid from the spot was actuated to a waste reservoir and removed with a KimWipe. Viral production steps were then done immediately after cell seeding.

2.2.2 Viral Production

HEK293T cells were seeded and cultured on the 1.6 mm diameter hydrophilic spot (following the cell culture protocol) at a suspension cell density of ~2.5 x 10^6 – 3.0 x 10^6 cells/mL. For viral production, we performed a reverse transfection protocol by first co-transfecting a mixture containing 0.75 µg of pMDLg/pRRE, 0.75 µg of pRSV-Rev, 1.5 µg of pMD2.g and 3 µg of the transfer vector pLv-mCherry with 12.5 µL of Lipofectamine 3000 and 12 µL of P3000 reagent for a total volume of 500 µL with Opti-MEM. After 20 min of incubation, 0.05% w/v of Pluronics F-127 were added to the mastermix to prepare for actuation on device. 1.5 µL of the Lipofectamine mastermix was actively dispensed and actuated towards the seeded HEK293T cells. The formulation (3 µL total volume) was mixed in a circular fashion at the lentivirus production region by actuating adjacent electrodes (highlighted in the red box in **Figure 2-1a**).

2.2.3 Optimization of Viral Titers and Transduction

HEK293T cells were seeded and cultured at the 'target cell' region at cell densities between 1-1.5 x 10^6 cells/mL following our cell culture protocol. After 24 h, four dilutions were generated containing the lentiviral particle-filled supernatant of the HEK293T cells at the production area. A dilution of 1:3 (DMEM and viral titers) was implemented by merging 1 µL of DMEM (10% heat-inactivated FBS, 8 µg/mL polybrene, 0.05% w/v Pluronics F-127; dispensed from the cell media reservoir) with 2 µL of the supernatant containing the viruses (**Figure 7-1a**). 1 µL of the

merged product was split and actuated to a 'target cell' region while the remainder (2 µL) was saved for other dilutions. This procedure was repeated three times to generate dilutions 1:6, 1:12, and 1:24. Two additional spots were used for controls where cells at the same density were cultured with complete medium with 8 µg/mL polybrene on the first spot and without polybrene on the second spot. The device was flipped upside down and incubated overnight. After 24 and 48 h incubation, the device was imaged using an Olympus IX73 inverted microscope (Olympus Canada, Mississauga, ON, Canada) containing excitation and emission filters with wavelengths 585 nm and 608 nm respectively for mCherry fluorescence. We counted the fluorescent cells and estimated the viral titer using Equation 1 (following Gill et al.):[152]

$$\frac{\#\ cells\ transduced\ \times\ \%fluorescent \times dilution\ factor}{transduction\ in\ volume}$$

$$= Transducing\ units\ per\ mL\ = (\frac{TU}{mL})$$

For CRISPR and shRNA optimization experiments, we followed the same procedures for cell culturing, viral production, and optimization of viral titers. The only changes to these procedures were the transfer plasmids were replaced with MISSION® shRNA plasmids (i.e. TRCN00000003300, non-target shRNA plasmid) and pLentiCRISPR-mCherry-NeoRv2 (LCMNv2) all-in-one Cas9 and sgRNA plasmids (**Figure 7-1**) for the shRNA and CRISPR experiments respectively.

2.2.4 Cell Transfer

The next day, the transduced target cells were retrieved, pooled together with their corresponding dilutions 24 hours post-transduction. For example, 2 microwells that were subjected to the first serial dilution were pooled, 2 microwells that were subjected to the second serial dilution were pooled. The device was brought to a biological safety cabinet where the top-plate was taken apart from the bottom plate. 5 µL of PBS was pipetted onto the microwells and aspirated using a pipette, leaving only adhered cells on the microwell. Cells were detached using 2 µL of trypsin-EDTA (0.25 % w/v) and the top-plate was placed back in the humidifying chamber, into the 37°C with 5 % CO2 incubator for 2 min. Two microwells subjected to the same serial dilution from the same device were then pooled together by resuspending each microwell with 10 µL of complete medium

and were added to 100 µL of complete media in a 96-well plate. The next day, the cultured wells were refreshed with complete medium supplemented with 1 µg/mL of puromycin for RNAi experiments and no antibiotics for CRISPR experiments. After seven days post-transduction, the cell lysate was collected for qRT-PCR assays or gene cleavage detection assays to verify gene knockouts.

2.3 Results and Discussion

2.3.1 Lentiviral Generation (LENGEN): Digital Microfluidics for Viral Production and Transduction

Figure 2-1a is a device to automate the production and the transduction of viral-derived vectors. Several design iterations were required to develop a device that is capable of producing and transducing virus particles. Two challenges were encountered in the process, including (1) generating the highest lentiviral titers that will enable efficient transduction and (2) to perform a 12-plex viral transduction analysis on-chip. These challenges called for several innovations with the device design. First, to package and to produce lentiviruses, a host is required (e.g., HEK293T cells) that is easily transfected and supports high-level of expression of the viral proteins to allow for efficient production of lentiviral titers. To enable such a process, we fabricated hydrophilic sites that are patterned on the device top-plate to serve as sites for cell seeding and proliferation. These hydrophilic sites enable a procedure known as "passive dispensing" where a droplet is actuated across the site, and a small volume (~1.5 µL) of the droplet adheres to the site, seeding it with media and cells. Although cells have been cultured on hydrophilic spots previously,[54,55,149–151] this is the first time that is being used for continuous cultures to generate, to produce and to deliver lentiviral particles. In initial experiments, we used a previous device design that cultured cells on ~1.2 mm diameter hydrophilic sites that enabled lipofection-mediated transfection with high efficiency.[149] However, using this device we observed: (1) the production of the lentiviral titers generated very low or near 0% transduction efficiency and (2) the electrode configuration made it difficult to mix droplets containing the DNA and lipids resulting in uneven distribution of viral particles when harvesting the virus from the generation site. We hypothesize the low transduction efficiency is due to the low viral titers being generated from the low cell density (~ 700 cells). Therefore, we created a larger cell culture site (~1.6 mm dia.) that houses ~ 2 500 cells

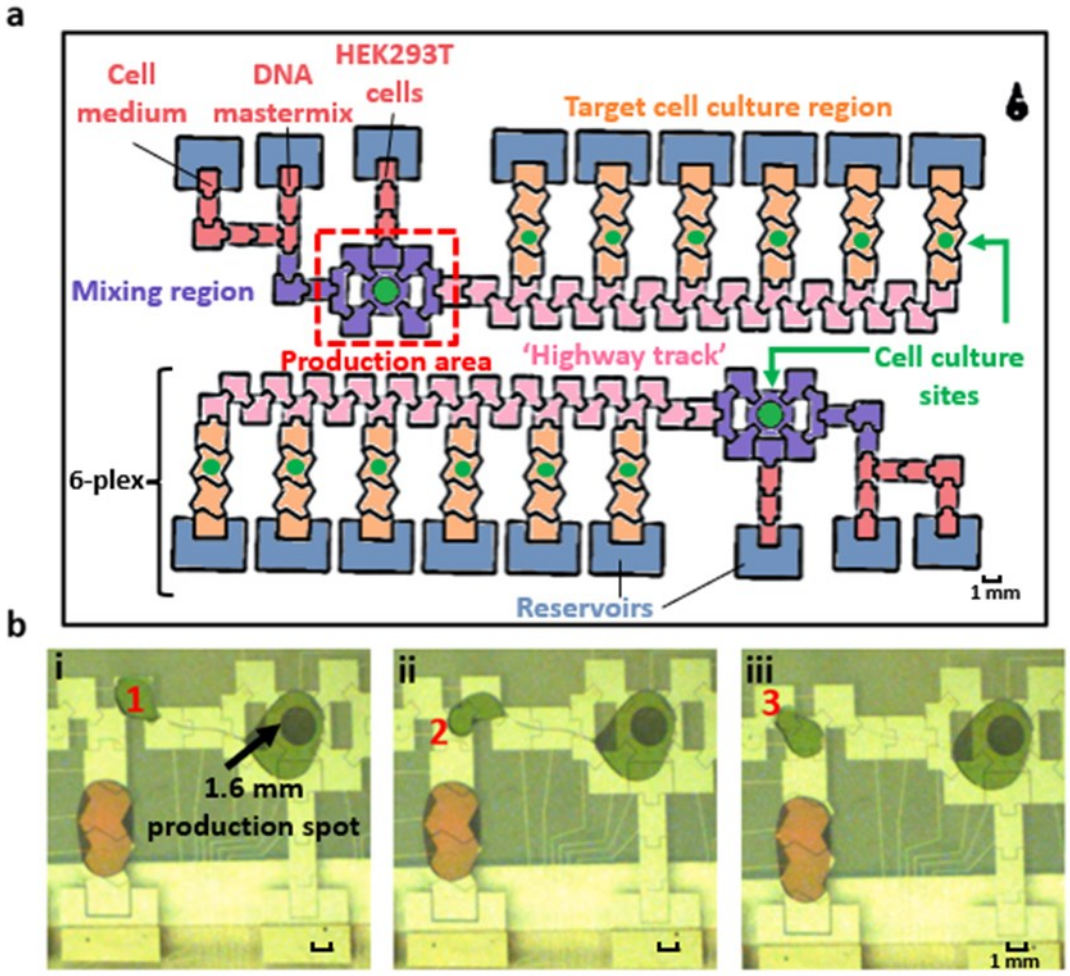

Figure 2-1: ***LENtiviral GENeration, packaging, transduction, and analysis (LENGEN) on a digital microfluidic platform.*** *(a) Top-view schematic representation of the LENGEN device. The bottom plate contains two sets of 79 electrodes each for lentiviral generation and packaging, cell culturing, transduction, and analysis. For each set, there is one patterned 1.6 mm dia. cell culture site for production and six ~1.2 mm dia. site for transduction and analysis. The production area houses a 3 μL droplet which is split into unit droplets (~ 1 μL) that covers the area of an electrode and actuated to the cell culturing sites. Two sets of electrodes enable replicates or different conditions to be performed in parallel. (b) Frames from a movie depicting (i) the droplet resting on electrode 1, (ii) droplet moves to electrode 2 when it is activated and (iii) droplet shows uni-directional movement onto electrode 3 (and not electrode 1) when electrodes 1 and 3 are bussed. The "highway track" of electrodes is used to enable delivery of the lentiviral particles to the cells with minimal electrode connections and to provide multiplexing capabilities on digital microfluidic devices. Droplets in the frames consisted of water, 0.05% Pluronics F-127 and food dye.*

at the optimal 50-70% confluency. Although increasing the cell culture site can generate more viral titers and increase transduction efficiency, droplet movement away from the hydrophilic culture site can be challenging.[150] This is especially problematic if we are to generate a dilution series which requires droplet movement away from the generation/packaging site and then mix/merge with dilution buffer. Hence, with a larger diameter (1.6 mm) a balance is struck between the lentiviral generation and the droplet movement forces to ensure we can generate dilutions, obtain high transduction efficiency, and continue to maintain reliable droplet movement.

In addition, we created a four-prong electrode system (highlighted as the 'production area') that is directed towards the hydrophilic site. The latter innovation was particularly important for reliable droplet mixing and splitting since the droplet is continuously circulated around the four-prong electrode to facilitate uniform mixing and is easily extended to facilitate "necking" during droplet splitting. To fulfill the 12-plex capabilities, the device design contains a 'highway track' to enable one-directional movement towards the cell-culturing site, and the delivery of the lentiviral particles to 6 target sites. Generally, square or inter-digitated electrodes are used to facilitate the droplet operations on a digital microfluidic device,[149,153,154] however, these types of electrodes require complicated wiring schemes that can be difficult to design as we increase the electrode density (unless you use multi-layer fabrication techniques)[33]. Instead, we modified the electrode design such that the droplet only moves towards the overlapping "prong"-electrodes (**Figure 2-1b**). Using such a design allows the electrodes to be bussed through a minimal two connections – i.e., on our device design we connected 22 electrodes using only 2 wired connections (instead of 22 wired connections) – saving time on design. Moreover, the reduction in connections enabled us to incorporate a symmetrical design on the device to allow 12 transduction assays to be conducted simultaneously – replicating the 6-plex design on the same substrate. We anticipate that future designs can use such electrode designs to overcome multiplexing challenges that is commonly associated with digital microfluidics.

With this configuration, a five-step procedure was developed to facilitate the automated generation, packaging, and delivery of the virus system. The schematic shows the events at the genetic level with an image-based representation of the droplet movements on the device. As shown in **Figure 7-2**, in step (i), the producer cells (HEK293T) are in a droplet suspension and actuated to the production area by loading and dispensing from reservoirs. In step (ii), a unit droplet of liposomes and viral DNA plasmids (pMDLg/pRRE, pRev, pMD2.G and transfer plasmid (**Figure 7-3**) are dispensed and merged and are thoroughly mixed using a 4-electrode linear array (~ 1 for mixing). The lipofectamine mixture was incubated at room temperature for ~15- 20 minutes for the DNA-liposomal complexes to be formed. In step (iii-iv), the lipofectamine mixture was actuated to the HEK293T cells and actively mixed for 1 min via three continuous circulations in the production area containing 8 electrodes to replicate the reverse transfection procedure on device (i.e., adding transfection mixture to unseeded cells). Finally, in step (v), after 24 h, the lentiviral particles were produced in the supernatant (cells are adhered to the hydrophilic spot) and

specific dilutions (1:3, 1:6, 1:12, and 1:24) are formed via electrode actuation (with ~98 % accuracy)[154] to infect target cells following the step-by-step procedure shown in in the **Figure 7-1a**. This five-step procedure can be performed in ~ 5 minutes and is the first (to our knowledge) that is capable of automating the procedures of preparation, production, and transduction with viral-derived vectors at a faster rate than the macroscale techniques.[144]

Breast cancer cell lines (MCF-7 and T47DKB-Luc) were chosen as models for our lentiviral study to show that our automated platform can genetically modify oncogenes and use this method to potentially find therapeutic targets against these genes.[155] For all results described here, a droplet comprised of the breast cancer cells (at various cell densities) were loaded into the reservoirs. These droplets were dispensed into smaller volumes and actuated towards the cell culturing sites using passive dispensing techniques (as described above). Two parameters were evaluated: cell viability and transduction efficiency. As described in the Supporting Information (**Figure 7-4**), both cell lines were viable on the device and showed comparable viability when cultured in well-plates. We also evaluated the cell viability after 48 and 72 h (since the gene knockouts after lentiviral transduction occurs within this timeframe)[156,157] and we observed an average viability of 83.7 and 85.7 % for MCF-7 and 98.4 and 88.6 % for T47DKB-Luc on the device respectively. **Figure 7-5a** shows representative fluorescently labeled images of the MCF-7 and T47DKB-Luc cells, and as shown, the cells are proliferative, and the morphologies of the cultured breast cancer cells were similar to the cells cultured in well-plates (**Figure 7-4c-d**). An additional assay was developed to determine if transduction can be performed (after generation and packaging) on device, and as shown in **Figure 7-5b**, the efficiency is ~43.0 % after 48 h post-transduction and improves to ~60.1% after 96 h post-transduction for T47DKB-Luc cells. These efficiencies are also a significant improvement from lipid-based transfection (see **Figure 7-6**), which is a trend usually observed for hard-to-transfect cell lines like T47DKB-Luc.[158]

From literature, a critical factor to determine successful lentiviral transduction is the functional titer, which is the transduction unit of virus capable of infecting cells and expressing the transgene.[159,160] Hence, we performed four serial dilutions of the lentiviral particles containing a non-targeting plasmid mCherry to determine the optimal concentration of functional lentiviral obtained in HEK293T cells. A number of mCherry transduced cells were counted (using imaging

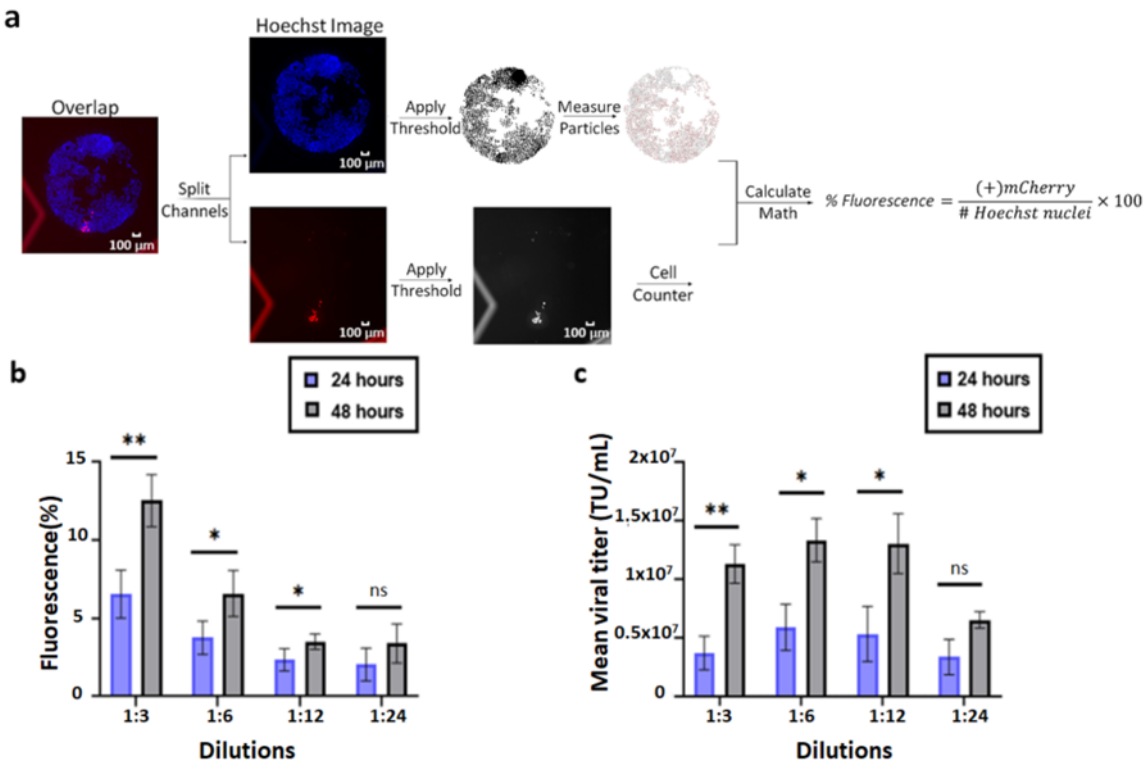

Figure 2-2: ***Optimizing lentiviral production.*** *Schematic (a) showing the imaging pipeline used to measure the fluorescence of mCherry positive cells. Plots are showing the (b) fluorescence efficiency and (c) mean viral titer as a function of supernatant dilutions (1:3, 1:6, 1:12, and 1:24) for positive mCherry HEK293T cells after 24 and 48 h lentiviral production and transduction. For (a), the schematic is showing the workflow to calculate the % fluorescence (of mCherry) after viral transduction. Mean viral titer can then be calculated using Equation 1. For (b), positive mCherry cells were counted and divided by non-transduced mCherry cells. For (c), the estimated mean viral titer amount was calculated by multiplying the number of cells transduced with the percentage of fluorescence, dilution factor, and dividing the total by the volume of lentiviral particles used for transduction (i.e., transducing units (TU) per milliliter). A student's t-test ($P < 0.05$) was used to evaluate the significance (* for a $P \leq 0.05$, ** for a $P \leq 0.01$ and ns for $P > 0.05$) between the dilutions. Error bars for both plots represent ± 1 S.D. with N = triplicates.*

techniques - see **Figure 2-2a**) on the hydrophilic spot after 24 h and 48 h (**Figure 2-2b**). As shown, the most optimal concentration of lentiviral particles was observed after 48 h transduction - achieving a range 6.5 x 10^6 to 1.33 x 10^7 TU/mL with the 1:3 dilution. These values were also translated to a viral titer (using Equation 1 from the Experimental Section) and on-device, we are able to obtain a functional titer of ~ 1 x 10^7 TU/mL after 24 or 48 h respectively (**Figure 2-2c**) - values very similar to titers obtained from benchtop methods.[161,162] Furthermore, we calculated the amount of transducing units generated per cell on the device and compared to the macroscale techniques. On average, we produced 1.56 TU/cell and 2.65 TU/cell on device after 24 and 48 h respectively, which is very similar to the benchtop after five days of harvesting (~2.80 TU/cell) (**Table 2-1**; see **Figure 7-7** for sample calculations). The fast production of titers and droplet manipulations (and larger surface area to volume ratio) enables the drastic time reduction (up to 2

Table 2-1: Comparison of lentiviral production on LENGEN vs macroscale per cell

Microscale (24 hours)		Microscale (48 hours)		Macroscale (5 days)	
Dilutions	TU/cell	Dilutions	TU/cell	Dilution	TU/cell
1:03	1.23	1:03	3.55	3:10	2.81
1:06	1.92	1:06	2.60	2:10	2.73
1:12	1.77	1:12	2.30	1:10	1.95
1:24	1.33	1:24	2.13	0.5:10	3.73
Average	1.56	Average	2.65	Average	2.80

weeks,[157,163] to ~ 2 days) in packaging, producing, and transducing on device. In practice, it was decided that 24 h post-transduction step was sufficient for the gene silencing and editing assays given the titers generated at 24 h are sufficient for observing knockdown and knockout events (see below).

Other factors that affect the transduction efficiency are the size of the lentiviral payload[164,165] and cell-type.[166] Since shRNA and CRISPR vectors are usually ~ 7.0 - 15.0 kb in size (compared to smaller ~ 4 kb plasmids containing fluorescent reporter mCherry), we used the system above to evaluate the effects of the lentiviral payload of ~15.0 kb (using LCMNv2 – see **Figure 7-3**) in hard-to-transfect cell lines like H1299 and T47DKb-Luc. As shown in supplementary **Figure 7-8a**, we obtained the highest efficiency for the 1:3 dilution which correspond to ~ 10.8 % of H1299 cells that show mCherry fluorescence. Comparatively to H1299, T47DKb-Luc shows higher transduction efficiency with the 1:6 dilution at ~5 % (**Figure 7-8b**) which is expected given that different cell lines have different affinity for virus uptake.[167,168] It is generally observed that larger lentiviral payloads will lead to lower transduction efficiency,[169] but there is no clear mechanism to predict which cell line will transduce more efficiently.[170] However, the results do suggest that for a particular cell type there should be focus on optimizing MOIs or lentiviral dilutions and post-infection incubation times to obtain effective transduction. In the future, it may be important to further to study different strategies[171,172] for effective transduction of lentiviral particles especially if the application calls for a wide variety of cell types (immortalized, primary, stem, etc.).

2.3.2 LENGEN for Lentiviral Knockdown and Knockout Assays

To evaluate the potential of our system for knockdown and knockout assays, we packaged shRNA and CRISPR plasmids that will target the estrogen receptor alpha (ESR1) in breast cancer

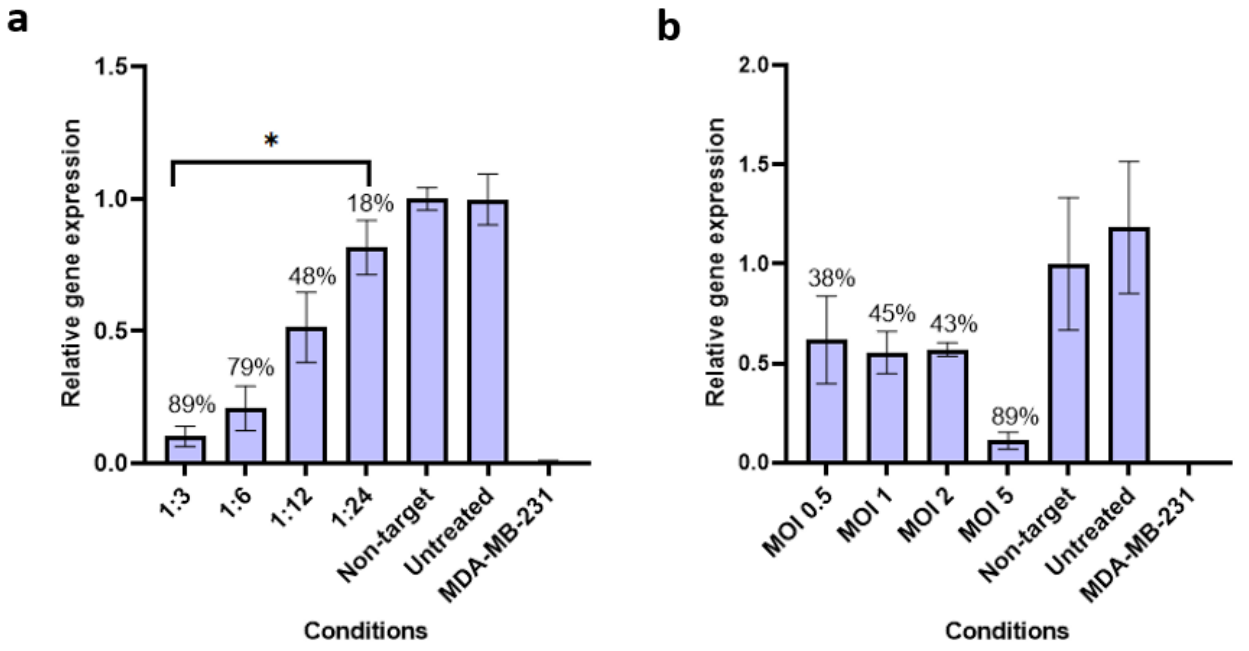

Figure 2-3: ***shRNA knockdown assays for ESR1.*** *Evaluating the relative gene expression of Estrogen Receptor 1 (ESR1) in MCF-7 cells that were performed in (a) LENGEN device and (b) well-plates. We generated, packaged lentiviral particles containing shRNAs targeting ESR1 and transduced them in MCF-7 cells. shRNA-mediated silencing of ESR1 was assessed using a ΔΔCq method to determine relative gene expression from qRT-PCR data with ACTB (β-actin) as an endogenous reference gene. The cells exhibited MOI-dependent viral delivery of shRNA#1 targeting ESR1 knockdown, with mRNA reduction by 38%, 45%, 43% and 89% when cells were treated with MOI of 0.5, 1, 2 and 5 respectively. In the case with LENGEN, the cells exhibited dilution-dependent viral delivery of shRNA#1 targeting ESR1 knockdown, with mRNA reduction by 89%, 79%, 48% and 18% when cells were treated with dilutions 1:3, 1:6, 1:12 and 1:24 respectively. Significance between dilutions 1:3 and 1:24 is significant (shown as * for P ≤ 0.05). Comparison of non-targeting shRNA to untreated samples shows no significant effect on gene expression. A negative control depicts ESR1's relative downregulated (almost zero expression levels) expression in MDA-MB-231 cells. Error bars for both plots represent ± 1 S.D. with N = triplicates.*

cells using our LENGEN system and then isolating single clones for expansion. ESR1 controls a wide range of physiological and regulatory processes in the development of the female reproductive system and is expressed in approximately 70% of breast cancer tumors.[173] Thus, there is much interest to systematically investigate genes whose loss affects cell growth or increases the estrogen-independent growth of ER+ breast cancer cells.[174] In this part of the work, we applied our system to automate the process of generating, packaging, and transducing the lentiviral particles containing the ESR1 target and examining the knockdown (shRNA) or knockout (CRISPR-Cas9) of the target gene.

To test the effectiveness of our method for gene expression analysis, RNAi assays were performed on the LENGEN device. The transfer plasmid targeting the ESR1 are packaged and produced using HEK293T cells and the supernatant are diluted to different viral concentrations using DMF actuation (1:3, 1:6, 1:12, 1:24; see **Figure 7-1a**) which are used to transduce MCF-7

cells. Expression values from LENGEN protocols were obtained by qRT-PCR methods by removing the top-plate containing the transduced cells from the DMF device (via trypsinization) and transferring 'pooled' cells (~ 2800 cells) to well-plates for analysis after outgrowth for seven days. For higher dilution (1:24) and lower dilution concentrations (1:3), the relative reduction in gene knockdown is 18 ± 8.8 and 89 ± 37.6 % respectively (**Figure 2-3a**) and are very similar to the observed in lentiviral well-plate conditions (**Figure 2-3b**). The gene expression percentages for both LENGEN and standard conditions were confirmed by a ΔΔCq method[175] (values obtained from **Figure 7-9** - qPCR amplification curves) which show that the LENGEN method is capable of gene silencing using viral delivery.

The knockout assay was motivated by the wide-spread interest in using CRISPR for identifying essential genes related to cancer and other diseases.[176–178] Similar to the RNAi assays, MCF-7 cells were seeded, grown, and transduced by a dilution series (generated on-chip) of lentiviruses containing an all-in-one plasmid with the Cas9 gene cassette and a sgRNA guide targeting ESR1. As shown in **Figure 2-4a**, the trend is very similar to what is observed with the RNAi experiments – i.e., at 1:3 dilution, we observed more cells being transduced - and this trend was identical to that observed in standard conditions (**Figure 2-4b**) and in literature.[179] To verify the knockout, we performed downstream analysis by removing the MCF-7 cells (~ 2800 cells) from the device and culturing them in well-plates in preparation for a genomic cleavage assay (**Figure 2-4c**). The band patterns and their cleavage percentages are similar to what is observed in the genomic cleavage gel from MCF-7 cells transduced (and lentiviral generation and packaging) in well-plates at different MOIs (**Figure 2-4d**). Since genome editing efficiency varies with different cell lines,[180] we implemented the gene-editing workflow[61] on H1299 cells and similarly observed successful knockout of integrated eGFP (gene cleavage efficiency of 16.1 %) (**Figure 7-10**). Although downstream gene editing analysis of CRISPR knockouts from microfluidic devices have been shown previously,[118,181–183] this is the first demonstration showing integration of lentiviral packaging, generation, and transduction on a microfluidic device followed by downstream gene editing analysis (single clone isolation and expansion).

As depicted in **Figure 2-1**, this "proof-of-principle" method was carried out in a 12-plex format (through the use of "highway tracks") and we propose that this will be straightforward to expand this technique to much higher levels of multiplexing given the electrode and bussing

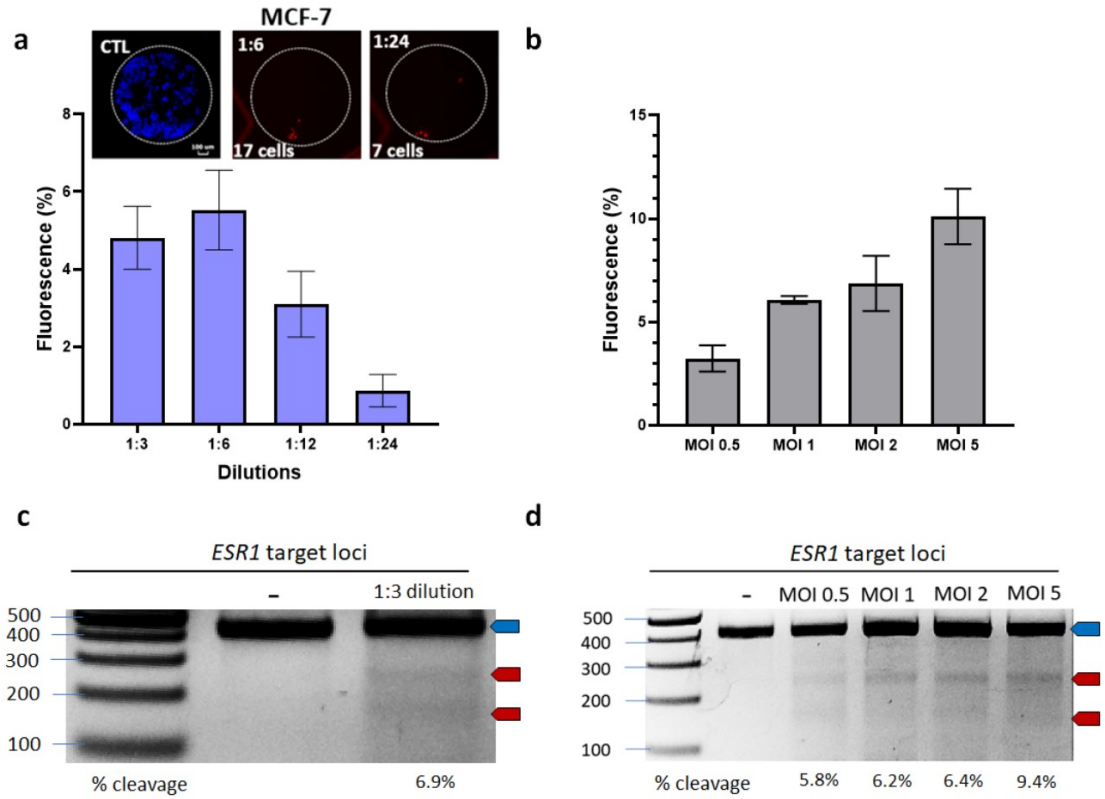

Figure 2-4: ***Knockout assays for ESR1.*** *Evaluating the knockout efficiency of ESR1 in MCF-7 cells performed in well-plates and on LENGEN. Lentiviral particles containing all-in-one Cas9/sgRNA targeting ESR1 were generated, packaged, and transduced using (a) LENGEN or (b) well-plate protocols. Plots of mCherry fluorescence (% of positive cells) were measured at (a) different dilutions (1:3, 1:6, 1:12, 1:24) and (b) different MOIs (0.5, 1, 2 and 5) by staining wild-type MCF-7 cells with Hoechst 33342 and compared to transduced (+)mCherry cells. (c-d) Each transduction was verified by a genomic cleavage assay after seven days post-transduction. The parental band is 409 bp (shown by the blue arrow arrow) and the cleavage bands are 235 bp and 174 bp (shown by red arrows). Following LENGEN protocols, cells were removed from the top-plate, transferred to a well-plate, and the 1:3 transduced cells were pooled together to perform the genomic cleavage assay. Error bars for both plots represent ± 1 S.D. with N = triplicates.*

techniques presented here (and particularly with recent reports of active matrix methods)[33,39]. Using our system for lentiviral packaging, production, and transduction, we obtained very similar gene expression profiles (via RNAi and CRISPR techniques) compared to benchtop assays, with shorter timescales to obtain viral titers at sufficient levels (days vs. weeks), 100-fold savings in volumes to save precious lentiviral samples, and minimal number of cells (~ 1000-3000 cells). In addition, in the macroscale, generating very concentrated amounts of viral titer requires several days of lentiviral harvests within large batches of culture and rounds of ultracentrifugation - a process that is not required with LENGEN techniques. Although this device generates a low number of transduced cells (i.e., ~1400 cells per target spot), we believe a future generation of this platform will allow for more transduced cells via 'pooling' of target cells by increasing the target spot area or increasing the droplet volumes in the production area to mL range. Therefore, our

current platform is aimed to reduce the time for lentiviral packaging, production and transduction of target cells, which has substantially decreased from generally two weeks[158,163] to two days (**Figure 7-12**) , and to eliminate the tedium needed for packaging and producing (and transducing) lentiviruses.

Chapter 3. A Tri-Droplet Liquid Structure for Highly Efficient Intracellular Delivery in Primary Mammalian Cells Using Digital Microfluidics

This chapter is a taken from a first author research article documenting a novel approach for miniaturized electroporation of both primary and immortalized human cells on a digital microfluidic platform. This chapter is adapted from the following publication: Samuel R. Little, Ziuwin Leung, Angela B. V Quach, Alison Hirukawa, Fatemeh Gholizadeh, Mehri Hajiaghayi, Peter J. Darlington, and Steve C. C. Shih. 2023. "A Tri-Droplet Liquid Structure for Highly Efficient Intracellular Delivery in Primary Mammalian Cells Using Digital Microfluidics." Advanced Materials Technologies, 2023, 2300719: doi: 10.1002/admt.202300719.

Abstract

Automated techniques for mammalian cell engineering are needed to examine a wide range of unique genetic perturbations especially when working with precious patient samples. We introduce an automated and miniaturized technique making use of digital microfluidics to electroporate a minimal number of mammalian cells (~40,000) at a time on a scalable platform. Our system functions by merging three droplets into a continuous droplet chain, which we call triDrop. In the triDrop configuration, the outer droplets are comprised of high conductive liquid while an inner or middle droplet is comprised of low conductivity liquid that contains the cells and biological payloads. In this work, we show that applying a voltage to the outer droplets generated an effective electric field throughout the tri-droplet structure allowing for insertion of the biological payload into the cells without sacrificing long term cell health. We show this technique for a range of biological payloads including plasmids, mRNA, and fully formed proteins being inserted into adherent and suspension cells which include primary T-cells. The unique features of flexibility and versatility of triDrop shows that our platform can be used for the automation of multiplexed gene edits with benefits of low reagent consumption and minimal cell numbers.

3.1 Introduction

Recent advances in ex-vivo cell engineering has led to new frontiers for cellular therapies.[184–186] Adding biological payloads (DNA, RNA, or protein) into a cell can supply these cells with a customized function. Specifically, in the field of immunotherapy, removing immune cells from the human body, engineering the cells, and injecting them into a patient has shown to be a robust treatment regimen for a wide range of ailments including both hematological[5,187] and solid[6,188] forms of cancer, infection,[189] and autoimmunity[190]. To further advance the field of cellular therapy, and more specifically the field of immunotherapy, researchers need the capability to assess large arrays of genetic perturbations, allowing them to cycle through design iterations in rapid succession. To integrate any of these functions, biological payloads must be inserted into the cells, and this generally relies on three mechanisms: biological[191] (viral transduction), chemical[84] (cationic polymer, calcium phosphate, cationic lipid, or cationic amino acid), and physical[89] (electroporation, mechanoporation, sonoporation, hydrodynamic-poration, or microinjection). Concerns over immunogenicity, semi-random transgene integration, and cytotoxicity have resulted in viral transduction becoming less popular, while low transfection efficiencies have led to decreased enthusiasm for chemical techniques.[82] Physical transfection techniques are still the preferred approach as they generate temporary nanopores in the cell membrane allowing the cargo suspended in the surrounding media to permeate the cell where it remains trapped after the pores heal.[89]

In the last two decades, microfluidics has emerged as a leading contender for automating mammalian cell transfection[105] with several techniques excelling at the transfection of immortalized cell lines and primary T cells.[94,106,193,194,107,108,110–112,116,182,192] Most of these methods have relied on channel microfluidic devices for clinical manufacturing applications that require processing of large numbers of cells (> millions). However, these devices are limited in their ability to easily control unique transfection parameters in parallel or to perform transfection at smaller cell quantities which is useful for research and development. For instance, Bloemberg et al.[195] detailed the development of 15 unique chimeric antigen receptors (CARs) targeting a solid tumour specific antigen (EGFRvIII) constructed using a rapid modular cloning strategy. After screening and testing in Jurkats, five high performing variants were selected for insertion via viral transduction into primary T cells. To test their entire library using primary T cells, optimized

electroporation protocols[196] would require upwards of 30 million cells which can be difficult to obtain from a single donor without lengthy ex vivo expansion protocols. To facilitate rapid screening of large libraries, such as the one developed by Bloemberg et al., and to reduce the time needed to culture and grow cells, an alternative approach is needed for effective delivery of target payloads with lower cell numbers and with the potential for parallelization and automation. Moreover, cell-based immunotherapies require inactivated primary T-cells[197] or natural killer cells or more rare immune cells such as tumor infiltrating leukocytes[198], or gamma-delta T cells[199] which are challenging to recover and to expand.[200] Optimized protocols for working with primary immune cells have shown that using fewer cells has a detrimental effect on viability and efficiency.[196,201]

Digital microfluidics (DMF) is a droplet-based technique that relies on the generation of electrostatic forces to actuate nL-μL droplets across a grid of electrodes via application of an electric potential.34 DMF has been used extensively for applications with mammalian cells,[52] and is also a promising platform for large scale parallelization with simple PCB-based designs capable of handling up to 50 samples in parallel[39] and more complex designs can handle 1000s of droplets at a time.[33] In recent years, DMF has been used to automate viral transfection[202] as well as lipid-based transfection[115] using mammalian cells, however, efforts to integrate physical transfection methods such as electroporation onto a DMF platform have been limited to only microbial cells.[130,131] Both of these systems resulted in >98% of all cells dying and only 2.3 %[130] or up to 9 %[131] of surviving cells being successfully transfected making the proposed designs not suitable for mammalian cells due to high cell death. The two major causes of cell death using previously shown DMF electroporator designs are excessive current generation during pulsing leading to joule heating,[96] and the effects of electrochemical reactions occurring at the metallic anode and cathode leading to a pH change in the media.[98] Several channel-based microfluidic systems have rectified these problems, reducing current by creating a high resistance electroporation environment,[97] and protecting cells from electrochemical species by isolating cells away from metallic electrodes.[112,203] To our knowledge, we are not aware of a robust method for implementing high efficiency, high viability physical transfection onto a DMF chip for mammalian cells.

In this work, we show for the first time a three-droplet assemblage for facilitating DMF electroporation, which we refer to as triDrop electroporation. The triDrop system consists of three droplets merged into a sequential chain, with the flanking droplets comprised of high conductivity media and the middle droplet comprised of low conductivity media containing cells and target payloads. Using this droplet arrangement, the platform enables superior electroporation results, compared to simpler single droplet arrangements, and we can achieve high electroporation efficiencies (> 95%) with high viabilities (> 95%) for a diverse range of easy-to-transfect cell types while delivering large cargo (2000 kDa FITC-tagged dextran molecules and mRNA) and complex biological cargo such as plasmids (~5 kb) and Cas9 ribonucleic proteins for genetic engineering applications. Next, we show that the triDrop system can be used for the electroporation of primary human T cells with minimal cell numbers, high efficiency (~90 %), high viability ratios 24-hours after transfection (~90 %) and with the ability to grow at rates comparable to non-electroporated samples for up to a week post-transfection. Finally, we show applications of CRISPR-Cas9 gene editing in primary human T cells by first showcasing the knockout of a well characterized gene with up to 80% efficiency, and an automated arrayed gene editing assay where we perform 10 unique editing conditions with two replicates (totalling 20 electroporation reactions) while using fewer than one million cells from a single donor. We propose that the triDrop represents an important tool in genetic engineering which can be easily implemented into current pipelines for engineering immune cells for the development of novel cellular immunotherapies**.**

3.2 Results and Discussion

3.2.1 triDrop Electroporation Using Digital Microfluidics

Figure 3-1a illustrates the triDrop workflow for electroporating 20,000 - 40,000 mammalian cells. This process involves several steps: sample preparation and collection, which entails preparing immortalized cell lines or primary cells extracted from a patient; resuspending the cells in electroporation buffer to achieve a concentration of at least 2 x 10^7 cells/mL, along with the desired payload; and loading them into the reservoirs of the DMF device. Notably, the use of low cell numbers in this workflow signifies a significant reduction in the required cell quantity when compared to existing systems. Presently, commercial platforms for primary T cell electroporation necessitate larger cell inputs, with manufacturer-recommended protocols suggesting a minimum of 200,000 cells for the Neon System (10 µL at a concentration of 2 x 10^7 cells / mL), and at least

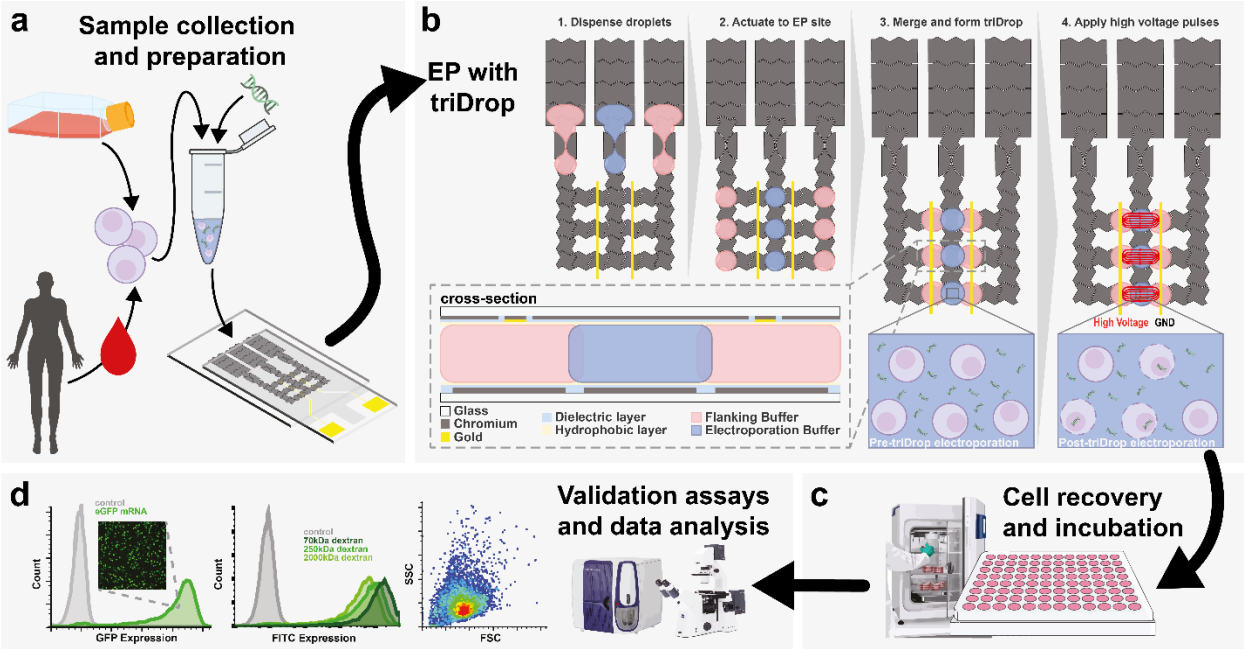

Figure 3-1: TriDrop platform design and overall experimental workflow. (a) Cell sample was cultured and prepared by resuspending it in electroporation buffer with target delivery molecules. (b) The schematic illustration shows top-view of the DMF device and the formation of the triDrop through a series of electrode actuations. The red lines (in frame 4) indicate the electric field lines generated during application of high voltage pulses. The inset shows the cross-sectional view of the triDrop. (c) After electroporation, samples were then incubated (> 24 h) for cell recovery and followed by (d) analysis using FACS or with fluorescent microscopy or any analytical method of interest.

1 million cells for the Lonza and Celetrix systems (20 µL at a concentration of 5 x 10^7 cells / mL). By employing the triDrop method, it becomes feasible to perform downstream assays such as flow cytometry and sequencing while starting with a reduced cell population.

The triDrop instrument is comprised of multiple components (**Figure 8-1**): the DMF device for the droplet manipulations, our imaging setup for visualizing the droplets on the device, an electroporation pulse circuit, and a DMF actuation circuit with open-source code (see BitBucket registry in Methods). The DMF device is comprised of two plates: the bottom plate, which contains the reservoir and driving electrodes to create the triDrop structure and the top plate, which contains Au-lines for applying the electroporation pulses to the triDrop structure as well as the grounding plane for the DMF driving voltage. The droplets sandwiched between the plates are comprised of either high, or low conductivity buffer containing mammalian cells and various payloads for delivery. Once the samples are loaded, the triDrop structure can be formed easily using our previously shown DMF platform[44,202] which allows for complete automation of all dispensing, actuation, and merging as well as automating the application of programmable high voltage pulses for electroporation.

The process of triDrop electroporation is shown in **Figure 3-1b**. A key feature of the system is the use of low cell numbers – users can input a low number of cells 20,000 to 40,000 cells per reaction for efficient transfection. Upon inputting cells into the reservoirs, three 1 μL droplets were dispensed, actuated to an electroporation site, and merged into a sequential chain as shown in **Figure 3-1b** (hereby referred to as the triDrop structure). Within the triDrop structure, the inner droplet (hereby referred to as the sample droplet) was comprised of low conductivity media ($\sigma \sim$ 8 mS/cm) and contained mammalian cells in suspension along with the payload to be delivered into the cells (in our work, the payloads used are dextran molecules of various sizes, mRNA, plasmids, or Cas9 proteins). The outer droplets (hereby referred to as the liquid electrodes) were comprised of high conductive media ($\sigma \sim$ 16 mS/cm) and were in contact with gold electrodes fabricated into the device top plate and provide an electrical connection between the metal electrodes and the sample droplet, similar to forming a liquid electroporation cuvette. After merging the three droplets into the triDrop structure, mixing was limited to diffusion and the structure consisted of three discrete regions for over 30 s post merge (**Figure 8-2a**), which allowed time for delivering high voltage pulses to the gold electrodes and electroporating the cells. The electroporation process was complete within 5 s of droplet merging and the total time for triDrop implementation from reservoir loading to electroporation was ~3 minutes for three triDrop structures. Immediately after electroporation, cells were loaded off chip for post-electroporation culture for up to 7 days (**Figure 3-1c**) and were analyzed using microscopy, flow cytometry and validated with fluorescent-based assays (**Figure 3-1d**). To our knowledge, the triDrop system shows state-of-the-art transfection efficiency with exceptional viability throughout and is the first technique shown for scalable mammalian cell electroporation on DMF devices and joins a small collection of microfluidic devices capable of transfecting primary human immune cells.[94,106,193,194,107,108,110–112,116,182,192]

3.2.2 Characterization of the triDrop System

In initial experiments, we explored the use of co-planar electrodes paired with various droplet structures to generate a sufficient electric field to insert 70 kDa FITC-tagged dextran into the easy to transfect HEK293 cell line. The droplet structures tested here are shown in **Figure 3-2a** and described as follows: (1) a uniform structure – one homogenous 3 μL droplet comprised of either high or low conductivity medium with the cells and payload distributed homogenously throughout,

(2) a focused structure – three 1 µL droplets comprised of the same media that are merged together with only the middle droplet containing cells and payload, and (3) a triDrop structure – two droplets of high conductivity buffer flanking a droplet with low conductivity buffer containing cells and payload. Three, 200 V_{DC} pulses, 10 ms in duration (determined via numerical simulations) were applied to the droplet structures and the results were analyzed using three metrics, transfection efficiency (TE), viability ratio (VR), and mean fluorescence intensity (MFI)

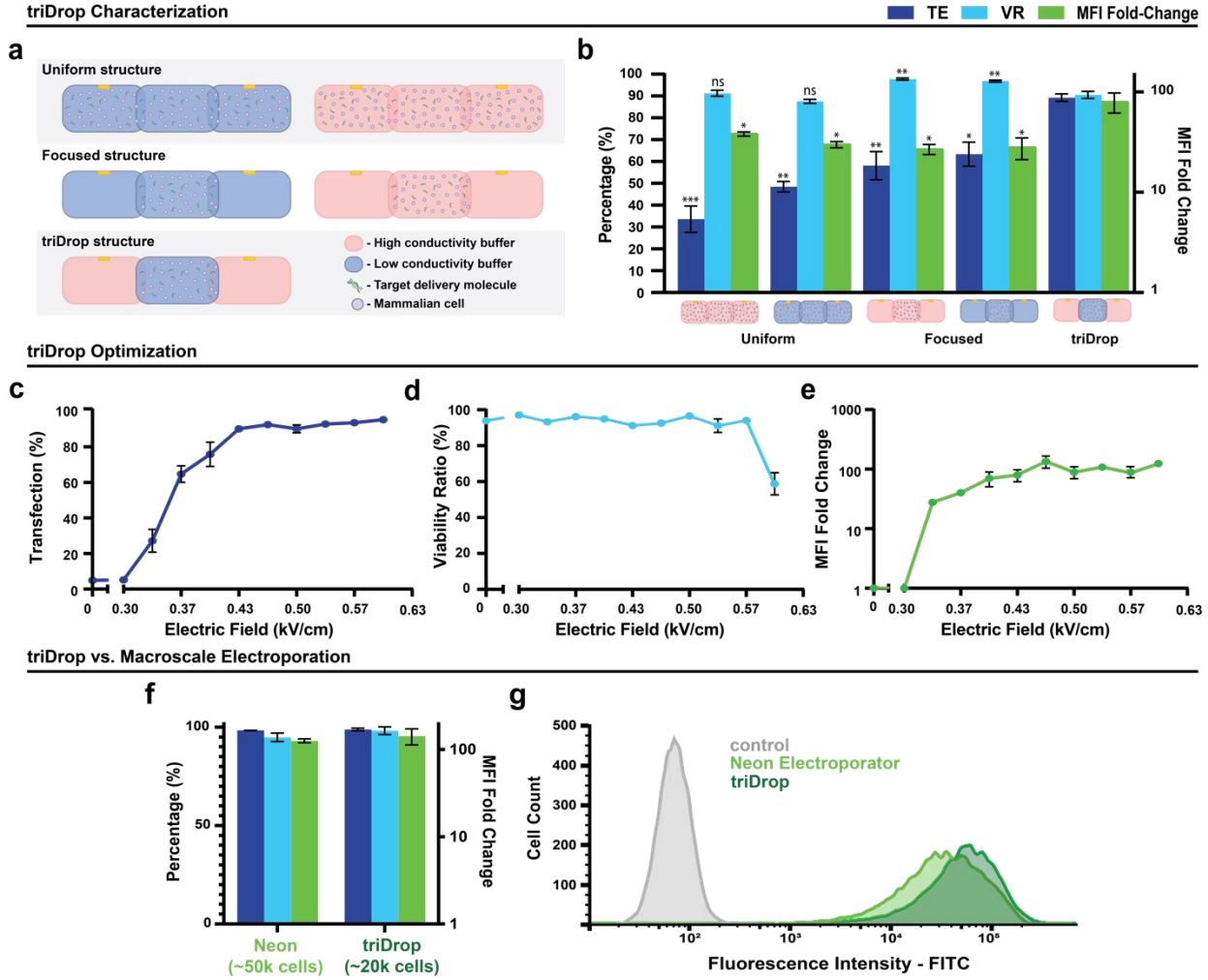

*Figure 3-2: System characterization and optimization for triDrop electroporation with HEK293 cells. (a) Illustrations showing different droplet liquid structures used for electroporation characterization. Pink droplets represented high conductivity media (σ ~ 16 mS/cm) and blue droplets represent low conductivity media (σ ~ 8 mS/cm). (b) Plots showing transfection efficiency (TE; dark blue), viability ratio (VR; light blue) and mean fluorescence intensity (MFI) fold-change (green) for five different droplet electroporation structures when inserting a 70 kDa FITC-tagged dextran molecule. Significance markers (P < 0.05, n = 3) are in reference to the triDrop arrangement. Plots showing the (c) transfection efficiency, (d) viability ratio, and (e) MFI fold-change with respect to the applied electric field using the triDrop system for the insertion of 70kDa FITC-tagged dextran molecule into HEK293 cells. The statistical analysis was performed via an ordinary one-way ANOVA (n = 3). Graphical representation showing the (f) efficiency, viability ratio, and MFI fold-change for the Neon (standard) versus the triDrop system. These quantitative values were obtained from (g) the cell counts displaying FITC fluorescence from electroporated and non-electroporated samples from the Neon system and the triDrop. SEM are calculated based of n = 3. n.s indicated no significant difference, *, **, and *** represents P-values below 0.05, 0.01, and 0.001 respectively. Statistical analysis was performed using an ordinary one-way ANOVA.*

fold change. **Figure 3-2b** shows that the triDrop structure has significantly higher TE (89%) and MFI fold change (79) than any of the other droplet structures while still maintaining a viability ratio of > 90 % ($P < 0.05$, $n = 3$). Additionally, we show that the success of the triDrop structure can be recreated without significant difference when the middle droplet is comprised of another low conductivity electroporation buffer ($\sigma \sim 7.4$ mS/cm) but not when using high conductivity electroporation buffers ($\sigma > 15$ mS/cm) (**Figure 8-3**). To understand the experimental results above, we developed a COMSOL simulation of the uniform and triDrop structure described in **Appendix C Figure 8-4**, and the results shown in **Figure 8-5** and **9-6**. The simulation of the uniform structure shows the outer regions of the structure experience electric fields that are low for mammalian electroporation (< 0.2 kV/cm),[204] regions close to the gold electrodes have a high but inconsistent electric field (~0.7 kV/cm), and the middle section of the droplet structure has a homogenous electric field that is too low for electroporation (0.35 kV/cm). Comparing this to the simulation of the triDrop structure shown in **Figures 8-6c**, forming the outer droplets using high conductive media and the inner droplet using low conductivity media results in a homogenous electric field (0.55 kV/cm) that focuses across the middle of the triDrop structure, solving the problem of heterogenous electric field generation that has plagued other droplet electroporation systems.[120] In the triDrop configuration, all the cells (which are entirely located in the middle droplet) experience a consistent electric field while being exposed to significantly lower current than common benchtop systems (~30 mA vs 3000 mA)[121] (**Figure 8-7**). This is an important result because isolating the cells in the middle of the droplet structure will prevent harmful electrochemical species (generated at the metal-liquid interface)[101] from changing the pH of the cell media and negatively affecting the health of the cells (see images of pH test in **Figure 8-2b**). Given these observations, the triDrop structure offers optimal results compared to the uniform or focused liquid structures when using identical electroporating conditions.

We hypothesized that the three quantitative metrics (TE, VR, and MFI-fold change) for the triDrop structure might be improved by varying the applied electric field. To test this hypothesis, a range of electric fields were applied to determine the optimal field for inserting a 70 kDa FITC tagged dextran molecules into HEK293 cells. These data, shown as line graphs in **Figure 3-2c-e**, confirm that there is range of fields (0.5-0.63 kV/cm) to achieve excellent TE (~ 90 %), VR (~ 90 %), and MFI fold change (> 80). Repeating this optimization for Jurkat and HeLa cells (**Figure 8-8**) reveal a slightly higher effective range (0.75-0.90 kV/cm). These applied fields place us

within the expected range reported by other high performance electroporation devices.[97,112] A list of all electroporation conditions tested throughout this study and the corresponding parameters can be found in **Table 9-1**.

To evaluate the triDrop method relative to gold standard practices (Neon™ transfection system), a series of transfections were performed using HeLa cells and dextran as the payload. All pulse parameters for triDrop are identical to those described above and the Neon™ was operated using the manufacturer recommended settings. The key differences between the systems are that the cell numbers used for the triDrop was lower than the Neon™ and sample volumes for transfection were reduced. When working with HeLa cells the Neon™ requires 10 μL of sample at a concentration of 5 x 10^7 cells/mL (50,000 total cells) whereas the triDrop requires only 1 μL at a concentration of 2 x 10^7 cells/mL (20,000 total cells). As shown in **Figure 3-2f**, cells transfected with the triDrop show very similar high metrics as the Neon™ (TEs > 98 %, VRs > 95 % and MFI fold change > 125). The transfection efficiency was calculated by flow cytometry analysis with the results of the FITC fluorescence counts (for ~15,000 events) to be very similar for both systems (but different than the non-electroporated control cells) (**Figure 3-2g**). These experiments show that our technique can achieve similar metrics as the standard mammalian-based transfection system with lower cell numbers. As described below, these low cell numbers enabled our work with primary T-cells, which is usually difficult to transfect when cell numbers are below 1 x 10^6 cells since their post-electroporation viability decreases significantly.[196,201]

3.2.3 Immortalized Cells

To further evaluate the capacity to transfect mammalian cells, different payloads were delivered to three commonly used immortalized cell types: HEK293, HeLa, and Jurkat cells. Each set of cells were prepared and loaded into the DMF platform (as in **Figure 3-1b**) and were transfected with four different payloads: 70 kDa, 250 kDa, and 2000 kDa FITC-tagged dextran, and a 5 kb eGFP plasmid. **Figure 3-3a** and **Figure 3-3b** shows the quantitative metrics for the typical model transfection cell line HEK293 and HeLa cells for the three different dextran sizes (along with a non-electroporated control) respectively. As shown, the metrics are excellent, with a TE > 90 % (left-side y-axis), VR > 90 % (left-side y-axis), and > 80 MFI fold-change (right-side y-axis). In fact, the triDrop system was able to insert the large 2000 kDa FITC-tagged dextran molecule (hydraulic diameter ~ 55 nm)[205] into both HEK293 and HeLa cell lines with a TE and VR of > 90

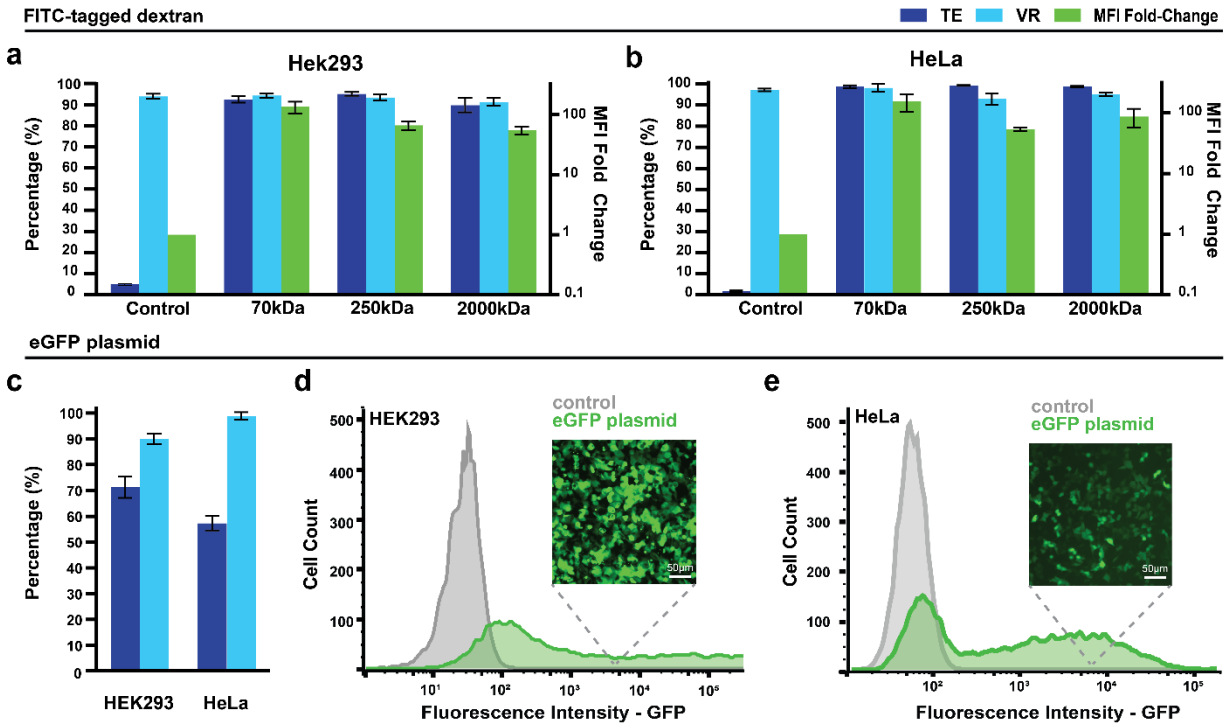

Figure 3-3: Intracellular delivery of diverse payloads in HEK293 and HeLa cells using triDrop electroporation. Plots of transfection efficiency, viability ratio, and MFI fold-change comparing an un-electroporated control vs the triDrop system for the insertion of a 70 kDa, 250 kDa, and 2000 kDa FITC-tagged dextran molecules for (a) HEK293 cells and (b) HeLa cells. (c) Plots of transfection efficiency and viability ratio for HEK293 and HeLa when inserting an eGFP plasmid. Fluorescence intensity histograms showing GFP expression for (d) HEK293 cells and (e) HeLa cells vs an non-electroporated control. Inset shows fluorescence images of (d) HEK293 cells and (e) HeLa cells expressing the eGFP plasmid. All plots with error bars are based on standard error of the mean for n = 3 replicates.

%. These results show that the delivery of large molecules into the cytosol of HEK293 and HeLa cells using triDrop is efficient and suggests that the system will be capable of delivering fully formed proteins of similar size or other large molecules.[108]

Moving towards a more biologically relevant payload, we performed the same protocol for delivering plasmids. **Figure 3-3c** shows the TE and VR for HEK293 and HeLa cells, as shown, we obtained a TE and VR of 71 % and 90 % for HEK293 and 60 % and 99 % for HeLa with both cell types showing healthy morphology after transfection (**Figure 8-9**). These results were obtained via flow cytometry and approximately 15,000 cell events were collected for each sample and the frequency fluorescence histogram is depicted in **Figure 3-3d** (HEK293) and **Figure 3-3e** (HeLa). In both cases, the control population showed very minimal fluorescence (see grey histogram) while the eGFP positive cells (showing successful triDrop electroporation) were shifted towards higher fluorescence than the control (see green plots). We note that plasmid transfection poses a greater challenge as it requires nuclear delivery rather than just cytosolic delivery.

Consequently, the delivery rates of plasmids are often lower compared to dextran molecules or mRNA molecules.[206,207] Regardless, these data confirm the triDrop system can be used to insert

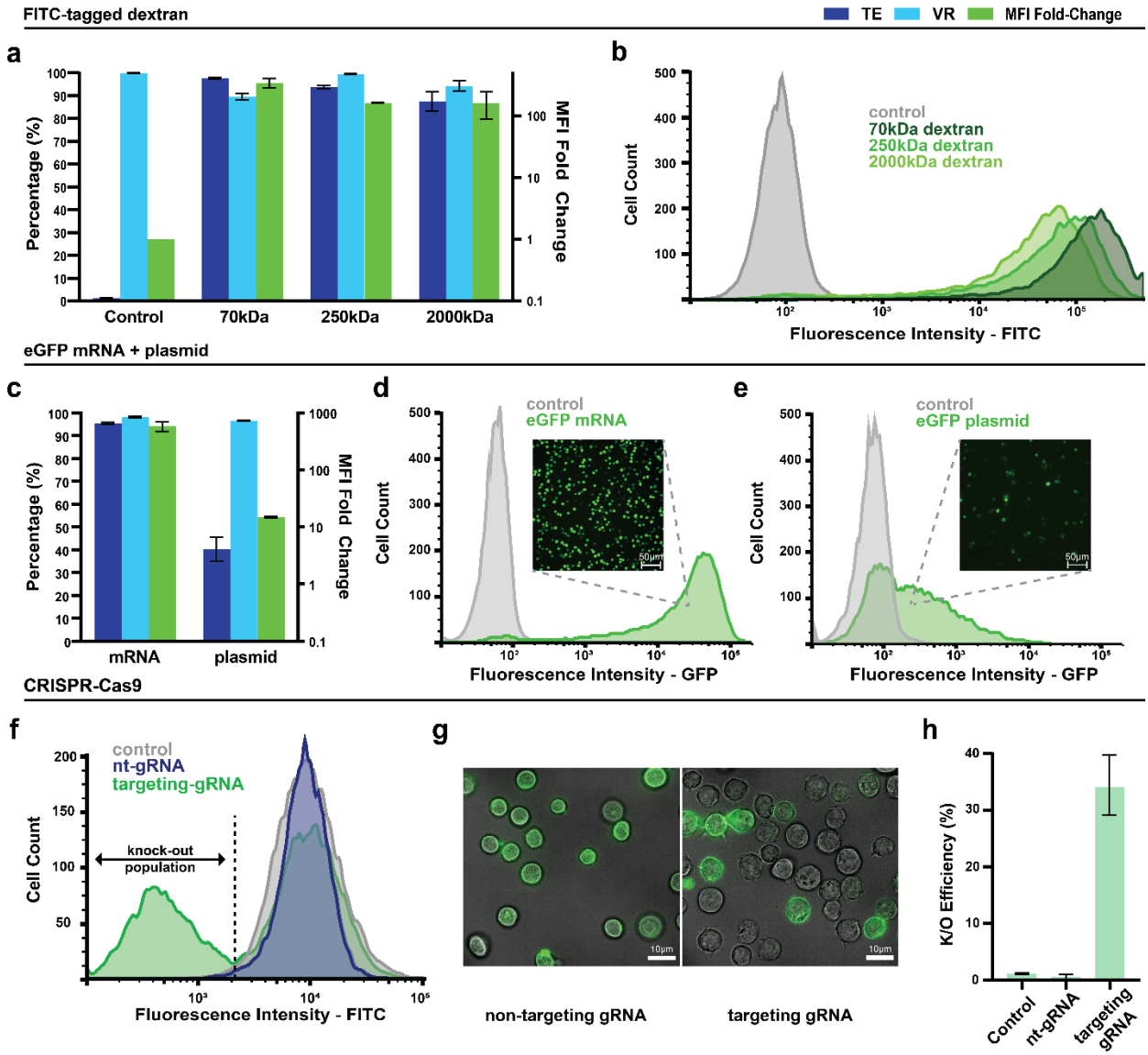

*Figure 3-4: Intracellular delivery of diverse payloads into **Jurkat** cells using **triDrop** electroporation. (a) Plots of transfection efficiency, viability ratio, and MFI fold-change comparing an un-electroporated control vs the triDrop system for the insertion of a 70kDa, 250kDa, and 2000kDa FITC-tagged dextran molecules. (b) Fluorescence intensity histograms showing the FITC expression comparing the control with the three different dextran molecules inserted using the triDrop system. (c) Plots of transfection efficiency, viability ratio, and MFI fold-change for the insertion of eGFP-mRNA, and eGFP-plasmid using the triDrop system. Fluorescence intensity histograms showing GFP expression for (d) eGFP-mRNA and (e) eGFP-plasmid inserted using triDrop electroporation vs. an non-electroporated control. Inset show fluorescence images for cells expressing (d) eGFP-mRNA and (e) eGFP-plasmid. (f) Fluorescence intensity histograms showing the FITC expression comparing a control vs. non-targeting gRNA vs β2M targeting gRNA populations after staining with a FITC-tagged anti-β2M antibody. (g) Fluorescence images overlaid with bright field images showing (left) cells electroporated with a non-targeting (nt) gRNA and (right) cells electroporated with a gRNA targeting the β2M gene and stained with a FITC-tagged anti-β2M antibody. (h) Plots of β-2-microglobulin knockout efficiency comparing an non-electroporated control vs. cells electroporated with a Cas9 protein conjugated with a non-targeting gRNA vs. cells electroporated with a Cas9 protein conjugated with a gRNA targeting the β-2-microglobulin gene. All plots with error bars are based on standard error of the mean for n = 3 replicates.*

both large payloads as well as biological payloads which have been challenging to deliver for other microfluidic based mammalian transfection devices.[208]

Next, we tested our system with Jurkat T-cells since they have been shown to be a suitable model in immunotherapy research[195] and have a reputation of being a more difficult to transfect cell line.[209] Here, we followed the same protocol as above - electroporating three different dextran molecules (70 kDa, 250 kDa, and 2000 kDa), and eGFP plasmid. Additionally, we included an mRNA payload given the increasing interest to use mRNA as an immunotherapeutic molecule.[210] **Figure 3-4a** shows the dextran results for our three metrics and are quantitatively similar to HEK293 and HeLa – VR and TE > 90 %. The flow cytometry histogram (**Figure 3-4b**) shows a full spectral shift towards higher fluorescence intensities for all three dextran sizes confirming that we can efficiently insert large molecules into Jurkat cells with minimal effect on viability. Furthermore, we transfected a 1 kb eGFP mRNA, and a 5 kb eGFP plasmid. Figure 3-4c shows results 24 hours post-transfection with the mRNA displaying an impressive TE of 95 % (measured via frequency histogram Figure 3-4d), a VR of 98 % and an MFI fold-change of > 500 while using only 2 pico grams of mRNA per cell. Electroporation with both payloads did not negatively influence the morphology of the cells (**Figure 8-9**), however, the plasmid (measured 48-hours post-transfection) showed a modest TE of 40 % (measured via frequency histogram Figure 3-4e), and a VR of 96 % and a very modest MFI fold-change of ~12. Taken together, these data suggest that the triDrop technique is suitable for both types of payloads for Jurkat cell transfection, with mRNA having higher TE, similar to previous microfluidic transfection works.[116]

As a final proof-of-principle in Jurkat cells, the triDrop system was used for an on-chip CRISPR knock-out of the β-2-microglobulin (β2M) gene. The β2M gene codes for a protein that serves as a key structural element in all major histocompatibility (MHC) class 1 molecules[211] and when the gene is impaired it can no longer form and be expressed on the cell surface making this an ideal target for an easily detectable proof-of-concept knockout. Jurkat cells were mixed with a Cas9 RNP containing either a scrambled gRNA or a gRNA targeting the β2M gene and loaded on to the chip for triDrop electroporation, immediately post electroporation cells were moved off-chip and into recovery buffer and left to incubate for 72 hours. After recovery, cells were blocked for non-specific binding and then stained with a FITC-tagged antibody targeting MHC class 1 molecules. **Figure 3-4f** depicts histogram data for the three different conditions – control (no

triDrop electroporation, grey line), non-targeting gRNA (triDrop electroporation with a scrambled gRNA, blue line), and β2M targeting gRNA (triDrop electroporation with a β2M specific gRNA, green line). All three populations had high viabilities (~95%), however, only cells that were electroporated with the β2M specific gRNA show a knockout population which is represented by cells with a lower fluorescence intensity (i.e., a peak is shown on the left of the dotted line). As illustrated in representative images after staining, cells remain healthy after 72 hours (~ 95% viability) and only those with knocked out β2M shows cells with no fluorescence (**Figure 3-4g)**. The knockout efficiency is summarized in **Figure 3-4h** and show an average knockout efficiency of 35 % for the cells electroporated with the β2M targeting gRNA whereas the two control populations both have < 2 % knockout. In sum, the gene-editing application here shows that the triDrop platform can deliver complex payloads into mammalian cells.

3.2.4 Primary T Cells

With the rise of immunotherapy showing promise for cancer patients, much research has been put into transfecting primary T cells.[88] While Jurkat cells can provide promising initial indicators for immunotherapies, final tests must be done in primary human immune cells.[195] Currently, there is no technology that is capable of generating libraries of engineered primary T cells in an automated and arrayed fashion without requiring millions of cells. To demonstrate the high-impact applicability of the triDrop system, we demonstrate the transfection process for primary human CD4+ T cells.

We first optimized the triDrop electroporation protocol for the insertion of the 2000 kDa dextran payload. Given the sensitive nature of these cells, we explored reducing the pulse duration as this parameter is known to have a significant effect on cell viability.[204] For each condition 3, 450 V pulses were applied with a duration of 1 ms, 3 ms, or 10 ms. As shown in **Figure 8-10a-d**, reducing the pulse duration (1 and 3 ms) was found to have the optimal metrics with 3 ms yielding the highest TE while still yielding VRs more than 90%. The system was further assessed with a plasmid payload. The representative images of the cells after 48 h post-transfection with an eGFP plasmid shows healthy morphology and cells are producing eGFP (**Figure 3-5a**). The electroporated cells were compared to cells that were not electroporated via flow cytometry histograms (**Figure 8-10e and f**). We quantified the VR as well as the TE, and as shown in **Figure 3-5b**, the triDrop electroporated cells shows a VR of 81 % and a TE > 38 %. These are good

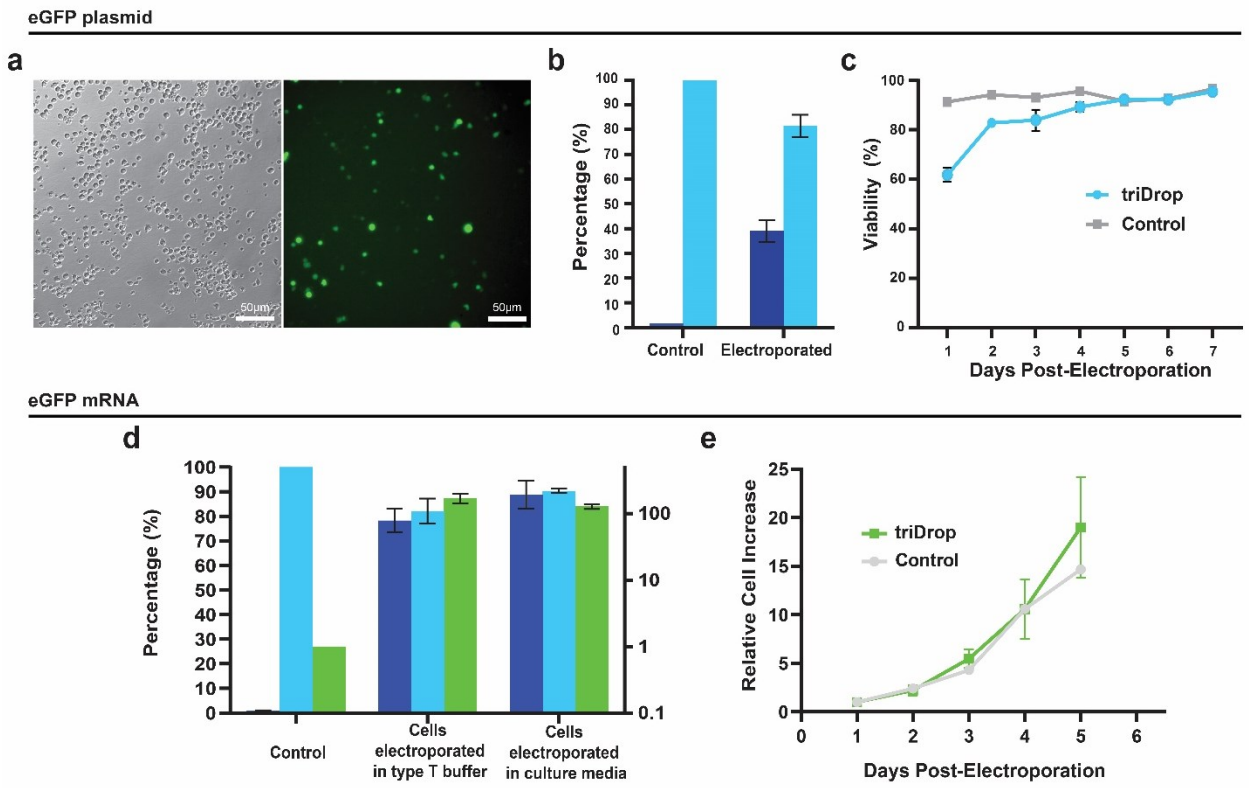

Figure 3-5: Intracellular delivery of valuable payloads into human primary CD4+ T cells using triDrop electroporation. (a) bright-field (left) and fluorescence (right) images showing GFP expression 48-hours post electroporation with the triDrop system. (b) Plots of transfection efficiency and viability ratio comparing an un-electroporated control vs the triDrop system for the insertion of a 5kb eGFP plasmid 48-hours post transfection. (c) Viability measurements for 7-days of post electroporation culture comparing a non-electroporated control vs. the triDrop system. (d) Plots of transfection efficiency, viability ratio, and MFI fold-change comparing samples electroporated with different electroporation buffers. (e) The cell increase of samples relative to day 1 for 7-days of post electroporation for samples electroporated vs. non-electroporated control. All plots with error bars are based on standard error of the mean for n = 3 replicates.

metrics for plasmid delivery into primary T cells comparing modestly with some commercially available systems such as the Neon™ (64 % TE and 94 % viability)[212], the Lonza system (70 % TE, 60 % viability)[213], or the Celetrix system (40 % TE, 50 % viability).[196] The viability of electroporated cells were monitored daily for the one week post-electroporation and compared against a non-electroporated control. It was observed that the health of the electroporated cells is comparable to that of non-electroporated cells by day 5 (**Figure 3-5c**) and, 7 days post electroporation, both the control population and the electroporated population had viabilities > 95% (also shown by the forward and side scatter plots – **Figure 8-10g)**.

In addition, we show the delivery of eGFP mRNA using cell culture media as our electroporation buffer. The deleterious effects of long term exposure to electroporation buffer on mammalian cells are well-documented[214] and many buffer manufacturers recommend minimizing

the time cells spend in the buffer. Furthermore, proprietary electroporation buffers can be prohibitively expensive.[100] A unique feature of our triDrop system is the ability to generate the electric field focusing effect on a wide variety of different media if the flanking droplets are comprised of a higher conductivity solution. We created a very high conductive solution ($\sigma \sim 32$ mS/cm, recipe in **Table 8-2 and 8-3**) to use as a flanking buffer for primary T cells suspended in RPMI ($\sigma \sim 15$ ms/cm) to maintain the high-low-high buffer conductivity triDrop structure. **Figure 3-5d** shows a comparison between cells electroporated in low conductivity buffer with the original triDrop configuration compared to cells electroporated in culture media using the very high conductive flanks. Both conditions show impressive results, however, as predicted, the cells electroporated in the culture media had superior VR (90 % vs 82 %) and had higher TE (89 % vs 78 %). The electroporated cells were allowed to grow out for 5-days post electroporation and were found to proliferate at a rate comparable to that of non-electroporated cells. After 5 days of culture electroporated cells and control cells show a similar fold increase with a ~19 and ~15-fold population increase respectively (**Figure 3-5e)**. Compared against four recent high-performance microfluidic transfection systems[111,112,116,194] for the insertion of mRNA into primary human T cells, the triDrop can achieve the best percentage of cells that are both living and transfected while using the least amount of mRNA per cell **(Figure 8-11)**.

Finally, we showcase our triDrop system for CRISPR-Cas9 gene editing in primary human CD4+ T cells. First, we performed a knockout targeting a well-established β2M gene. **Figure 3-6a** depicts histogram data for a non-electroporated condition (grey line), a condition electroporated with a non-targeting gRNA (blue line) and a condition electroporated with a β2M-targeting gRNA (green line). All cells were stained with a FITC-tagged anti-β2M antibody four days post-electroporation. As expected, the control condition, and the condition electroporated with a non-targeting gRNA show complete expression of the β2M protein, however, the condition electroporated with the targeting gRNA show a significant leftward shift indicating substantially reduced β2M expression (i.e., reduced fluorescence). In addition, **Figure 3-6b** shows that after four days post-electroporation, the triDrop system (and the editing) has no observable impact on cell health when compared to the control condition as determined by staining with DAPI. We also measured the knockout efficiency for these three conditions, and as shown in **Figure 3-6c**, the targeted β2M gRNA shows an average knockout efficiency of 70 %, which is similar to previously shown microfluidic gene editing systems when targeting this gene in primary cells.[215]

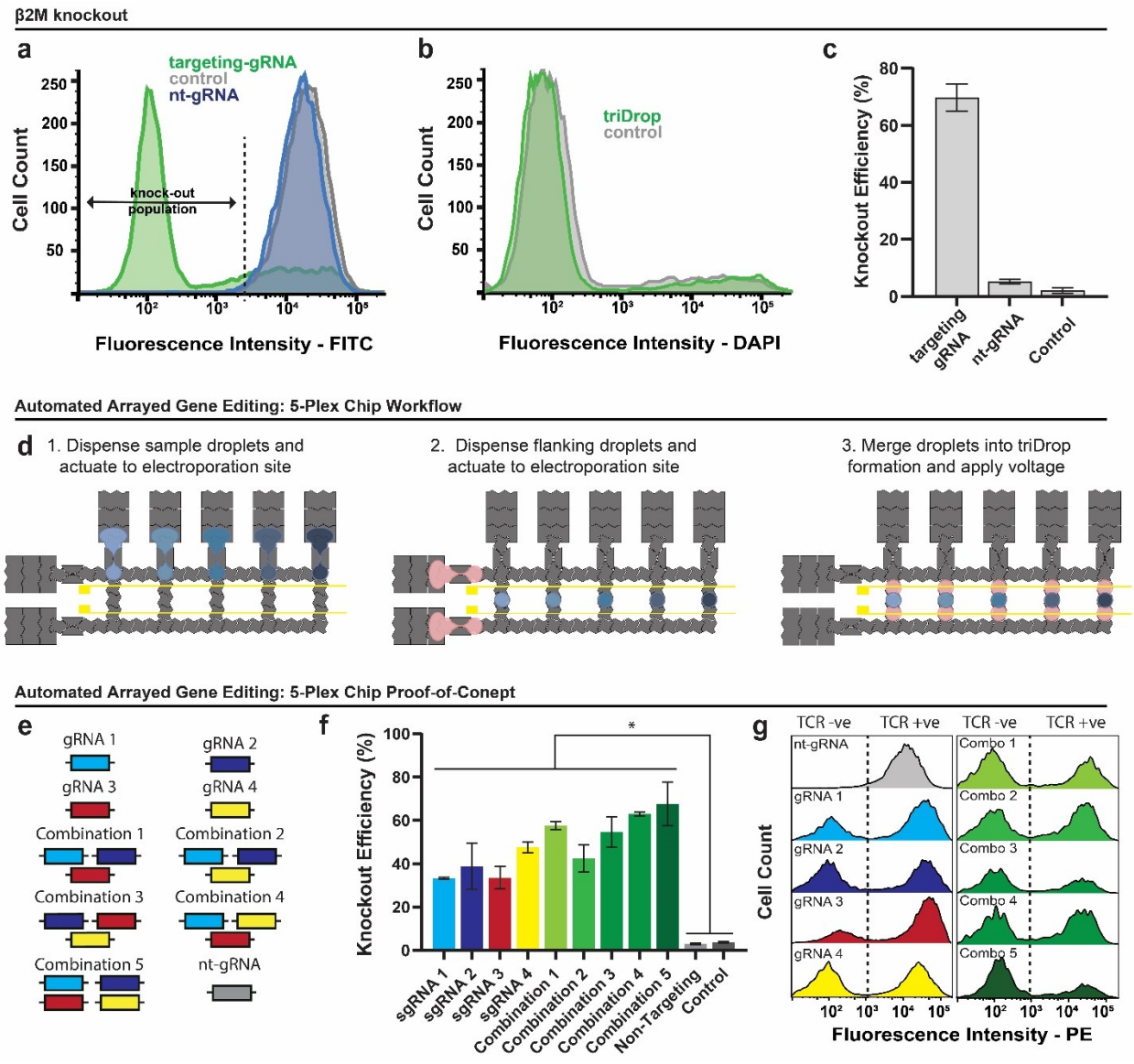

*Figure 3-6: CRISPR-Cas9 gene editing applications in human primary CD4+ T cells using triDrop electroporation. (a) Fluorescence intensity histograms showing the FITC expression comparing a control vs. non-targeting gRNA vs β2M targeting gRNA populations after staining with a FITC-tagged anti-β2M antibody. (b) Fluorescence intensity histograms showing the DAPI staining comparing a control vs. electroporated population after four days of culture. (c) β2M knockout efficiency summary for three conditions. (d) Schematic illustrations showing the operations of an automated DMF platform capable of the simultaneous electroporation of 5 unique samples. (e) Summary of all conditions for the arrayed automated gene editing experiment. (f) Summary of TRAC-knockout efficiency for all 10 conditions plus a non-electroporated control. (g) Fluorescence intensity histograms showing TCR expression for all 10 analyzed conditions. Error bars are based on standard error of the mean for (c) n = 3 replicates and (f) n = 2 replicates. * Represents P-values below 0.05. Statistical analysis was performed using an unpaired T-test.*

The final assay was motivated by widespread interest in performing arrayed gene editing on primary T cells for immunotherapeutic discovery.[216] We combined the triDrop gene editing capabilities with our DMF platform's capacity for parallelized automation to perform an automated, 5-plex arrayed gene editing experiment. As a model system, we targeted the knockout

of the T cell receptor alpha constant (TRAC) locus due to the recent interest in using this site for T cell receptor therapies.[62] The device and method shown in **Figure 3-6d** was designed with additional sample reservoirs to hold cells suspended in low conductivity electroporation buffer mixed with one of the unique guide conditions and additional electroporation sites to increase parallel processing. Four gRNAs were designed (sequence in **Table 8-4**) and arranged into 10 unique conditions to target the TRAC locus as summarized in **Figure 3-6e**. To perform this experiment, we followed the same protocol as before except using a chip capable of performing five unique triDrop electroporations in parallel (**Figure 8-12**). Generally, these types of multiplexed experiments require at least 200,000 cells per condition[216], however, for our experiments (20 total electroporation reactions), fewer than 1 million cells from a single donor were used for all conditions. **Figure 3-6f** summarizes the knockout results as measured via flow cytometry 4-days post electroporation. As expected, all conditions had knockout efficiencies significantly different than the non-targeting and the control ($P < 0.05$), with each condition achieving at least 30 % average knockout. Interestingly, cells electroporated with multiple gRNAs had significantly higher knockout efficiencies than cells electroporated with only one gRNA ($P < 0.001$, **Figure 8-13)**, and the full combination of all four gRNAs together had the highest average knockout (67 %) which is inline with previously shown results.[217] Histogram plots depicting TCR expression with the best result from each condition are shown in **Figure 3-6g**. These results show that triDrop electroporation can be combined with high throughput DMF automation to perform arrayed CRISPR experiments with high value cell lines.

The capability to perform electroporation at these lower cell numbers is a significant challenge with current commercially available techniques, rather these systems are required to use at least ~ 200,000 cells, and usually between 1-2 million cells per condition when working with sensitive cell lines. TriDrop is an efficient technique with excellent viabilities and transfection efficiencies (> 90 %) for immortalized and primary cells alike while requiring only 40,000 cells for a single reaction. Moreover, we have shown that the triDrop system can be combined with DMF for a simple arrayed CRISPR screen while using fewer than one million primary human T cells, and we hope in the future this capability can be expanded to test large libraries of novel constructs on rare cells. This capability will both accelerate the pace of immune cell engineering, requiring less time and resources to grow and culture cells during research and development stages, while also making it more affordable due to less consumption of expensive reagents like Cas9

proteins and gRNAs. We believe the triDrop system will help lift barriers in immune cell engineering and open the door to discovering new therapeutic breakthroughs via high throughput arrayed screening.

3.3 Conclusion

We show for the first time the ability to perform highly efficient and highly viable electroporation of immortalized and primary mammalian cells on a DMF platform using a tri-droplet liquid structure. Moreover, our platform can work with low quantities of mammalian cells, which can be cost-efficient and expedite the engineering workflow for mammalian cells. We compared our system with the Neon system and showed very comparable transfection results. Additionally, as an application, we described results relating to performing five unique CRISPR edits in parallel while using the human primary T cells. We propose such a platform would be potentially integrated with other DMF devices for end-to-end automation of mammalian cell engineering[218] similar to what has been shown previously for microbial cells[113,114] and be used for applications related to the field of genome editing and cell-based immunotherapies.

3.4 Materials and Methods

3.4.1 Reagents and Materials

Unless specified otherwise, general-use chemicals and kits were purchased from Sigma-Aldrich (St. Louis, MO). Device fabrication reagents and supplies included chromium-coated glass slides, and gold-coated glass slides with AZ1500 photoresist from Telic (Valencia, CA), MF-321 positive photoresist developer from Rohm and Haas (Marlborough, MA), chromium etchant 9051 and gold etchant TFA from Transene (Danvers, MA), AZ-300T photoresist stripper from AZ Electronic Materials (Somerville, NJ), Teflon-AF 1600 from DuPont Fluoroproducts (Wilmington, DE). Transparency masks for device fabrication were printed from ARTNET Pro (San Jose, CA) and polylactic acid (PLA) material for 3D printing were purchased from 3Dshop (Mississauga, ON, Canada). General chemicals for tissue culture were purchased from Wisent Bio Products (Saint-Bruno, QC, Canada). eGFP plasmid (**Figure 8-14**) and mRNA (**Table 8-4** for sequences) for this study were acquired from Addgene (catalog: 54767) and TriLink Biotechnologies (catalog: L-7201) respectively. Electronic components were obtained from DigiKey (Thief River Falls, MI). Electroporation buffers were obtained from Harvard Apparatus Canada (St Laurent, QC), Thermo

Fisher Scientific (Burlington, ON), or made in-house (see **Table 8-3**). Neon™ transfection reagents were purchased from Thermo Fisher Scientific (Burlington, ON).

3.4.2 TriDrop Device Fabrication and Setup

TriDrop devices, each comprising of a bottom plate with Cr-based electrodes and a top-plate with Au-based electroporation electrodes, were fabricated at Concordia's cleanroom facility using transparent photomasks printed at 25 400 dpi (Artnet Pro, Bandon, OR). An overview of the fabrication process is illustrated in **Figure 8-15**. DMF bottom plates bearing chromium electrodes coated with a SU-8 5 dielectric and Teflon-AF hydrophobic layer were formed using previously outlined methodology[38]. Each bottom plate features an array of 30 actuation electrodes (2 mm by 2 mm), 12 reservoir electrodes (2.9 mm by 5.5 mm) arranged into 3 reservoirs, 6 active dispensing electrodes (2 mm by 2 mm), and 3 splitting electrodes (3.8 mm x 3 mm). The electrode array has inter-electrode gaps of 150 mm and each electrode was connected to a pogo-pin holder.

TriDrop top plates bearing gold electrodes (0.2 mm wide) were formed from a glass substrate coated with 100 nm gold adhered to seed chromium layer (~12 nm). To form the gold electrodes, top plates were spin-coated (10 s 500 rpm, 30 s 3000 rpm, 20 s 5000 rpm) in S1811, exposed through a transparent mask, developed using Microposit MF321 (2 min), washed with DI water, submerged in gold etchant (2 min), washed with DI water, and submerged in AZ stripper to remove the remaining photoresist before being washed with acetone, IPA, and DI water, and dried with nitrogen. To disconnect the chromium from the gold wiring, we followed the above protocol except using CR-4 etchant to remove the chromium. To insulate the gold electroporation electrodes from the Cr-grounding layer, the top plate was surface treated for 45 s in a plasma cleaner (Harrick Plasma PDC-001, Ithaca, NY) before coating a 5 µm dielectric of SU8-5. Briefly, the photoresist was spin-coated (10 s 500 rpm, 30 s 2500 rpm), followed by a soft bake (65 °C 2 min, 95 °C, 10 min), exposed to UV light through a custom mask (5 s), post-exposure baked (65 °C 2 min, 95 °C 10 min), developed in SU8 developer (15 s), rinsed with IPA and DI water, dried with nitrogen, and then hard baked (180 °C, 10 min). Bottom plates were spin-coated with Teflon-AF 1600 in 2 % w/w in Fluorinert FC-40 (10 s 500rpm, 30s 1500rpm). To assemble the completed triDrop device, the top and bottom plates were assembled using two layers of double-sided tape (180 µm total thickness, 3M) and the gold electrode on the top plate were aligned directly above electroporation sites on the bottom plate.

3.4.3 Cell Culture

HeLa and HEK293 cells were cultured in Dulbecco's Modified Eagle Medium (DMEM) and Jurkat cells in RPMI-1640 (kindly provided by Prof. Alisa Piekny, Concordia). All media contained 10 % heat-inactivated fetal bovine serum (FBS) and 100 U/mL penicillin/streptomycin. Cells were passaged every 2-3 days and maintained in a humidified chamber at 37 °C with 5% CO_2. For triDrop experiments, HeLa and HEK293 cells were passaged by first washing with PBS, then trypsinizing with 0.25 % trypsin-EDTA followed by washing with DMEM before seeding cells in a fresh flask at 2 x 10^5 cells/mL. Jurkat cells were passaged by centrifuging at 300 g for 5 min to pellet the cells, aspirating the media and resuspending in RPMI before seeding at 1 x 10^5 cells/mL. Prior to electroporation, aliquots of 600,000 cells were prepared and resuspended with target molecules in EP buffer to a final volume of either 15 µL or 30 µL.

Primary human CD4+ T cells were either purchased from BPS bioscience (catalog #79752, San Diego, CA) or separated from fresh primary blood and purified using EasySep Human CD4 T cell Isolation kit to a purity of 95 % (STEMCELL Technologies, Canada, Catalog # 17952) (**Figure 8-16**). All cells were kept in liquid nitrogen prior to use. For experiments with plasmid, mRNA, and dextran, cells were thawed and cultured in complete culture medium consisting of RPMI-1640 with 10 % FBS, 100 U/mL penicillin/streptomycin, and 100 IU/mL recombinant human IL-2 (Fisher Scientific Ottawa, ON). After 24 h, the cells were activated with Human T-Activator CD3/CD28 Dynabeads (Fisher Scientific Ottawa, ON, #11131D) and were incubated up to 48 hours. After incubation, activator beads were removed following manufacturers protocol by first gently pipetting up and down to release cells from the activator beads followed by transferring the cells to a magnetic tube rack for 1-2 minutes to allow for cells and beads separation and the supernatant containing cells was transferred to a fresh tube. Primary T cells were counted using TC20 Automated Cell Counter (BioRad, CA) and maintained at 1 x 10^6 cells/mL by daily addition of complete culture media. Prior to electroporation, cell aliquots of 600,000 cells were prepared and resuspended with target molecules with EP buffer to a final volume of 15 µL for each unique condition. For gene editing experiments with primary T cells, culture conditions were adapted from Roth et al.[201] Briefly, cells were thawed into culture media supplemented with, 10 % FBS, 200 IU/mL IL-2, 10 ng/mL IL-7 (Peprotech, cat no: 200-07), and 5 ng/mL IL-15 (Peprotech, cat

no: 200-15). Post electroporation cells were recovered in the same media cocktail but with IL-2 levels increased to 500 IU/mL.

3.4.4 Bulk Electroporation

Prior to electroporation, HeLa cells were seeded the day before transfection (day 0) to reach 70-80% confluency by day 1. Immediately before electroporation, adherent cells were trypsinized (using 0.25% trypsin-EDTA), washed, and re-suspended in media, and counted with TC20 Automated Cell Counter (BioRad, CA). The Neon™ transfection system (Thermo Fisher) was then used to electroporate cells using manufacturer's protocol following four steps: (1) cells were centrifuged at 300 g for 3 min and washed with 500 µL PBS before being resuspended 5 x 10^6 cells/mL in the Neon™ electroporation buffer. (2) FITC-tagged dextran molecules were then added to a final concentration of 300 µg/mL. (3) the electroporation sample was mixed (via gentle up-and-down pipetting) and transferred to the Neon™ capillary electroporation tip and were electroporated using the parameters recommended by the manufacturer for HeLa (1005 V, 2 pulse, 35 ms), and (4) immediately after electroporation, cells are placed into a 6 well plate containing 2 mL of pre-warmed culture media for cell recovery. Cells were only maintained in their proprietary electroporation buffer for a maximum duration of 20 min to preserve cell viability.

3.4.5 TriDrop Automation and Operation

The bottom plate of the triDrop device was placed on a pogo pin holder that has been propped to a height 20 cm above the benchtop using a chassis constructed from T-slotted aluminum extrusions purchased from McMaster-Carr (catalog #: 47065T101, Aurora, OH) and machined and assembled in-house. The system is connected to a 720 pixel, 30 frames-per-second camera (Skybasic, Houston TX.) to visualize droplet movements on the device (**Figure 8-1**). A 12-input card edge connector from Digikey (catalog #: 151-1410-ND, Thief River Falls, MI), was attached to the top plate of the triDrop device and connected via three leads (DMF ground, High Voltage DC, DC ground). Two DC leads were connected to an electroporation pulse circuit (**Figure 8-1**) and one lead was used to provide the electrical connection for the DMF ground. The electroporation circuit consisted of an 8 pin optocoupler (Model #: AQW216EH) purchased from Digikey was connected to a Z650-0.32-U DC power source (TDK-Lambda) and controlled by an Arduino Uno running a custom pulse generating program, creating custom pulses of varying amplitudes and durations (100 - 450 V_{DC}, 1-10 ms in duration). For automating droplet movement on the device, see our

previous published work for circuit and connectivity.[44] The electroporation and DMF actuation circuit were controlled by our in-house software which is available on our bitbucket registry (https://bitbucket.org/shihmicrolab/littleleung_2023). Droplet movements were programmed by application of AC potentials (300 – 400 V_{RMS}) at 15 kHz between the top and bottom plates. The DMF actuation software was also used to initiate the electroporation pulse circuitry to ensure immediate and uniform pulse application after triDrop merging.

3.4.6 TriDrop Electroporation

Prior to a triDrop experiment, HEK293, HeLa, Jurkat, and primary T-cells were centrifuged at 300 g for 3 min, washed twice with a custom 1SM buffer, and resuspended in Type T electroporation buffer. For experiments using dextran molecules, cells and dextran molecules were prepared at a final concentration of 2 x 10^7 cells/mL and 0.03 ng/cell respectively. For experiments with eGFP plasmid or mRNA, the payload was added to the cell sample to achieve a concentration of 1.275 pg/cell and 2 pg/cell respectively, with a final cell concentration of 4 x 10^7 cells/mL. For CRISPR knock-out experiments, per 1 million cells,100 pmol of sgRNA and 50 pmol of Cas9 were mixed and incubated at room temperature for 10 minutes to allow for the formation of Cas9 RNP. The Cas9 RNP was then immediately used or stored on ice until use, where it was then added to cells in electroporation buffer for a final concentration of 4 x10^7 cells/mL.

TriDrop operation included four droplet operations and were implemented using the triDrop automation system described previously. The four steps included: (1) reservoir filling, (2) triDrop dispensing, (3) triDrop merging, and (4) triDrop electroporation. The device consisted of three reservoirs: two outer reservoirs were filled with PBS containing 0.05 % Pluronics F-68 (which we refer to as high conductivity buffer, $\sigma \sim 16$ mS/cm) and the middle reservoir was filled with cells and the desired payload suspended in electroporation buffer containing 0.05 % Pluronics F68 surfactant. Reservoirs were filled by pipetting 6 µL each onto the bottom plate at the edge of the top plate and applying driving potentials to the three reservoir electrodes to draw the fluids into the reservoir. Next, ~1 µL single droplet was dispensed from each reservoir by pulling and necking the liquid out of the reservoir using a modified droplet dispensing system[219]. The cell containing droplet was actuated to the center of the electroporation site and the two high conductive droplets were actuated to the outer edges of the electroporation site. The three droplets were merged by actuating the high conductive droplets towards the cell containing droplet creating a continuous

three droplet structure. Immediately upon merging, the electroporation circuit was automatically triggered to deliver a sequence of high voltage DC square-wave pulses to the exposed Au-electrodes (on the top plate) that were in direct contact with the PBS droplets (see **Table 8-1** for triDrop electroporation parameters). For experiments using the uniform electroporation arrangement, all three reservoirs contained the same media with cells and payload suspended in either electroporation buffer or PBS with 0.05 % Pluronics F-68 surfactant. For experiments using the focused electroporation arrangement, all three reservoirs contain the same media (either electroporation buffer or PBS with 0.05 % Pluronics F68 surfactant), however only the middle reservoir contains cells and payload.

Immediately after triDrop electroporation, the top plate is removed, and the electroporated cells (total volume ~ 3 μL) were immediately removed from the chip via pipetting and placed in a well plate that was pre-loaded with warmed culture media. HEK293 and HeLa cells were cultured in flat bottom 48 well plates post electroporation for cell recovery. Jurkat and Primary T cells were cultured in a U-bottom 96 well plate post electroporation for cell recovery. All experiments with cells were incubated for a maximum time of 20 minutes in electroporation buffer to preserve optimal cell health.

3.4.7 Arrayed Gene Editing

An optimized gRNA design tool available from Synthego™ was used to design four unique gRNAs targeting the TRAC locus and were purchased from Synthego™ (see **Table 9-4** for sequences). The four unique guides were arranged into 10 unique combinations: four individual guides, four conditions containing any three gRNA combinations, one combination containing all four guides, and one non-targeting gRNA. Prior to reservoir filling on the device, all guide combinations were prepared in equal parts: 0.9 μL of each gRNAs (100 pmol/μL) combined with 1.2 μL of a Cas9 protein (30 pmol/μL) and were incubated for 10 minutes to form the RNP complex. 4 μL of primary T-cells (see Cell Culture section for preparation) in type T electroporation buffer of a density 4 x 10^7 cells/mL were mixed with 0.6 μL of the RNP complex in a PCR tube for each combination. Immediately after preparation, cells and the RNP complex solution as well as the high conductivity were loaded onto the device following the reservoir filling protocol above. TriDrop electroporation and post-electroporation procedures followed the protocol described above.

3.4.8 pH Measurements

Following previously established methods for analyzing pH change in microfluidic electroporators[98], DMF reservoirs were loaded with either high conductivity buffer (flanking reservoirs) or low conductivity media with HEK293 cells at a concentration of 2 x 10^7 cells/mL (middle reservoir) containing either phenolphthalein or Congo red to test the pH changes above 9.0 and between 3 – 5.2, respectively. The triDrop structure was formed following the procedure described above and 3, 200 V pulses 10 ms in duration were applied. Images of the droplets were taken every 1 s for 30 s using a wireless digital microscope (Skybasic, Houston, TX) to monitor colour changes in the middle droplet.

3.4.9 Current Measurements

Electrical current was measured by placing a 100 Ω shunt resistor in series and downstream of the triDrop top plate. An oscilloscope was connected across the shunt resistor and the voltage peak was recorded across the resistor during an application of the electric potential (after forming the triDrop structure). The system current was determined using the Ohm's law relationship ($I_{measured} = V_{peak}/100\ \Omega$).

3.4.10 Flow Cytometry

Viability, transfection efficiency (TE) and mean fluorescent intensity (MFI) were measured using a BD FACS Melody (BD Bioscience, Canada). The FACS was equipped with three excitation lasers (405 nm, 488 nm, 561 nm) in a 2B-2V-4YG configuration. For all experiments with dextran molecules, plasmids, or mRNA, cells were resuspended in 500 µL of culture media, washed by centrifuging (300 g, 5 min), and then resuspending in 1 mL FACS buffer (1x PBS, 1 mM EDTA, 25 mM HEPES, 1 % FBS, pH 7.0), then centrifuged (300 g, 5 min), aspirated, and resuspended in 600 µL of FACS buffer. For all samples, viability was assessed by staining dead cells using 0.6 µL of DAPI (50 ng/µL) added to the sample immediately prior to FACS and mixed thoroughly with the sample by pipetting. Dextran, plasmids, and mRNA were excited by a 488 nm laser and viewed through a 527/32 filter. DAPI was used as an indicator for dead cells and was excited by a 405 nm laser. Our gating protocol is shown in **Figure 8-17**. Briefly, a non-electroporated control containing payload was prepared using the above method and loaded into the FACS machine. First, the data was analyzed comparing forward scatter and side scatter to identify which data

points are cells. Next, the cell population was analyzed comparing side scatter height and side scatter width to identify singlets. Once singlets were identified, a histogram plot was generated for DAPI staining - separating living cells (DAPI negative) from dead cells (DAPI positive). Finally, the living cell population was used to generate a histogram showing FITC expression and this histogram was used to define the lower boundary of transfection with the gate being set to include ~1 % of the control population as transfected to account for endocytosis. For each condition, 15,000 events were collected at a rate of 100 events/s.

For CRISPR gene knockout experiments, cells were maintained in culture for 72 hours post-electroporation. Following maintenance, the cells were centrifuged (300 g, 5 min) and resuspended in 50 µL of culture media. 48 µL of culture media and 2 µL of Human TruStain FcX™ (Fc Receptor Blocking Solution, BioLegend catalog #: 422301) were mixed to prevent non-specific binding followed by 5 minutes of incubation at room temperature. After blocking, cells were spun down at 300 g for 5 minutes with the supernatant removed, resuspended in 98 µL of culture media plus 2 µL of FITC anti-human HLA-A,B,C Antibody (BioLegend catalog #: 311403) and incubated for an additional 20 minutes in the dark at 4 °C. After staining, the cells were then washed twice in 1 mL of FACS buffer, centrifuged (300 g, 5 min) to remove the supernatant, and resuspended in 600 µL of FACS buffer. Similar to above, FACS gates are determined by running a non-electroporated control to define normal β2M expression and electroporated samples are compared against the control.

3.4.11 Post-Electroporation Analysis

FACS data was analyzed using FlowJo (Ashland, OR). After gating out the doublets and cell debris, the viability was measured as the percentage of living cells (DAPI negative) from a sample. The viability ratio (VR) was then calculated as the ratio of the viability of electroporated sample to the non-electroporated cells (i.e., control).

$$VR = \frac{Viability_{electroporated}}{Viability_{Unelectroporated}} \; x \; 100$$

TE was calculated as the number of fluorescent living cells above the threshold divided by the total number of living cells.

$$TE = \frac{number\ of\ transfected\ living\ cells}{total\ number\ of\ living\ cells}\ x\ 100$$

The background fluorescence of the cells was defined by using samples with cells only with no electroporation.

MFI fold-change was calculated by measuring the mean fluorescent intensity for non-transfected control cells as shown previously[116]. This parameter measures a relative increase in brightness compared to a control.

$$MFI\ fold-change = \frac{MFI_{transfected\ cells}}{MFI_{untransfected\ cells}}$$

Relative cell increase was calculated by dividing the cell count on each day post-electroporation by the cell count from day 1 post-electroporation. The cell count was calculated by measuring the cell centration using T20 Automated Cell Counter (BioRad, CA) and the volume of culture medium in each well.

Knockout efficiency was determined by dividing the number of living cells below a fluorescence threshold by the total number of living cells.

$$Knockout\ Efficiency = \frac{number\ of\ living\ cells\ below\ fluorescence\ threshold}{total\ number\ of\ living\ cells}\ x\ 100$$

For visual analysis, 48 hours post electroporation, bright field and fluorescent images were taken a with 20x objective on an Olympus IX73 inverted microscope (Olympus Canada, Mississauga, ON, Canada) and a 100x objective on a Zeiss Axio Observer 7 with an excitation wavelength of 480 nm and a 470/40 nm excitation and 525/50 nm emission filter set (catalog # 49002, Chroma Technology Corporation, Bellows Falls, VT). The brightness and contrast of images were adjusted using ImageJ.

3.4.12 Statistical Analysis

Statistical analysis was performed using an ordinary one-way ANOVA with Prism V8.4 (Graphpad) with n = 3 replicates for **Figure 3-2** and **Figure 8-3**. For **Figure 3-2**, we obtained a F-value of 13.7, 20.73, and 6.4 for transfection efficiency, viability ratio, and mean fluorescence intensity, respectively with a Dfn of 4 and Dfd of 10. For **Figure 8-3**, we obtained a F-value of

97.23, 4.08, and 11.36 for transfection efficiency, viability ratio, and mean fluorescence intensity, respectively with a Dfn of 3 and Dfd of 8. For **Figure 3-6** statistical analysis was performed using an unpaired T test.

Chapter 4. A Digital Microfluidic Platform for the Microscale Production of Functional Immune Cell Therapies

This chapter is taken from a first author research article comparing our novel DMF cell engineering platform against two state-of-the-art commercially available electroporators. The following article thoroughly tests our hypothesis that miniaturized droplet-based electroporation can allow for a substantial reduction in reagent consumption while producing cells with improved viability and functionality compared to existing macroscale solutions. This chapter is adapted from the following publication: Samuel R. Little, Niloufar Rahbari, Fatemeh Gholizadeh, Mehri Hajiaghayi, Alison Hirukawa, Hugo Sinha, Fanny-Mei Cloarec-Ung, David JHF Knapp, Peter J. Darlington, and Steve C. C. Shih (2024) "A Digital Microfluidic Platform for the Microscale Production of Functional Immune Cell Therapies". It is currently under review at ACS Nano.

Abstract

Genetically engineering human immune cells has been shown to be an effective approach for developing novel cellular therapies to treat a wide range of diseases. To expand the scope of these cellular therapies while solving persistent challenges, extensive research and development is still required. Electroporation has recently emerged as one of the most popular techniques for inserting biological payloads into human immune cells to perform genetic engineering. However, several recent studies have reported that electroporation can negatively impact cell functionality. Additionally, the requirement to use large amounts of cells and expensive payloads to achieve efficient delivery can drive up the costs of development efforts. Here we use a digital microfluidic enabled electroporation system (referred to as triDrop) and compare against two state-of-the-art commercially available systems for the engineering of human T cells. We describe the ability to use triDrop for highly viable, highly efficient transfection while using substantially fewer cells and payload. Subsequently, we perform transcriptomic analysis on cells engineered with each of the three systems and show that electroporation with triDrop lead to less dysregulation of several functionally relevant pathways. Finally, in a direct comparison of immunotherapeutic functionality, we show that T cells engineered with triDrop have an improved ability to mount an

immune response when presented with tumor cells. These results show that the triDrop platform is uniquely suited to produce functionally engineered immune cells while also reducing the costs of cell engineering compared to other commercially available systems.

4.1 Introduction

Reprogramming the functionality of human T cells by inserting novel biological payloads has shown to be a promising avenue of therapeutic development.[65] Removing immune cells from a patient, functionally modifying the cells to fight disease, and reinjecting them into the patient has been shown as a viable treatment for both hematological cancers,[5,220,221] and solid cancers.[188] However, manufacturing of these therapies is challenging,[65] and a drawback with current available therapies is the lack of specificity can cause deleterious side effects.[11] Efforts have been made to engineer immune cells for improved targeting to avoid so called "on-target, off-tumour" toxicities.[222] However, developing cellular therapies for cancer that is affordable, as well as safe and efficient will require additional complex genetic engineering and substantial R&D.[64,223]

A key challenge in the cell engineering pipeline is the delivery of biological payloads across the cell membrane and into the cells, which must be done efficiently while preserving the viability, and functionality of the cells. There are a handful of recently reported techniques that can introduce payloads into cells either biologically (retroviruses,[71] lentiviruses,[72,73] herpes simplex virus,[74] adenovirus,[75] and adeno-associated virus),[76] chemically (cationic lipids,[83] lipid nanoparticles),[84] or physically (electroporation,[92] mechanoporation,[108] sonoporation,[224] or microinjection).[225] Concerns over immunogenicity, semi-random transgene integration, and cytotoxicity have resulted in viral transduction becoming less popular,[79,80] while low transfection efficiencies have led to decreased enthusiasm for chemical techniques.[82] Physical transfection techniques are becoming the preferred approach as they generate temporary nanopores in the cell membrane allowing the cargo suspended in the surrounding media to permeate the cell where it remains trapped after the pores heal.[89] Given that pre-clinical R&D is a substantial driver of cost and time when bringing a new cell therapy to market,[69] a platform capable of automating laborious procedures and processing numerous samples in parallel, while requiring only small inputs of cell and reagents per reaction could reduce the cost and length of many cellular therapy development programs. Currently, there are several popular commercially available platforms used for cell therapy, however these platforms either require performing each reaction serially (one-at-a-time)

for testing multiple conditions,[216] or require large cellular and reagent inputs,[201] which is expensive and at times requires pooling numerous donors together convoluting the data.

Microfluidic-based platforms are emerging as potential technologies for the physical transfection of human immune cells using techniques such as mechanical squeezing or compression,[107,108,110,116,194] fluidic shearing,[109,111] and electroporation.[112,193]A primary goal for this field has been to develop a platform capable of clinical-scale production, specifically, a device that is able to efficiently insert a single type of payload into cells while operating continuously with a throughput > 10^6 cells / minute.[105] Towards that goal, Weaver et al.[226] recently detailed the final results of phase 1 clinical trial where a microfluidic mechanoporation method was used to produce four doses per patient each containing upwards of 5 x 10^6 cells / kg for patients with HPV16+ solid tumours. Another example is the development of a viscoelastic-mechanoporation method from Sevenler et al.[109] capable of processing 2.5 x 10^8 cells / minute. These are important techniques for clinical manufacturing, but we are not aware of a robust, parallel microfluidics platform capable of inserting multiple unique payloads and conditions while minimizing the cost and consumption of each single reaction.

We previously published a novel three-droplet system that allowed for efficient electroporation (EP) of human T cells on a digital microfluidic (DMF) platform.[227] Our technique minimizes the generation of electrical current and protects the cells from harmful electrochemical reactions that can occur during EP. Further, our proposed platform (referred to as triDrop) required < 50,000 cells per reaction and by using the multiplexing capabilities of DMF, numerous reactions can be performed in parallel. However, a major drawback of electroporation is that cells engineered via EP have been shown in the past to suffer from impaired functionality and genetic dysregulation post transfection.[94,95,105] Here, we use our triDrop electroporation system and compare against two commercially available state-of-the-art electroporation systems: Invitrogen Neon Electroporation System™ (hereby referred to as the Neon), and the Lonza 4D-Nucleofector™ (hereby referred to as the Nucleofector). Herein we describe how triDrop efficiently transfects reduced amounts of cells while using less payload compared to the Neon and Nucleofector systems. Additionally, triDrop can deliver both simple (mRNA) and complex (CRISPR gene-editing reagents) payloads with improved viability and proliferation capabilities after EP. We conducted a transcriptomic analysis to benchmark triDrop, revealing that cells

engineered with triDrop exhibit significantly less genetic dysregulation compared to using Neon and Nucleofector. Finally, we show a proof-of-concept immunotherapeutic assay, demonstrating that the triDrop platform is uniquely suited as a miniaturized platform for the research and development of novel immunotherapies.

4.2 Results and Discussion

4.2.1 Comparing Electroporation Platforms

We analyzed three electroporation (EP) systems that are schematically overviewed in **Figure 4-1a-c**. **Figure 4-1a** is the Invitrogen Neon Electroporation System™ (Neon)[97], the system operates by placing 10 µL (or 100 µL) of cells and payload suspended in EP buffer inside a capillary tube with an anode placed at the top of the capillary tube and the bottom submerged in an electrolytic buffer that is in contact with a cathode. Applying a voltage across the anode and the cathode generates an electric field throughout the capillary tube. **Figure 4-1b** is the Lonza 4D-Nucleofector and it operates by placing 20 µL of EP buffer containing cells and payload into a cuvette with parallel anode and cathode. The sample is placed directly between the electrodes and a voltage is applied. **Figure 4-1c** is a recently published,[227] droplet-based, electroporation system that relies on digital microfluidics hereby referred to as the triDrop system. The triDrop operates by merging three 1 µL droplets into a sequential chain, the outer droplets are comprised of a high conductivity media (~ 16 mS / cm) and the inner droplet is comprised of low conductivity buffer (~ 8 mS / cm) and contains cells and payload. We previously demonstrated that by placing the anode and cathode in contact with the outer droplets and applying a voltage, a homogenous electric field is generated across the inner droplet inserting the payload into the cells while protecting the cells from excessive current generation and harmful electrolytic byproducts often found at the anode and the cathode during electroporation. The Neon and Nucleofector have been shown extensively for transfection of primary human T cells, however we propose that the triDrop can offer two key advantages over these existing systems. First, is the ability to achieve high performance transfection while using fewer cells and less payload providing up to a 20-fold reduction in the overall cost of T cell engineering (**Table 9-1**). In addition, using lower quantities of cells per reaction enables larger libraries to be tested on a single donor and opens the possibility

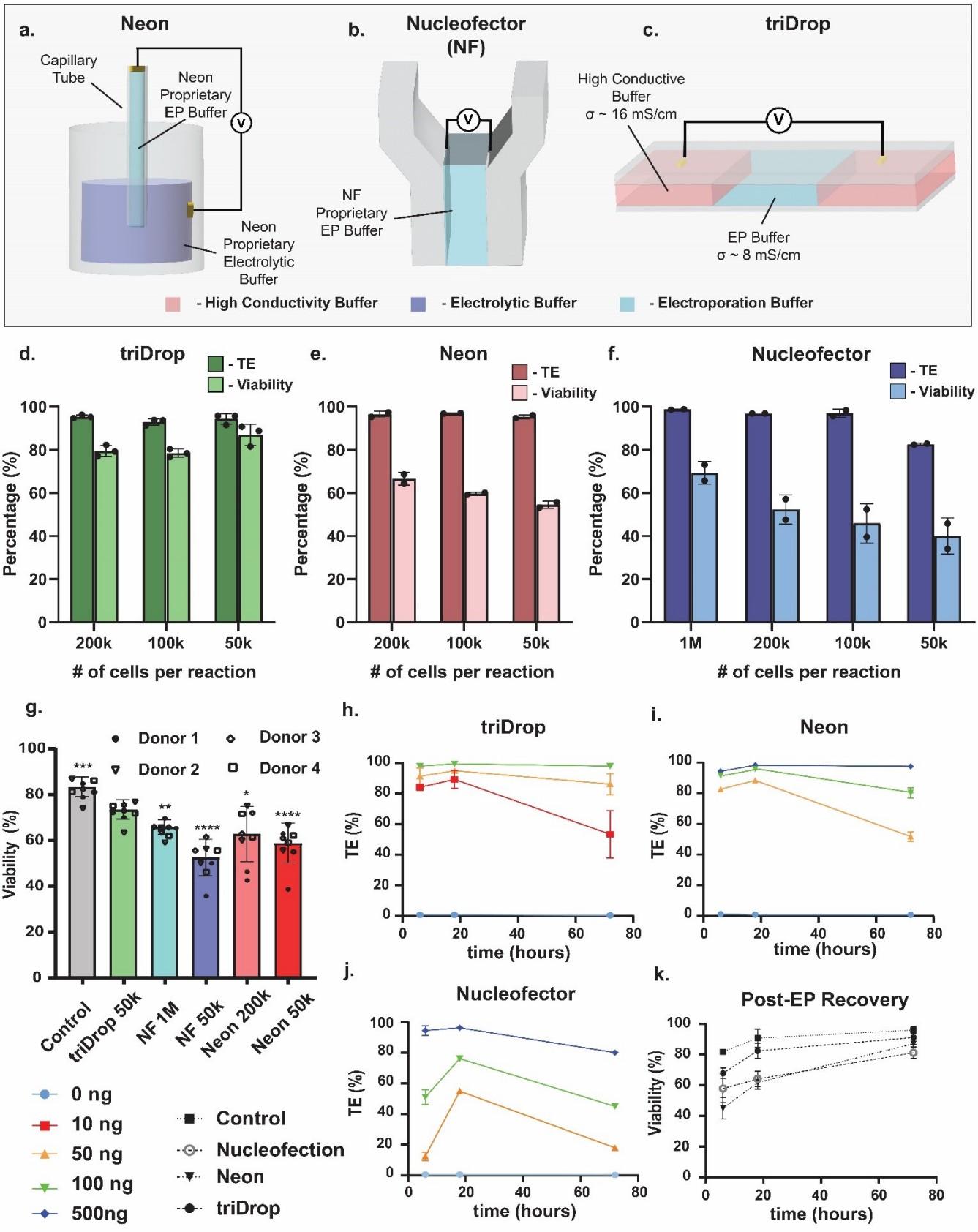
a.
Neon
Capillary Tube
Neon Proprietary EP Buffer
V
Neon Proprietary Electrolytic Buffer
b.
Nucleofector (NF)
V
NF Proprietary EP Buffer
c.
triDrop
High Conductive Buffer
σ ~ 16 mS/cm
V
EP Buffer
σ ~ 8 mS/cm
- High Conductivity Buffer
- Electrolytic Buffer
- Electroporation Buffer
d.
triDrop
- TE
- Viability
Percentage (%)
200k
100k
50k
# of cells per reaction
e.
Neon
- TE
- Viability
Percentage (%)
200k
100k
50k
# of cells per reaction
f.
Nucleofector
- TE
- Viability
Percentage (%)
1M
200k
100k
50k
# of cells per reaction
g.
Donor 1
Donor 2
Donor 3
Donor 4
Viability (%)
Control
triDrop 50k
NF 1M
NF 50k
Neon 200k
Neon 50k
0 ng
10 ng
50 ng
100 ng
500ng
Control
Nucleofection
Neon
triDrop
h.
triDrop
TE (%)
time (hours)
i.
Neon
TE (%)
time (hours)
j.
Nucleofector
TE (%)
time (hours)
k.
Post-EP Recovery
Viability (%)
time (hours)

*Figure 4-1: **Three electroporation systems**. Schematic overview of three electroporation systems used in this work where a) Neon, b) Nucleofector, and c) triDrop. Bar graphs depicting transfection efficiency (TE; dark colours) and viability (light colours) when performing electroporation using varying numbers of cells per reaction for d) triDrop, e) Neon, and f) Nucleofection. g) Viability measurements taken six hours post-EP for cells electroporated using either the manufacturer recommended number of cells or 0.5 x 105 cells per reaction. Four donors (shown as polygons) were used for this study with two technical replicates. Statistical significance markers represent comparison between triDrop and all other conditions (n = 8). Line graphs depicting transfection efficiency over 72 hours post-EP when using 10 ng (red line), 50 ng (orange line), 100 ng (green line) and 500 ng (blue line) of mRNA for h) triDrop, i) Neon, j) Nucleofection. k) Line graph depicting viability over 72 hours post-EP for cells electroporated with all three EP systems and a control. All error bars represent mean ± 1 SD. Statistical n.s indicates no significant difference, *, **,***, and **** represent p-values below 0.05, 0.01, 0.001 and 0.0001 respectively. Statistical analysis was performed using a Student's t-test.*

to perform electroporation with rare cell types. Second, by limiting the exposure of cells to excessive electrical current and harmful electrolytic byproducts (such as pH changes as a result of the reduction and oxidation of water molecules, chlorine and hydrogen gas bubbles, and metal ions),[101] the health and functionality of the cells can be preserved post-electroporation. It has been shown that joule heating as a result of electrical current, and exposure to electrolysis are significant contributing factors to cell death as a result of EP,[96] and that cell death increases as the cells get closer to the anode and cathode[98]. The triDrop was specifically designed to isolate cells away from the anode and cathode, reducing exposure to the electrolytic byproducts, and to create a highly resistive environment limiting the generation of electrical current.[227] Further, using fewer cells than the recommendation given by the Neon and Nucleofector would reduce the overall electrical resistance of their system, leading to increased electrical current during pulsing and potentially more joule heating and severe electrolysis.[99]

We hypothesize that the triDrop platform has the ability to use fewer cells per reaction to achieve high transfection efficiency and cell viability post-electroporation. To test this hypothesis, three primary T-cell concentrations (0.5, 1, and 2 x 10^5 cells per reaction) were electroporated with an eGFP-mRNA payload using one out of the three systems. As shown in **Figure 4-1d**, we found that while all three platforms were able to deliver mRNA molecules with efficiencies > 95 %, the triDrop had the highest reported viability as measured 18 hours post electroporation. The triDrop maintained viabilities above 80 % for 1, 2 x 10^5 cell conditions and 85 % viability for electroporation reactions using 0.5 x 10^5 cells. In comparison, **Figure 4-1e** and **4-1f** show the Neon and Nucleofector achieved peak viabilities of ~ 65 % (in line with previously published results[228]) when using the manufacturer recommended condition (1 x 10^6 cells per reaction for Nucleofection, and 2 x 10^5 cells per reaction for Neon). Interestingly, reducing the number of cells per reaction results in decreasing viabilities for both the Neon and the Nucleofector, achieving ~ 60 % and ~ 45 % viability respectively for EP reactions when using only 0.5 x 10^5 cells per reaction

(**Figure 4-1g**). To validate the effects of using reduced cell amounts on viability, we conducted EP using either the recommended number of cells or 0.5 x 10^5 cells per reaction and measured viability 6 hours post-EP. While all systems led to a reduction in viability compared to the control, the triDrop system showed a significant improvement in viability in comparison to the Neon and Nucleofector regardless of how many cells were used. In addition, reducing the number of cells used by the Nucleofector leads to a significant reduction in viability (65 % vs. 51 %, P = 0.001), which could be related to our hypothesis of high current generation and electrolysis.

Next, we investigated the effects of using differing amounts of payload per reaction on transfection efficiency and viability. Cells were electroporated with a range of mRNA amounts using one of the three systems at their optimal cell concentrations (0.5 x 10^5 cells for triDrop, 2 x 10^5 cells for Neon, and 1 x 10^6 cells for Nucleofector) and were analyzed with flow cytometry after 6, 18, and 72 hours. **Figure 4-1h-j** shows line graphs depicting transfection efficiency for each condition over 72 hours following EP. While the Neon and triDrop perform similarly, the Nucleofector requires approximately 10 times as much payload to achieve results comparable to the triDrop (500 ng vs 50 ng). In fact, the triDrop achieved > 80 % transfection efficiency while using the lowest tested amount of mRNA (10 ng). Furthermore, **Figure 4-1k** shows the measured viability of each system over 72 hours when using 100 ng of mRNA per reaction for the triDrop, 500 ng for Neon, and 1000 ng for Nucleofection (optimal amounts based on the results from **Figure 4-1h-j**). The data confirms that the triDrop has the highest viability of the three systems and by 18 hours post-EP cells treated with the triDrop have a viability of > 80 % compared to a viability of ~ 60 % (consistent with results shown in **Figure 4-1d-f**). It is only after 72 hours post-electroporation that all three systems have a recovered viability > 80 %. When the cells are permeabilized by EP, the concentration gradient between the surrounding environment and the inside of the cell leads to payload being driven through the pores across the cell membrane.[229] TriDrop uses smaller volumes for the system (electroporated volume of ~ 1 µL), and as such, substantially less payload is required to achieve concentrations optimal for insertion into the cell.

4.2.2 Knockout and Knock-In Gene Editing Efficiency

The well-characterized CRISPR system has been used for engineering human immune cells to create new cellular immunotherapies.[201] Additionally, screening large libraries of CRISPR edits

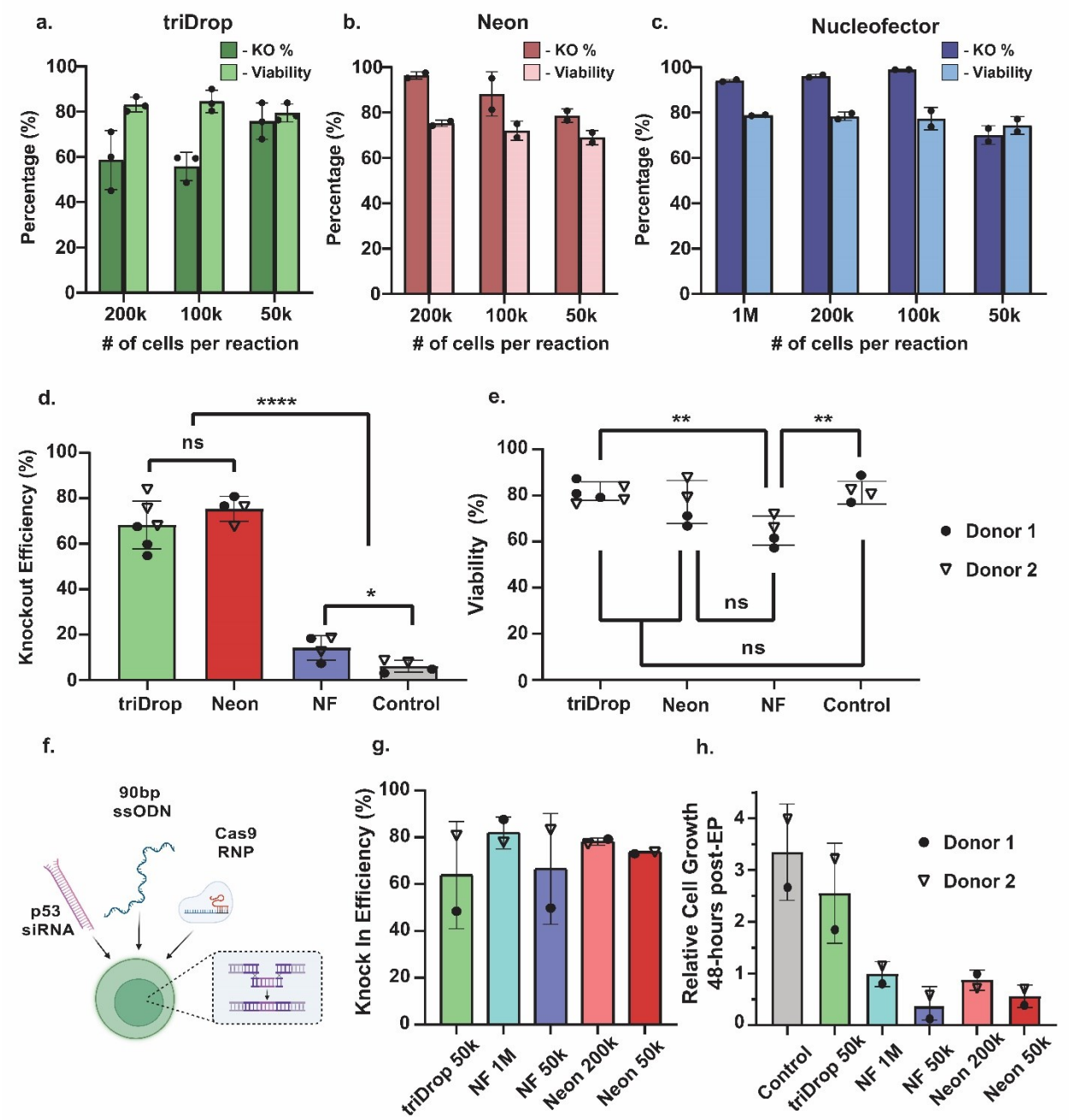

Figure 4-2: ***Gene editing.*** *Bar graphs depicting knockout efficiency (dark colours) and viability (light colours) measured four days post EP when electroporating varying amounts of cells per reaction when using a) triDrop, b) Neon, and c) Nucleofector. Bar graphs showing d) knockout efficiency and e) viability for 0.5 x 10^5 cells electroporated with 2.5 pmol of RNP using the three EP systems (n = 4 - 6). f) Schematic showing the payloads required for CRISPR knock-in (created with BioRender.com). Bar graphs showing g) knock-in efficiency and h) relative cell growth post EP for two donors electroporated using manufacturer recommended number of cells or 0.5 x 10^5 cells per reaction. All error bars represent mean +/- 1 SD. Statistical n.s indicated no significant difference, *, **,***, and **** represent p-values below 0.05, 0.01, 0.001 and 0.0001 respectively. Statistical analysis was performed using a Student's t-test.*

has been shown as a successful avenue for immunotherapeutic discovery.[216] The first step for such an application is to use delivery methods (such as electroporation) to introduce gene-editing components into cells. First, we investigated the performance of all three systems to conduct

CRISPR knockouts targeting the TRAC locus. A range of cell concentrations were electroporated with an sgRNA cocktail complexed with a Cas9 protein to form a ribonucleic protein (RNP) and knockout efficiency was evaluated by staining with an anti-human alpha-beta TCR antibody and analyzed with flow cytometry four days post transfection. **Figure 4-2a-c** show the effects of knockout with all three systems using 0.5, 1, 2 x 10^5 cells per reaction as well as a 1 million cell condition for the Nucleofector. In these experiments, RNP was normalized to the reaction volume to ensure consistent payload concentration as recommended by Hultquist et al.[230] and Oh et al.[231] and was added at a ratio of 50 pmol per 20 µL of reaction.. The triDrop achieved an optimal knockout efficiency of 75 % with a viability of 80 % when using 0.5 x 10^5 cells per reaction, and the Neon and Nucleofector were both able to achieve knockout efficiencies ~ 95 % when using higher numbers of cells. However, decreasing cell amounts to 0.5 x 10^5 cell per reaction led to the efficiency dropping to 78 % and 70 % respectively.

Given the substantial volume differences between the three systems, adding payload in proportion to volume leads to a significant difference in the total amounts of Cas9 enzymes and sgRNA needed per reaction (i.e. 50 pmol of RNP for 1 nucleofection reaction vs 2.5 pmol for 1 triDrop reaction). To account for this difference, we tested conditions by normalizing payload to the number of cells being electroporated via addition of 50 pmol of RNP for every 1 million cells being used as recommended by Roth et al.[201] We found that when using the Nucleofector, decreasing the payload in proportion to the number of cells being electroporated led to a decrease in knockout efficiency suggesting that volumetric normalization is more important than cellular normalization for achieving high delivery efficiency (**Figure 9-1**). **Figure 4-2d** and **e,** show a side-by-side comparisons of two donors when electroporating only 0.5 x 10^5 cells with 2.5 pmol of Cas9 RNP. Both the Neon and the triDrop were able to achieve 75 % and 68 % knockout efficiency respectively with no significant difference between the two ($p = 0.26$), however, the Nucleofector was only able to achieve 14 % knock out efficiency with these conditions, which is significantly lower than the other two systems ($p < 0.0001$). Additionally, we observed that the decreased number of cells had a significant impact on the health of cells electroporated with the Nucleofector even after four days of recovery. Compared to the control the triDrop and Neon, both had no significant differences in cell viability ($p = 0.67$, and $p = 0.3$ respectively) whereas the Nucleofector had viabilities significantly less than both the control ($p = 0.004$) and cells treated

with the triDrop ($p = 0.0008$). These show further evidence that the triDrop system can achieve efficient editing while requiring significantly less expensive payload.

After validating triDrop as a reliable method for knockout, we introduced donor templates to perform CRISPR knock-ins using the three methods. We followed a recent protocol published by Cloarec-Ung et al.[232], which involved simultaneously co-delivering a Cas9 RNP targeting the SRSF2 gene, a 90 bp ssODN HDR-template, and an siRNA molecule targeting p53 (**Figure 4-2f**; all sequences in **Table 9-2**). Cells from two donors were electroporated using the Neon with 0.5 and 2 x 10^5 cells per reaction, the Nucleofector using either 0.5 or 10 x 10^5 cells per reaction, or the triDrop with 0.5 x 10^5 cells per reaction. The amount of payload was normalized to the reaction volume such that the Nucleofector and Neon used 20- and 10-times more payload than the triDrop respectively. Cells were collected 48 hours post EP and the total number of viable cells were counted prior to being lysed and prepared for knock-in confirmation via Sanger sequencing. **Figure 4-2g** shows that all systems achieve average knock-in efficiencies of > 60 % and up to 80 % insertion efficiency, which is in line with recently published results.[233] Interestingly, as shown in **Figure 4-2h,** we observed that the cells electroporated with the triDrop had proliferation capacities most similar to the control (2.5 fold increase in total viable cells vs 3.3 fold increase respectively), and more surprisingly, Nucleofector and Neon showed minimal proliferation post-EP. When using only 0.5 x 10^5 cells per reaction, these systems showed a reduction in proliferative capacity, a 0.3 and 0.5 fold-change respectively in total viable cells demonstrating that using fewer cells with these commercial systems leads to impaired proliferation capabilities. These data suggest that all three systems can transfect both easy-to-deliver (mRNA) and hard-to-deliver payloads (Cas9 RNPs + HDR templates). However, the triDrop offers substantial improvements in both cell viability and proliferation capacity immediately after electroporation as well as requiring significantly less payload (at least 10x) and fewer cells.

4.2.3 Transcriptomic Analysis

The triDrop was developed to perform the efficient electroporation of primary human T cells for the purposes of developing and testing cellular therapies. To this end, it is important that cells engineered with the triDrop maintain their functionality following electroporation. To test for

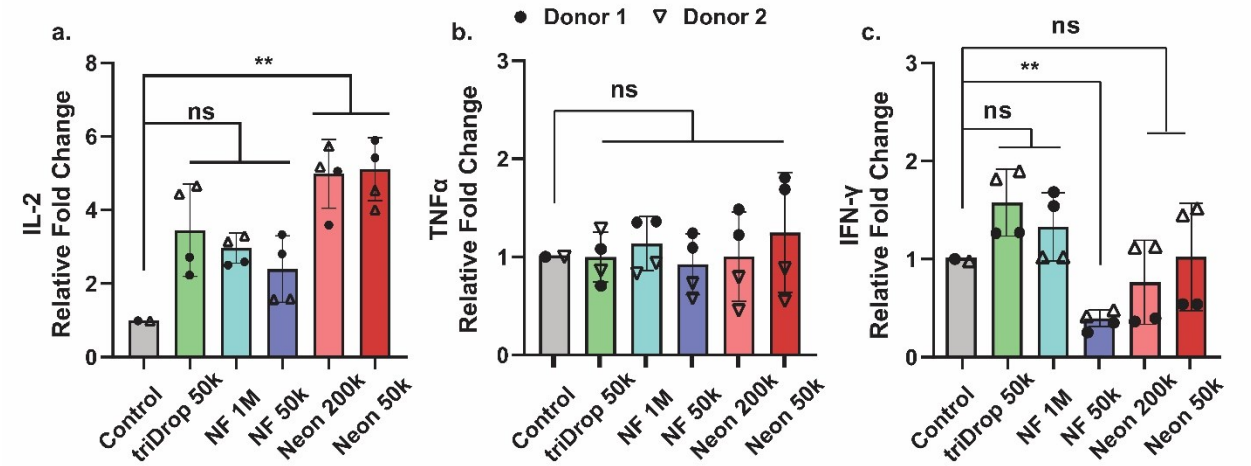

*Figure 4-3: qPCR examination of key genes for cellular therapies. Bar graphs showing relative gene expression (2^(-ΔΔCt)) 6 hours post EP for two donors electroporated using manufacturer recommended number of cells or 0.5 x 105 cells per reaction for a) IL-2, b) TNF-α, and c) IFN-γ. All error bars represent mean +/- 1 SD. Significance n.s indicates no significant difference, and ** represents p-values below 0.01. Statistical analysis was performed using a Student's t-test. (n = 4).*

these effects, we carried out transcriptional profiling of human T cells post-electroporation. In the first type of test, we used qPCR to look at critical cytokines (IL-2, TNF-α, and IFN-γ) in the immune system that play significant roles in cellular therapies.[234] Dysregulation of these genes lead to non-specific response or an impaired response in the presence of a target antigen.[235,236] Cells were electroporated in all three systems using either manufacturer recommended conditions or 0.5 x 10^5 cells per reaction and RNA was recovered from the cells 6 hours post EP. As shown in **Figure 4-3a-c**, cells treated with the triDrop shows no significant dysregulation in any of the three examined genes. Cells treated with the Neon, regardless of the number of cells used, shows no significant dysregulation of TNF-α, and IFN-γ, but there is a significant upregulation of IL-2 (relative fold change of 4.99, P = 0.005, and 5.11 P = 0.003) compared to the control. Similarly, when using the Nucleofector, cells treated with the manufacturer recommended conditions showed no dysregulation of the three genes, however, when using 0.5 x 10^5 cells per EP reaction, IFN-γ was significantly downregulated (relative fold change of 0.38, P = 0.0006), indicating that cells electroporated under this condition may experience a reduced capacity to secrete this important cytokine. Intrigued by the results above, we used RNA sequencing to examine the entire transcriptional landscape of cells treated with all three systems. Electroporated cells from three different donors using the manufacturer recommended conditions for the Neon and Nucleofector and using 0.5 x 10^5 cells per reaction for the triDrop were used to study the differential expression of genes between treated samples and a control.

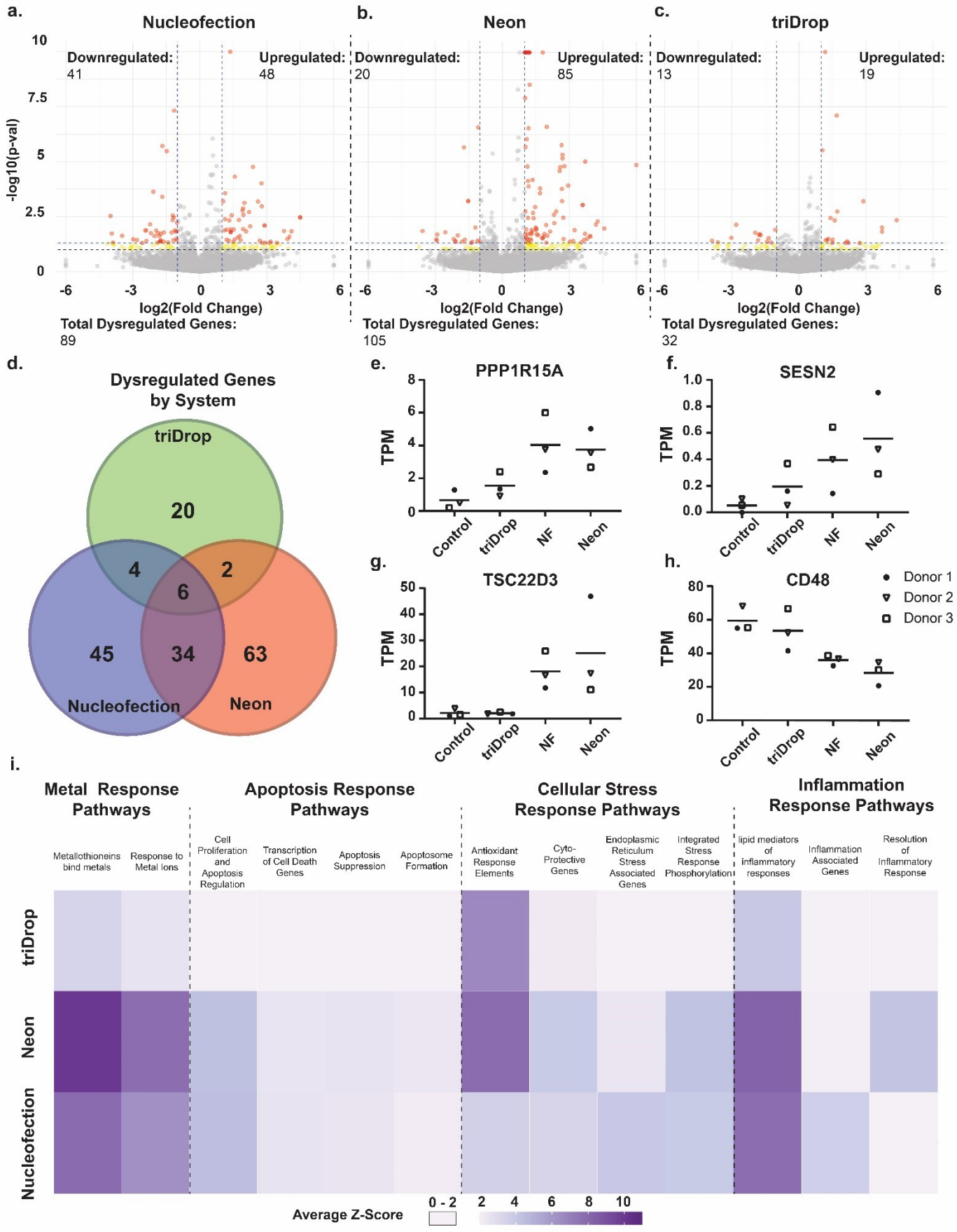
a.
Nucleofection
Downregulated: 41
Upregulated: 48
-log10(p-val)
log2(Fold Change)
Total Dysregulated Genes: 89
b.
Neon
Downregulated: 20
Upregulated: 85
log2(Fold Change)
Total Dysregulated Genes: 105
c.
triDrop
Downregulated: 13
Upregulated: 19
log2(Fold Change)
Total Dysregulated Genes: 32
d.
Dysregulated Genes by System
triDrop
20
4
2
6
45
34
63
Nucleofection
Neon
e.
PPP1R15A
TPM
Control
triDrop
NF
Neon
f.
SESN2
TPM
g.
TSC22D3
TPM
h.
CD48
TPM
Donor 1
Donor 2
Donor 3
i.
Metal Response Pathways
Apoptosis Response Pathways
Cellular Stress Response Pathways
Inflammation Response Pathways
Metallothioneins bind metals
Response to Metal Ions
Cell Proliferation and Apoptosis Regulation
Transcription of Cell Death Genes
Apoptosis Suppression
Apoptosome Formation
Antioxidant Response Elements
Cyto-Protective Genes
Endoplasmic Reticulum Stress Associated Genes
Integrated Stress Response Phosphorylation
lipid mediators of inflammatory responses
Inflammation Associated Genes
Resolution of Inflammatory Response
triDrop
Neon
Nucleofection
Average Z-Score
0 - 2
2
4
6
8
10

Figure 4-4: ***Transcriptomic analysis.*** *Volcano plots depicting p-values and fold change for individual genes for cells from three different donors 6 hours post EP when electroporated with a) Nucleofection, b) Neon, and c) triDrop. Genes with a log fold change > 1 or < -1 with a p value < 0.05 (red dots) and < 0.1 (yellow dots) are highlighted. d) Venn diagram showing the number of genes that are uniquely dysregulated or mutually dysregulated between the three EP systems. Transcripts per million (TPM) values for three donors comparing the control, triDrop, Nucleofector, and Neon for e) PPP1R15A, f) SESN2, g) TSC22D3, and h) CD48. i) Heatmap showing the average Z-scores for 13 selected pathways for cells electroporated with all three EP systems.*

Figures 4-4a-c show volcano plots depicting the differential gene expression for all three electroporation systems compared to the control (with no electroporation). The x-axis depicts the log fold change of expression with the left and right displaying down- or up- regulated expression respectively, and the y-axis depicting the confidence in the gene expression changes represented by $-\log_{10}$(p-values). Using the cut-off metrics of > 1 or < -1 log fold change and a p–value of 0.05, we sorted genes into the categories of significantly dysregulated (red dots) or non-significant genes (grey dots). In addition, genes meeting the less stringent condition of p–values < 0.1 are shown as yellow dots. Based on these cutoffs, the Neon shows a dysregulation of 105 genes, the Nucleofector showing 89 genes, and only 32 genes for the triDrop. A principal component analysis showed the triDrop to be most similar to control cells (**Figure 9-4**). To understand these results, we classified them by grouping the genes that are commonly dysregulated between the systems **(Figure 4-4d)**. Six genes are commonly dysregulated between all systems and are shown in **Table 9-3.** Interestingly, 34 genes are commonly dysregulated between the Neon and the Nucleofector but not dysregulated with the triDrop. A collection of four such genes are highlighted in **Figure 4-4e-h**. The first two genes, PPP1R15A (2.7- and 2.8-fold increase for Neon and Nucleofector respectively), and SESN2 (3.6- and 2.9- fold increase for Neon and Nucleofector respectively), are implicated in integrated stress response pathways with SESN2 being implicated in pathways responding to oxidative DNA damage[237] and PPP1R15A encoding for the growth arrest and DNA damage inducible protein.[238] The upregulation of these two genes may partially explain the reduced viability and proliferation seen by cells electroporated with the Neon and the Nucleofector. The two other genes are TSC22D3 (2.9- and 2.4-fold change for Neon and Nucleofector respectively) and CD48 (-1.7- and -1.4-fold change for Neon and Nucleofector respectively) which are both known to affect the functionality of immune cells especially in the context of immunotherapy. First, TSC22D3 encodes for an anti-inflammatory molecule that is known to have immunosuppressive effects.[239] The upregulation of this gene has been shown to compromise anti-tumour immunity in mice[240] and corresponds with non-responsiveness in anti-CD19 CAR T trials in humans.[241] Second, CD48 is a crucial member of lymphocyte activation and down regulation of this gene may impair the ability of T cells to respond to antigen presenting cells.[242] Therefore,

these two genes could impair the ability of cells engineered with the Neon and Nucleofector to adequately perform in immunotherapeutic assays.

For a more complete understanding of how genes were dysregulated in response to EP, all genes were assigned a z-score to quantify the different levels of expression relative to the control. Genes were then grouped into high level genetic pathways using the Reactome data base[243] and the average z-score for the whole pathway was calculated. Out of the ~ 2600 pathways analyzed, the triDrop showed a dysregulation of 79 pathways (defined as a pathway with an average z-score > 2.0 or < -2.0), the Neon with 130, and the Nucleofector showing 134. **Figure 4-4i** summarizes a collection of noteworthy pathways that are further documented in **Table 9-4.** As shown, all systems upregulate pathways responding to metal ion contaminates with the lowest z-score of upregulation shown by the triDrop. It is known that metal particulates can be secreted from the anode and cathode during electrolysis.[101] The difference in z-scores observed for these pathway may be due to the Neon and Nucleofector placing cells in direct contact with at least one electrode whereas the triDrop isolates cells from both limiting contact with metal contaminates. Additionally, the Neon and the Nucleofector upregulate pathways corresponding to apoptosis and cellular stress which may further explain earlier data showing reduced viabilities and proliferation capabilities for cells treated with these systems. Finally, we observed upregulation of three inflammation pathways which are minimally upregulated or not upregulated with the triDrop. Upregulation of these pathways is concerning for cells being engineered for immunotherapy applications because chronic inflammation is known to lead to premature T cell exhaustion[244] which can impair the function of CAR T cells.[12]

In summary, it is evident that cells engineered with the triDrop system have fewer dysregulated genes and dysregulated pathways relative to the Neon and Nucleofection systems. Using the Neon or Nucleofector, up-regulates genes and pathways associated with cellular stress, impairment of anti-tumour activity, as well as inflammation, which are either not upregulated or are minimally upregulated in cells engineered with the triDrop.

4.2.4 Functional CAR-T assays

A final series of experiments was performed to highlight the triDrop's ability to engineer cells with immunotherapeutic capabilities. As a model system, T-cells were engineering to express an anti-CD19 CAR molecule (**Figure 4-5a**). Cells were electroporated using either manufacturer

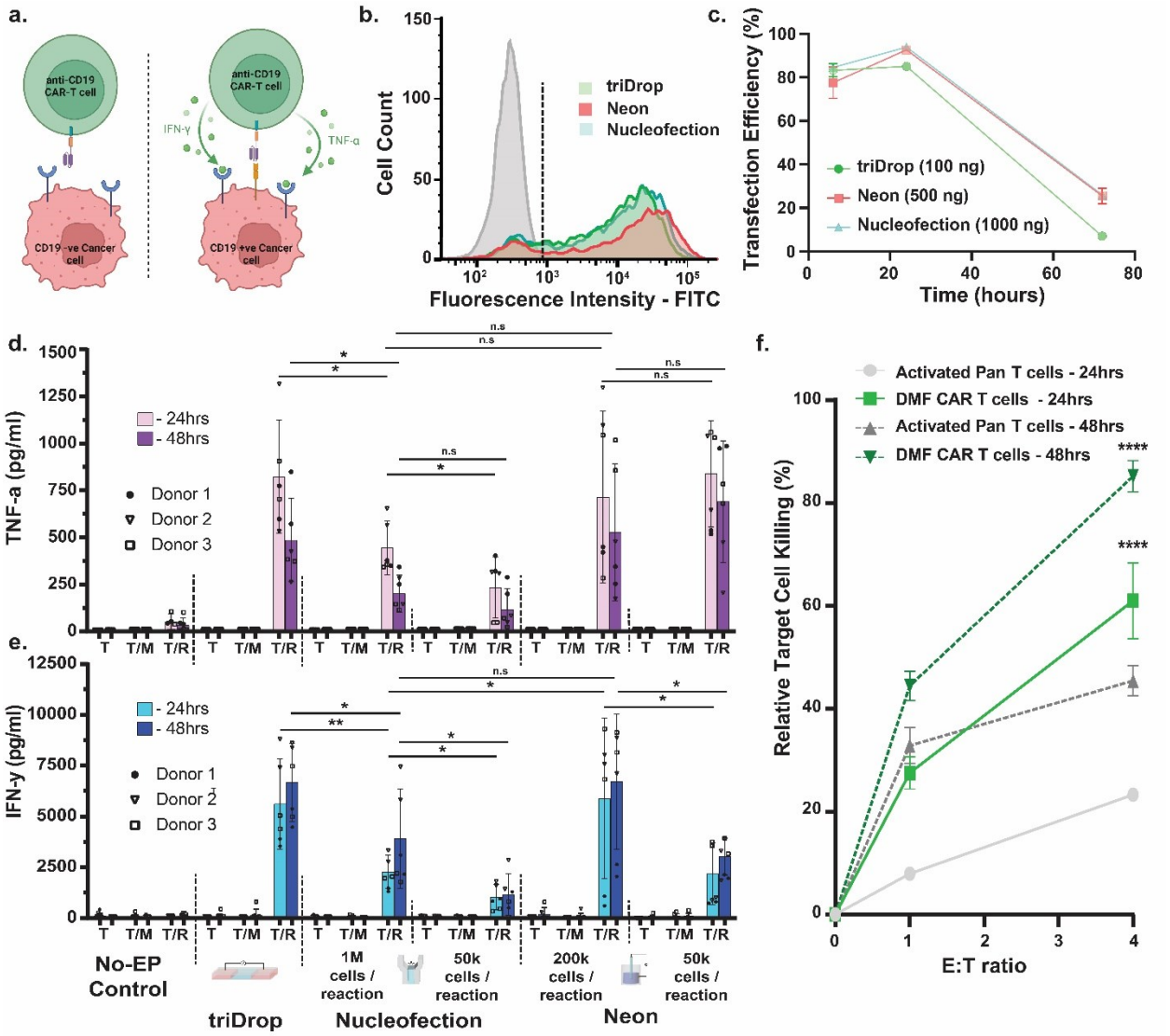

Figure 4-5: ***Functional CAR-T assays.*** *a) Overview of immunotherapeutic testing assay detailing an anti-CD19 CAR T cell interacting with a CD19 negative or positive tumor cell line. Created with BioRender.com. b) Fluorescence intensity histograms showing FITC expressions for cells stained with a FITC-tagged CD19 protein from a control (grey), triDrop (green), Nucleofection (blue), and Neon (red). c) Line graphs depicting expression of an anti-CD19 CAR molecule at 6, 24, and 72 hours post EP when using the triDrop (green, 100ng of mRNA), Neon (red, 500ng of mRNA), and Nucleofection (blue, 1000ng of mRNA). Bar graphs depicting measured levels of d) TNF-α and e) IFN-γ after 24 hours (light purple and light blue) and 48 hours (dark purple and dark blue) of culture for cells electroporated using all three systems using either manufacturer recommended conditions or 0.5 x 10^5 cells per reaction. Engineered cells are either cultured by themselves (T), or at a 1:1 ratio with MCF-7 cells (T/M), or with Raji cells (T/R). (n = 6) f) Line graphs depicting relative killing of Raji cells cocultured with activated Pan T cells at 1:1 ratio and 4:1 ratio after 24 hours (light grey, solid line) and 48 hours (dark grey, dashed line) or with triDrop engineered CAR T cells at a 1:1 and 4:1 ratio after 24 hours (light green, solid line), and 48 hours (dark green, dashed line). Statistical significance markers indicate difference between engineered cells and activated pan T cells for each timepoint. (n = 4). All error bars represent mean +/- SD. n.s indicated no significant difference, *, **,***, and **** represent p-values below 0.05, 0.01, 0.001 and 0.0001 respectively. Statistical analysis was performed using a student's t-test.*

recommended conditions or 0.5 x 10^5 cells per reaction with an anti-CD19 CAR mRNA payload. We used optimal amounts of payload for each system (see **Figure 4-1**) and used flow cytometry to validate the delivery of the mRNA payload. **Figure 4-5b** shows the expression of the anti-CD19

protein by staining electroporated cells with a FITC-tagged CD19 protein. The expression of the CAR protein was > 80 % for all systems 6 hours post EP and peaked at 24 hours, then slowly declined over the subsequent two days (**Figure 4-5c**). Therefore, for the functionality assays, 6 hours post EP, 2.5 x 10^4 engineered T-cells were cultured by themselves, or co-cultured with either 2.5 x 10^4 MCF-7 cells (CD19-negative) or 2.5 x 10^4 Raji cells (CD19-positive). **Figure 4-5 d and e** show bar graphs depicting the cytokine levels of IFN-γ and TNF-α in the supernatant for cells under various treatments and culture conditions after 24 hours and 48 hours of co-culture. None of the engineered cells produced either of the anti-tumour cytokines when cultured by themselves or in the presence of CD19 negative cells, indicating a highly specific response of the anti-CD19 CAR. When cultured with CD19-positive targets, cells engineered with the triDrop show significantly increased production of both IFN-γ (24 h: $p = 0.006$, 48 h: $p = 0.05$), and TNF-α (24 h: $p = 0.02$, 48 h: $p = 0.016$), compared to cells engineered with the Nucleofector when using with manufacturer recommend conditions. Cells engineered with the Neon also have higher cytokine production than Nucleofection but lack statistical significance across the 24 and 48 h timepoints. Additionally, using 0.5 x 10^5 cells per reaction with the Nucleofector leads to a significant reduction in cytokine production capabilities. This aspect suggests that the Nucleofector impairs immune function immediately following EP (as seen by the transcriptional sequencing data) and that attempting to use fewer cells than recommended by the manufacturer further exacerbates this impairment. While the Neon was able to produce similar average levels of cytokines compared to triDrop, the response was highly variable across donors. Further, similar to the Nucleofector, using 0.5 x 10^5 cells per reaction with the Neon surprisingly led to a significant reduction in the cells' ability to produce IFN-γ (although not TNF-α). This suggests that, as hypothesized, using either the Neon or the Nucleofector with fewer than recommended cells lead to those cells having impaired functionality.

Finally, we test the ability to use cells engineered with our triDrop platform for killing Raji cells in co-culture. For this experiment, 2.5 x 10^4 Raji cells were co-cultured with either 2.5 x 10^4 or 10 x 10^4 triDrop generated CAR T-cells or non-electroporated activated pan T cells. Coculture began 6 hours post EP. After 24 and 48 hours of co-culture, cells were collected and analyzed via flow cytometry by staining CD3 antibodies to separate target cells and effector cells and DAPI was used to differentiate living and dead cells. **Figure 4-5f** shows, as expected, the activated pan T cells elicit a small cytotoxic effect on the Raji cells, leading to ~23 % (24h) and 45 % (48h)

killing of target cells when co-cultured at the 4:1 effector : target ratio. However, when cultured with the triDrop engineered CAR T cells, approximately 27 % (24h) and 45 % (48h) of target cells are killed when cultured at a 1:1 ratio and 61 % (24h) and 85% (48h) are killed at a 4:1 effector : target ratio indicating a robust killing effect. Overall, the results detailed in **Figure 4-5** show that the triDrop platform can engineer cells capable of improved functional ability in immunotherapeutic assays while using less payload and fewer cells than either the Neon or Nucleofector EP systems. This capability will pave the way for high throughput immune cell engineering assays that can be both faster and more affordable than previous assays while producing reliable results.

4.3 Materials and Methods

DMF device fabrication and assembly, droplet operations, and the electroporation circuit are described in **Appendix D**.

4.3.1 Reagents and Materials.

Unless specified otherwise, general-use chemicals and kits were purchased from Sigma-Aldrich (St. Louis, MO). Device fabrication reagents and supplies included chromium-coated glass slides, and gold-coated glass slides with AZ1500 photoresist from Telic (Valencia, CA), MF-321 positive photoresist developer from Rohm and Haas (Marlborough, MA), chromium etchant 9051 and gold etchant TFA from Transene (Danvers, MA), AZ-300T photoresist stripper from AZ Electronic Materials (Somerville, NJ), Teflon-AF 1600 from DuPont Fluoroproducts (Wilmington, DE). Transparency masks for device fabrication were printed from ARTNET Pro (San Jose, CA) and polylactic acid (PLA) material for 3D printing were purchased from 3Dshop (Mississauga, ON, Canada). General chemicals for tissue culture were purchased from Wisent Bio Products (Saint-Bruno, QC, Canada). Electronic components were obtained from DigiKey (Thief River Falls, MI). eGFP mRNA was purchased from TriLink Biotechnologies (catalog #: L-7201). Anti-CD19 CAR mRNA was purchased from Med Chem Express (catalog #: HY-153084). Cas9 and sgRNAs were purchased from Synthego (Redwood City, USA).

4.3.2 Cell Culture

Primary T-cell culturing. Primary human T cells were separated from fresh venous primary blood using LympPrep gradient centrifugation (Wisent Bio) and purified using either the EasySep

Human CD4 T cell Isolation kit or EasySep Human T cell isolation kit to a purity of 95 % (STEMCELL Technologies, Canada, Catalog # 17952, and Catalog # 17951). All cells were kept in liquid nitrogen prior to use. Cells were thawed and cultured in complete culture medium consisting of RPMI-1640 with 10 % Fetal Bovine Serum (FBS), 100 IU / mL penicillin/streptomycin, and 200 IU / mL recombinant human IL-2 (STEMCELL Technologies, Canada, Catalog # 78220). Unless specified otherwise, cell culture was performed in U-bottom 96 well plates. After 24 hours post-thaw, the cells were activated with Human T-Activator CD3/CD28 Dynabeads (Fisher Scientific Ottawa, ON, #11131D) at a 1:1 cell to bead ratio and were incubated for 48 hours. After incubation, activator beads were removed following manufacturers protocol by first gently pipetting up and down to release cells from the activator beads followed by transferring the cells to a magnetic tube rack for 1-2 minutes to allow for cells and beads separation and the supernatant containing cells was transferred to a fresh tube. Cells were electroporated within 24 hours of bead removal. Primary T cells were counted using the ViCell Blu automated cell counter (Beckman Coulter, Canada) and maintained at 0.25 - 1 x 106 cells / mL by daily addition of complete culture media. Post electroporation cells were recovered in the same media cocktail as above but with IL-2 levels increased to 400 IU / mL.

Immortalized cell culture. Raji and MCF-7 cells were grown in cell culture media formed from RPMI (Raji) or DMEM (MCF-7), supplemented with 10% fetal bovine serum (FBS). Cells were grown to near confluency in complete media in T-25 flasks in an incubator at 37 °C with 5% CO2. Prior to each experiment, cells were detached using a solution of trypsin (0.25% w/v) and EDTA (1 mM), centrifuged, then resuspended in complete media. Cell lines were passaged every 2-3 days by media removal, PBS wash, trypsinization (for adherent cells), resuspension in fresh culture media and split at a 1:10 ratio into fresh media. All immortalized cell lines were kept below passage 10.

4.3.3 Electroporation

For all electroporation platforms primary human T cells were electroporated within 24 hours after the removal of activation beads. Cells were in electroporation buffer for a maximum of 15 minutes and were transferred to recovery buffer promptly after pulse application using one of the three systems. For both the Neon and Nucleofector a wide range of pulse parameters (voltage amplitude, number of pulses, and pulse duration) have been shown for effective electroporation. In this work

we use the pulse parameters recommended by the manufacturer for working with activated primary human T cells[213,245] and shown to be effective by Zhang et al.[93] and Schumann et al.[246] which are three, 1600 V_{DC} pulses, 10 ms in duration for the Neon and pulse code EO-115 for the Nucleofector.

triDrop Electroporation. Detailed explanations of the triDrop platform can be found in our previous manuscript.[227] Unless specified otherwise, 5 x 10^5 cells were centrifuged (300 g, 5 min), washed in PBS, centrifuged, and resuspended in 10 µL of electroporation buffer with conductivity σ ~ 8 mS / cm (Neon Type T buffer containing 0.05% Pluronic F68 surfactant) and payload was added as described below. 7.5 µL of a buffer with conductivity σ ~ 16 mS / cm (PBS containing 0.05% Pluronic F68 surfactant) was pipetted into each of the device's flanking reservoirs and 7.5 µL of the cell solution was pipetted into the middle reservoir. DMF actuation was used to dispense three unit droplets, ~ 1 µL in volume, from each reservoir and actuate them to the three on-chip electroporation sites. Driving potentials (i.e. actuation) was used to merge the droplets into the triDrop configuration, and a pulse generation circuit was automatically triggered to deliver five, 550 V_{DC} pulses, 500 µs in duration to the droplet structure. After electroporation cells were immediately removed from the chip via pipetting and transferred to recovery buffer. Cells from each of the three electroporation sites were loaded into their own well and served as technical triplicates.

Neon Electroporation. Neon electroporation was performed using manufacturer recommended protocols for the Neon Transfection System 10 µL kit (Thermo Fisher, Catalog # MPK 1025). For each unique condition, 4.4 x 10^5 cells were centrifuged (300 g, 5 min), washed in PBS, centrifuged again, and finally resuspended in 22 µL of type R buffer. 10 µL Neon tips were used a maximum of two times to serve as technical replicates. Three, 1600 V_{DC} pulses, 10 ms in duration were applied. Immediately, electroporation cells were transferred to recovery buffer.

To explore the effects of cell density on electroporation performance, 8 x 10^5 cells were washed in PBS and resuspended in 40 µL of Buffer R. The cell solution was diluted with fresh Buffer R in the following ratios, 5.5 µL: 16.5 µL and 11 µL: 11 µL, creating aliquots containing 1.1 x 10^5 cells and 2.2 x 10^5 cells respectively. These aliquots were used to perform two electroporation reactions each containing ~ 5 x 10^4 cells per reactions and ~ 1 x 10^5 cells per reaction respectively. The remaining cell solution was used to perform two reactions with 2 x 10^5

cells per reaction (manufacturer recommended amount). All conditions were cultured at 5 x 10^4 cells per well for post-electroporation analysis.

Lonza Electroporation. Lonza electroporation was performed using manufacturer recommended protocols for the P3 Primary Cell 4D-Nucleofector X Kit S (Lonza, Canada, Catalog # V4XP-3032). For each condition, 1.1 x 10^6 cells were centrifuged (300 g, 5 min), washed in PBS, centrifuged, and resuspended in 22 µL of P3 buffer. 20 µL of cell solution was pipetted into the nucleofector cuvette and pulse code E0-115 was used for electroporation. Immediately following electroporation 100 µL of pre-warmed recovery buffer was added to each cuvette and the sample was incubated for 10 minutes prior to be transferred to a well plate.

To determine the effects of cell density on electroporation efficacy, 3 x 10^6 cells were washed in PBS and resuspended in 60 µL of P3 buffer. The cell solution was mixed with fresh P3 buffer in the following ratios, 2:38, 4:36, and 8:32, creating aliquots containing 1 x 10^5 cells, 2 x 10^5 cells, and 4 x 10^5 cells. These aliquots were each used to perform two electroporation reactions containing 5 x 10^4 cells per reaction, 1 x 10^5 cells per reaction or 2 x 10^5 cells per reactions respectively. The remaining cell solution was used to perform two reactions with 1 x 10^6 cells per reaction (manufacturer recommended amount). All conditions were cultured at 50,000 cells per well for post-electroporation analysis.

4.3.4 Transfection Protocols

mRNA transfection. mRNA transfection was performed by preparing cells for electroporation using the techniques outlined above and adding mRNA immediately prior to electroporation. Unless specified otherwise, mRNA was added at 50 ng / µL for each system (50 ng per reaction for triDrop, 500 ng per reaction for Neon, and 1000 ng per reaction for Lonza). eGFP and anti-CD19 CAR mRNA were stored at -80 $^{\circ}$C in 5 µL aliquots with a stock concentration of 1 and 2 µg / µL respectively. The eGFP-mRNA sequence can be found in **Table 9-2**.

For experiments exploring the effects of mRNA concentration on electroporation efficacy, 100 ng, 50 ng, and 10 ng per reaction conditions were explored using the triDrop. Three tubes were prepared, each containing 5 x 10^5 cells resuspended in 10 µL of electroporation buffer as described above. 1 µL of stock eGFP-mRNA (1 µg / µL) was added to the first tube, 0.5 µL of stock solution was added to the second tube, and for the final tube 1 µL of stock mRNA was diluted

with 9 µL of type T electroporation buffer and 1 µL of the dilution was added to the cell mixture. For Neon, 500 ng, 100 ng, and 50 ng reaction conditions were explored. Three tubes each containing 4.4 x 10^5 cells resuspended in 22 µL of electroporation buffer were prepared as outlined above. 1 µL of stock mRNA (1 µg / µL) was added to the first tube. Next, 1 µL of stock mRNA was diluted in 9 µL of type R electroporation buffer. 2 µL of this dilution was added to the second tube, and 1 µL was added to the third tube. Each tube was used for two electroporation reactions. For the Lonza, 500 ng, 100 ng, and 50 ng per reaction conditions were explored. Three tubes each containing 2.2 x 10^6 cells resuspended in 44 µL of electroporation buffer was prepared as outlined above. 1 µL of stock mRNA (1 µg / µL) was added to the first tube. Next, 1 µL of stock mRNA was diluted in 9 µL of P3 electroporation buffer. 2 µL of this dilution was added to the second tube, and 1 µL was added to the third tube. Each aliquot was used for two electroporation reactions.

Gene Editing. TRAC knockouts were performed by complexing TrueCut Cas9 protein V2 (Thermo Fisher, Canada, catalog #: A36496) with an sgRNA cocktail designed by Synthego to target the TRAC locus (Synthego, SKU: 052-1020-000-1.5n-0). Cas9 proteins and gRNAs were kept at -20 °C at a stock concentration of 30 pmol / µL and 100 pmol / µL respectively. The amount of gRNA and Cas9 protein added to each sample was controlled by either normalizing to the number of cells per reaction or by normalizing to the volume of the reaction. For normalization to the number of cells per reaction, 50 pmol of Cas9 was mixed with 100 pmol of gRNA for every 1 million cells used. For normalization to reaction volume, 50 pmol of Cas9 was mixed with 100 pmol of gRNA for every 20 µL of reaction volume (equivalent to volume required for one Lonza nucleofection cuvette). After mixing of the Cas9 protein with the gRNA, the mixture was left at room temperature for 10 minutes to allow for the formation of the ribonucleic protein (RNP) complex and either immediately added to the cell mixture or kept on ice for no more than 30 minutes before being added to the cell mixture.

CRISPR knock-ins were performed by using the protocol originally described by Cloarec-Ung et al..[232] crRNA (200 pmol / µL, IDT) was mixed with tracrRNA (200 pmol / µL, IDT) at a 1:1 ratio and annealed by heating at 95℃ for 5 minutes followed by cooling to room temperature at a rate of 0.1℃ / s in a thermocycler to form sgRNA at a concentration of 100 pmol / µL. the resulting sgRNA was then mixed with Cas9 (30 pmol / µL) at a 2:1 ratio and left to complex for 10 minutes at room temperature to form RNPs. A single stranded oligonucleotide (ssODN) HDR

repair template (400 pmol / µL, IDT) was diluted 1:8 in electroporation buffer prior to electroporation. p53 siRNA (100 pmol / µL, Thermo Fisher, Catalog # 4390824) was diluted 1:1000 in nuclease free water. For every 20 µL of reaction volume, 50 pmol of RNP, 50 pmol of ssODN, and 20 fmol of p53 siRNA was added to cells already in electroporation buffer immediately prior to electroporation. Following electroporation cells were recovered in the recovery buffer described above with the addition of 0.5 µM AZD7648 (Cayman Chemical, Item # 28598).

4.3.5 Analysis

RT-qPCR. RT-qPCR was performed in accordance with the Minimum Information for Publication of Quantitative Real Team PCR Experiments (MIQE) guidelines[247] and associated data (including primer sequences, qPCR validation, and data analysis) can be found in **Figure 9-2** and **Table D5**. RT-qPCR was performed on the Eco Real Time PCR System (catalog # EC-101-1001) using the Eco study V5.0 software. Cells from two donors were electroporated in technical replicates with each system using the methods outlined above using either the manufacturer recommended conditions or 5 x 10^4 cells per reaction. Post electroporation all cells were cultured at 5 x 10^4 cells cells per well in 200 µL of recovery buffer (recipe above). 6 hours after electroporation cells were washed in PBS, lysed and prepared for RT-qPCR using Power SYBR green cells-to-Ct kit (Thermo Fisher, Catalog #4402954). PCR cycling conditions were as follows: 95℃, 10 min; 40x (95℃ 15s, 60℃ 1 min). 18s rRNA was used as a reference gene.[248,249]

Knock-In. 48-hours post-electroporation genomic DNA (gDNA) was recovered from the cells using the DNeasy Blood and Tissue Kit (Qiagen, Catalog # 69504). gDNA was amplified using 0.5 µM of pri077F+R primers (**Table 9-2**) with the following thermal cycle: 98℃ 30s; 35x (98℃ 10s, 60℃ 10s, 72℃ 30s); 72℃ 5 min. Following amplification, PCR products were purified with the GeneJET PCR purification kit (Thermo Fisher, Catalog #K0702). Purified PCR products were quantified by Nanodrop at a range of 20 – 40 ng / µL, and 5-15 ng were sent for Sanger sequencing at the IRIC Genomics core with the primer pri0003-A1(**Table 9-2**). Chromatograms for each condition were aligned against a control sample using SnapGene's alignment tool and validated with Synthego's ICE Analysis. (**Figure 9-3**).

Transcriptomic sequencing and analysis. Transcriptomic sequencing was performed using the Oxford Nanopore minION Mk1B with flow cell R9.4.1. Cells from three donors were

electroporated using the optimized or manufacturer (Neon and Nucleofector) recommended condition. All cells post-electroporation were cultured at 5 x 10^4 cells per well in 200 µL of recovery buffer. Six hours post electroporation cells were washed in PBS, lysed, and RNA was extracted using RNeasy Mini Kit (Qiagen, catalog #74104). As per manufacturer's recommendations, 200 ng of total RNA was used from each condition as an input to the kit with an RNA integrity number > 10. The RNA library was prepared using the PCR-cDNA Barcoding Kit (Oxford Nanopore, catalog #SQK-PCB111.24) following the manufacturer's protocol. Briefly, by taking full-length polyadenylated RNA, complementary strand synthesis and strand switching were performed using kit-supplied oligonucleotides. The kit contained 24 primer pairs, 12 of which were used to generate and then amplify double-stranded cDNA by PCR amplification using rapid attachment barcode primers with the following thermal cycle: 95℃ 30s; 18x (95℃ 15s, 62℃ 15s, 65℃ 120s), 65℃ 360s, 4℃ hold. These primers contained 5' tags and facilitated the ligase-free attachment of Rapid Sequencing Adapters and their sequences are listed in the **Table 9-2**. 1 µL of amplified cDNA from each condition was analyzed using a 4200 Tapestation System (Agilent) prior to sequencing to confirm sample quality and a concentration of at least 1000 pg / µL. Amplified and barcoded samples were then pooled together, and Rapid Sequencing Adapters were added to the pooled mix. The final pooled library loaded on to the flow cell contained 2 fmol of cDNA from each barcoded condition for a total of 24 fmol.

Base calling was performed using Oxford Nanopore's Dorado software. Sequencing reads were aligned with the Homo Sapiens GRCh38 transcriptome using Minimap2.[250] Transcript counts were performed using Salmon[251] and mapped to genomic data using the R/Bioconductor package biomaRt.[252] Differential expression was calculated using DESeq2.[253] Z – scores were used to quantify variation from the control based on the number of transcripts per million (TPM) that were counted for each gene using the following formula:

$$Z_{score} = \frac{TPM_{Treated} - TPM_{control}}{SD_{control}}$$

Genes were grouped into high level genetic pathways using the Reactome data base[243] and analyzed using the ReactomePA package.[254]

Flow Cytometry. Flow cytometry was performed using the BD FACS Melody (BD Bioscience, Canada). The FACS was equipped with three excitation lasers (405 nm, 488 nm, 561 nm) in a 2B-

2V-4YG configuration. TRAC knockouts were detected via staining with anti-human alpha/beta TCR FITC (Thermo Fisher Scientific, catalog #11-9955-42). Anti-CD19 CAR expression was detected using FITC-labelled human CD19 protein (Acro Biosystems, catalog # CD9-HF251-25ug). CD3 expression was detected using PE-CD3 monoclonal antibody (Thermo Fisher Scientific, catalog #12-0038-42). CD19 expression was detected using a FITC Mouse anti-Human CD19 antibody (BD Bioscience, catalog #560994). All staining was performed in accordance with manufacturer guidelines, cells were incubated with the appropriate stains for 30 – 60 minutes at 4 $^{\circ}$C followed by three PBS wash steps to remove any unbound antibodies. For all samples, viability was assessed by staining dead cells using DAPI (50 ng / µL) added to the sample immediately prior to FACS and mixed thoroughly with the sample by pipetting. Lymphocytes were separated from debris using forward scatter vs side scatter dot plots and singlets were separated from doublets by plotting side scatter – pulse width vs side scatter – pulse height.

4.3.6 CAR-T Assays

mRNA coding for a second-generation anti-CD19 CAR molecule with a 41BB-CD3z coactivation domain was used. For each electroporation system, > 4 x 10^5 activated pan T cells were electroporated with anti-CD19 CAR mRNA using either the manufacturer recommended conditions or by performing eight reactions using 0.5 x 10^5 cells each (1 x 10^6 cells were used for the Nucelofector). Immediately post electroporation cells were incubated in 200 µL recovery buffer at 0.5 x 10^5 cells per well.

Four hours prior to the tumour cell killing assay, 2.5 x 10^4 Raji cells per well were seeded in a U-bottom well plate in 100 µL of fresh RPMI with 10 % FBS and 2.5 x 10^4 MCF-7 cells per well were seeded in a treated flat-bottom 96 well plate in 100 µL of fresh RPMI with 10 % FBS. Control wells were seeded with 100 µL of fresh RPMI containing no cells.

After six hours of recovery, electroporated and control cells were counted, washed in PBS, and resuspended in fresh RPMI with 10% FBS at a concentration of 2.5 x 10^4 cells per 100 µL. 100 µL of cell solution form each condition was then added in technical replicates to wells prepared earlier containing either just media, MCF-7 cells, or Raji cells. Supernatant was collected after 24-hours and 48-hours by centrifuging the plates for 3 min at 300 g to pellet the cells and pipetting 180 µL from the top of each well. Supernatant was analyzed via ELISA using the manufacturer

recommended protocol for INF-γ (BD Biosciences, catalog # 555142) and TNF-α (BD Biosciences, catalog # 555212).

Tumour cell killing was performed by co-culturing CAR T cells or control activated pan T cells with Raji cells at a 1:1 (2.5 x 10^4 T cells : 2.5 x 10^4 Raji cells) or 4:1 ratio (1 x 10^5 T cells : 2.5 x 10^4 Raji cells). Raji cell death was validated via flow cytometry.[125] After 24-hours of co-culture, cells are recovered and washed before being stained with PE-CD3 monoclonal antibody and prepared for flow cytometry. Immediately before flow cytometry DAPI is added to visualize cell viability. PE-CD3 staining allows for the differentiation between T cells and Raji cells, and DAPI allows for the visualization of living and dead cells. A detailed gating overview is shown in **Figure S5**. Relative Killing Efficiency was measure using the following formula:

$$\eta_{killing} = \left[1 - \left(\frac{Target\ Cell\ Viability_{treated}}{Target\ Cell\ Viability_{untreated}}\right)\right] x\ 100$$

Where the treated target cell viability represents the viability of Raji cells cocultured with either activated pan T cells or CAR T cells, and the untreated viability represents the viability of Raji cell cultured by themselves under the same conditions over the same period.

Chapter 5. Conclusions, Future work, and Reflections

5.1 Future Directions

Discovering the breakthroughs of tomorrow will involve screening a nearly limitless library of possibilities in silico, bringing the most promising candidates to the wet lab, and narrowing down only the best options for the clinic. In this work we have shown how droplet microfluidics can be used to miniaturize, automate, and improve mammalian gene editing workflows. But to truly make a meaningful difference in the world of cell and gene therapy discovery these technologies must be integrated into high throughput robotic workflows to allow for true end-to-end automation. The current limitations and opportunities for improvement for the presented works are as follows:

- **Chapter 2 and 3:** The platforms presented here are limited by the number of electrodes that could be fabricated into the glass DMF platform. Increasing the number of electrodes and transitioning to a chip with a slightly larger footprint could facilitate more transfection sites and more reservoirs to contain unique sets of payload or cell types.
- **Chapter 2:** The LENGEN chip required an overnight incubation in a 37℃, 5 % CO2 incubator. To facilitate this, the operator was required to manually move the chip from a biosafety cabinet where microfluidic operation was performed to an incubator and back. Additionally, to prevent droplet evaporation the chip was loaded inside a specially designed humidity chamber. For this technology to significantly improve current workflows, DMF operation should be integrated into an incubator environment. Or alternatively, the DMF device can be sealed and the local environment around the chip can be adapted for cell culture conditions.
- **Chapter 2 and 3**: Both systems required the manual addition of reagents on to the chip via pipette. Additionally, sample retrieval was performed by removing DMF top plates and pipetting off the surface of the chip. This involves substantial human labour. Complete automation would involve integrating these platforms with plate handling and pipetting robots. Plate manipulators could be used to grab and place DMF chips as needed and pipetting robots could be used to load samples through pre-designed sample

ports. After operation on the DMF chip the sample could be actuated back to the port where the robot could retrieve the sample and prepare it for down stream analysis.

- **Chapter 3 and 4:** A major innovation of the platform presented in chapter three and proven in chapter 4 is the ability to use small amounts of reagents. However, manually pipetting extremely small quantities of cell or enzyme solutions often made this prohibitively difficult. To truly achieve state of the art gene-editing with significant reduction in reagent consumption a technique for nanoliter dispensing should be integrated with the DMF electroporation system. This could either be a microfluidic solution relying on additional DMF capabilities or it could be an existing commercial system such as an acoustic dispenser.
- **Chapter 4:** Cells engineered on our DMF platform were demonstrated to have improved efficacy in vitro with a transiently expressed immunotherapeutic molecule. To confirm the long-term improved functionality of cells engineered on the DMF platform this analysis should also be performed for cells with a genetically integrated immunotherapeutic molecule in a mouse model.

5.2 Conclusion

In this thesis we demonstrated how droplet microfluidics can significantly improve mammalian cell engineering workflows. We first demonstrated how the automation capabilities of DMF can allow for tedious workflows such as the generation and delivery of viral particles can be miniaturized and automated. Subsequently we proposed a new technique for performing electroporation on a DMF platform. By harnessing the novel droplet mechanics observed in DMF systems we were able to solve several long-standing problems that have prevented success for droplet-based electroporators. Further, we also demonstrated that our novel platform offered significant benefits over existing state-of-the-art macroscale electroporation systems including the ability to reduce the cost of cell engineering, perform arrayed cell engineering using small populations of cells (including rare cell types), and to significantly improve the health and functionality of cells after electroporation.

In the future, we hope these technologies will be used in two ways. First, by cell therapy researchers who wish to screen large libraries of payloads with single donor resolution or when using rare cells, and second, by microfluidic engineers who wish to use our cell engineering

techniques as a module in a larger platform that could automate numerous aspects of cell therapy building and testing together on a single platform.

Appendix A: Contributions

6.1 Peer-Reviewed Journal Articles

6.1.1 Currently Under Review

2024 Title: "*A Digital Microfluidic Platform for the Micro-Scale Production of Functional Immune Cell Therapies*". Authors: **Samuel R Little**, Niloufar Rahbari, Fatemeh Gholizadeh, Mehri Hajiaghayi, Joel Phillips, Peter J Darlington, Steve CC Shih. Status: Submitted, ACS Nano.

2024 Title: "*Modulatory Effect of M3 Muscarinic Acetylcholine Receptor on Human Memory Th cells*". Authors: Fatemeh Gholizadeh, Mehri Hajiaghayi, Jennifer S. Choi, **Samuel R. Little**, Niloufar Rahbari, Kelly Brotto, Eric Han, Steve CC Shih, Peter J Darlington. Status: Submitted, Journal of Immunology.

2024 Title: "*β2-Adrenergic Biased Agonist Inhibits the Development of Th17 and the Response of Memory Th17 Cells in an NF-κB-Dependent Manner*". Authors: Mehri Hajiaghayi, Fatemeh Gholizadeh, Eric Han, **Samuel R. Little**, Niloufar Rahbari, Isabella Ardila, Carolina Lopez Naranjo, Karsa Tehranimeh, Steve CC Shih, Peter J Darlington. Status: Submitted, Frontiers in Immunology.

6.1.2 Published

2024 Title: "*An Automated Single-Cell Droplet-Digital Microfluidic Platform for Monoclonal Antibody Discovery*". Authors: Fatemeh Ahmadi, Hao Tran, Natasha Letourneau, **Samuel R Little**, Annie Fortin, Anna Moraitis, Steve C. C. Shih. Journal: Small

2023 Title: "*A Tri-Droplet Liquid Structure for Highly Efficient Intracellular Delivery in Primary Mammalian Cells Using Digital Microfluidic*". Authors: **Samuel R. Little**, Ziuwing Leung, Angela B.V. Quach, Alison Hirukawa, Fatemeh

Gholizadeh, Mehri Hajiaghayi, Peter J Darlington, Steve CC Shih. Journal: Advanced Materials Technologies.

2023 Title: "*An electrochemical aptasensor for Δ9-tetrahydrocannabinol detection in saliva on a microfluidic platform*". Authors: László Kékedy-Nagy, James M. Perry, **Samuel R. Little**, Oriol Y. Llorens, Steve.C.C. Shih. Journal: Biosensors and Bioelectronics.

2022 Title: "*Viral Generation, Packaging, and Transduction on a Digital Microfluidic Platform*" Authors: Angela BV Quach, **Samuel R Little**, SCC Shih. Journal: Analytical Chemistry.

2020 Title: "*Droplet Microfluidics: Applications in Synthetic Biology*" Authors: **Samuel R Little**, James M Perry, Kenza Samlali, Steve CC Shih. Book Chapter: Droplet Microfluidics.

6.2 Conference Talks and Proceedings

6.2.1 Oral presentations

2024 Society for Laboratory Automation and Screening
Oral Presentation Topic: "*An automated single-cell droplet digital microfluidic platform for Monoclonal Antibody Discovery"*.

2023 SynBio5.0
Oral Presentation Topic: "*An automated platform for engineering primary human T cells with digital microfluidics"*
Awarded 3rd prize in student speaking competition.

2021 Micro Total Analytical Systems
Oral Presentation Topic: "*Viral Generation, Packaging, and Transduction on a Digital Microfluidic Platform"*

6.2.2 Posters

2024 Micro Total Analytical Systems
Poster Topic: "*A Digital Microfluidic Platform for the Micro-Scale Production of Functional Immune Cell Therapies"*

2023 Society for Laboratory Automation and Screening
Poster Topic: "*An automated platform for engineering primary human T cells using digital microfluidics"*
Awarded 1 of 3 best student posters.

2021 Micro Total Analytical Systems
Poster Topic: "*High viability transfection of mammalian cells using tri-droplet electroporation on a digital microfluidic platform"*

6.3 Patents

2022 *System and Methods for Applying Voltages Within Droplet-Based Systems*
US Patent Office, Publication No. WO/2022/256604

Appendix B: Supplementary Information for Chapter 2

7.1 Supplementary Tables

Table 7-1: CRISPR Cas9 sgRNA sequences

Custom LentiCRISPRv2 plasmids	Custom sequence	PAM	Source
LCV2_eGFP_12	Oligo1:CACCGGGGCGAGGAGCTGTTCACCG Oligo2: AAACCGGTGAACAGCTCCTCGCCCC	GGG	Shalem et al., 2014
LCV2_ESR1_76	Oligo7: CACCGCGCCGTGTACAACTACCCCG Oligo8: AAACCGGGGTAGTTGTACACGGCGC	AGG	This study

Table 7-2: RNAi shRNA sequences

shRNA plasmid	Sequence (5'-3')	Source
Non-target shRNA	5'- GCGCGATAGCGCTAATAATTT -3'	Dr. Sylvie Mader's lab
ERα shRNA 1	5'- CTACAGGCCAAATTCAGATAA -3'	Sigma-Aldrich TRCN0000003300

Table 7-3: Primer Sequences

Primer	Purpose	Sequence (5'–3')
LCV2_eGFP_12_F	Colony PCR	TTTTCTGCTCGCCGCTCAGGAA
LCV2_ESR1_76_F	Colony PCR	CACCGCGCCGTGTACAACTA
LCV2_cPCR_R	Colony PCR	TGTCCACCACTTCCTCGAAGTTCC
NeoRoverhang_F	Overhang PCR	TTGCATTCTAGACTGAGGCGGAAAGAACCAG
NeoRoverhang_R	Overhang PCR	CACAGCTTCTAGATGACGCTCAGTGGAACGA
LCMN_EcoRI_F	PCR amplification	TTGAATTCTAGACTGAGGCGGAAAG
LCMN_overhang_R	PCR amplification & overhang PCR	ACTGAACGTCTCTTAACGCGTCACTTGTACAGC
LCV2_overhang_F	PCR amplification & overhang PCR	TAGTTAAGAGACGCGTTAAGTCGACAATCAACCTCTG
LCV2_EcoRI_R	PCR amplification	TTCAAGACCTAGCTAGCGAATTCA
LCMNv2_cPCR_R	cPCR	CGCCAAAGTGGATCTCTGCTGTC
hU6_prom_F	Sequencing	GAGGGCCTATTTCCCATGATTC
NeoR_F	Sequencing	GAACAAGATGGATTGCACGC

Table 7-4: 6-well plate template for lentiviral transduction for flow cytometry assessment of lentiviral titer

Lentiviruses: 100 µL Media: 400 µL	Lentiviruses: 50 µL Media: 450 µL	Lentiviruses: 25 µL Media: 475 µL
Lentiviruses: 12.5 µL Media: 487.5 µL	Lentiviruses: 6.25 µL Media: 493.75 µL	Lentiviruses: None Media: 500 µL

Table 7-5: RT-qPCR Primers

Gene-specific primers	Sequence (5'-3')
ERα - Forward	TTGACCCTCCATGATCAGGTC
ERα - Reverse	GCAAACAGTAGCTTCCCTGG
β-actin - (Forward & reverse)	Proprietary (ThermoFisher)

Table 7-6: Primers used for gene cleavage detection assay

Gene target amplification – primer	Sequence (5'-3')	Product size (bp)	Expected cleaved bands' size (bp)
eGFP - Forward	GCCTCTGCCTCTGAGCTATTC	433	293 & 160
eGFP - Reverse	TGAAGAAGATGGTGCGCTCC		
ERα - Forward	CATGACCCTCCACACCAAAG	409	235 & 174
ERα - Reverse	TTCTCCAGGTAGTAGGGCAC		

7.2 Supplementary Figures

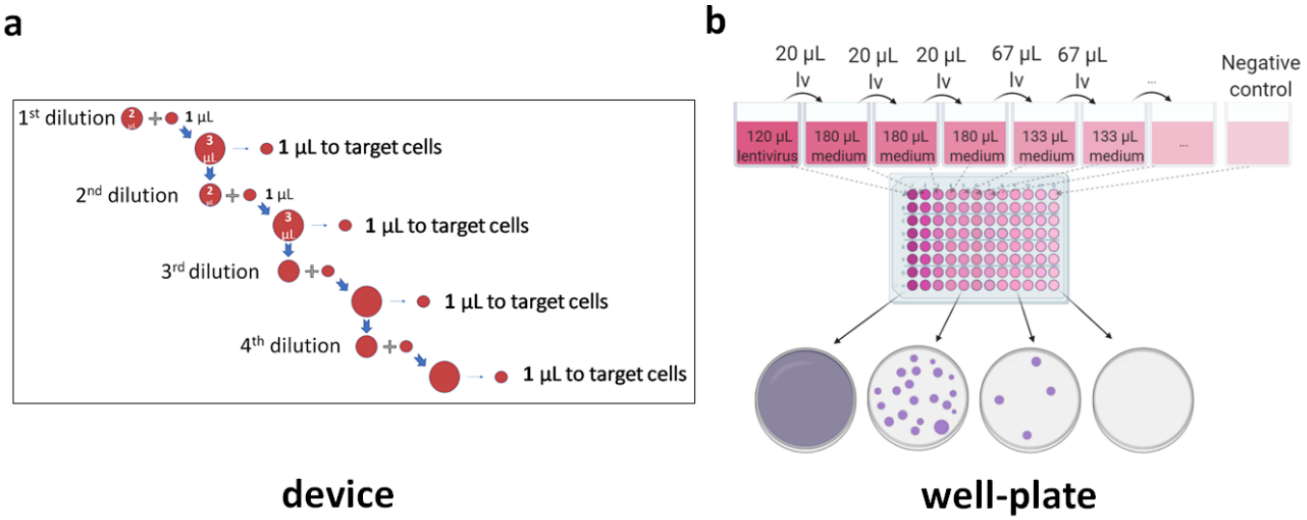

Figure 7-1: ***Lentiviral transduction dilutions to measure mean viral titer in the device and well-plate.*** *(a) Serial dilutions of 1:3, 1:6, 1:12, and 1:24 of lentiviral supernatant are formed at the production area following a dilution protocol. Each 1 µL unit DMEM droplet is applied to HEK293T cells in a serial fashion. A dilution of 1:3 (DMEM and viral titers) was implemented by merging 1 µL of DMEM with 2 µL of the supernatant containing the viruses. 1 µL of the merged product was split and actuated to a 'target cell' region while the remainder (2 µL) was saved for other dilutions. This procedure was repeated three times to generate dilutions 1:6, 1:12, and 1:24. After monitoring for two days, viral titer via the fluorescence of target cells was calculated based on Equation 1. (b) Serial dilutions of lentiviruses (lv) are applied to HEK293T cells in a 96-well plate. Colonies were allowed to grow in the presence of the puromycin for 7-8 days with medium renewal each 2 days and stained with 0.1 % w/v crystal violet in 20% ethanol and counted when the negative control well was completely dead. Counted colonies were converted into transducing units per mL via Equation 2 shown in the methodology.*

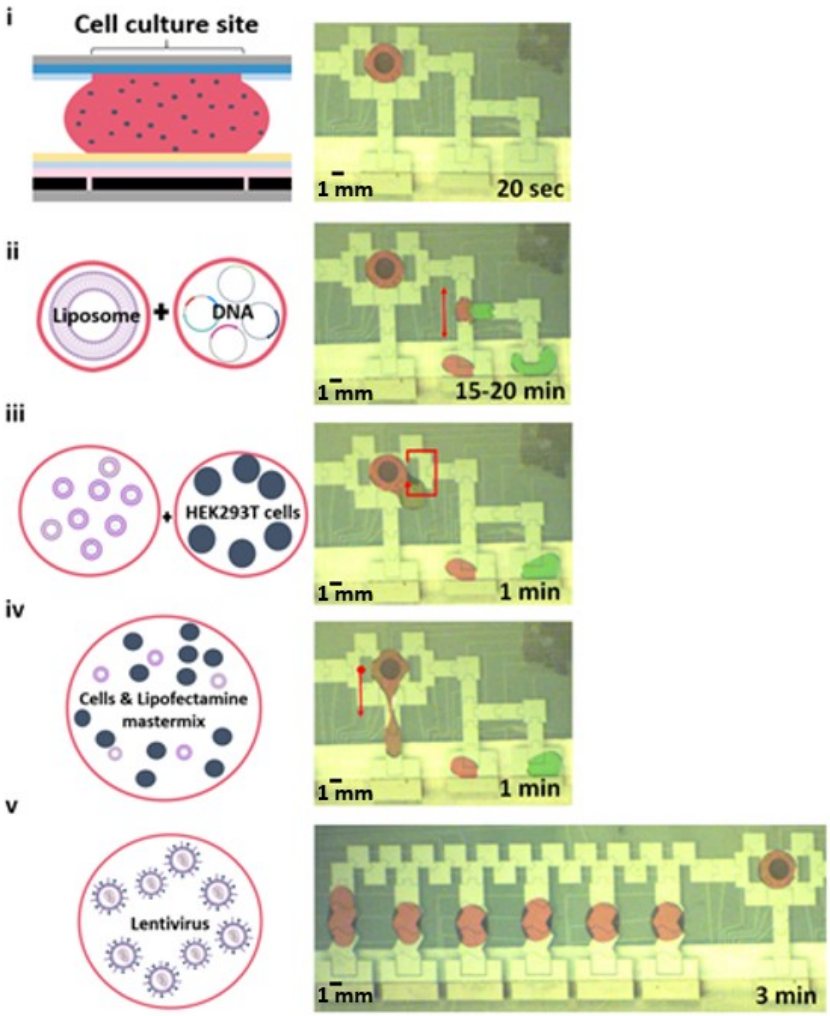

Figure 7-2: ***Lentiviral production and transduction strategy on the LENGEN platform.*** *The schematic shows the events at the genetic level with an image-based representation of the droplet movements (containing food dye) on the device. Left: the graphical representation of the five-step lentiviral generation, production, transduction, and analysis (drawings are not to scale). Right: images from a movie for each of the five steps along with the time taken for each step. Coloured food dyes were used to show the droplet. Step (i) HEK293T cells in a droplet are seeded at the production region. (ii) Plasmids and lipids from separate reservoirs are dispensed and merged and incubated for 20 mins. (iii) The DNA and lipids are dispensed into the HEK293T cell culture region and are mixed in a circular fashion around the adjacent electrodes. (iv) Excess mixture (containing plasmid, lipids, media) is dispensed away from the HEK293T cell culture region for removal. (v) After seeding the target cell line at the cell culture regions, unit droplets containing lentiviral particles with the plasmid of interest is split from the production region and actuated to a cell culture region (transduction). Analysis of the cells can be performed via microscopy after 24 or 48 h. For transduction analysis, cells can be removed by trypsin and cultured in well-plates for verification analysis (e.g., qRT-PCR, gene cleavage) or for sorting and isoclonal expansion (not shown).*

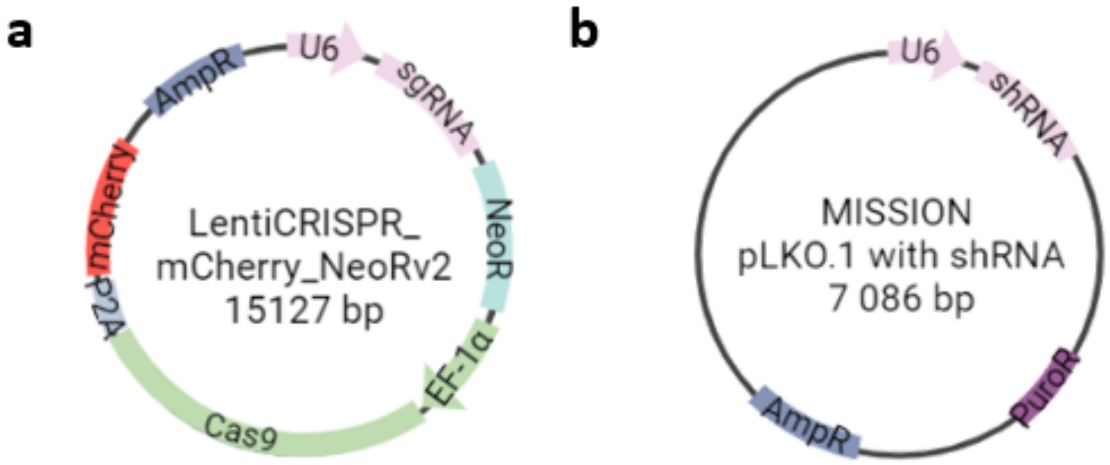

Figure 7-3: ***Transfer plasmids used in this study.*** *(a) LentiCRISPR_mCherry_NeoRv2 (LCMNv2) is a viral transfer vector that contains an sgRNA (targeting either eGFP or ESR1) under the promoter U6 and a spCas9 gene cassette linked to a fluorescent reporter, mCherry, via a P2A linker which are all under the promoter EF-1α. A neomycin/kanamycin resistance was assembled into the plasmid. (b) MISSION® pLKO.1 constructs contain an shRNA targeting ESR1 under the promoter of U6 and has a puromycin resistance cassette. The first plasmid is deposited into the online Addgene repository (Cambridge, MA).*

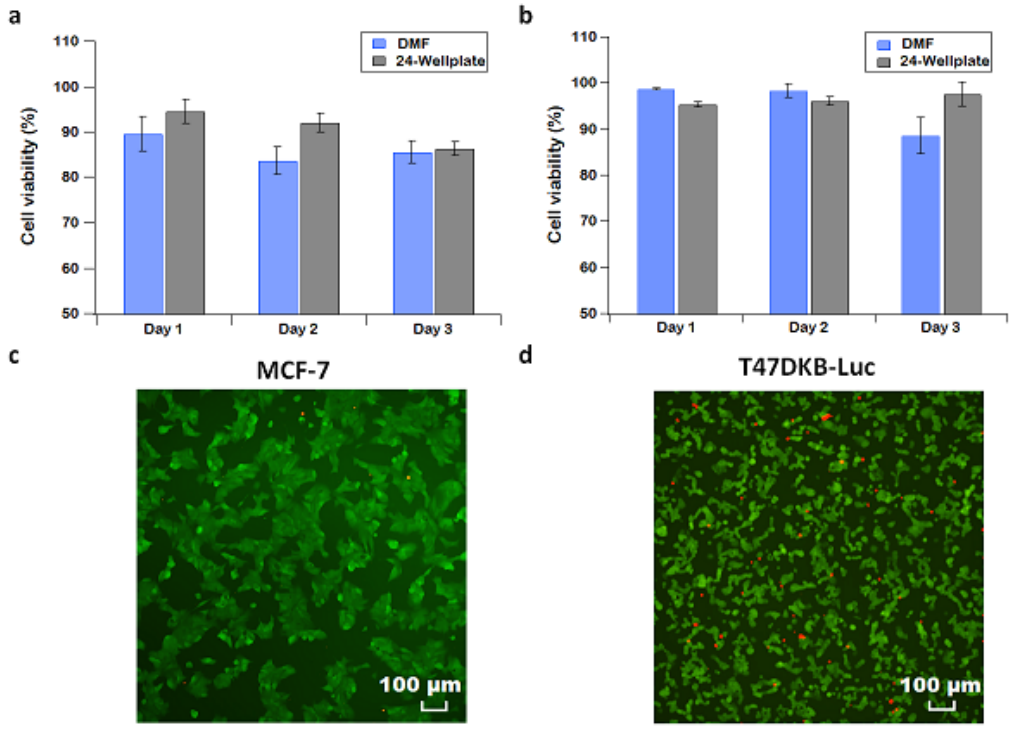

Figure 7-4: ***Cell viability of breast cancer cells (MCF-7 & T47DKB-Luc) on DMF and 24-wellplate throughout 3 days.*** *(a-b) Viability bar graph of MCF-7 and T47DKB-Luc cells. An average viability of 83.7 and 85.7 % for MCF-7 and 98.4 and 88.6 % for T47DKB-Luc was observed on the device respectively. (c-d) Qualitative images of cell viability for breast cancer cells stained with FDA/PI in 24-well plate after 3 days.*

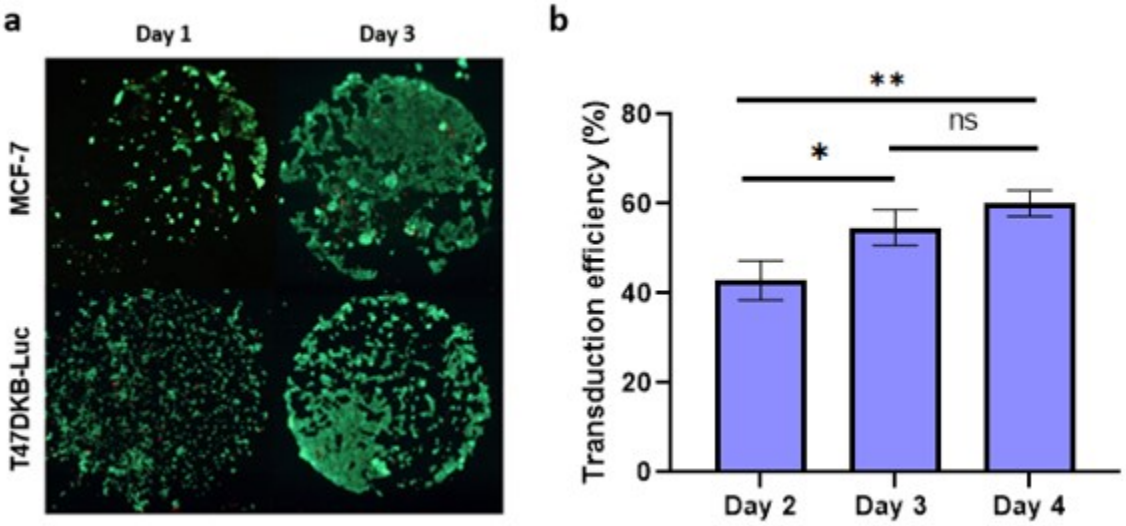

Figure 7-5: ***Optimizing viability and transduction efficiency for breast-cancer cell lines (MCF-7 and T47DKB-Luc) on the LENGEN device.*** *(a) Fluorescent images of each cell line treated with fluorescein diacetate (green) stains live cells and propidium iodine (red) stains for dead cells on the cell culturing sites for day 1 and 3. (b) Graph showing the transduction efficiency on T47DKB-Luc with a pLV-mCherry plasmid on the LENGEN platform for days 2-4. A student's t-test ($P < 0.05$) was used to evaluate the significance (* for a $P \leq 0.05$, ** for a $P \leq 0.01$ and ns for $P > 0.05$) between each day. Error bars represent ± 1 S.D. with N = triplicates.*

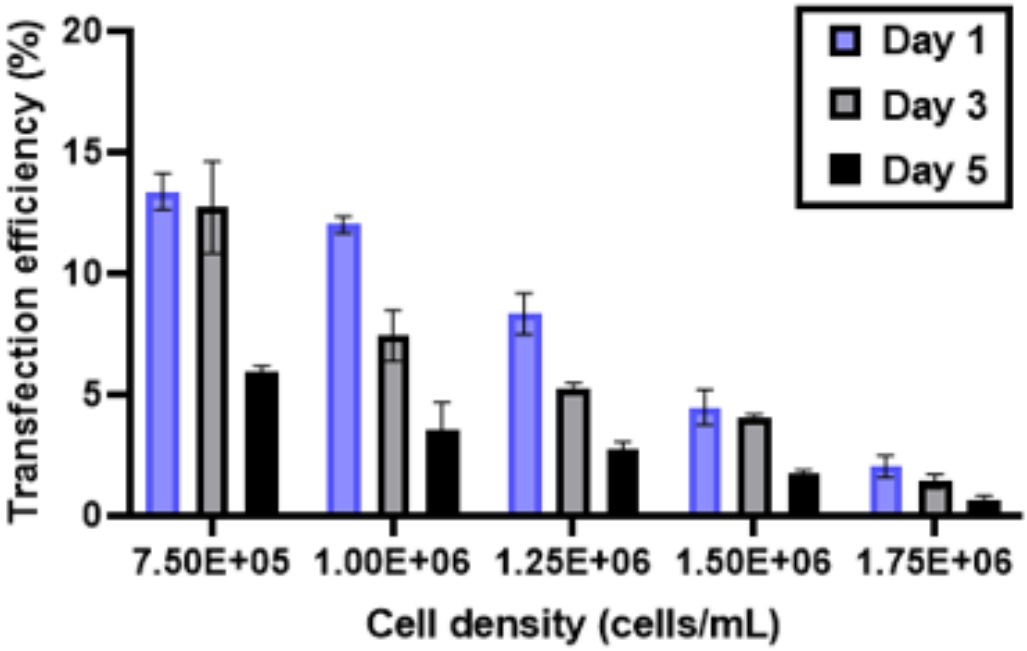

Figure 7-6: ***Lipid-mediated transfection efficiency of T47DKB-Luc with plasmid eGFP-N1 in 24-wellplate over 5 days.*** *Different cell densities were seeded in a well-plate for evaluation of transfection efficiency based on the observation of eGFP fluorescence in T47DKB-Luc cells. 750 ng of DNA plasmid was transfected into the cells. Within the first day, the highest transfection efficiency was observed at the lowest cell density is ~ 13.4%. Error bars for both plots represent ± 1 S.D. with N = triplicates.*

Sample calculations:

For dilution 1:3 on microscale, seeding density is 3 x 10^6 cells/mL with an average viral titer of 3.68 x 10^6 TU/mL after **24 hours**

$$\frac{3.68 \times 10^6\ TU/mL}{3 \times 10^6\ cells/ml} \approx 1.23\ TU\ per\ cell$$

For dilution 1:3 on microscale, seeding density is 3 x 10^6 cells/mL with an average viral titer of 1.05 x 10^7 TU/mL after **48 hours**

$$\frac{1.05 \times 10^7\ TU/mL}{3 \times 10^6\ cells/ml} \approx 3.55\ TU\ per\ cell$$

For dilution 3:10 on macroscale, seeding density is 5 x 10^6 cells/mL with an average viral titer of 1.4 x10^7 TU/mL after **5 days** of harvesting

$$\frac{1.4 \times 10^7 TU/mL}{5 \times 10^6 cells/ml} \approx 2.81\ TU\ per\ cell$$

Figure 7-7: ***Sample calculations for measuring the transducing units packaged per producer cell****. The cell seeding density was divided by the obtained mean viral titer to calculate the approximate transducing units packaged per producer cell on macroscale and microscale.*

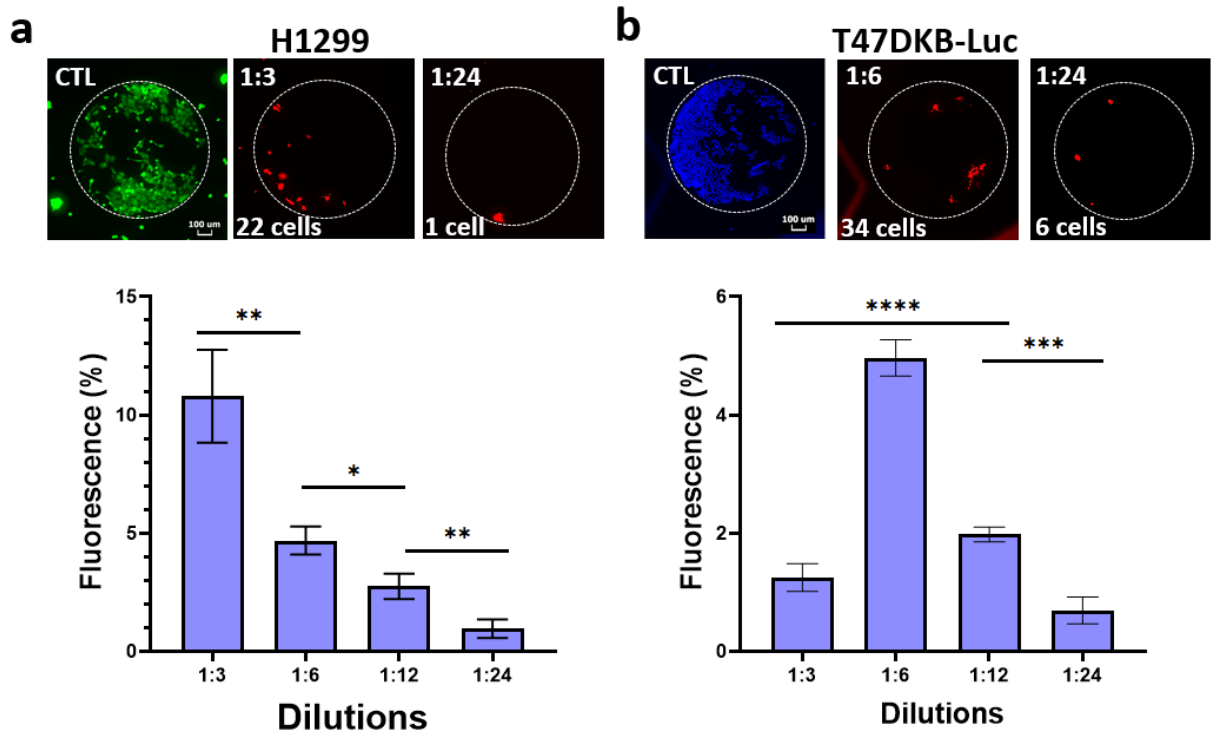

Figure 7-8: ***Evaluating the effect of a large lentiviral payload (~15 kb) for different cell lines****: (a) H1299 and (b) T47DKb-Luc. Each plot is accompanied with pictures showing the cells seeded on the hydrophilic spot (white outline) situated on the LENGEN device. Wild-type H1299 cells contained eGFP integrated into the cells (from Genecopeia) and wild-type T47DKb-Luc were fluorescently labeled with Hoechst 33342 stain. All cells were transduced with the lentiviral particles (at different dilutions 1:3, 1:6, 1:12, and 1:24) containing an mCherry fluorescent reporter. (+)mCherry cells were counted to generate the % fluorescence efficiency. A student's t-test ($P < 0.05$) was used to evaluate the significance (shown as * for a $P \leq 0.05$, ** for a $P \leq 0.01$, *** for a $P \leq 0.001$, **** for a $P \leq 0.0001$) between the dilutions. Error bars for both plots represent ± 1 S.D. with N = triplicates.*

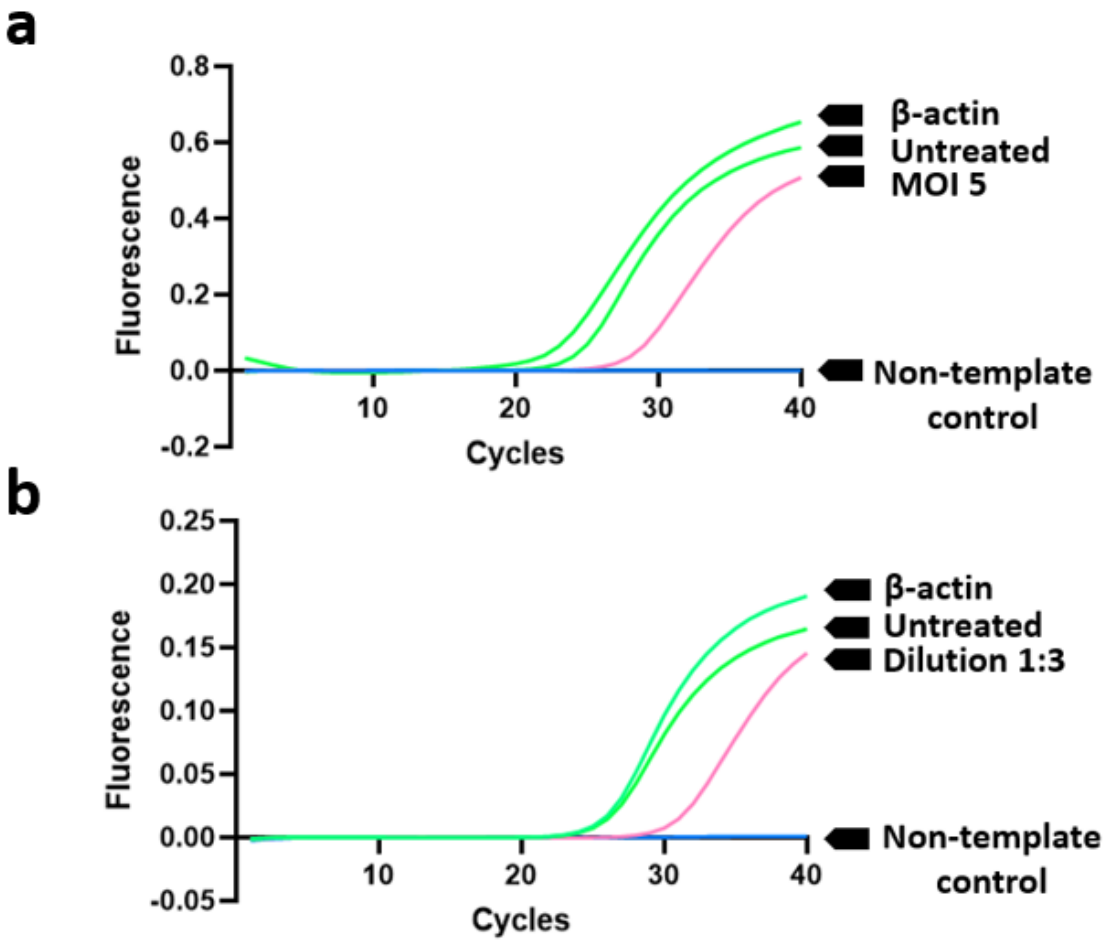

Figure 7-9: ***RT-qPCR raw data examples: RNAi assay on MCF-7's on LENGEN and in a 96-well plate****. Amplification plots measuring gene expression of ESR1 and ACTB (as a reference gene) in MCF-7 cells from (a) LENGEN and (b) well-plate platforms. Pooled 1:3 dilutions were transferred into a well-plate for analysis. All cells grown in well-plates were selected using puromycin antibiotic after seven days.*

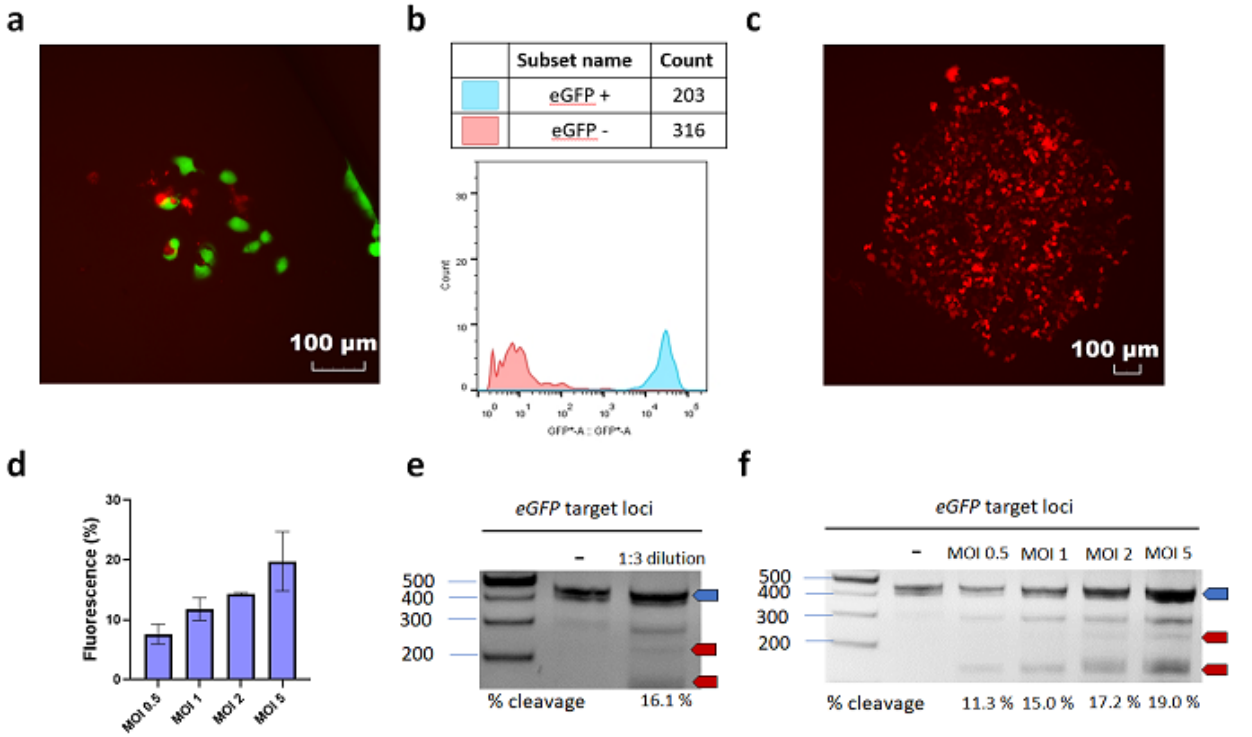

Figure 7-10: ***Expansion of eGFP knockout cells transduced on LENGEN on device and in well-plate.*** *(a) Pooled dilutions (1:3) of H1299 transduced on device transferred into a 96-well plate. Overlay images of mCherry and eGFP images show the knockout of eGFP in some cells five days post-transduction. (b) Cell sorting of H1299 grown from pooled dilutions (1:3). Flow cytometry data showing the count of eGFP knockout cells versus (+)eGFP cells. (c) Single cell expansion of (-)eGFP/(+)mCherry H1299 cells after ~2 weeks post-sorting. The heterogenous population was cell sorted for single cell expansion of knocked out eGFP and integrated mCherry-expressing cells. (d) Plot of fluorescence percentage at different MOIs (0.5, 1, 2 and 5) was measured in H1299 cells, two days post-transduction in a 96-well plate. Error bars represent ± 1 S.D. with N = triplicates. Genomic cleavage assay after seven days post-transduction on H1299 cells transduced with (e) the 1:3 dilution generated on LENGEN and (f) the indicated MOIs in well-plates along with a negative control (non-targeting sgRNA). The wildtype band is 433 bp (shown by the blue arrow arrow) and the expected cleavage bands are 293 bp and 160 bp (shown by the red arrows). There is presence of un-specific bands (~400 bp and ~310 bp) due to many repeated sequences located near the target loci.*

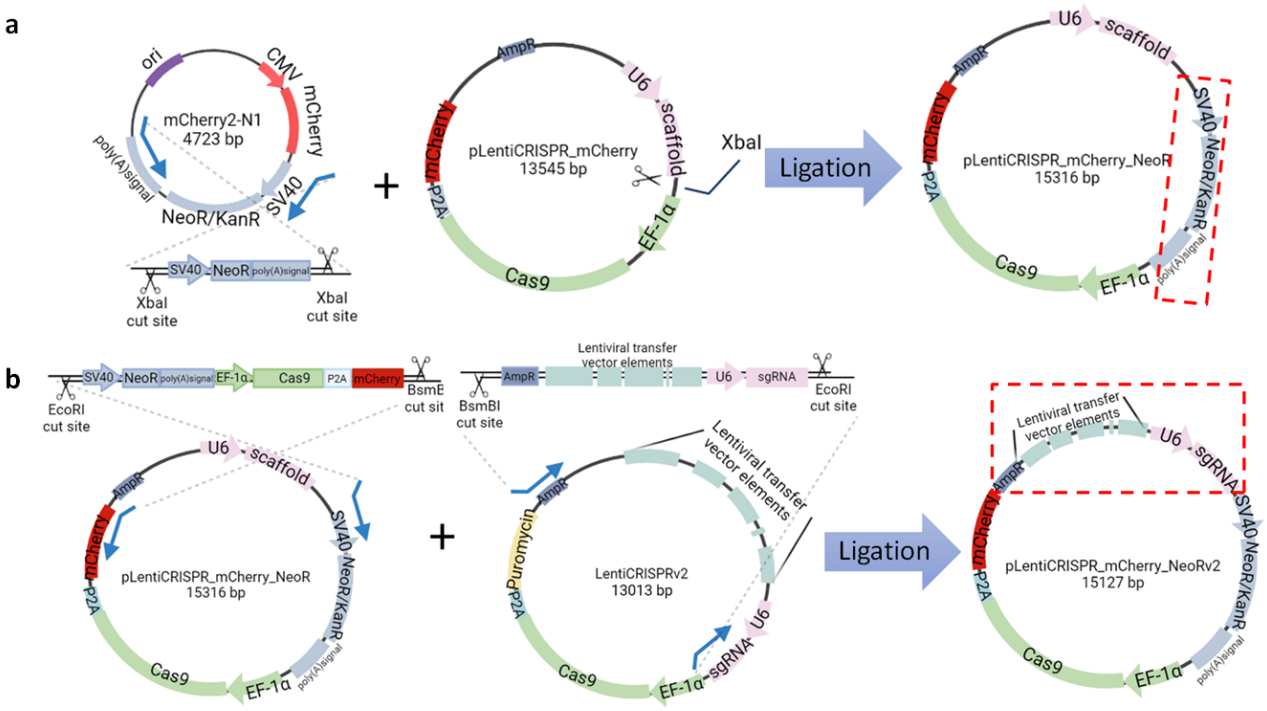

Figure 7-11: ***Schematic showing the two-step cloning procedures for the construction of pLentiCRISPR_mCherry_NeoRv2.*** *Cloning steps shown for (a) the construction of pLentiCRISPR_mCherry_NeoR by adding gene fragments of the neomycin resistance to the plasmid pLentiCRISPR_mCherry and (b) the construction of pLentiCRISPR_ mCherry_NeoRv2 by ligating part of the pLentiCRISPR_mCherry_NeoR (neomycin resistance, Cas9-P2A-mCherry) to part of the LentiCRISPRv2 plasmid (ampicillin resistance, lentiviral transfer vector elements and the sgRNA). The dotted box shows the inserted part into the backbone.*

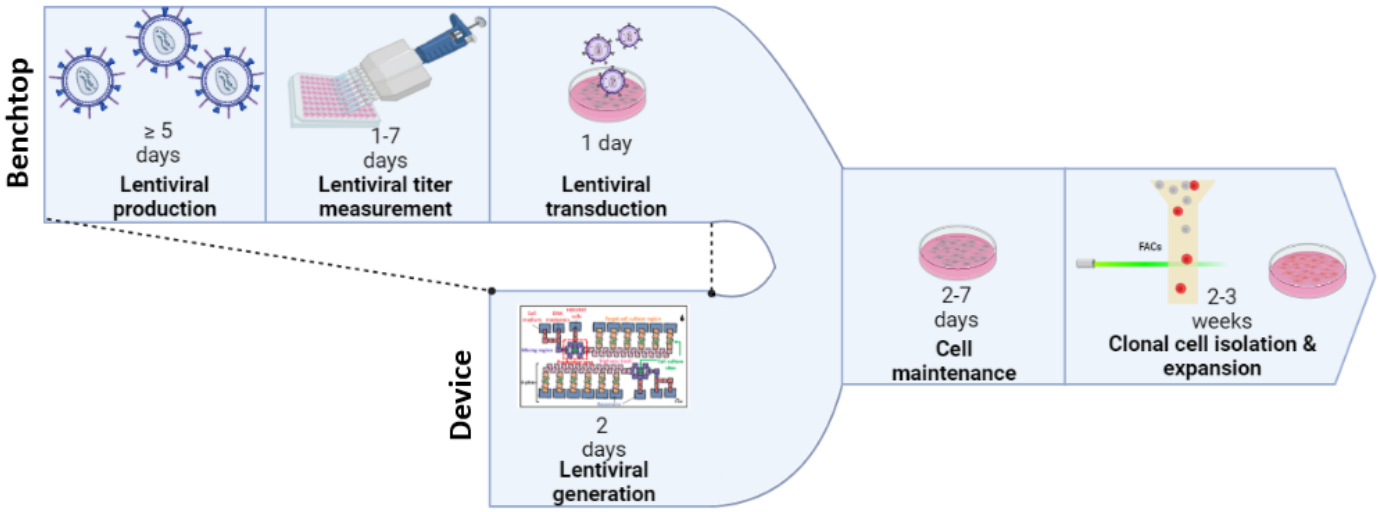

Figure 7-12: ***Schematic of the lentiviral generation process on benchtop versus device.*** *The timeline and timescale of the lentiviral generation process done on benchtop and on device are compared. The generation process includes production, titration measurement (depending on the technique chosen[6-7]) and transduction. Both are concluded with the cell maintenance, clonal cell isolation and expansion steps.*

Appendix C: Supplementary Information for Chapter 3

8.1 Supplementary Tables

Table 8-1: Electroporation parameters, cell densities, and required concentrations used for different cell lines and payloads

Cell type	Payloads	Concentration	Pulse Number	Pulse Duration	Cell density (cells/ml)	Voltage (V)	Electric field (kV/cm)
HEK293	70kDa FITC-Dextran 250kDa FITC-Dextran 2000kDa FITC-Dextran	1.2 µg / µl	3	10 ms	$2x10^7$ $4x10^7$	225	0.57
	5 kb eGFP-plasmid	51 ng / µl					
HeLa	70kDa FITC-Dextran 250kDa FITC-Dextran	1.2 µg / µl	3	10 ms	$2x10^7$	350	0.88

	2000kDa FITC-Dextran 5 kb eGFP-plasmid	51 ng / µl			$4x10^7$		
Jurkat	70kDa FITC-Dextran 250kDa FITC-Dextran 2000kDa FITC-Dextran 1 kb eGFP-mRNA 5 kb eGFP-plasmid Cas9 RNP	1.2 µg / µl 0.08 µg / µl 51 ng / µl 2 pmol / µl	3	5 ms	$4x10^7$ cells/ml	350	0.88
Primary T cells	2000kDa FITC-Dextran 1 kb eGFP-mRNA 5 kb eGFP-plasmid	1.2 µg / µl 0.08 µg / µl 51 ng / µl	3	3 ms	$4x10^7$ cells/ml	450	1.13

Table 8-2: Electroporation buffer conductivities and relative permittivity

Material	Characteristic	
	Electrical conductivity (mS/cm)	Relative permitivity
BTXpress	17.7	80
PBS	16	80
Type R buffer	15.6	80
Type T buffer	8.4	80
ISM(m) buffer	7.5	80
Very high conductive solution	32.0	80

Table 8-3: Recipes for various custom buffers

Buffer	Composition
1SM-Modified	5mM KCl, 15mM MgCl2.6H2O, 25mM Sodium succinate, 25mM Mannitol, pH 7.2
Very high conductive solution	120mM NaCl, 2.8mM KCl, 2mM MgCl2, 20mM CaCl2, 10mM HEPES, 11mM glucose, pH 7.2 with NaOH, 300 mOsm
FACs Buffer	1x PBS, 1mM EDTA, 25mM HEPES (pH7.0), 1% FBS

Table 8-4: eGFP mRNA sequence

mRNA sequence	AUGGUGAGCAAGGGCGAGGAGCUGUUCACCGGGGUGGUGCCCAUCC UGGUCGAGCUGGACGGCGACGUAAACGGCCACAAGUUCAGCGUGUC CGGCGAGGGCGAGGGCGAUGCCACCUACGGCAAGCUGACCCUGAAG UUCAUCUGCACCACCGGCAAGCUGCCCGUGCCCUGGCCCACCCUCGU GACCACCCUGACCUACGGCGUGCAGUGCUUCAGCCGCUACCCCGAC

	CACAUGAAGCAGCACGACUUCUUCAAGUCCGCCAUGCCCGAAGGCU ACGUCCAGGAGCGCACCAUCUUCUUCAAGGACGACGGCAACUACAA GACCCGCGCCGAGGUGAAGUUCGAGGGCGACACCCUGGUGAACCGC AUCGAGCUGAAGGGCAUCGACUUCAAGGAGGACGGCAACAUCCUGG GGCACAAGCUGGAGUACAACUACAACAGCCACAACGUCUAUAUCAU GGCCGACAAGCAGAAGAACGGCAUCAAGGUGAACUUCAAGAUCCGC CACAACAUCGAGGACGGCAGCGUGCAGCUCGCCGACCACUACCAGC AGAACACCCCCAUCGGCGACGGCCCCGUGCUGCUGCCCGACAACCAC UACCUGAGCACCCAGUCCGCCCUGAGCAAAGACCCCAACGAGAAGC GCGAUCACAUGGUCCUGCUGGAGUUCGUGACCGCCGCCGGGAUCAC UCUCGGCAUGGACGAGCUGUACAAGUAA

8.2 Supplementary Figures

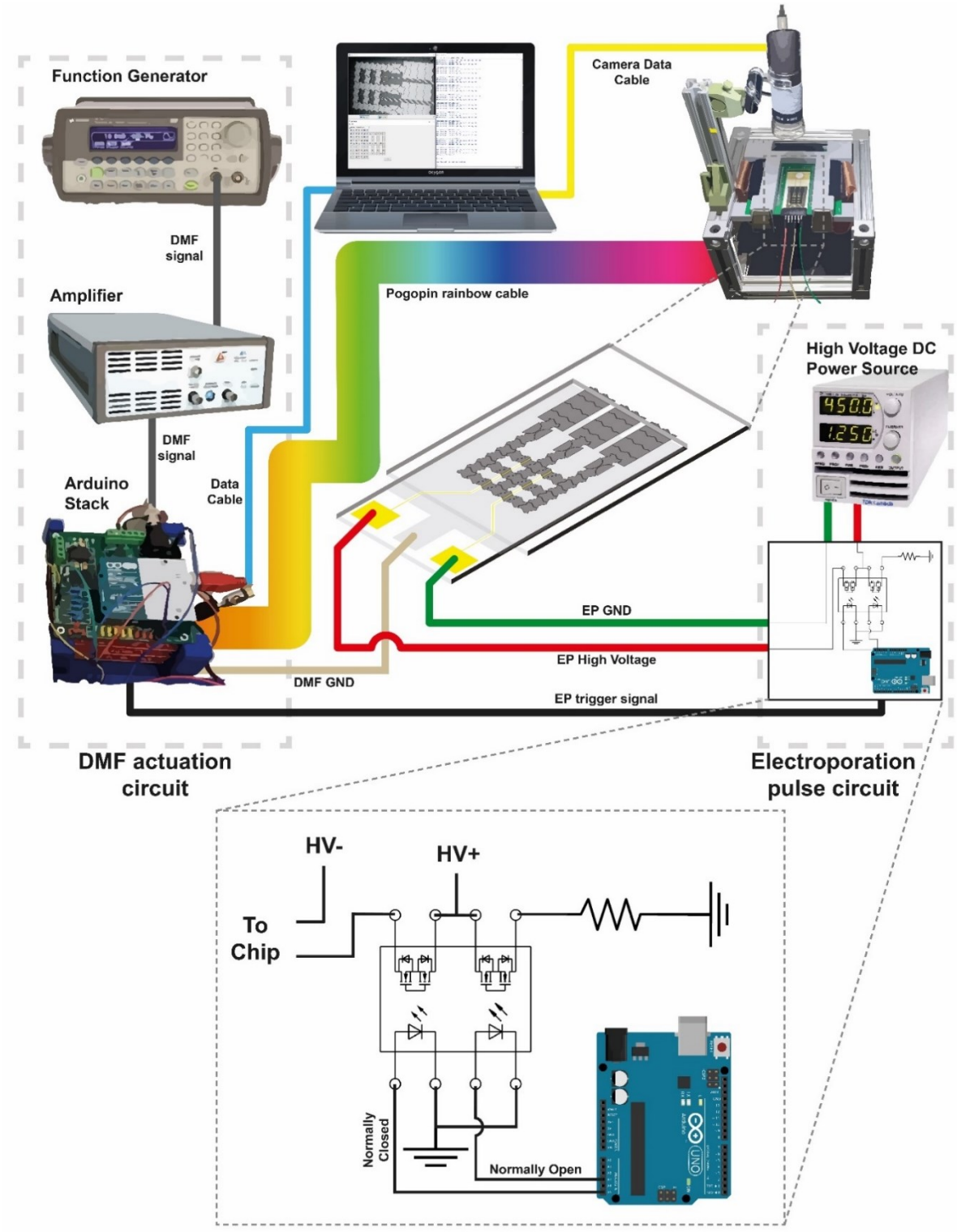

Figure 8-1: Schematic overview of the complete triDrop automation setup detailing the DMF actuation hardware, automated electroporation pulse generation circuit, and chip holder

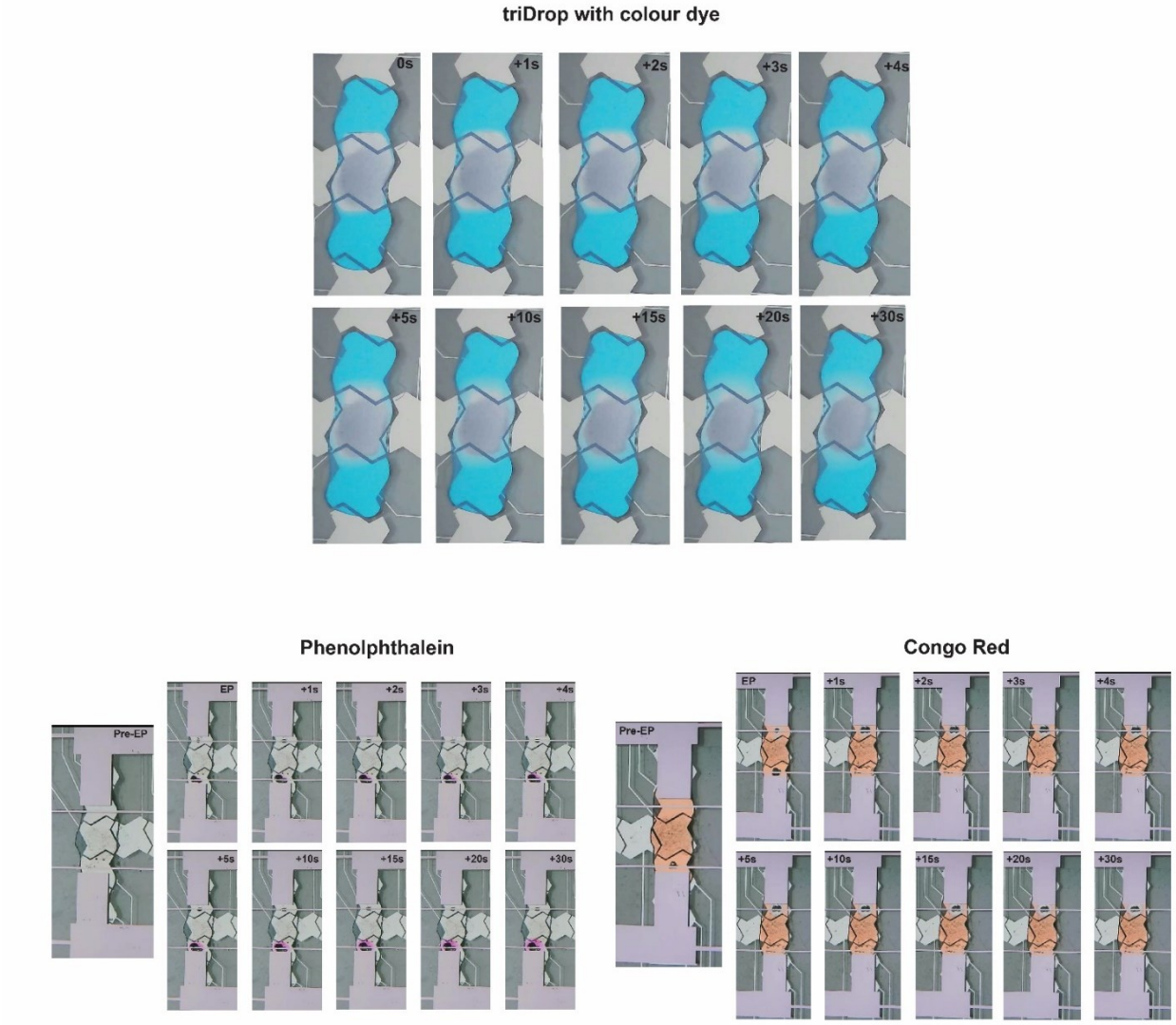

Figure 8-2: ***Qualitative assessment of droplet movement on the triDrop system.*** *(a) A triDrop merge operation performed using a standard bottom plate and a transparent Indium Tin Oxide top plate to help visualize liquid mixing. The outer droplets are comprised of high conductive media with 0.05% Pluronics F68 surfactant along with blue dye. The middle droplet is comprised of low conductive media with 0.05% Pluronics F68 surfactant and 4 x 10^7 cells/mL. Droplets are mixed using standard techniques and left to mix via diffusion for 30 s. (b) A triDrop electroporation procedure using a modified top plate allowing for visualization of the triDrop structure. All three droplets are either doped with phenolphthalein (pH indicator turning purple in the presence of pH above 8.5, left image set), or Congo red (pH indicator turning from red to blue at pH below 5.2, right image set). Three, 200 V_{DC}, 10 ms pulses are applied and the structure was observed for 30 s. The time stamp for each image is shown on the image.*

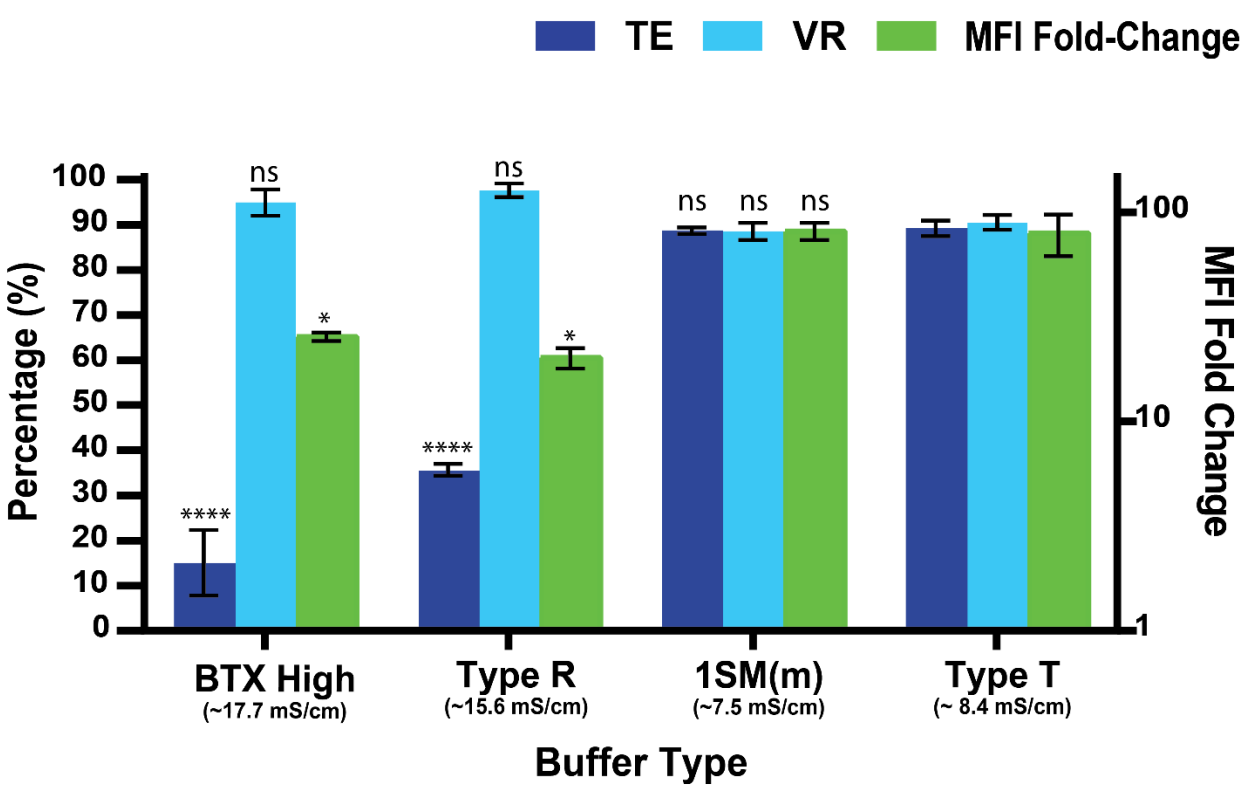

Figure 8-3: ***Comparison of electroporation buffer with varying conductivities.*** *Bar graph comparing triDrop electroporation to insert 70kDa FITC-tagged dextran into HEK293 cells using four different electroporation buffers to form the middle droplet. For each condition three 200 V_{DC} pulses, 10 ms in duration were applied. The outer droplets were comprised of high conductivity media and the middle droplets had cells at 2 x 10^7 cells/mL. SEM are calculated based of n = 3. n.s indicated no significant difference, *, **, and *** represents P-values below 0.05, 0.01, and 0.001 respectively. Statistical analysis was performed using an ordinary one-way ANOVA.*

Numerical simulations were performed using COMSOL Multiphysics software on a 3D structure. The 3D model of the triDrop structure was generated by taking a video of the triDrop merge sequence using PBS with colored dye as flanking buffers and using a transparent ITO top plate to help visualize the droplets and clearly see the boundaries between the flanking droplets and the sample droplet. The video was analyzed frame by frame and a digital image of the top-down view of the triDrop merge geometry was isolated at 2-seconds post-merge. The image was imported into AutoCAD and the boundaries of the individual droplets were traced to create a model of the triDrop structure. The AutoCAD file was imported into COMSOL Multiphysics and extruded to a final height of 180 µm (the gap between our top and bottom layer). The 3D COMSOL model, illustrated in the **Figure below**, was used in the simulations using a FINE mesh. Using the electric currents physics module, the following equations were used starting with the point form of *Ohm's law*:

$$\boldsymbol{J} = \boldsymbol{\sigma E} + \boldsymbol{J_e}$$

where **J** is the current density (SI unit: A/m^2), $\mathbf{J_e}$ is the externally generated current density (SI unit: A/m^2), $\boldsymbol{\sigma}$ is the electrical conductivity (SI unit: S/m), and **E** is the electric field (V/m). Converting this to its continuity then states

$$\boldsymbol{\nabla \cdot J} = -\boldsymbol{\nabla \cdot (\sigma \nabla V} - \boldsymbol{J_e}) = \mathbf{0}$$

As such, we can then solve for the scalar electric potential **V** which can then be used to calculate the electric field **E**. The material characteristics for each droplet is listed in **Appendix B Table B-2**. The initial conditions and boundaries used for solving the above model are as follows:

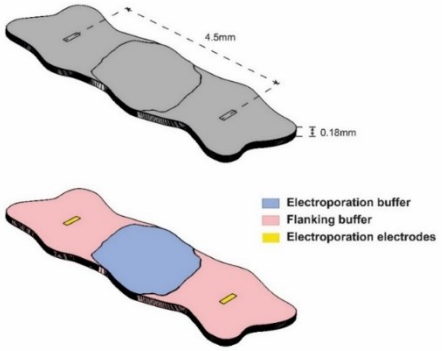

Figure 9-4: COMSOL overview

1. Temperature = 293.15 K
2. High voltage electroporation = 200 V
3. Ground potential and initial potential V = 0 V

where the high voltage and ground potential were set to the boundaries highlighted in yellow in the Figure below. Using these parameters, a stationary study was used to solve for the electric field **E** and **Figure 8-5 and 8-6** shows the simulated EF within the triDrop structure of different electroporation buffers with different conductivities.

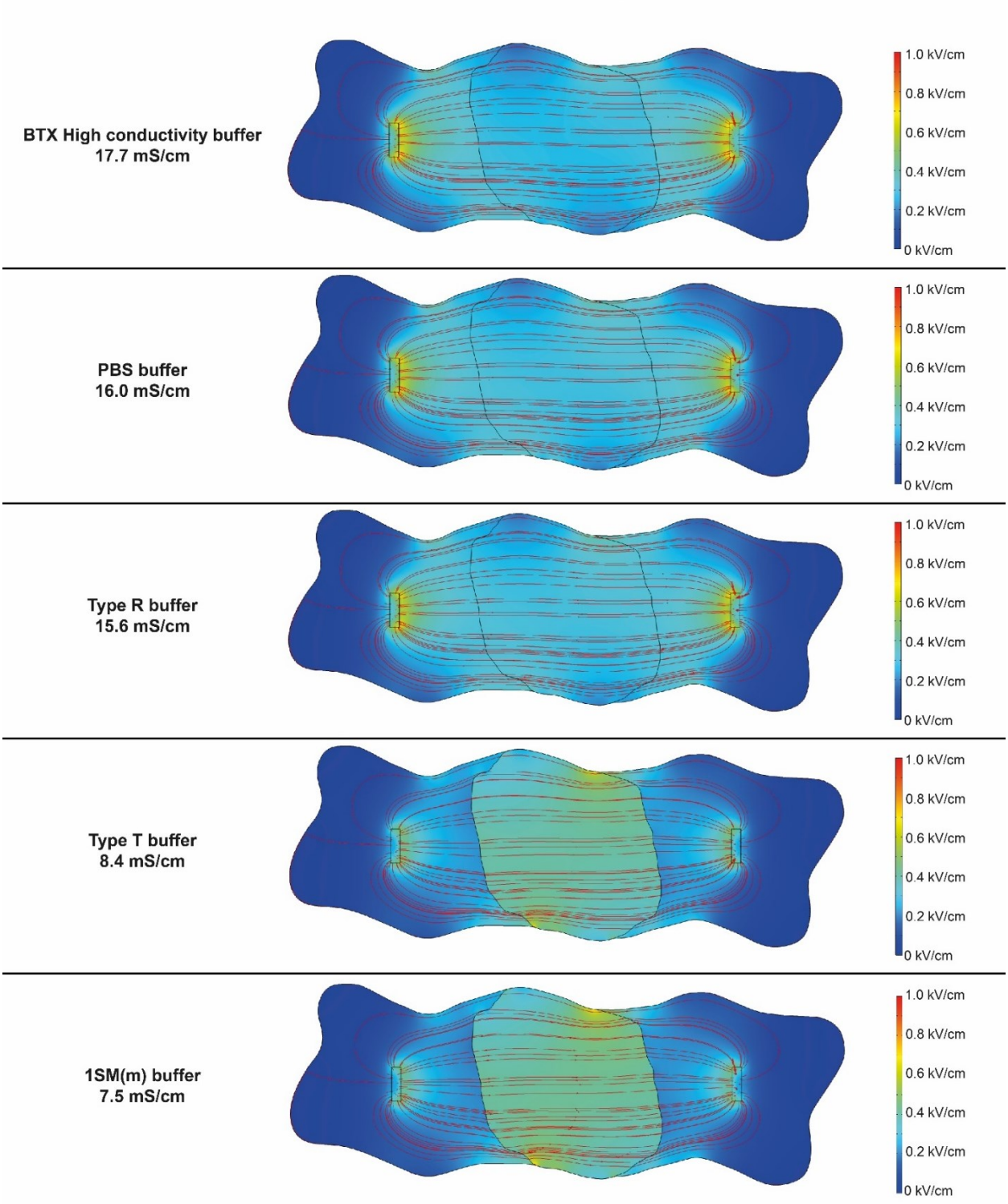

Figure 8-5: ***triDrop COMSOL simulations*** *showing the electric field generated inside of a triDrop structure when forming the middle droplet out of buffers with different conductivities.*

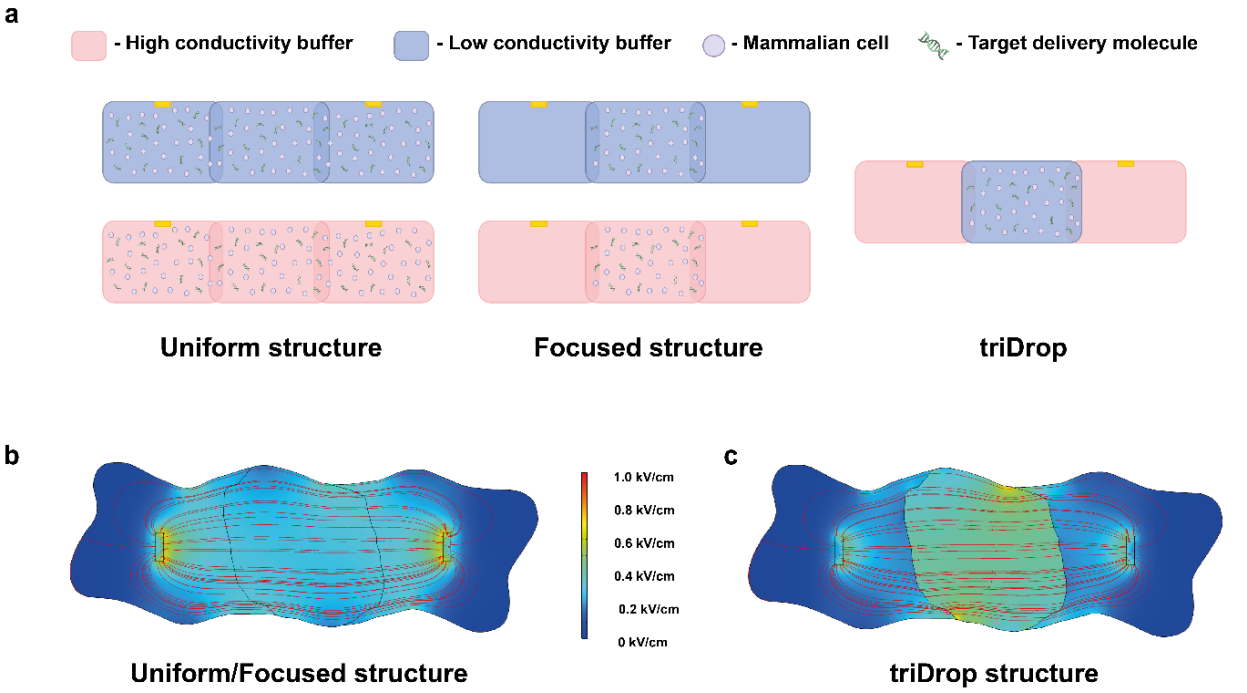

Figure 8-6: ***Droplet electroporation formats.*** *(a) Schematic representation of the 3 different electroporation structures investigated for effective DMF electroporation. (b) COMSOL simulations of the droplet structures when applying a 200V pulse.*

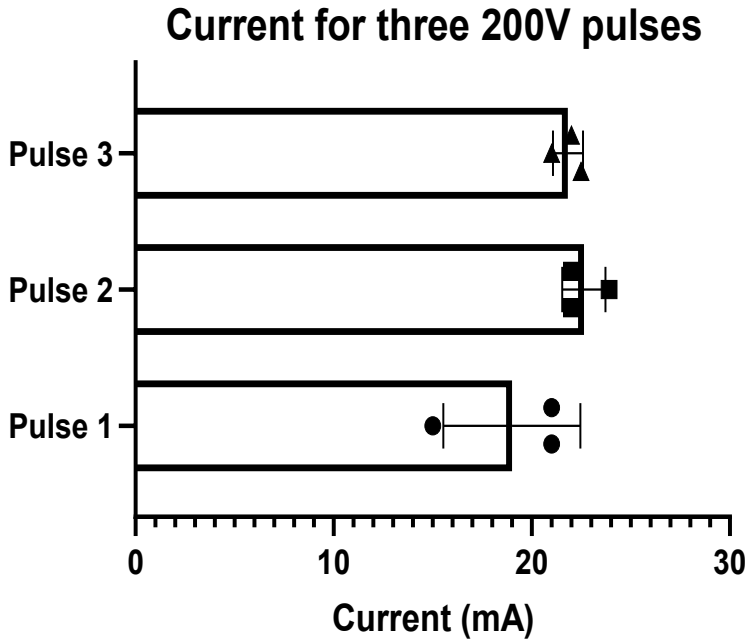

Figure 8-7: ***Current measurements*** *for all three pulses during a standard triDrop electroporation process. Three, 200 V_{DC} pulses, 10 ms in duration were applied to a triDrop structure containing 2 x 10^7 cells/mL. Error bars are based on standard error of the mean for n = 3 replicates.*

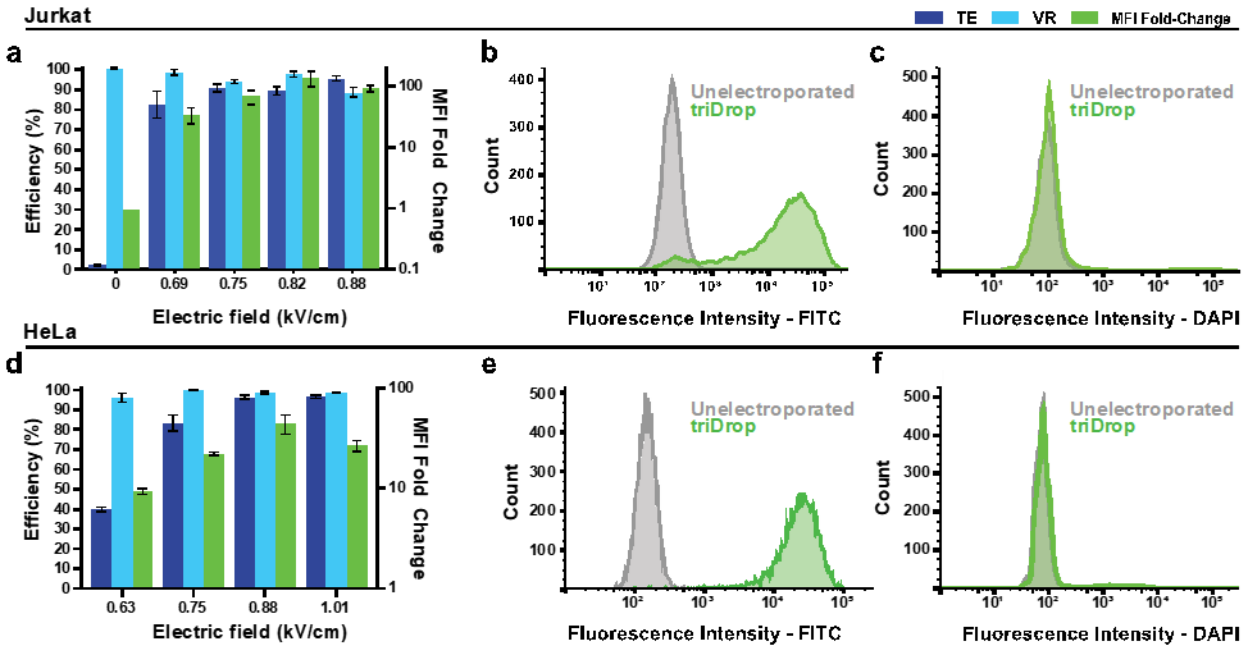

Figure 8-8: ***Electroporation parameter optimization for Jurkat and HeLa cells.*** *(a) Voltage optimization using 3, 5 ms pulses on Jurkat cells. (b) FITC fluorescence and (c) DAPI staining comparing an electroporated population (green, 350 V_{DC}) vs an unelectroporated population (grey). (d) Voltage optimization using 3, 10 ms pulses on HeLa cells. (e) FITC fluorescence and (f) DAPI staining comparing an electroporated population (green, 350 V_{DC}) vs an unelectroporated population (grey). All plots with error bars are based on standard error of the mean for n = 3 replicates.*

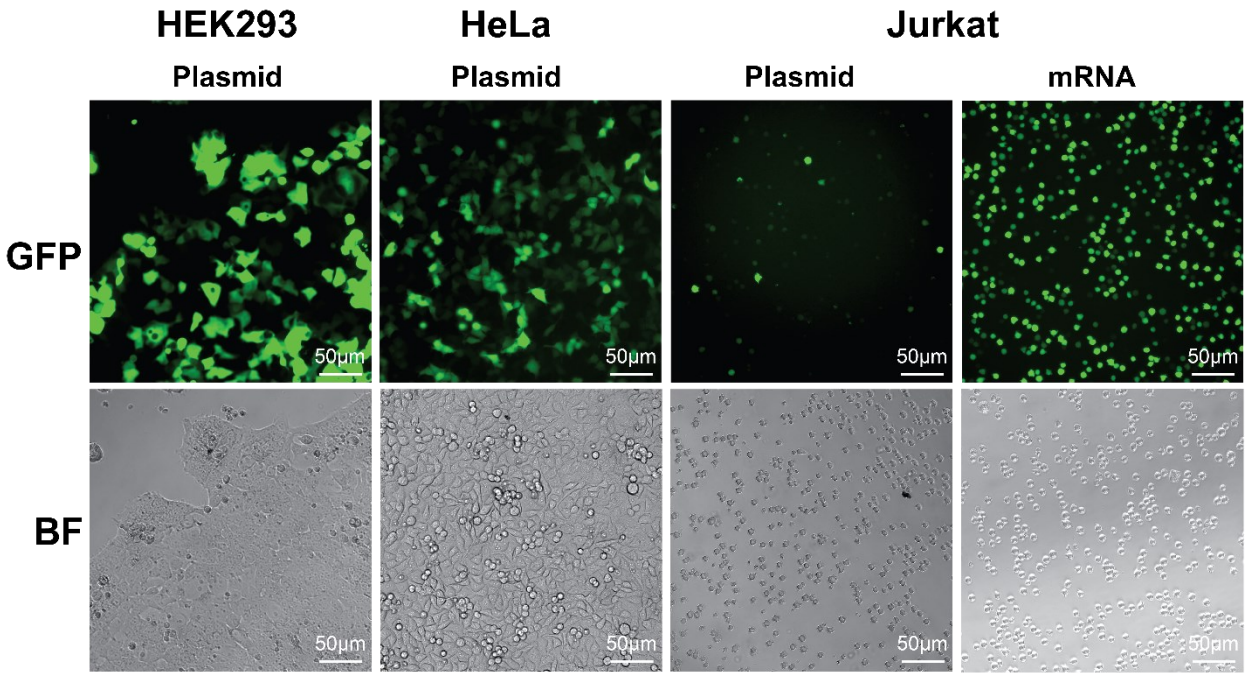

Figure 8-9: ***GFP vs brightfield*** *(BF) images for electroporated HEK293, HeLa, and Jurkat cells.*

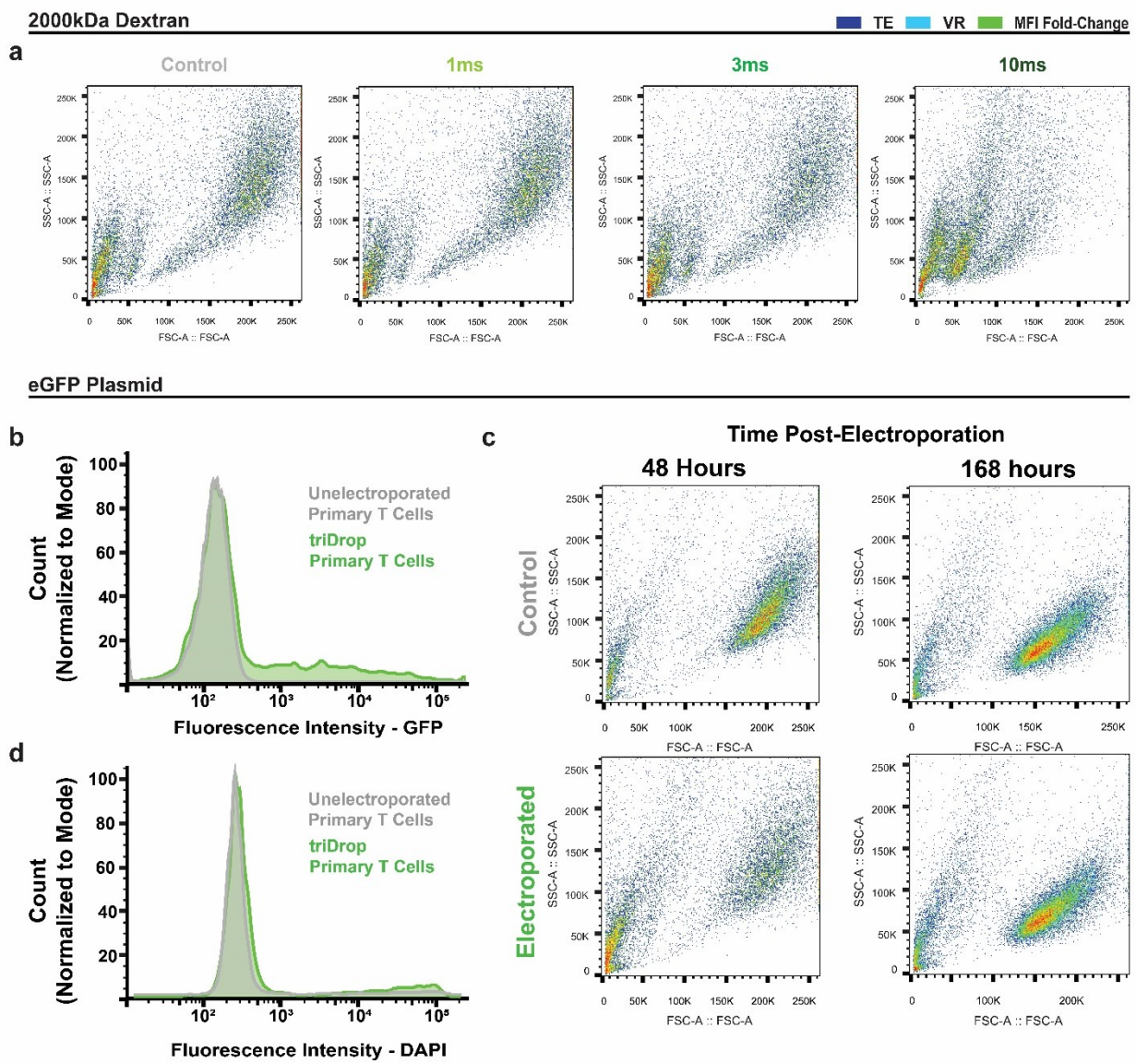

Figure 8-10: ***Additional information for primary T cell electroporation****. (a) Side scatter vs. forward scatter plots for a control population and populations electroporated with 3 pulses with a duration of 1 ms, 3 ms, and 10 ms. (b) GFP expression histogram and (c) DAPI staining histogram for primary T cells electroporated with an eGFP plasmid (green) vs a control (grey) 48-hours post electroporation. (d) Side scatter vs. forward scatter for a control population and an electroporated population and control population 48 hours and 168 hours post-electroporation.*

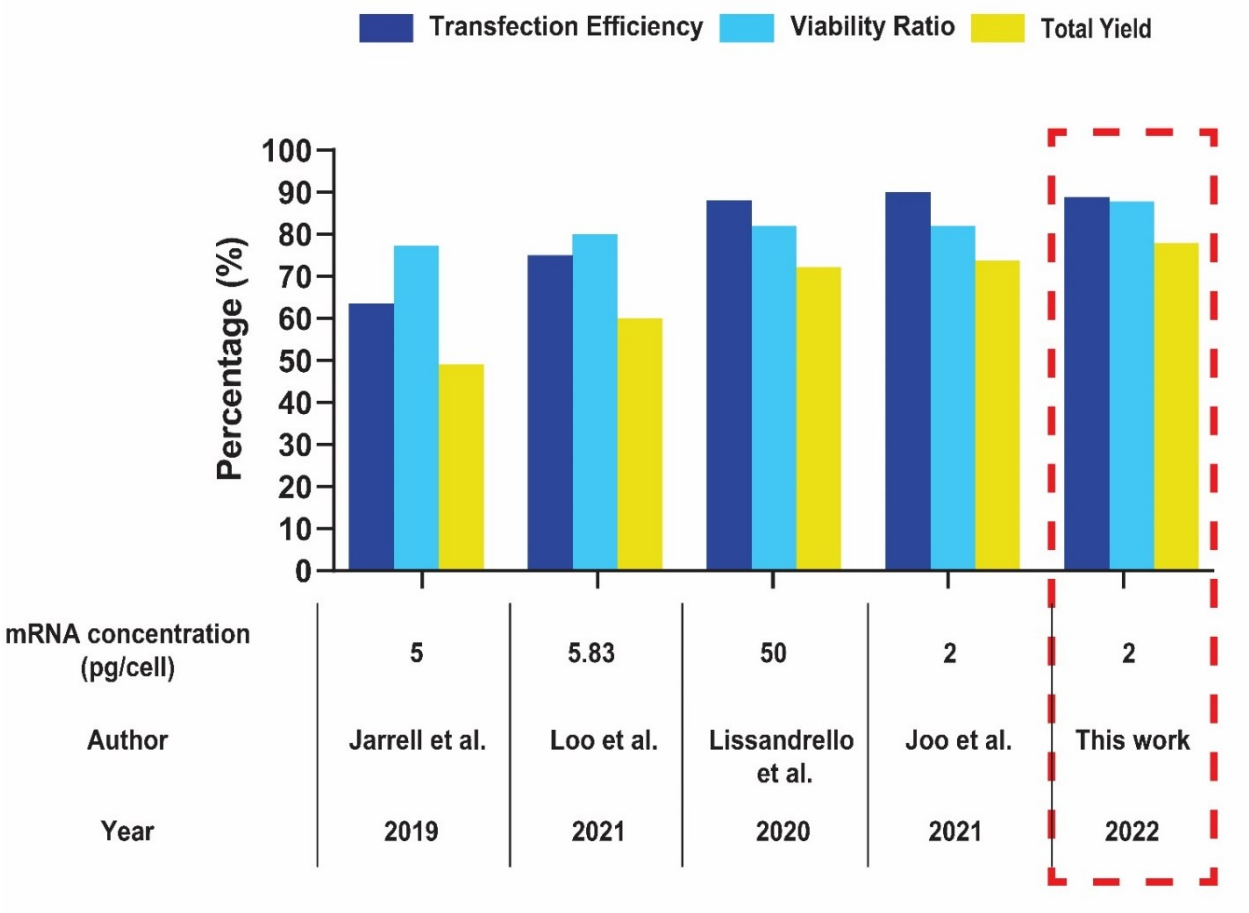

Figure 8-11: ***Comparison of four recent microfluidic transfection systems*** *for the insertion of eGFP mRNA into primary human T cells.*

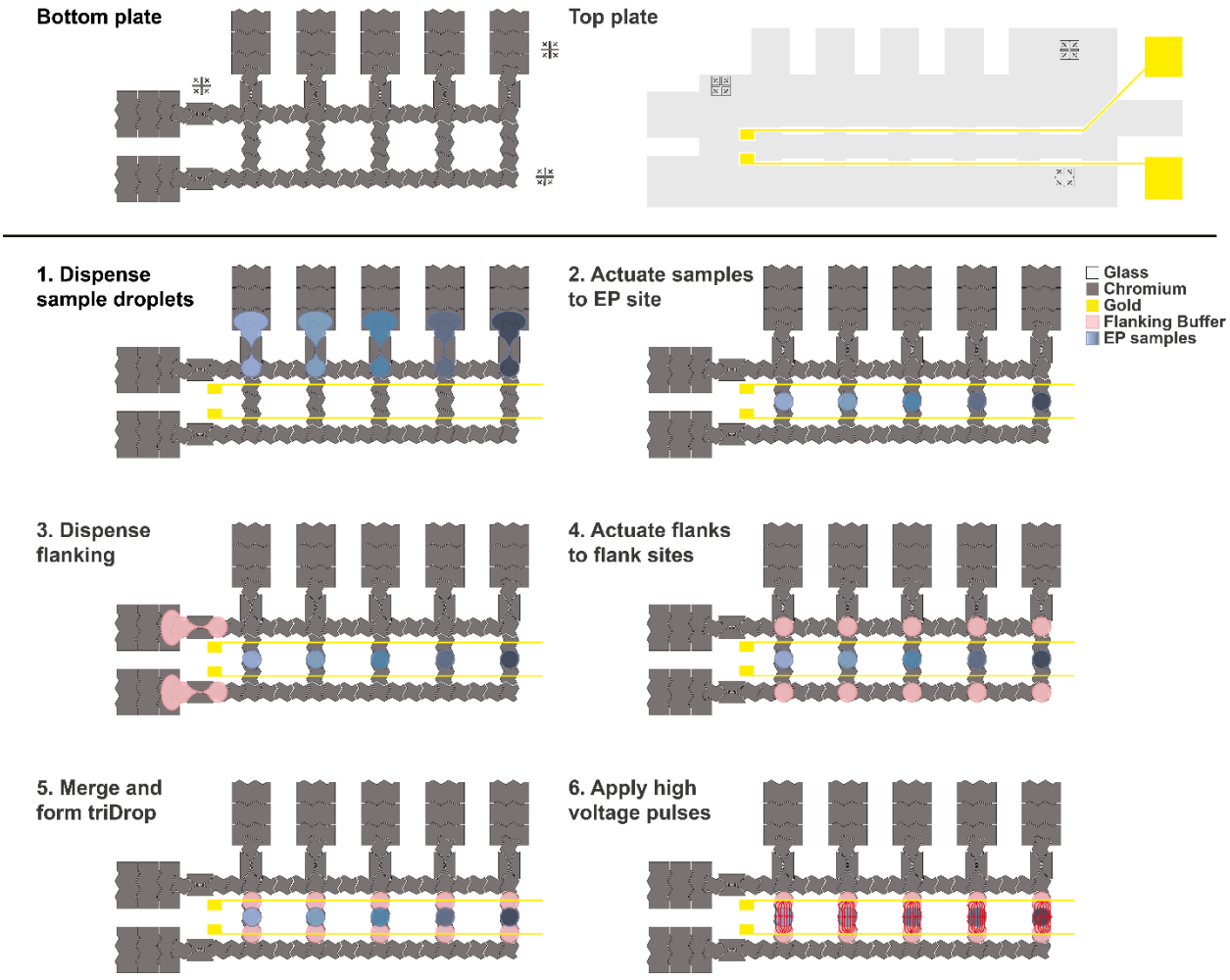

Figure 8-12: (Top) ***Electrode designs for bottom and top plates used in the 5-plex device****. (Bottom) The five step on-chip automated droplet movements for the formation of five triDrop electroporations in parallel. The different coloured "blue" droplets represent the different guide combinations with primary T-cells that can be dispensed and electroporated with the high conductivity buffer (shown as pink)*

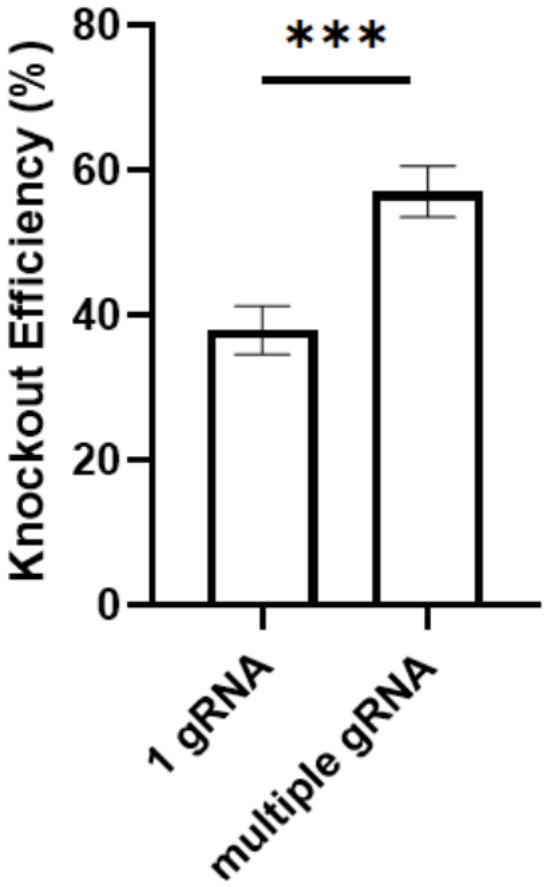

Figure 8-13: ***Single guide vs multi-guide knockouts****. Comparison of primary human T cells electroporated with one gRNA targeting the TRAC locus vs cells electroporated with multiple gRNAs (combinations of three and four guides). Error bars are based on standard error of the mean for n = 8 and n = 10 replicates respectively. Statistical analysis was performed using an unpaired T test. P < 0.001.*

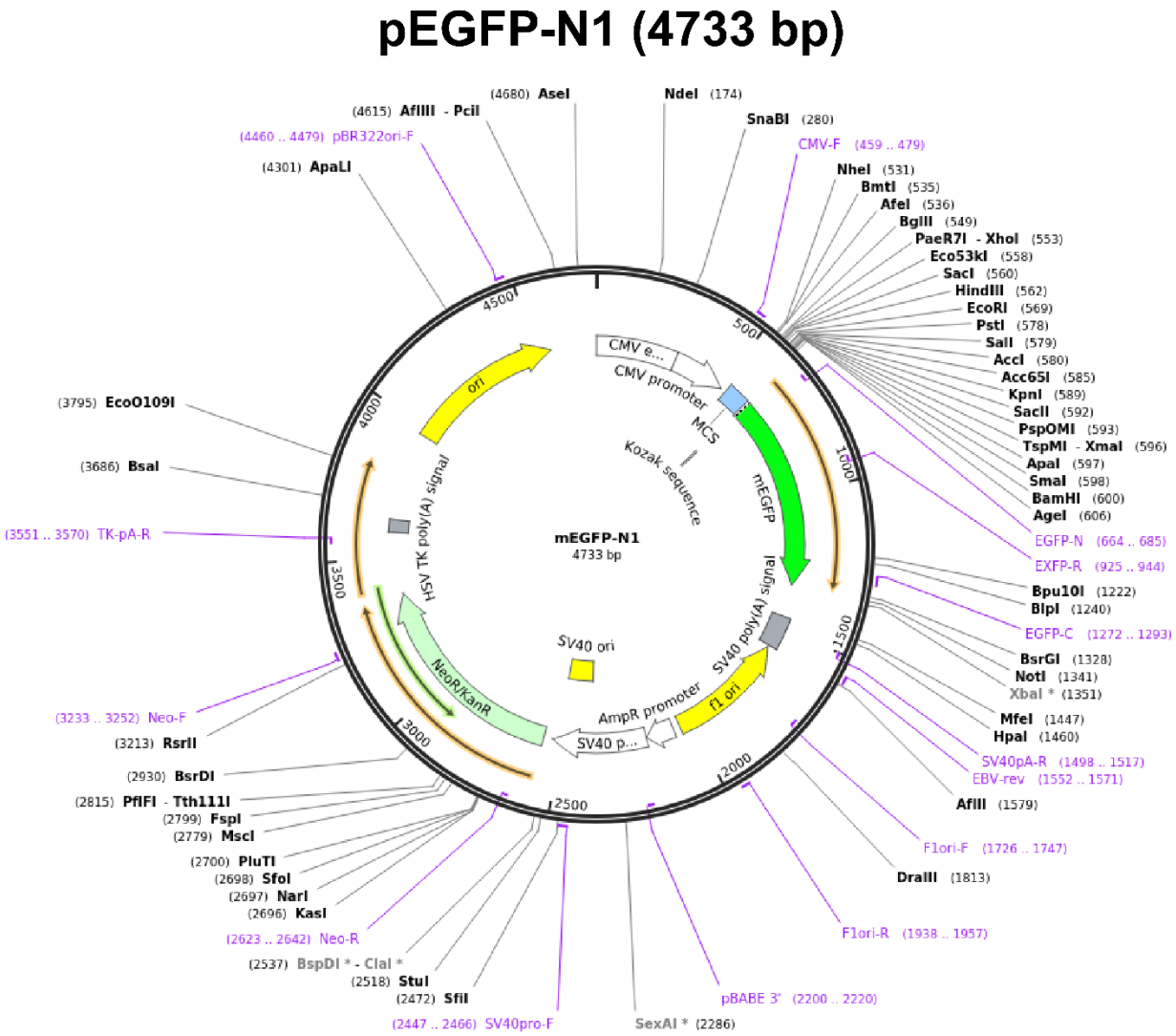

Figure 8-14: ***eGFP plasmid map****. The plasmid map contains a neomycin or kanamycin resistance marker. The eGFP is driven by a CMV promoter. More information can be found from Addgene (catalog no. 54767).*

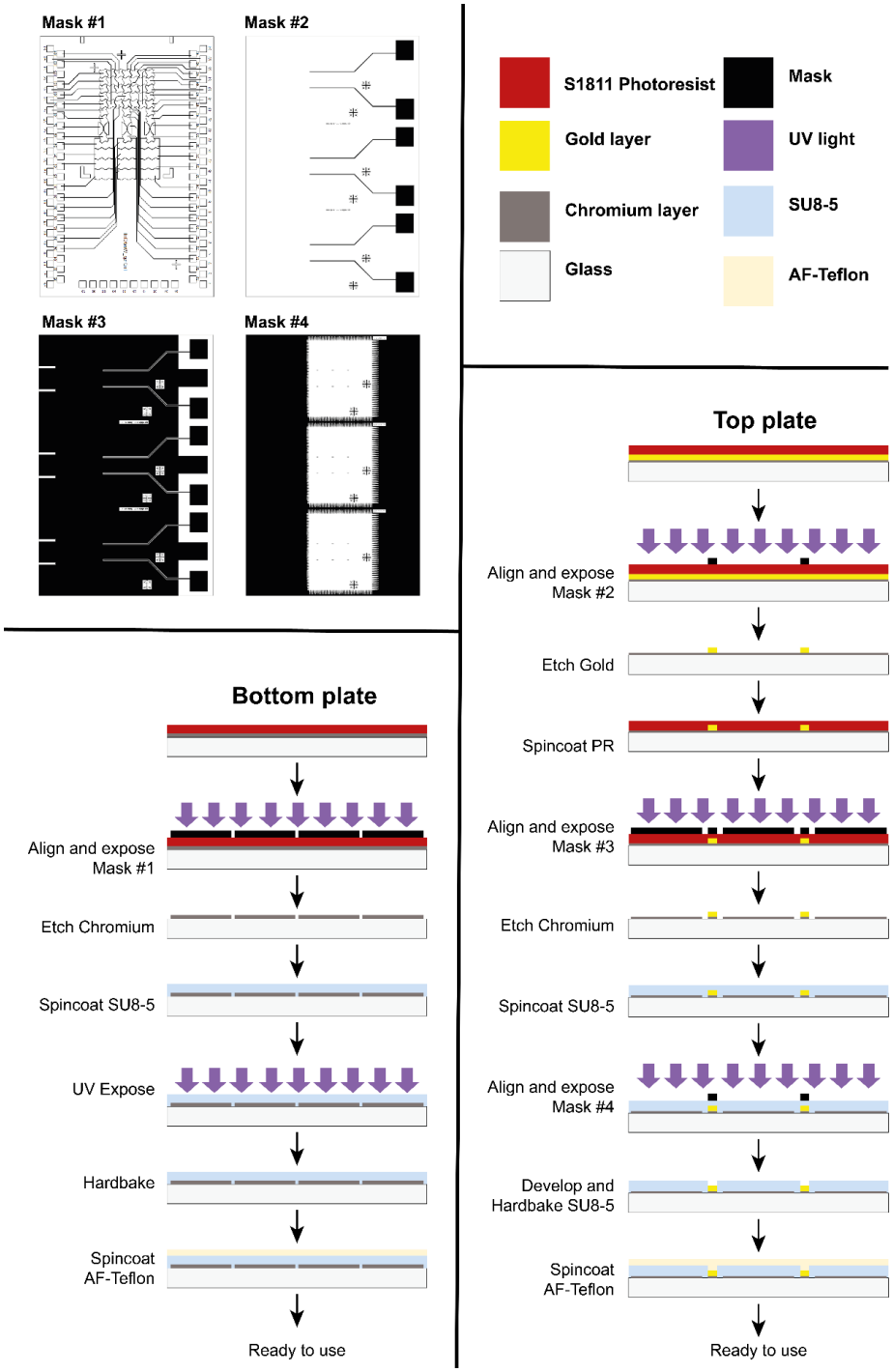

Figure 8-15: ***Fabrication procedure shown for the triDrop electroporation digital microfluidic device****. The bottom plate shows the general procedure for digital microfluidic bottom plate electrode fabrication. The top-plate shows how to fabricate the gold-lines for electroporating the triDrop structure and to create a semi-transparent top-plate to visualize the droplets. After fabrication, the top-plate is aligned with electrodes on the bottom-plate to ensure the flanking (outside) droplets are touching the gold lines (not shown).*

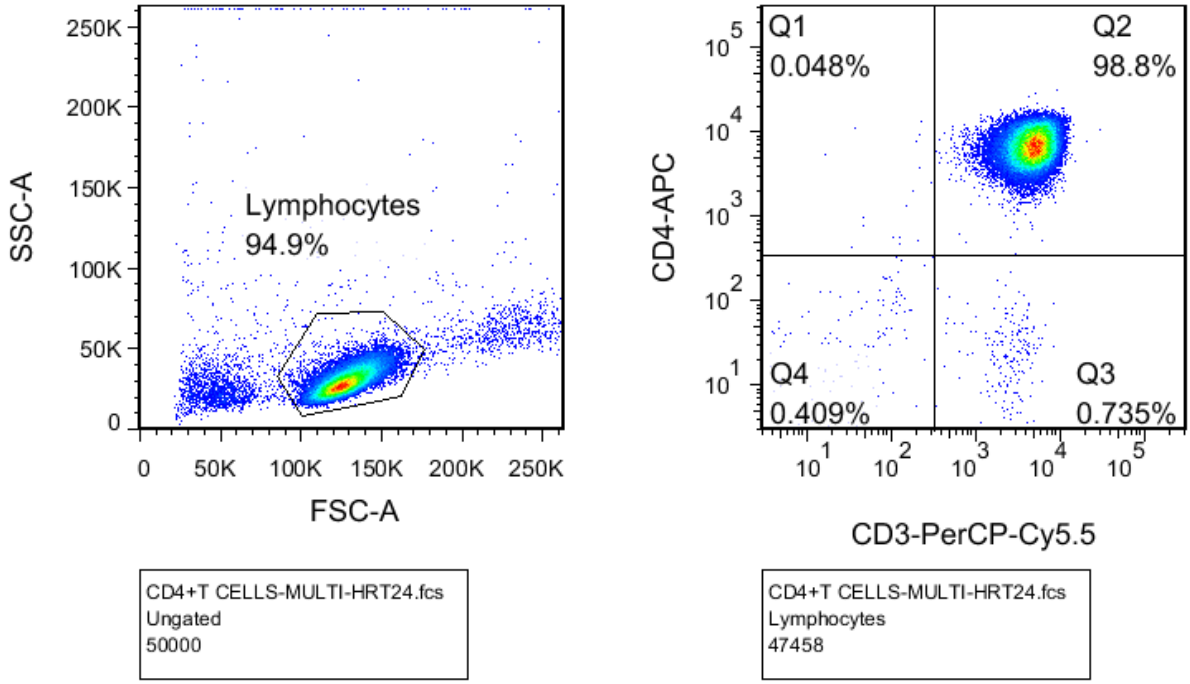

Figure 8-16: ***FACS data showing the isolation of CD4+ cell*** *from fresh human blood using the EasySep Human CD4 T cell Isolation kit*

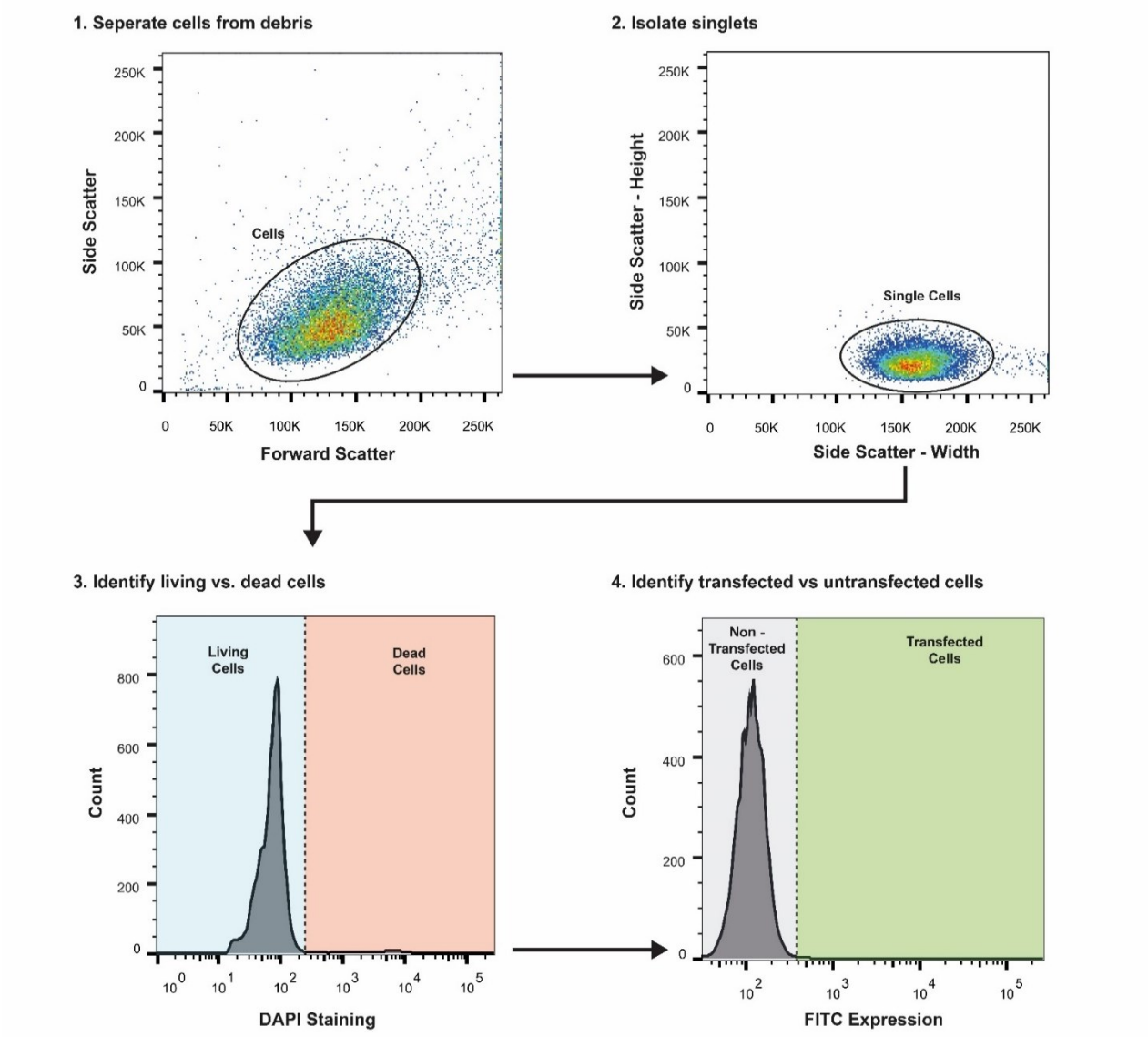

Figure 8-17: ***Flow cytometry gating overview.*** *A non-electroporated sample mixed with the prospective payload is used to define gating. First, cells are separated from debris. Next, single cells are isolated from doublets. This is followed by identifying live/dead cells which are determined with DAPI staining. Finally, successfully electroporated living cells are identified.*

Appendix D: Supplementary Information for Chapter 4

9.1 Supplementary Tables

Table 9-1: Cost of Genetically Engineering Primary Human T cells

Process	Material	Material Cost (CAD)	Nucleofector		Neon		triDrop	
			Amount Needed per reaction	Cost (CAD)	Amount Needed per reaction	Cost (CAD)	Amount Needed per reaction	Cost (CAD)
Pan T Cell Isolation	Leukopack	4757 (~ 5 x 10^9 cells)	1 x 10^6 cells	0.95	2 x 10^5 cells	0.19	5 x 10^4 cells	0.05
	Isolation Kit	979 (1 x 10^9 cells)	1 x 10^6 cells	0.98	2 x 10^5 cells	0.2	5 x 10^4 cells	0.05
Cell Culture	Media + Serum w/ cytokines	85 (500 mL)	1 mL	0.17	0.2 mL	0.03	0.05 mL	<0.01
	Activation Beads	1195 (2 mL)	0.025 mL	15	0.005 mL	3	0.00125 mL	0.75
Gene Editing	Cas9 Nuclease	1294 (500 µg/3nmol)	50 pmol	21.50	10 pmol	4.32	2.5 pmol	1.08
	sgRNA	95 (1.5 nmol)	100 pmol	6.33	20 pmol	1.24	5 pmol	0.31
TOTAL COST FOR 1 REACTION			**$44.90**		**$8.98**		**$2.25**	

NOTE: Reagent costs are validated as of June 2024 and may change with bulk purchasing or institutional pricing. It is assumed that ~50% of cells in a Leukopak are pan T cells. Costs will change depending on what cell line is being engineered. Leukopak – StemCell Technologies (catalog # 70500); Isolation Kit – StemCell Technologies (catalog # 17951); serum – Thermo Fisher (catalog # A5670701); cytokines – Thermo Fisher (catalog #200-02-1MG); activation beads – Thermo Fisher (catalog #11161D); Cas9 Nuclease - Thermo Fisher (catalog #A36496); gRNA – Synthego (SKU: SKU: 052-1020-000-1.5n-0)

Table 9-2: Import Sequences

Name	Sequence
eGFP mRNA	AUGGUGAGCAAGGGCGAGGAGCUGUUCACCGGGGUGGUGCCCAUCCUGGUCG AGCUGGACGGCGACGUAAACGGCCACAAGUUCAGCGUGUCCGGCGAGGGCGA GGGCGAUGCCACCUACGGCAAGCUGACCCUGAAGUUCAUCUGCACCACCGGCA AGCUGCCCGUGCCCUGGCCCACCCUCGUGACCACCCUGACCUACGGCGUGCAG UGCUUCAGCCGCUACCCCGACCACAUGAAGCAGCACGACUUCUUCAAGUCCGC CAUGCCCGAAGGCUACGUCCAGGAGCGCACCAUCUUCUUCAAGGACGACGGCA ACUACAAGACCCGCGCCGAGGUGAAGUUCGAGGGCGACACCCUGGUGAACCGC AUCGAGCUGAAGGGCAUCGACUUCAAGGAGGACGGCAACAUCCUGGGGCACA AGCUGGAGUACAACUACAACAGCCACAACGUCUAUAUCAUGGCCGACAAGCAG AAGAACGGCAUCAAGGUGAACUUCAAGAUCCGCCACAACAUCGAGGACGGCA GCGUGCAGCUCGCCGACCACUACCAGCAGAACACCCCCAUCGGCGACGGCCCC GUGCUGCUGCCCGACAACCACUACCUGAGCACCCAGUCCGCCCUGAGCAAAGA CCCCAACGAGAAGCGCGAUCACAUGGUCCUGCUGGAGUUCGUGACCGCCGCCG GGAUCACUCUCGGCAUGGACGAGCUGUACAAGUAA
SRSF2 gRNA	/AlTR1/rCrGrGrCrUrGrUrGrGrUrGrUrGrArGrUrCrCrGrGrGrUrUrUrUrArGrArGrCrUr ArUrGrCrU/AlTR2/
ssODN HDR template	T*G*GACGGCCGCGAGCTGCGGGTGCAAATGGCGCGCTACGGCCGCCCTCCAGAT TCACACCACAGCCGCCGGGGACCGCCACCCCGCAG*G*T
Pri077 F	AGCGATATAAACGGGCGCAG
Pri077 R	TCGCGACCTGGATTTGGATT
Pri0003-A1	T*/iC*/GGCGACGTGTACATCC
Barcode Flanking Sequence (Top Strand)	5' - ATCGCCTACCGTGA - barcode - TTGCCTGTCGCTCTATCTTC - 3'
Barcode Flanking Sequence (Bottom Strand)	5' - ATCGCCTACCGTGA - barcode - TCTGTTGGTGCTGATATTGC - 3'
Barcode 01	AAGAAAGTTGTCGGTGTCTTTGTG
Barcode 02	TCGATTCCGTTTGTAGTCGTCTGT
Barcode 03	GAGTCTTGTGTCCCAGTTACCAGG
Barcode 04	TTCGGATTCTATCGTGTTTCCCTA
Barcode 05	CTTGTCCAGGGTTTGTGTAACCTT
Barcode 06	TTCTCGCAAAGGCAGAAAGTAGTC
Barcode 07	GTGTTACCGTGGGAATGAATCCTT
Barcode 08	TTCAGGGAACAAACCAAGTTACGT
Barcode 09	AACTAGGCACAGCGAGTCTTGGTT
Barcode 10	AAGCGTTGAAACCTTTGTCCTCTC
Barcode 11	GTTTCATCTATCGGAGGGAATGGA
Barcode 12	CAGGTAGAAAGAAGCAGAATCGGA

Table 9-3: Mutually Dysregulated Genes (p <0.05)

Gene Symbol	Gene Name	Ensembl Gene ID	Fold Change			Putative Function
			triDrop	Neon	Nucleofection	
ACBD3	acyl-CoA binding domain containing 3	ENSG00000182827	3.71228801	3.77293021	4.26957006	Involved in the maintenance of Golgi structure and function
MT1M	Metallothionein 1M	ENSG00000205364	2.87867827	2.77319454	3.70987145	Member of the metallothionein superfamily
SLC7A11	Solute carrier family 7 member 11	ENSG00000151012	4.36751455	4.49961256	3.7043796	Implicated in ferroptosis[255]
PMCH	Pro-Melanin Concentrating Hormone	ENSG00000183395	1.59762742	2.38135295	2.6530848	Expression in immune cells may inhibit proliferation[256]
CRIP1	Cysteine rich protein 1	ENSG00000213145	1.17007127	1.3629836	1.80771559	LIM/double zinc finger protein family
RPL38P4	Ribosomal Protein L38 Pseudogene 4	ENSG00000250562	1.19873041	1.38231401	1.49196731	Pseudogene

Table 9-4: Reactome Pathway Analysis

Reactome		Z-scores		
Pathway ID	**Brief description**	**Nucelofection**	**triDrop**	**Neon**
R-HSA-5661231	Metallothioneins bind metals	7.857664356	3.423042716	9.99969
R-HSA-5660526	Response to metal ions	6.395220981	2.653043923	7.833048
R-HSA-2028269	regulation of cell proliferation and apoptosis	4.41568806	1.176575666	4.359968
R-HSA-9614657	transcription of cell death genes	2.637279679	0.401525923	2.575192
R-HSA-9635465	suppression of apoptosis	2.544866109	1.800080837	2.624122
R-HSA-111458	formation of apoptosome	2.210876005	1.340514592	2.419572
R-HSA-9818027	cytoprotective genes	3.355447126	2.238439352	3.910091
R-HSA-9818035	endoplasmic reticulum stress associated genes	3.99123084	-0.123698357	2.488199
R-HSA-9648895	integrated stress response phosphorylation	3.915343024	1.7811285	4.282006
R-HSA-111995	lipid mediators involved in inflammatory responses	7.810607731	4.059175677	8.231199
R-HSA-9818026	inflammation associated genes	3.683541285	-0.287309368	2.024568
R-HSA-75876	resolution of inflammatory response	1.643061815	0.390802551	4.152934

Table 9-5: qPCR Primer Sequences

Gene Symbol	Gene Name	Ensemble ID	Primer sequence	PCR product (bp)	Product Melting Point (°C)
18srRNA	18s ribosomal RNA	NCBI ID: 106631781	**F:** 5'-CTC AAC ACG GGA AAC CTCAC-3' **R:** 5'-CGC TCC ACCAAC TAA GAACG-3'	110	82.3
IL-2	Interleukin-2	ENSG00000109471	**F:** 5'-CACAGCTACAACTGGAGCATTTAC-3' **R:** 5'-TTCAGTTCTGTGGCCTTCTTGG-3'	133	76.6
IFNG	Interferon gamma	ENSG00000111537	**F:** 5'- GAGTGTGGAGACCATCAAGGA -3' **R:** 5'-GGACATTCAAGTCAGTTACCGAA-3'	113	78.1
TNFα	Tumor necrosis factor	ENSG00000232810	**F:** 5'- AACCTCCTCTCTGCCATCAA -3' **R:** 5'- GGAAGACCCCTCCCAGATAG -3'	100	84

9.2 Supplementary Figures

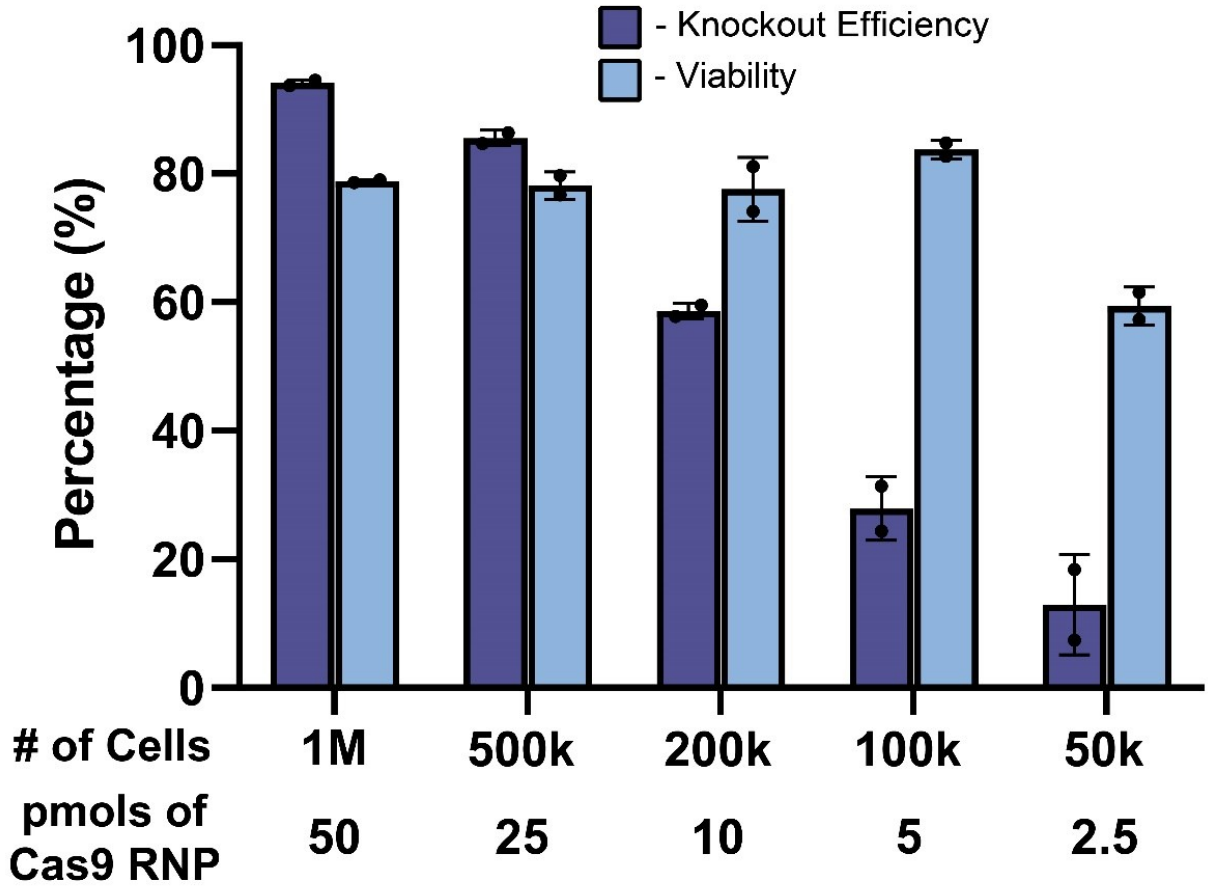

Figure 9-1: ***Reducing Payload and Cell Count with the Nucleofector****. Bar graphs showing knockout efficiency (dark blue) and viability (light blue) measured four days post-EP for cells engineered with the Nucleofector. The number of cells and amount payload are indicated under each set of bars. All error bars represent mean +/- 1 SD.*

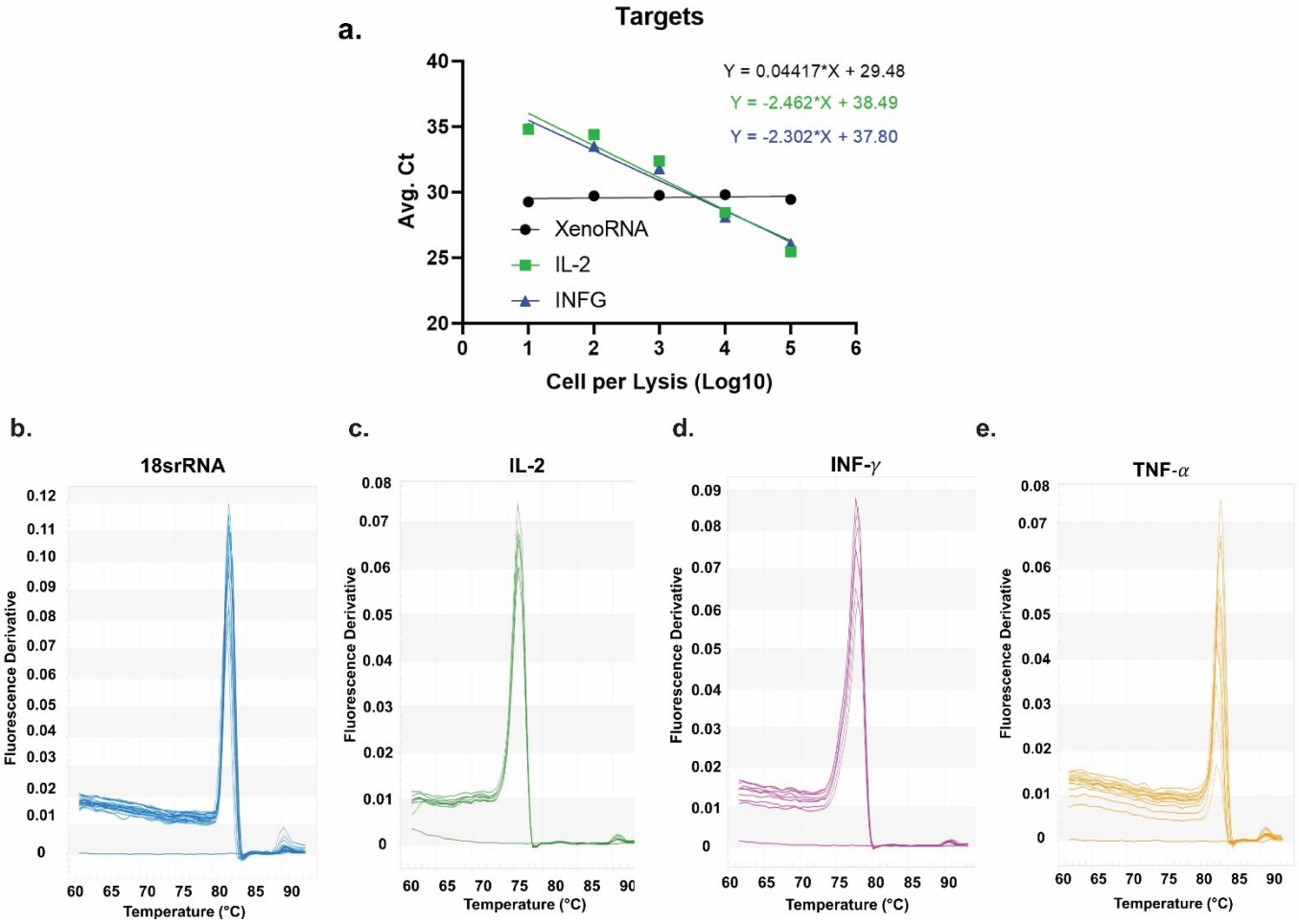

Figure 9-2: ***qPCR raw data****. a) Standard curve depicting relationship between threshold cycle and number of lysed cells. Melting curves for b) 18srRNA, c) IL-2, d) IFN-γ, e) TNF-α showing product melt point consistent with that predicted in Table S5.*

Wild Type Sequence

tggacggccgcgagctgcgggtgcaaatggcgcgctacggccgccccccggactcacaccacagccgccggggaccgccaccccgcaggt

ssODN HDR Template Sequence

tggacggccgcgagctgcgggtgcaaatggcgcgctacggccgcccTccAgaTtcacaccacagccgccggggaccgccaccccgcaggt

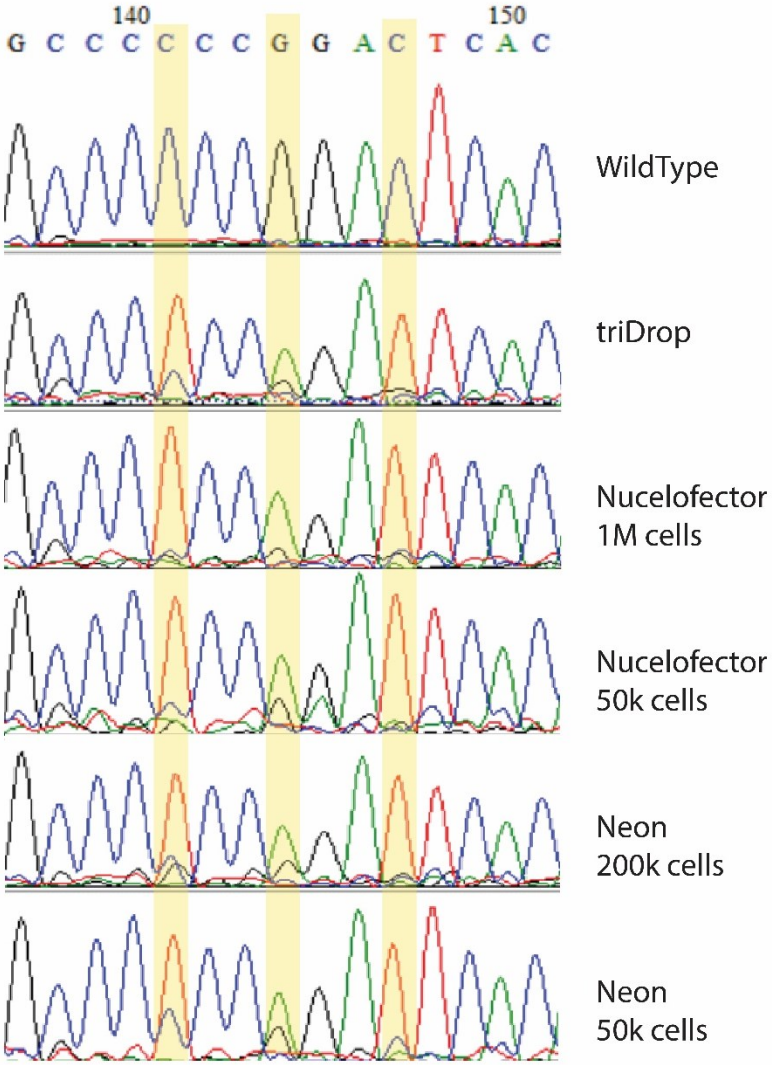

Figure 9-3: ***Sanger Sequencing*** *. Wild type sequence and ssODN HDR template sequence with difference between the sequences highlighted. Chromatograms produced via Sanger for cells electroporated with all three EP systems using varying amounts of cells per reaction. Chromatograms are aligned using snap gene and = the yellow highlight is to show the difference between wild type and knock-in sequence.*

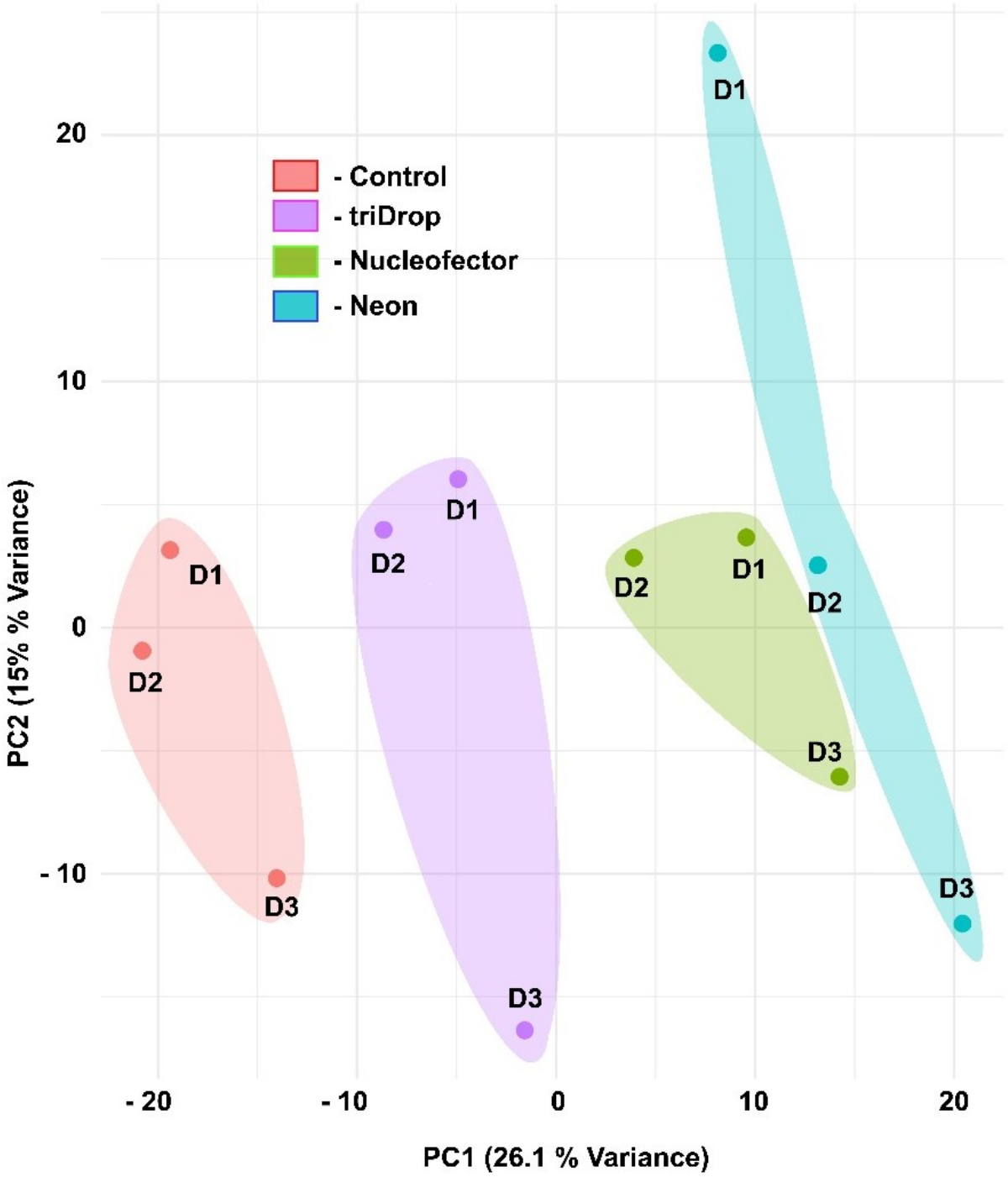

Figure 9-4: ***RNAseq data.*** *Principal component analysis performed across all genes for three donors electroporated with the three EP systems. Control (red cluster), triDrop (purple cluster), Nucleofector (green cluster) and Neon (blue cluster) are all shown. Cluster proximity indicates increased similarity between samples meaning the triDrop is most similar to the control six hours post EP. Graph was generated using DESeq2*

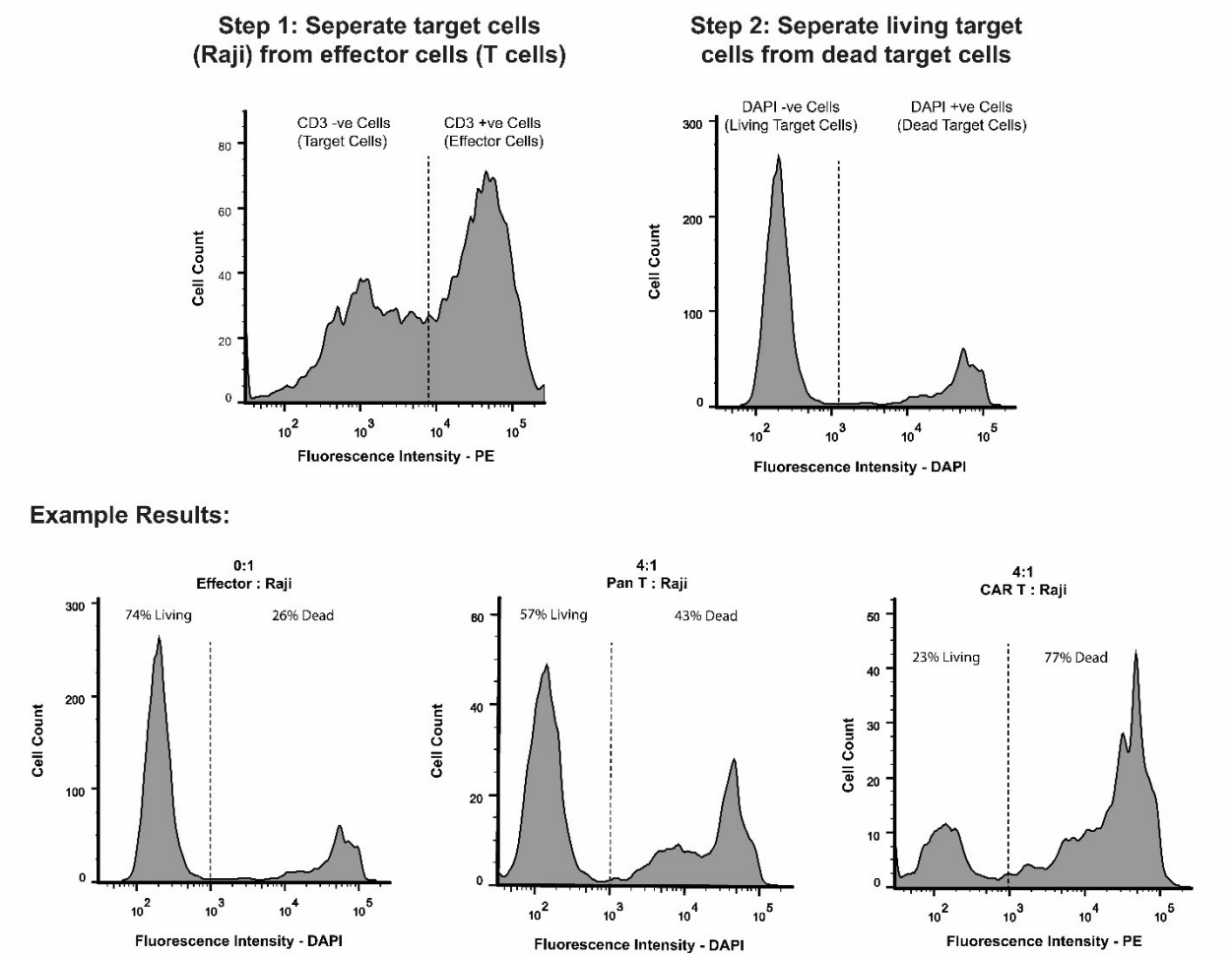

Figure 9-5: ***CAR Killing-Assay Flow Cytometry Pipeline****. Flow cytometry gating pipeline for target cell killing analysis. Cells are stained with CD3-PE (Phycoerythrin) antibody and DAPI prior to flow cytometry. Histogram showing PE fluorescence intensity is generated for all lymphocytes showing two peaks allowing for effector and target cells to be differentiated. CD3 negative target cells (i.e. PE negative) are isolated and a new histogram is generated showing DAPI fluorescence intensity allowing for the differentiation of living and dead cells. Sample live-dead plots are shown for control Raji cells, and Raji cells cultured for 24 hours at a 4:1 ratio with activated pan T cells and triDrop engineered CAR T cells.*

References

1. Narayanan, S. & Shami, P. J. Treatment of acute lymphoblastic leukemia in adults. *Crit. Rev. Oncol. Hematol.* **81**, 94–102 (2012).

2. Hossain, M. J., Xie, L. & McCahan, S. M. Characterization of Pediatric Acute Lymphoblastic Leukemia Survival Patterns by Age at Diagnosis. *J. Cancer Epidemiol.* **2014**, 865979 (2014).

3. Brentjens, R. *et al.* CD19-targeted T cells rapidly induce molecular remissions in adults with chemotherapy-refractory acute lymphoblastic leukemia. **5**, 177ra38 (2013).

4. Park, J. H. *et al.* Long-Term Follow-up of CD19 CAR Therapy in Acute Lymphoblastic Leukemia. *N. Engl. J. Med.* **378**, 449–459 (2018).

5. June, C. H. & Sadelain, M. Chimeric Antigen Receptor Therapy. *N. Engl. J. Med.* **379**, 64–73 (2018).

6. Marofi, F. *et al.* CAR T cells in solid tumors: challenges and opportunities. *Stem Cell Res. Ther.* **12**, 81 (2021).

7. Maldini, C. R., Ellis, G. I. & Riley, J. L. CAR T cells for infection, autoimmunity and allotransplantation. *Nat. Rev. Immunol.* **18**, 605–616 (2018).

8. Blache, U., Tretbar, S., Koehl, U., Mougiakakos, D. & Fricke, S. CAR T cells for treating autoimmune diseases. *RMD Open* **9**, e002907 (2023).

9. von Baumgarten, L., Stauss, H. J. & Lünemann, J. D. Synthetic Cell-Based Immunotherapies for Neurologic Diseases. *Neurol. Neuroimmunol. neuroinflammation* **10**, e200139 (2023).

10. Wang, L. L. *et al.* Cell therapies in the clinic. *Bioeng. Transl. Med.* e10214 (2021) doi:10.1002/btm2.10214.

11. Kennedy, L. B. & Salama, A. K. S. A review of cancer immunotherapy toxicity. *CA. Cancer J. Clin.* **70**, 86–104 (2020).

12. Gumber, D. & Wang, L. D. Improving CAR-T immunotherapy: Overcoming the challenges of T cell exhaustion. *eBioMedicine* **77**, 103941 (2022).

13. Lim, H., Kim, H., Kim, S., Lim, H. & Chung, A. J. Expanding CAR-T cell immunotherapy horizons through microfluidics. **24**, 1088 (2024).

14. Feynman, R. Plenty of room at the bottom. *Am. Sci.* **100**, 226–233 (1959).

15. Purcell, E. M. Life at low Reynolds number. *Am. J. Phys.* **45**, 3–11 (1977).

16. Brody, J. P., Yager, P., Goldstein, R. E. & Austin, R. H. Biotechnology at low Reynolds numbers. *Biophys. J.* **71**, 3430–3441 (1996).

17. Whitesides, G. M. The origins and the future of microfluidics. **442**, 368–373 (2006).

18. Moragues, T. *et al.* Droplet-based microfluidics. *Nat. Rev. Methods Prim.* **3**, 32 (2023).

19. Squires, T. M. Microfluidics : Fluid physics at the nanoliter scale. *Rev. Mod. Phys.* **77**, 977–1026 (2005).

20. Umbanhowar, P. B., Prasad, V. & Weitz, D. A. Monodisperse Emulsion Generation via Drop Break Off in a Coflowing Stream. 347–351 (2000).

21. Matuła, K., Rivello, F. & Huck, W. T. S. Single-Cell Analysis Using Droplet Microfluidics. **4**, 1900188 (2020).

22. Shembekar, N., Hu, H., Eustace, D. & Merten, C. A. Single-Cell Droplet Microfluidic Screening for Antibodies Specifically Binding to Target Cells. *Cell Rep.* **22**, 2206–2215 (2018).

23. Agresti, J. J. *et al.* Ultrahigh-throughput screening in drop-based microfluidics for directed evolution. *Proc. Natl. Acad. Sci. U. S. A.* **107**, 4004–9 (2010).

24. Ahmadi, F., Samlali, K., Vo, P. Q. N. & Shih, S. C. C. An integrated droplet-digital microfluidic system for on-demand droplet creation, mixing, incubation, and sorting. *Lab Chip* **19**, 524–535 (2019).

25. McDonald, J. C. *et al.* Fabrication of microfluidic systems in poly(dimethylsiloxane). *Electrophoresis* **21**, 27–40 (2000).

26. Clausell-Tormos, J. *et al.* Droplet-Based Microfluidic Platforms for the Encapsulation and Screening of Mammalian Cells and Multicellular Organisms. *Chem. Biol.* **15**, 427–437 (2008).

27. Eduati, F. *et al.* A microfluidics platform for combinatorial drug screening on cancer biopsies. *Nat. Commun.* **9**, 2434 (2018).

28. Ronteix, G. *et al.* High resolution microfluidic assay and probabilistic modeling reveal cooperation between T cells in tumor killing. *Nat. Commun.* **13**, 3111 (2022).

29. Agnihotri, S. N. *et al.* Droplet microfluidics for functional temporal analysis and cell recovery on demand using microvalves: application in immunotherapies for cancer. *Lab Chip* **22**, 3258–3267 (2022).

30. Wheeler, M. A. *et al.* Droplet-based forward genetic screening of astrocyte–microglia cross-talk. *Science (80-.).* **379**, 1023–1030 (2023).

31. Sart, S., Ronteix, G., Jain, S., Amselem, G. & Baroud, C. N. Cell Culture in Micro fl uidic Droplets. *Chem. Rev.* **122**, 7061–7088 (2022).

32. Wang, Y., Liu, M., Zhang, Y., Liu, H. & Han, L. Recent methods of droplet microfluidics and their applications in spheroids and organoids. *Lab Chip* **23**, 1080–1096 (2023).

33. Anderson, S., Hadwen, B. & Brown, C. Thin-film-transistor digital microfluidics for high valuein vitrodiagnostics at the point of need. *Lab Chip* **21**, 962–975 (2021).

34. Choi, K., Ng, A. H. C., Fobel, R. & Wheeler, A. R. Digital Microfluidics. *Annu. Rev. Anal. Chem.* **5**, 413–440 (2012).

35. Berthier, J. *et al.* Actuation potentials and capillary forces in electrowetting based microsystems. *Sensors Actuators, A Phys.* **134**, 471–479 (2007).

36. Chatterjee, D., Hetayothin, B., Wheeler, A. R., King, D. J. & Garrell, R. L. Droplet-based microfluidics with nonaqueous solvents and solutions. *Lab Chip* **6**, 199–206 (2006).

37. Chatterjee, D., Shepherd, H. & Garrell, R. L. Electromechanical model for actuating liquids in a two-plate droplet microfluidic device. *Lab Chip* **9**, 1219 (2009).

38. Moazami, E., Perry, J. M., Soffer, G., Husser, M. C. & Shih, S. C. C. Integration of World-

to-Chip Interfaces with Digital Microfluidics for Bacterial Transformation and Enzymatic Assays. *Anal. Chem.* **91**, 5159–5168 (2019).

39. Xing, Y. *et al.* A robust and scalable active-matrix driven digital microfluidic platform based on printed-circuit board technology. *Lab Chip* **21**, 1886–1896 (2021).

40. Fobel, R., Fobel, C. & Wheeler, A. R. DropBot: An open-source digital microfluidic control system with precise control of electrostatic driving force and instantaneous drop velocity measurement. *Appl. Phys. Lett.* **102**, 193513 (2013).

41. Ng, A. H. C. *et al.* A digital microfluidic system for serological immunoassays in remote settings. *Sci. Transl. Med.* **10**, eaar6076 (2018).

42. Samiei, E., Tabrizian, M. & Hoorfar, M. A review of digital microfluidics as portable platforms for lab-on a-chip applications. *Lab Chip* **16**, 2376–2396 (2016).

43. Zhang, Y. & Liu, Y. Advances in integrated digital microfluidic platforms for point-of-care diagnosis: A review. *Sensors and Diagnostics* **1**, 648–672 (2022).

44. Perry, J. M., Soffer, G., Jain, R. & Shih, S. C. C. Expanding the limits towards 'one-pot' DNA assembly and transformation on a rapid-prototype microfluidic device. *Lab Chip* **21**, 3730–3741 (2021).

45. MiroCanvas: Fully Automated NGS Library Prep. https://www.integra-biosciences.com/canada/en/ngs-automation/miro-canvas.

46. TraxION: A Transformative Aproach to Sequencing. https://nanoporetech.com/products/sequence/traxion.

47. Volta Labs: UNLOCKING THE UTILITY OF GENOMICS FOR THE WORLD. https://www.voltalabs.com/.

48. Nuclera: Access Your Target Proteins On Demand. https://www.nuclera.com/.

49. Nicoya: The world's first digital high-throughput benchtop SPR system. https://nicoyalife.com/.

50. Li, J. & Kim, C. J. Current commercialization status of electrowetting-on-dielectric (EWOD) digital microfluidics. *Lab Chip* **20**, 1705–1712 (2020).

51. Drop Genie: Accelerating the Pace of Discovery. https://www.drop-genie.com/.

52. Barbulovic-Nad, I., Yang, H., Park, P. S. & Wheeler, A. R. Digital microfluidics for cell-based assays. *Lab Chip* **8**, 519–526 (2008).

53. Barbulovic-Nad, I., Au, S. H. & Wheeler, A. R. A microfluidic platform for complete mammalian cell culture. *Lab Chip* **10**, 1536 (2010).

54. Srigunapalan, S., Eydelnant, I. A., Simmons, C. A. & Wheeler, A. R. A digital microfluidic platform for primary cell culture and analysis. *Lab Chip* **12**, 369–375 (2012).

55. Lamanna, J. *et al.* Digital microfluidic isolation of single cells for -Omics. *Nat. Commun.* **11**, 5632 (2020).

56. Au, S. H., Chamberlain, M. D., Mahesh, S., Sefton, M. V. & Wheeler, A. R. Hepatic organoids for microfluidic drug screening. *Lab Chip* **14**, 3290 (2014).

57. Piwocka, O. *et al.* Navigating challenges: optimising methods for primary cell culture isolation. *Cancer Cell Int.* **24**, 28 (2024).

58. Richter, M. *et al.* From Donor to the Lab: A Fascinating Journey of Primary Cell Lines. *Front. Cell Dev. Biol.* **9**, 711381 (2021).

59. Cong, L. *et al.* Multiplex Genome Engineering Using CRISPR/Cas Systems. *Science (80-.).* 819–824 (2013).

60. Mali, P., Esvelt, K. M. & Church, G. M. Cas9 as a versatile tool for engineering biology. *Nat. Methods* **10**, 957–963 (2013).

61. Ran, F. A. *et al.* Genome engineering using crispr-cas9 system. *Nat. Protoc.* **8**, 197–217 (2013).

62. Eyquem, J. *et al.* Targeting a CAR to the TRAC locus with CRISPR/Cas9 enhances tumour rejection. *Nature* **543**, 113–117 (2017).

63. Vonderheide, R. H. & June, C. H. Engineering T cells for cancer: Our synthetic future. *Immunol. Rev.* **257**, 7–13 (2014).

64. Wellhausen, N., Agarwal, S., Rommel, P. C., Gill, S. I. & June, C. H. Better living through

chemistry: CRISPR/Cas engineered T cells for cancer immunotherapy. *Curr. Opin. Immunol.* **74**, 76–84 (2022).

65. Finck, A. V., Blanchard, T., Roselle, C. P., Golinelli, G. & June, C. H. Engineered cellular immunotherapies in cancer and beyond. *Nat. Med.* **28**, 678–689 (2022).

66. Lino, C. A., Harper, J. C., Carney, J. P. & Timlin, J. A. Delivering crispr: A review of the challenges and approaches. *Drug Deliv.* **25**, 1234–1257 (2018).

67. Maude, S. L., Teachey, D. T., Porter, D. L. & Grupp, S. A. CD19-targeted chimeric antigen receptor T-cell therapy for acute lymphoblastic leukemia. *Blood* **125**, 4017–4024 (2015).

68. Fraietta, J. A. *et al.* Disruption of TET2 promotes the therapeutic efficacy of CD19-targeted T cells. *Nature* **558**, 307–312 (2018).

69. Dodson, B. P. & Levine, A. D. Challenges in the translation and commercialization of cell therapies. *BMC Biotechnol.* **15**, 70 (2015).

70. Li, X. *et al.* Viral Vector-Based Gene Therapy. *Int. J. Mol. Sci.* **24**, 7736 (2023).

71. Bulcha, J. T., Wang, Y., Ma, H., Tai, P. W. L. & Gao, G. Viral vector platforms within the gene therapy landscape. *Signal Transduct. Target. Ther.* **6**, 53 (2021).

72. Wolff, J. H. & Mikkelsen, J. G. Delivering genes with human immunodeficiency virus-derived vehicles: still state-of-the-art after 25 years. *J. Biomed. Sci.* **29**, 79 (2022).

73. Naldini, L., Trono, D. & Verma, I. M. Lentiviral vectors, two decades later. *Science (80-.).* **353**, 1101–1102 (2016).

74. Aldrak, N. *et al.* Oncolytic herpes simplex virus-based therapies for cancer. *Cells* **10**, 1541 (2021).

75. Syyam, A. *et al.* Adenovirus vector system: construction, history and therapeutic applications. *Biotechniques* **73**, 297–305 (2022).

76. Li, C. & Samulski, R. J. Engineering adeno-associated virus vectors for gene therapy. *Nat. Rev. Genet.* **21**, 255–272 (2020).

77. Zhao, Z., Anselmo, A. C. & Mitragotri, S. Viral vector-based gene therapies in the clinic.

Bioeng. Transl. Med. **7**, e10258 (2022).

78. Atasheva, S. & Shayakhmetov, D. M. Cytokine Responses to Adenovirus and Adenovirus Vectors. *Viruses* **14**, 888 (2022).

79. Au, H. K. E., Isalan, M. & Mielcarek, M. Gene Therapy Advances: A Meta-Analysis of AAV Usage in Clinical Settings. *Front. Med.* **8**, 809118 (2022).

80. Yoder, K. E., Rabe, A. J., Fishel, R. & Larue, R. C. Strategies for Targeting Retroviral Integration for Safer Gene Therapy: Advances and Challenges. *Front. Mol. Biosci.* **8**, 662331 (2021).

81. Wagner, D. L., Koehl, U., Chmielewski, M., Scheid, C. & Stripecke, R. Review: Sustainable Clinical Development of CAR-T Cells – Switching From Viral Transduction Towards CRISPR-Cas Gene Editing. *Front. Immunol.* **13**, 865424 (2022).

82. Kim, T. K. & Eberwine, J. H. Mammalian cell transfection: The present and the future. *Anal. Bioanal. Chem.* **397**, 3173–3178 (2010).

83. Ponti, F., Campolungo, M., Melchiori, C., Bono, N. & Candiani, G. Cationic lipids for gene delivery: many players, one goal. *Chem. Phys. Lipids* **235**, 105032 (2021).

84. Zhang, L. *et al.* Lipid nanoparticle-mediated efficient delivery of CRISPR/Cas9 for tumor therapy. *NPG Asia Mater.* **9**, e441 (2017).

85. Mashima, R. & Takada, S. Lipid Nanoparticles: A Novel Gene Delivery Technique for Clinical Application. *Curr. Issues Mol. Biol.* **44**, 5013–5027 (2022).

86. Hou, X., Zaks, T., Langer, R. & Dong, Y. Lipid nanoparticles for mRNA delivery. *Nat. Rev. Mater.* **6**, 1078–1094 (2021).

87. Kraft, J. C., Freeling, J. P., Wang, Z. & Ho, R. J. Y. Emerging research and clinical development trends of liposome and lipid nanoparticle drug delivery systems. *J. Pharm. Sci.* **103**, 29–52 (2014).

88. Raes, L., De Smedt, S. C., Raemdonck, K. & Braeckmans, K. Non-viral transfection technologies for next-generation therapeutic T cell engineering. *Biotechnol. Adv.* **49**, 107760 (2021).

89. Fajrial, A. K., He, Q. Q., Wirusanti, N. I., Slansky, J. E. & Ding, X. A review of emerging physical transfection methods for CRISPR/Cas9-mediated gene editing. *Theranostics* **10**, 5532–5549 (2020).

90. Yarmush, M. L., Golberg, A., Kotnik, T. & Miklavˇ, D. Electroporation-Based Technologies for Medicine : Principles , Applications , and Challenges. *Annu. Rev. Biomed. Eng.* **16**, 295–320 (2014).

91. Kotnik, T. & Bobanovid, F. Sensitivity of transmembrane voltage induced by applied electric fields a theoretical analysis. **43**, 285–291 (1997).

92. Campelo, S. N., Huang, P.-H., Buie, C. R. & Davalos, R. V. Advancements in Electroporation Technologies: From Bench to Clinic. *Annu. Rev. Biomed. Eng. 2023* **25**, 78–94 (2023).

93. Zhang, J. *et al.* Non-viral, specifically targeted CAR-T cells achieve high safety and efficacy in B-NHL. *Nature* **609**, 369–374 (2022).

94. DiTommaso, T. *et al.* Cell engineering with microfluidic squeezing preserves functionality of primary immune cells in vivo. *Proc. Natl. Acad. Sci. U. S. A.* **115**, E10907–E10914 (2018).

95. Hur, J. *et al.* Genetically Stable and Scalable Nanoengineering of Human Primary T Cells via Cell Mechanoporation. *Nano Lett.* **23**, 7341–7349 (2023).

96. Rols, M.-P. Parameters Affecting Cell Viability Following Electroporation In Vitro. *Handb. Electroporation* **75**, 1449–1465 (2017).

97. Kim, J. A. *et al.* A novel electroporation method using a capillary and wire-type electrode. *Biosens. Bioelectron.* **23**, 1353–1360 (2008).

98. Li, Y. *et al.* Electroporation on microchips: The harmful effects of pH changes and scaling down. *Sci. Rep.* **5**, 17817 (2015).

99. Hoffman, A, G. Animal Cell Electroporation And Electrofusion Protocols: Instrumentation. *Cell Electroporation Electrofusion Protoc.* **3**, 41–59 (1995).

100. Chicaybam, L., Sodre, A. L., Curzio, B. A. & Bonamino, M. H. An Efficient Low Cost

Method for Gene Transfer to T Lymphocytes. *PLoS One* **8**, e60298 (2013).

101. Saulis, G., Lape, R., Pranevičiute, R. & Mickevičius, D. Changes of the solution pH due to exposure by high-voltage electric pulses. *Bioelectrochemistry* **67**, 101–108 (2005).

102. MaxCyte. https://maxcyte.com/.

103. Nucleofector. bioscience.lonza.com.

104. Neon NxT Electroporation System. https://www.thermofisher.com/au/en/home/life-science/cell-culture/transfection/neon-electroporation-system.html.

105. Hur, J. & Chung, A. J. Microfluidic and Nanofluidic Intracellular Delivery. *Adv. Sci.* **8**, 2004595 (2021).

106. Szeto, G. L. *et al.* Microfluidic squeezing for intracellular antigen loading in polyclonal B-cells as cellular vaccines. *Sci. Rep.* **5**, 10276 (2015).

107. Li, J. *et al.* Microfluidic-Enabled Intracellular Delivery of Membrane Impermeable Inhibitors to Study Target Engagement in Human Primary Cells. *ACS Chem. Biol.* **12**, 2970–2974 (2017).

108. Sharei, A. *et al.* Ex vivo cytosolic delivery of functional macromolecules to immune cells. *PLoS One* **10**, e0118803 (2015).

109. Sevenler, D. & Toner, M. High throughput intracellular delivery by viscoelastic mechanoporation. *Nat. Commun.* **15**, 115 (2024).

110. Hur, J. *et al.* Microfluidic cell stretching for highly effective gene delivery into hard-to-transfect primary cells. *ACS Nano* **14**, 15094–15106 (2020).

111. Jarrell, J. A. *et al.* Intracellular delivery of mRNA to human primary T cells with microfluidic vortex shedding. *Sci. Rep.* **9**, 3214 (2019).

112. Lissandrello, C. A. *et al.* High-throughput continuous-flow microfluidic electroporation of mRNA into primary human T cells for applications in cellular therapy manufacturing. *Sci. Rep.* **10**, 18045 (2020).

113. Shih, S. C. C. *et al.* A Versatile Microfluidic Device for Automating Synthetic Biology.

ACS Synth. Biol. **4**, 1151–1164 (2015).

114. Gach, P. C. *et al.* A Droplet Microfluidic Platform for Automating Genetic Engineering. *ACS Synth. Biol.* **5**, 426–433 (2016).

115. Sinha, H., Quach, A. B. V., Vo, P. Q. N. & Shih, S. C. C. An automated microfluidic gene-editing platform for deciphering cancer genes. *Lab Chip* **18**, 2300–2312 (2018).

116. Joo, B., Hur, J., Kim, G. B., Yun, S. G. & Chung, A. J. Highly Efficient Transfection of Human Primary T Lymphocytes Using Droplet-Enabled Mechanoporation. *ACS Nano* **15**, 12888–12898 (2021).

117. Lee, J. H. & Chung, A. Highly efficient mRNA transfection with droplet cell squeezing for cellular engineering. *IEEE Int. Conf. Nano/Molecular Med. Eng. NANOMED* 133–136 (2023).

118. Li, X., Aghaamoo, M., Liu, S., Lee, D. H. & Lee, A. P. Lipoplex-Mediated Single-Cell Transfection via Droplet Microfluidics. *Small* **14**, 1802055 (2018).

119. Pérez-Sosa, C. *et al.* Droplets for Gene Editing Using CRISPR-Cas9 and Clonal Selection Improvement Using Hydrogels. *Micromachines* **15**, 413 (2024).

120. Zhan, Y., Wang, J., Bao, N. & Lu, C. Electroporation of cells in microfluidic droplets. *Anal. Chem.* **81**, 2027–2031 (2009).

121. Im, D. J. & Jeong, S. N. Transfection of Jurkat T cells by droplet electroporation. *Biochem. Eng. J.* **122**, 133–140 (2017).

122. Vasileiou, T., Foresti, D., Bayram, A., Poulikakos, D. & Ferrari, A. Toward Contactless Biology: Acoustophoretic DNA Transfection. *Sci. Rep.* **6**, 20023 (2016).

123. Arai, T., Sato, T. & Matsubara, T. Effective Cell Transfection in An Ultrasonically Levitated Droplet for Sustainable Technology. *Adv. Sci.* **9**, 2203576 (2022).

124. Billingsley, M. M. *et al.* Ionizable Lipid Nanoparticle-Mediated mRNA Delivery for Human. *Nano Lett.* **20**, 1578–1589 (2020).

125. Kiesgen, S., Messinger, J. C., Chintala, N. K., Tano, Z. & Adusumilli, P. S. Comparative analysis of assays to measure CAR T-cell-mediated cytotoxicity. *Nat. Protoc.* **16**, 1331–

1342 (2021).

126. Iwai, K. *et al.* Scalable and automated CRISPR-based strain engineering using droplet microfluidics. *Microsystems Nanoeng.* **8**, (2022).

127. Iwai, K. *et al.* Automated flow-based/digital microfluidic platform integrated with onsite electroporation process for multiplex genetic engineering applications. *MEMS 2018* 1229–1232 (2018).

128. Qu, B., Eu, Y. J., Jeong, W. J. & Kim, D. P. Droplet electroporation in microfluidics for efficient cell transformation with or without cell wall removal. *Lab Chip* **12**, 4483–4488 (2012).

129. Yoo, B. S. *et al.* A continuous droplet electroporation system for high throughput processing. *Analyst* **143**, 5785–5791 (2018).

130. Madison, A. C. *et al.* Scalable Device for Automated Microbial Electroporation in a Digital Microfluidic Platform. *ACS Synth. Biol.* **6**, 1701–1709 (2017).

131. Moore, J. A. *et al.* Automated electrotransformation of Escherichia coli on a digital microfluidic platform using bioactivated magnetic beads. *Biomicrofluidics* **11**, 014110 (2017).

132. Simpson, K. J. *et al.* Identification of genes that regulate epithelial cell migration using an siRNA screening approach. *Nat. Cell Biol.* **10**, 1027–1038 (2008).

133. Shalem, O. *et al.* Shalem et al., 2014. *Science (80-.).* **343**, 84–87 (2014).

134. Aiuti, A. *et al.* Lentiviral hematopoietic stem cell gene therapy in patients with wiskott-aldrich syndrome. *Science (80-.).* **341**, (2013).

135. McGarrity, G. *et al.* Patient monitoring and follow-up in lentiviral clinical trials. *J. Gene Med.* **14**, 44–53 (2012).

136. Townsend, M. H., Shrestha, G., Robison, R. A. & O'Neill, K. L. The expansion of targetable biomarkers for CAR T cell therapy. *J. Exp. Clin. Cancer Res.* **37**, 163 (2018).

137. Wang, J., Hu, Y. & Huang, H. Current development of chimeric antigen receptor T-cell therapy. *Stem Cell Investig.* **5**, 44 (2018).

138. Simon, B. *et al.* Enhancing lentiviral transduction to generate melanoma-specific human T cells for cancer immunotherapy. *J. Immunol. Methods* **472**, 55–64 (2019).

139. Segura, M. M., Garnier, A., Durocher, A., Coelho, H. & Kamen, A. Production of Lentiviral Vectors by Large-Scale Transient Transfection of Suspension Cultures and Affinity Chromatography Purificatio. *Biotechnol. Bioeng.* **98**, 789–799 (2007).

140. Tiscornia, G., Singer, O. & Verma, I. M. Production and purification of lentiviral vectors. *Nat. Protoc.* **1**, 241–245 (2006).

141. Geraerts, M., Willems, S., Baekelandt, V., Debyser, Z. & Gijsbers, R. Comparison of lentiviral vector titration methods. *BMC Biotechnol.* **6**, 34 (2006).

142. Merten, O. W. *et al.* Large-scale manufacture and characterization of a lentiviral vector produced for clinical Ex vivo gene therapy application. *Hum. Gene Ther.* **22**, 343–356 (2011).

143. Kutner, R. H., Puthli, S., Marino, M. P. & Reiser, J. Simplified production and concentration of HIV-1-based lentiviral vectors using HYPERFlask vessels and anion exchange membrane chromatography. *BMC Biotechnol.* **9**, 10 (2009).

144. Tran, R. *et al.* Microfluidic Transduction Harnesses Mass Transport Principles to Enhance Gene Transfer Efficiency. *Mol. Ther.* **25**, 2372–2382 (2017).

145. Moore, N. *et al.* A Microfluidic Device to Enhance Viral Transduction Efficiency During Manufacture of Engineered Cellular Therapies. *Sci. Rep.* **9**, 15101 (2019).

146. Cimetta, E. *et al.* Microfluidic-driven viral infection on cell cultures: Theoretical and experimental study. *Biomicrofluidics* **6**, 024127 (2012).

147. Silva, P. N. *et al.* Highly efficient adenoviral transduction of pancreatic islets using a microfluidic device. *Lab Chip* **16**, 2921–2934 (2016).

148. Chuck, A. S., Clarke, M. F. & Palsson, B. O. Retroviral infection is Limited by Brownian Motion. **1534**, 1527–1534 (1996).

149. Sinha, H., Quach, A. B. V., Vo, P. Q. N. & Shih, S. C. C. An automated microfluidic gene-editing platform for deciphering cancer genes. *Lab Chip* **18**, 2300–2312 (2018).

150. Eydelnant, I. A., Uddayasankar, U., Li, B., Liao, M. W. & Wheeler, A. R. Virtual microwells for digital microfluidic reagent dispensing and cell culture. *Lab Chip* **12**, 750–757 (2012).

151. Zhai, J. *et al.* A digital microfluidic system with 3D microstructures for single-cell culture. *Microsystems Nanoeng.* **6**, 6 (2020).

152. Gill, K. P. & Denham, M. Optimized Transgene Delivery Using Third-Generation Lentiviruses. *Curr. Protoc. Mol. Biol.* **133**, e125 (2020).

153. Husser, M. C., Vo, P. Q. N., Sinha, H., Ahmadi, F. & Shih, S. C. C. An Automated Induction Microfluidics System for Synthetic Biology. *ACS Synth. Biol.* **7**, 933–944 (2018).

154. Leclerc, L. M. Y., Soffer, G., Kwan, D. H. & Shih, S. C. C. A fucosyltransferase inhibition assay using image-analysis and digital microfluidics. *Biomicrofluidics* **13**, 034106 (2019).

155. Saunderson, E. A. *et al.* Hit-and-run epigenetic editing prevents senescence entry in primary breast cells from healthy donors. *Nat. Commun.* **8**, 1450 (2017).

156. Vijayraghavan, S. & Kantor, B. A protocol for the production of integrase-deficient lentiviral vectors for CRISPR/Cas9-mediated gene knockout in dividing cells. *J. Vis. Exp.* **2017**, e56915 (2017).

157. Merten, O. W., Hebben, M. & Bovolenta, C. Production of lentiviral vectors. *Mol. Ther. Methods Clin. Dev.* **3**, 16017 (2016).

158. Cao, F. *et al.* Comparison of gene-transfer efficiency in human embryonic stem cells. *Mol. Imaging Biol.* **12**, 15–24 (2010).

159. Aznan, A. N., Karim, N. A., Wan Ngah, W. Z. & Jubri, Z. Critical factors for lentivirus-mediated PRDX4 gene transfer in the HepG2 cell line. *Oncol. Lett.* **16**, 73–82 (2018).

160. Gouvarchin Ghaleh, H. E., Bolandian, M., Dorostkar, R., Jafari, A. & Pour, M. F. Concise review on optimized methods in production and transduction of lentiviral vectors in order to facilitate immunotherapy and gene therapy. *Biomed. Pharmacother.* **128**, 110276 (2020).

161. Brown, L. Y., Dong, W. & Kantor, B. An Improved Protocol for the Production of Lentiviral Vectors. *STAR Protoc.* **1**, 100152 (2020).

162. McCarron, A., Donnelley, M. & Parsons, D. Scale-up of lentiviral vectors for gene therapy: advances and challenges. *Cell Gene Ther. Insights* **3**, 719–729 (2017).

163. Manceur, A. P. *et al.* Scalable Lentiviral Vector Production Using Stable HEK293SF Producer Cell Lines. *Hum. Gene Ther. Methods* **28**, 330–339 (2017).

164. Sinn, P. L., Sauter, S. L. & McCray, P. B. Gene therapy progress and prospects: Development of improved lentiviral and retroviral vectors - Design, biosafety, and production. *Gene Ther.* **12**, 1089–1098 (2005).

165. Counsell, J. R. *et al.* Lentiviral vectors can be used for full-length dystrophin gene therapy. *Sci. Rep.* **7**, 79 (2017).

166. Wotherspoon, S., Dolnikov, A., Symonds, G. & Nordon, R. Susceptibility of Cell Populations to Transduction by Retroviral Vectors. *J. Virol.* **78**, 5097–5102 (2004).

167. Pirona, A. C., Oktriani, R., Boettcher, M. & Hoheisel, J. D. Process for an efficient lentiviral cell transduction. *Biol. Methods Protoc.* **5**, bpaa005 (2021).

168. Hines, W. C., Yaswen, P. & Bissell, M. J. Modelling breast cancer requires identification and correction of a critical cell lineage-dependent transduction bias. *Nat. Commun.* **6**, 6927 (2015).

169. Kumar, M., Keller, B., Makalou, N. & Sutton, R. E. Systematic determination of the packaging limit of lentiviral vectors. *Hum. Gene Ther.* **12**, 1893–1905 (2001).

170. Ellis, B. L. *et al.* A survey of ex vivo/in vitro transduction efficiency of mammalian primary cells and cell lines with Nine natural adeno-associated virus (AAV1-9) and one engineered adeno-associated virus serotype. *Virol. J.* **10**, 74 (2013).

171. Klein, R. L., Dayton, R. D., Tatom, J. B., Henderson, K. M. & Henning, P. P. AAV8, 9, Rh10, Rh43 vector gene transfer in the rat brain: Effects of serotype, promoter and purification method. *Mol. Ther.* **16**, 89–96 (2008).

172. Hirsch, M. L. *et al.* Viral Single-Strand DNA Induces p53-Dependent Apoptosis in Human Embryonic Stem Cells. *PLoS One* **6**, e27520 (2011).

173. Traboulsi, T., El Ezzy, M., Gleason, J. L. & Mader, S. Antiestrogens: Structure-activity

relationships and use in breast cancer treatment. *J. Mol. Endocrinol.* **58**, R15–R31 (2017).

174. Xiao, T. *et al.* Estrogen-regulated feedback loop limits the efficacy of estrogen receptor–targeted breast cancer therapy. *Proc. Natl. Acad. Sci. U. S. A.* **115**, 7869–7878 (2018).

175. Taylor, S. C. *et al.* The Ultimate qPCR Experiment: Producing Publication Quality, Reproducible Data the First Time. *Trends Biotechnol.* **37**, 761–774 (2019).

176. Li, H. *et al.* Applications of genome editing technology in the targeted therapy of human diseases: mechanisms, advances and prospects. *Signal Transduct. Target. Ther.* **5**, 1 (2020).

177. Tian, X. *et al.* CRISPR/Cas9 – An evolving biological tool kit for cancer biology and oncology. *Precis. Oncol.* **3**, 8 (2019).

178. Liu, B., Saber, A. & Haisma, H. J. CRISPR/Cas9: a powerful tool for identification of new targets for cancer treatment. *Drug Discov. Today* **24**, 955–970 (2019).

179. Alimperti, S., Lei, P., Tian, J. & Andreadis, S. T. A novel lentivirus for quantitative assessment of gene knockdown in stem cell differentiation. *Gene Ther.* **19**, 1123–1132 (2012).

180. Xu, X. *et al.* Efficient homology-directed gene editing by CRISPR/Cas9 in human stem and primary cells using tube electroporation. *Sci. Rep.* **8**, 11649 (2018).

181. Samlali, K., Ahmadi, F., Quach, A. B. V, Soffer, G. & Shih, S. C. C. One Cell , One Drop , One Click : Hybrid Microfluidics for Mammalian Single Cell Isolation. **16**, 2002400 (2020).

182. Han, X., Liu, Z., Ma, Y., Zhang, K. & Qin, L. Cas9 Ribonucleoprotein Delivery via Microfluidic Cell-Deformation Chip for Human T-Cell Genome Editing and Immunotherapy. *Adv. Biosyst.* **1**, 1600007 (2017).

183. Han, X. *et al.* Microfluidic Cell Deformability Assay for Rapid and Efficient Kinase Screening with the CRISPR-Cas9 System. *Angew. Chemie - Int. Ed.* **55**, 8561–8565 (2016).

184. Doudna, J. A. & Charpentier, E. The new frontier of genome engineering with CRISPR-Cas9. *Science (80-.).* **346**, (2014).

185. Barrangou, R. & Doudna, J. A. Applications of CRISPR technologies in research and

beyond. *Nat. Biotechnol.* **34**, 933–941 (2016).

186. Doudna, J. A. The promise and challenge of therapeutic genome editing. *Nature* **578**, 229–236 (2020).

187. Lee, D. W. *et al.* T cells expressing CD19 chimeric antigen receptors for acute lymphoblastic leukaemia in children and young adults: A phase 1 dose-escalation trial. *Lancet* **385**, 517–528 (2015).

188. Patel, U. *et al.* CAR T cell therapy in solid tumors: A review of current clinical trials. *eJHaem* **3**, 24–31 (2022).

189. Jiang, Z. *et al.* HIV-1-Specific CAR-T Cells With Cell-Intrinsic PD-1 Checkpoint Blockade Enhance Anti-HIV Efficacy in vivo. *Front. Microbiol.* **12**, 684016 (2021).

190. Mukhatayev, Z., Ostapchuk, Y. O., Fang, D. & Le Poole, I. C. Engineered antigen-specific regulatory T cells for autoimmune skin conditions. *Autoimmun. Rev.* **20**, 102761 (2021).

191. Senís, E. *et al.* CRISPR/Cas9-mediated genome engineering: An adeno-associated viral (AAV) vector toolbox. *Biotechnol. J.* **9**, 1402–1412 (2014).

192. Jarrell, J. A., Sytsma, B. J., Wilson, L. H., , Fong L. Pan , Katherine H.W.J. Lau, G. T. S. K. & Lievano, A. A. Genome editing human primary T cells with microfluidic vortex shedding & CRISPR Cas9. *bioRxiv* **3**, 6 (2021).

193. Jayasooriya, V., Ringwelski, B., Dorsam, G. & Nawarathna, D. mRNA-based CAR T-cells manufactured by miniaturized two-step electroporation produce selective cytotoxicity toward target cancer cells. *Lab Chip* **21**, 3748–3761 (2021).

194. Loo, J. *et al.* Microfluidic transfection of mRNA into human primary lymphocytes and hematopoietic stem and progenitor cells using ultra - fast physical deformations. *Sci. Rep.* 21407 (2021).

195. Bloemberg, D. *et al.* A High-Throughput Method for Characterizing Novel Chimeric Antigen Receptors in Jurkat Cells. *Mol. Ther. - Methods Clin. Dev.* **16**, 238–254 (2020).

196. Zhang, Z., Qiu, S., Zhang, X. & Chen, W. Optimized DNA electroporation for primary human T cell engineering. *BMC Biotechnol.* **18**, 4 (2018).

197. Ghassemi, S. *et al.* Rapid manufacturing of non-activated potent CAR T cells. *Nat. Biomed. Eng.* **6**, 118–128 (2022).

198. Chamberlain, C. A. *et al.* Highly efficient PD-1-targeted CRISPR-Cas9 for tumor-infiltrating lymphocyte-based adoptive T cell therapy. *Mol. Ther. - Oncolytics* **24**, 417–428 (2022).

199. Rozenbaum, M., Meir, A., Aharony, Y., Itzhaki, O. & Schachter, J. Gamma-Delta CAR-T Cells Show CAR-Directed and Independent Activity Against Leukemia. **11**, 1347 (2020).

200. Hulen, T. M., Chamberlain, C. A., Svane, I. M. & Met, Ö. ACT Up TIL Now: The Evolution of Tumor-Infiltrating Lymphocytes in Adoptive Cell Therapy for the Treatment of Solid Tumors. *Immuno* **1**, 194–211 (2021).

201. Roth, T. L. *et al.* Reprogramming human T cell function and specificity with non-viral genome targeting. *Nature* **559**, 405–409 (2018).

202. Quach, A. B. V., Little, S. R. & Shih, S. C. C. Viral Generation, Packaging, and Transduction on a Digital Microfluidic Platform. *Anal. Chem.* **94**, 4039–4047 (2022).

203. Zhu, T. *et al.* Electroporation based on hydrodynamic focusing of microfluidics with low dc voltage. *Biomed. Microdevices* **12**, 35–40 (2010).

204. Pollard, J. W., Luqmani, Y., Bateson, A. & Chotai, K. DNA Transformation of Mammalian Cells. *Nucleic Acids* **130**, 321–332 (2003).

205. Lebrun, L. & Junter, G. A. Diffusion of dextran through microporous membrane filters. *J. Memb. Sci.* **88**, 253–261 (1994).

206. Bai, H., Lester, G. M. S., Petishnok, L. C. & Dean, D. A. Cytoplasmic transport and nuclear import of plasmid DNA. *Biosci. Rep.* **37**, BSR20160616 (2017).

207. Dean, D., Strong, D. & Zimmer, W. Nuclear entry of nonviral vectors DA. *Gene Ther.* **33**, 395–401 (2015).

208. Ding, X. *et al.* High-throughput nuclear delivery and rapid expression of DNA via mechanical and electrical cell-membrane disruption. *Nat. Biomed. Eng.* **1**, 0039 (2017).

209. Ayyadevara, V. S. S. A. & Roh, K. H. Calcium enhances polyplex-mediated transfection

efficiency of plasmid DNA in Jurkat cells. *Drug Deliv.* **27**, 805–815 (2020).

210. Schlake, T., Thess, A., Thran, M. & Jordan, I. mRNA as novel technology for passive immunotherapy. *Cell. Mol. Life Sci.* **76**, 301–328 (2019).

211. Wang, H., Liu, B. & Wei, J. Beta2-microglobulin(B2M) in cancer immunotherapies: Biological function, resistance and remedy. *Cancer Lett.* **517**, 96–104 (2021).

212. Invitrogen. Neon Transfection System Cell Protocols: Human T cells microporation.

213. Lonza. Amaxa ™ 4D-Nucleofector ™ Protocol for stimulated Human T Cells For 4D-Nucleofector ™ X Unit.

214. Hsi, P. *et al.* Acoustophoretic rapid media exchange and continuous-flow electrotransfection of primary human T cells for applications in automated cellular therapy manufacturing. *Lab Chip* **19**, 2978–2992 (2019).

215. Yen, J. *et al.* TRIAMF: A New Method for Delivery of Cas9 Ribonucleoprotein Complex to Human Hematopoietic Stem Cells. *Sci. Rep.* **8**, 16304 (2018).

216. Gurusamy, D. *et al.* Article Multi-phenotype CRISPR-Cas9 Screen Identifies p38 Kinase as a Target for Adoptive Immunotherapies ll Article Multi-phenotype CRISPR-Cas9 Screen Identifies p38 Kinase as a Target for Adoptive Immunotherapies. *Cancer Cell* **37**, 818–833 (2020).

217. Seki, A. & Rutz, S. Optimized RNP transfection for highly efficient CRI SPR/Cas9-mediated gene knockout in primary T cells. *J. Exp. Med.* **215**, 985–997 (2018).

218. Ahmadi, F., Quach, A. B. V. & Shih, S. C. C. Is microfluidics the 'assembly line' for CRISPR-Cas9 gene-editing? *Biomicrofluidics* **14**, 061301 (2020).

219. Wang, H. & Chen, L. Novel electrodes for precise and accurate droplet dispensing and splitting in digital microfluidics. *Nanotechnol. Rev.* **10**, 857–869 (2021).

220. Stadtmauer, E. A. *et al.* CRISPR-engineered T cells in patients with refractory cancer. *Science (80-.).* **367**, eaba7365 (2020).

221. Scholler, J. *et al.* Decade-long safety and function of retroviral-modified chimeric antigen receptor T cells. *Sci. Transl. Med.* **4**, 132ra53 (2012).

222. Hyrenius-wittsten, A. *et al.* SynNotch CAR circuits enhance solid tumor recognition and promote persistent antitumor activity in mouse models. *Sci. Transl. Med.* **13**, 591 (2021).

223. Ellis, I. G., Sheppard, C. N. & Riley, L. J. Genetic engineering of T cells for immunotherapy. *Nat. Genet. Rev.* **176**, 139–148 (2021).

224. Carugo, D. *et al.* Contrast agent-free sonoporation: The use of an ultrasonic standing wave microfluidic system for the delivery of pharmaceutical agents. *Biomicrofluidics* **5**, 44108–4410815 (2011).

225. Zhuang, S. *et al.* Microinjection in Biomedical Applications: An Effortless Autonomous Omnidirectional Microinjection System. *IEEE Ind. Electron. Mag.* **17**, 2–15 (2023).

226. Weaver, A. N. *et al.* Final outcomes analysis of the cell product SQZ - PBMC - HPV Phase 1 trial in incurable HPV16 + solid tumors shows improved overall survival in patients with increased CD8 + T cell tumor infiltration. **63**, 1421–1428 (2024).

227. Little, S. R. *et al.* A Tri-Droplet Liquid Structure for Highly Efficient Intracellular Delivery in Primary Mammalian Cells Using Digital Microfluidics. *Adv. Mater. Technol.* **8**, 2300719 (2023).

228. Aksoy, P., Aksoy, B. A., Czech, E. & Hammerbacher, J. Viable and efficient electroporation-based genetic manipulation of unstimulated human T cells. *bioRxiv* 466243 (2018).

229. Chopra, S., Ruzgys, P., Maciulevičius, M., Jakutavičiute, M. & Šatka, S. Investigation of plasmid DNA delivery and cell viability dynamics for optimal cell electrotransfection in vitro. *Appl. Sci.* **10**, 6070 (2020).

230. Hultquist, J. F. *et al.* CRISPR-Cas9 genome engineering of primary CD4+ T cells for the interrogation of HIV-host factor interactions. **14**, 1–27 (2019).

231. Oh, S. A., Seki, A. & Rutz, S. Ribonucleoprotein Transfection for CRISPR/Cas9-Mediated Gene Knockout in Primary T Cells. *Curr. Protoc. Immunol.* **124**, e69 (2019).

232. Cloarec-Ung, F. M. *et al.* Near-perfect precise on-target editing of human hematopoietic stem and progenitor cells. *Elife* **12**, RP91288 (2023).

233. Shy, B. R. *et al.* High-yield genome engineering in primary cells using a hybrid ssDNA repair template and small-molecule cocktails. *Nat. Biotechnol.* **41**, 521–531 (2023).

234. Mejía-Guarnizo, L. V., Monroy-Camacho, P. S., Turizo-Smith, A. D. & Rodríguez-García, J. A. The role of immune checkpoints in antitumor response: a potential antitumor immunotherapy. *Front. Immunol.* **14**, 1298571 (2023).

235. Gocher, A. M., Workman, C. J. & Vignali, D. A. A. Interferon-γ: teammate or opponent in the tumour microenvironment? *Nat. Rev. Immunol.* **22**, 158–172 (2022).

236. Ward-Kavanagh, L. K., Lin, W. W., Šedý, J. R. & Ware, C. F. The TNF Receptor Superfamily in Co-stimulating and Co-inhibitory Responses. *Immunity* **44**, 1005–1019 (2016).

237. Garaeva, A. A., Kovaleva, I. E., Chumakov, P. M. & Alexandra, G. Mitochondrial dysfunction induces SESN 2 gene expression through Activating Transcription Factor. *Cell Cycle* **15**, 64–71 (2016).

238. Magg, V. *et al.* Turnover of PPP1R15A mRNA encoding GADD34 controls responsiveness and adaptation to cellular stress. *CellReports* **43**, 114069 (2024).

239. Bereshchenko, O. *et al.* Glucocorticoid-Induced Leucine Zipper : A Novel Anti-inflammatory Molecule. **10**, 308 (2019).

240. Yang, H. *et al.* Stress–glucocorticoid–TSC22D3 axis compromises therapy-induced antitumor immunity. *Nat. Med.* **25**, 1428–1441 (2019).

241. Hong, C., Choi, Y. H., Wald, D. & Hwang, T. H. Identifying A Source Of Dysfunctional CAR T Cells Incorporating With PBMC scRNA Seq Data. *J. Cancer Immunother.* **11**, 1191 (2023).

242. Mcardel, S. L., Terhorst, C. & Sharpe, A. H. Roles of CD48 in regulating immunity and tolerance. *Clin. Immunol.* **164**, 10–20 (2016).

243. Croft, D. *et al.* The Reactome pathway knowledgebase. *Nucleic Acids Res.* **42**, 472–477 (2014).

244. Wherry, E. J. T cell exhaustion. *Nat. Immunol.* **12**, 492–499 (2011).

245. CRISPR / Cas9-mediated Genome Editing of Human Primary T-cells using the Neon ™ Transfection System.

246. Schumann, K. *et al.* Generation of knock-in primary human T cells using Cas9 ribonucleoproteins. *Proc. Natl. Acad. Sci. U. S. A.* **112**, 10437–10442 (2015).

247. Bustin, S. A. *et al.* The MIQE guidelines: Minimum information for publication of quantitative real-time PCR experiments. *Clin. Chem.* **55**, 611–622 (2009).

248. Bas, A., Forsberg, G., Hammarström, S. & Hammarström, M. L. Utility of the housekeeping genes 18S rRNA, β-actin and glyceraldehyde-3-phosphate-dehydrogenase for normalization in real-time quantitative reverse transcriptase-polymerase chain reaction analysis of gene expression in human T lymphocytes. *Scand. J. Immunol.* **59**, 566–573 (2004).

249. Geigges, M. *et al.* Reference Genes for Expression Studies in Human CD8+ Naïve and Effector Memory T Cells under Resting and Activating Conditions. *Sci. Rep.* **10**, 9411 (2020).

250. Li, H. Minimap2: Pairwise alignment for nucleotide sequences. *Bioinformatics* **34**, 3094–3100 (2018).

251. Patro, R., Duggal, G., Love, M. I., Irizarry, R. A. & Kingsford, C. Salmon provides fast and bias-aware quantification of transcript expression. **14**, 417–418 (2017).

252. Durinck, S., Spellman, P. T., Birney, E. & Huber, W. Mapping identifiers for the integration of genomic datasets with the R / Bioconductor package biomaRt. **4**, 1184–1191 (2009).

253. Love, M. I., Huber, W. & Anders, S. Moderated estimation of fold change and dispersion for RNA-seq data with DESeq2. *Genome Biol.* **15**, 550 (2014).

254. Yu, G. & He, Q.-Y. ReactomePA: an R/Bioconductor package for reactome pathway analysis and visualization. *Mol. Biosyst.* **12**, 477–479 (2016).

255. Wang, C. *et al.* Ferroptosis and Neurodegenerative Diseases: Insights into the Regulatory Roles of SLC7A11. *Cell. Mol. Neurobiol.* **43**, 2627–2642 (2023).

256. Lakaye, B., Coumans, B., Harray, S. & Grisar, T. Melanin-concentrating hormone and

immune function. *Peptides* **30**, 2076–2080 (2009).